The Jahn-Teller effect in icosahedral symmetry.

John Paul Cullerne.

Exeter College.

Trinity Term 1995.

To the memory of my aunt May.

Acknowledgements.

I would like to thank Prof. D. Sherrington for the privilege of working in his department. It is a pleasure to thank my supervisor Dr. M.C.M. O'Brien for all her guidance and patience over the past three years. I would also like to thank Dr. M.N. Angelova and Dr. C.C. Chancey for all their help and encouragement.

My colleagues in Office 1.3 have provided an enjoyable working atmosphere for which I am most grateful. My thanks goes especially to Mr. J.E. Santos and Mr. J.C. Johnston for their help with proof reading and for putting up with my virtual monopoly on the computer terminal.

Special thanks must go to Kay my fiancée who has given me so much encouragement and support over the past three years.

I must also thank my family who have supported and encouraged me throughout my D. Phil. and all of my studies. Without their support none of this would have been possible.

Finally I acknowledge the financial support of the EPSRC.

The Jahn-Teller effect in icosahedral symmetry.

John Paul Cullerne.

Exeter College, Oxford.

A thesis submitted for the degree of Doctor of Philosophy at the University of Oxford.

Trinity Term 1995.

ABSTRACT.

The resurgence of interest in properties of molecules of icosahedral symmetry follows the discovery of the C_{60} molecule. Due to the high symmetry of the icosahedron, almost all the electronic and vibrational levels are highly degenerate, so that in dealing with properties of these systems, the Jahn-Teller interaction must almost always be allowed for. This thesis primarily explores the properties of the icosahedral $G \otimes (g \oplus h)$ interaction and related subsystems in the strong coupling régime. Mappings of the adiabatic potential energy surfaces facilitate an analysis of the geometrical phase or Berry phase acquired by the quantal system on transportation around adiabatic circuits in parameter space. The Berry phase information in conjunction with an analysis of tunnelling, determines the properties of the ground state.

The use of Ham factors achieves a characterization of the various coupling régimes. However, characterization of G and H Jahn-Teller systems, requires an extension of the standard definition of these Ham factors. In such cases the extended matrix elements between and within vibronic tunnelling sublevels cannot be ignored. A calculation of all the standard and extended matrix elements is presented. A further introduction of a matrix of Ham factors facilitates the description of H multiplicity within an H manifold.

Finally, two problems are investigated numerically; aimed at making some allusion towards possible experimental manifestations of $G \otimes (g \oplus h)$. The first investigation considers the variations in the eigensystem and Ham factors of $G \otimes (g \oplus h)$, as a function of the coupling to the two modes. The second investigation considers the structure in the optical absorption line shapes for the transitions from orbital singlet to quartet, G, states in an icosahedral environment. The quartet states are subject to both spin-orbit and linear Jahn-Teller interactions.

Contents

Chapter 1

Basic Theory.

1.1 A brief review of Jahn-Teller interactions in icosahedral symmetry.

JAHN- Teller interaction effects constitute a field of investigation in the physics and chemistry of molecules and crystals combining all the phenomena and laws originating from the mixing of electronic states by nuclear displacements. Jahn and Teller [47] proved that if the electronic state of a non-linear molecular system is orbitally degenerate, forces will persist in the totally symmetric molecular configuration (the Jahn-Teller origin) and thus an equilibrium is in general impossible. Subsequent motion of the nuclei will then remove the electronic degeneracy. This *vibronic* coupling of nuclear and electronic degrees of freedom, arising from the degeneracy or near degeneracy of electronic states in the symmetric molecular configuration, is called "The Jahn-Teller effect".

In their original paper [47], Jahn and Teller invoked both vibration and perturbation theory. Their discussion of this effect was primarily on the energetics, i.e. their concern was with the non-zero matrix elements of the linear perturbation term. Indeed, a non-linear molecular system exhibiting such non-zero perturbation terms in its totally symmetric configuration, is subject to a force corresponding to the slope of the energy curve in the high symmetry origin.

The degenerate electronic states and normal modes of distortion may be classified according to the irreducible representations (irreps) of the point group of the Jahn-Teller origin. For spin-independent[1] electron systems, the normal mode distortions capable of lifting the degeneracy

[1] In the case of spin-dependent systems the electronic state is classified according to the irreps of the double point group of the Jahn-Teller origin. The corresponding Jahn-Teller active modes appear in the anti-symmetric square of the irrep of the electronic state.

belong to the non-singlet irreps appearing in the symmetric square of the irrep of the electronic state. The molecular distortions defined in this way are termed "Jahn-Teller active".

Until the recent discovery of the C_{60} molecule [54], icosahedral symmetry did not figure largely in discussions of the Jahn-Teller effect. It was not thought until the last decade that molecules with this high symmetry would be found to exist. In fact, the range of Jahn-Teller interactions within the different irreducible representations of this symmetry is so rich and varied, that they are well worth studying and classifying even before possible manifestations of some of them appear in the experimental record.

The full icosahedral group I_h may be considered as a direct product of I (the group of icosahedral rotations) and S_2 (the group made up of the identity and the inversion elements). The S_2 inversion symmetry has the effect of distinguishing irreps that are even and odd under inversion. The irreps of I_h are labelled accordingly by "gerade"(g) and "ungerade"(u) subscripts. However, in the notation for Jahn-Teller systems these subscripts are very often omitted because the Jahn-Teller active modes are necessarily invariant under inversion (see Subsection (1.4.1)). For simplicity, in all of the following any reference to the icosahedral group implies only icosahedral rotations since the inversion symmetry of an icosahedral molecule cannot be destroyed by Jahn-Teller distortions. Similarly, any reference to higher continuous symmetries which are reduced to I, will relate only to pure rotations, e.g. $SO(3)$ instead of $O(3) \equiv SO(3) \otimes S_2$.

There are five irreducible representations in I [49]: an invariant singlet, A, two triplets, T_1 and T_2, a quartet, G and a quintet, H (publications on this topic often use varying notations, but this is the notation used in this thesis). A study of the products of these representations yields seven Jahn-Teller couplings to be considered. Couplings involving only single modes are listed in the form, (electronic state, upper-case label)$\otimes$(vibrational mode, lower-case label), $T_1 \otimes h$, $T_2 \otimes h$, $G \otimes g$, $G \otimes h$, $H \otimes g$, $H \otimes h_2$ and $H \otimes h_4$ (coupling to the H state may involve more than one type of h vibration. The significance of the 2 and 4 in the subscripts is explained fully in the next chapter). A survey of continuous group invariances present in these Jahn-Teller systems involving several vibration modes was made by Pooler [80]. A résumé of properties of all the above mentioned systems is given below. For brevity, the following coupling schemes are denoted by just the symmetry designations with a subscript eq, for equal coupling[2].

$T \otimes h$ The interaction matrices in this system are identical to those of a triplet in cubic symmetry, simultaneously coupled to a doublet ϵ and a triplet τ_2 of vibrations acting as a quintet of modes i.e., $T \otimes (\epsilon \oplus \tau_2)_{eq}$. This case, which occurs surprisingly often in cubic symmetry

[2]See Subsection (1.4.2)

considering that it is an "accidental" degeneracy, has been extensively studied [70, 72, 73, 60, 17, 87]. The Hamiltonian has rotational symmetry in a three-dimensional sub-space of the five-dimensional phase space, with the result that the low-lying states are rather closely spaced, being pseudo-rotational. This type of coupling is important for low-lying excited electronic triplets of C_{60} [68, 55, 25, 5, 6].

$G \otimes (g \oplus h)$ The subject of this thesis. Since the symmetric square of G contains both G and H, the general Jahn-Teller system includes coupling to modes of both these types. Pooler [80] shows that when the coupling strengths to both types of mode are suitably adjusted i.e. $G \otimes (g \oplus h)_{eq}$, the Hamiltonian is invariant under $SO(4)$, so that there will be a continuum of minima. Ceulemans *et al.* [13] treat this coupling scheme, providing a general solution to the *static* case.

$G \otimes g$ Here the lowest adiabatic potential energy surface (APES) has minima as well as threefold degeneracies at points corresponding to distortions of tetrahedral ($\mathcal{T}$) symmetry, and saddle points and degeneracies at distortions of trigonal ($\mathcal{D}_3$) and dihedral ($\mathcal{D}_2$) symmetry.

$G \otimes h$ Here the lowest APES has ten points of minimum energy, corresponding to distortions of $\mathcal{D}_3$ symmetry, saddle points are at distortions of $\mathcal{D}_2$ and $\mathcal{D}_3$ symmetry, and degeneracies at distortions of pentagonal ($\mathcal{D}_5$) symmetry. Minima lie at the vertices of a dodecahedron embedded in the five-dimensional phase space, while the saddle points nearest in energy to the minima lie near the centres of the edges of the dodecahedron. A *duality* between this interaction and $H \otimes g$ is found to exist and may be utilized to obtain the ground state properties of both $G \otimes h$ and $H \otimes g$ *dynamical* systems in the limit of strong coupling (see Chapter 3).

$H \otimes (g \oplus h \oplus h)$ Ceulemans *et al.* [14] treat this coupling scheme, providing a general solution to the *static* case. An extra complication is introduced here because the H irreducible representation occurs twice in the symmetric square $[H \otimes H]$. As a result of this, the Wigner-Eckart theorem does not take its usual simple form, and there are two families of H matrices which must be multiplied by different coupling constants to represent a general Jahn-Teller interaction. A distinction between the two different types of H matrices is often made by deriving them from the $SO(3)$ irreducible representations $J = 2$ (h_2) and $J = 4$ (h_4). Some of the possible variations can then be listed as follows:

$H \otimes (g \oplus h \oplus h)$ Pooler [80] shows that this Hamiltonian can have $SO(3)$ or $SO(5)$ sym-

metry if all three sets of modes are included with appropriate coupling constants.

$H \otimes h_2$ This case was considered by Khlopin *et al.* [53]. The Hamiltonian possesses the continuous symmetry of $SO(3)$ [80]. The lowest APES is a four-dimensional hypersphere in the five-dimensional phase space, and it becomes degenerate with the next APES over a three-dimensional subspace. This can be expected to lead to even higher degeneracies in the closely spaced low-lying levels than in $T \otimes h$.

$H \otimes h_4$ This has no continuous group symmetry. The lowest APES has minima at points of $\mathcal{D}_5$ symmetry with degeneracies and saddles at $\mathcal{D}_3$ and $\mathcal{D}_2$ points respectively.

$H \otimes g$ This has no continuous group symmetry. The lowest APES has minima and degeneracies at points of $\mathcal{D}_3$ distortion, and saddle points and degeneracies at distortions of $\mathcal{T}$ symmetry. A *duality* between this interaction and $G \otimes h$ is found to exist and may be utilized to obtain the ground state properties of both $H \otimes g$ and $G \otimes h$ *dynamical* systems in the limit of strong coupling (see Chapter 3).

1.2 General discussion and plan of the thesis.

The icosahedral orbital quartet G is Jahn-Teller active under the nine normal mode distortions belonging to the icosahedral representation $(g \oplus h)$. Advances in the theoretical treatment of atomic clusters [18, 84, 32] predict some structures that may exemplify this kind of Jahn-Teller effect. In the case of carbon, an infinite series of icosahedral carbon shells is theoretically possible and such clusters fall into two disjoint classes [32]. The prototype for the first class is the truncated icosahedral C_{60} molecule which is known to exhibit $T \otimes h$ instability as a negatively charged species C_{60}^{-} or C_{60}^{3-}. However, the prototype for the second class is the dodecahedral C_{20} molecule, the singlularly charged cation of which, C_{20}^{+}, is found to have a four-fold degenerate G ground state and thus should be subject to a Jahn-Teller instability under the $(g \oplus h)$ distortions [13]. Theoretical work on silicon micro-clusters also predicts some features of icosahedral symmetry. There is also some experimental evidence which apparently vindicates these theoretical conclusions. An investigation of the cluster size dependence of the reaction rate constant for the addition of the first C_2H_4 molecule onto Si_n^{+} [18], has reaction minima for n=13,19 and 23. Chelikowsky *et al.* [18] interpret these 13,19 and 23 atom clusters as belonging to a pentagonal growth sequence [45] with the 13 atom cluster taking up an atom-centred icosahedral structure. The recent work of Gu *et al.* [35] on the electronic structure of icosahedral silicon clusters finds that the icosahedral Si_{13}^{+} cluster has a highest occupied molecular orbital (HOMO) of G_g symmetry but with only one electron occupation. Therefore, icosahedral Si_{13}^{+} is predicted to exhibit

Jahn-Teller instability appropriate to a G_g electronic state.

This thesis primarily explores the Jahn-Teller instability of an orbital G degeneracy in an icosahedral environment, which is usually referred to symbolically as $G \otimes (g \oplus h)$. The investigations presented here are within the strong coupling régime, where an adiabatic approximation may be applied. Although actual physical systems are very rarely strongly coupled, strong coupling studies have proved their worth in the past [89]. Such studies provide the strong coupling limits of various quantities which may be interpolated to the weak coupling limit so that their values may be estimated at intermediate coupling strengths where the calculation is very difficult. At the weak coupling limit, Jahn-Teller interactions are treated as perturbations to the oscillator Hamiltonian, and therefore involve a symmetry subduction from the dynamical symmetry group of the oscillator Hamiltonian to the point group of the Jahn-Teller origin. For the icosahedral group, the dynamical symmetries of the oscillator Hamiltonian can be as large as $U(9)$ in the case of $G \otimes (g \oplus h)$, or even $U(14)$ in the case of $H \otimes (g \oplus h \oplus h)$. Detailed studies of the many different subduction paths from these high symmetries to I have yet to be expounded. Weak coupling studies of general $G \otimes (g \oplus h)$ are therefore extremely complicated and until the subduction paths from $U(9)$ to I are better understood, the $G \otimes (g \oplus h)$ weakly coupled problem will remain relatively unmanageable.

The strong coupling Hamiltonian for $G \otimes (g \oplus h)$ is constructed from the symmetry coupling rules within a G manifold. These coupling rules are well documented and are readily available in tabular form [81, 34]. However, the availability of modern computing methods has made it possible to avoid a laborious inspection of tables. In Chapter 2 a *Mathematica* routine for calculating symmetry coupling coefficients is outlined which is very fast and easily implemented. The resulting Clebsch-Gordan matrices are not only used to construct Jahn-Teller Hamiltonians, but also facilitate an analysis of icosahedral invariant quantities which proves very useful in the later chapters of this thesis.

On the theoretical treatment of $G \otimes (g \oplus h)$, some work has been done in the *static* régime [13, 53]. The work of Ceulemans *et al.* [13] appealed to the *epikernel principle* [67, 15] to obtain the extremal configurations and extensive use was made of the finite and infinite invariances present in the system. In this vein, the symmetry of the system splits naturally into three categories: the symmetries of the infinite $SO(4)$ parent group, the finite icosahedral group of the Jahn-Teller origin, and the icosahedral sub-groups resulting from the symmetry-lowering distortions. Analyses in Chapters 3, 4 and 5 follow this descent in symmetry ($SO(4) \supset I \supset$ lower point groups) to explore the ground state properties of $G \otimes (g \oplus h)$ and related subsystems in the strong coupling régime.

The treatment in Chapter 3 utilizes the $SO(4) \supset I$ symmetry descent extensively in examining the *dynamical* ground state properties of $G \otimes (g \oplus h)$. A *biharmonic* parametrization facilitates the solution of $G \otimes (g \oplus h)_{eq}$ at strong coupling, which exhibits an $SO(4)$ invariance [80] and may be written as $(\frac{1}{2}, \frac{1}{2}) \otimes (1,1)$ of $SO(4)$. Solution of the Schrödinger equation of nuclear motion is over the three-dimensional "flat" trough of the lowest APES. The continuity of the vibronic wave function over the lowest APES facilitates the derivation of the ordering and degeneracy of the resulting pseudo-rotational states, the energies of these states to order $(1/V_o^2)$ where V_o is the strength of the Jahn-Teller coupling, and the ground state reduction factors or Ham factors [38, 37] of the $(1,1)$ operators [20]. An extention of the *biharmonic* parametrization simplifies the investigation of *dynamical* effects in the low-lying states of the icosahedral subsystems $G \otimes g$ and $G \otimes h$ [20].

A simple *duality* between $G \otimes h$ and $H \otimes g$ [20] leads to the diagonalization of the first order tunnelling matrices over the lowest APESs in both $G \otimes h$ and $H \otimes g$. In a similar analysis, a simple *self-duality* is utilized to diagonalize the first order tunnelling matrix for $G \otimes g$ [20]. An investigation such as this requires some knowledge of the variations in the electronic wave function over the lowest APES. It is useful to discuss these variations in terms of the Berry phases [9, 1] and a method is introduced for numerically tracking the electronic eigenstate over the lowest APES [20]. Introduction of a matrix method incorporating the Berry phase information, greatly simplifies the computation of symmetry adapted low-lying eigenstates, the energy eigenvalues of these states and therefore their ordering [20].

In Chapter 4, extension of the above methods facilitates the calculation of Ham factors for Jahn-Teller active operators within the low-lying states of $G \otimes g$, $G \otimes h$ and $H \otimes g$ [20]. The extra complication arising from the energy-proximity of the low-lying sublevels necessitates an extension [21] of the standard definition of the Ham factor. Consideration of the multiplicity of H irreps arising in the symmetric square $[H \otimes H]$ [21], requires the introduction of a matrix of Ham factors.

In Chapter 5, a numerical treatment of the $G \otimes (g \oplus h)$ eigenvalue problem [22], leads to a better understanding of the variations of eigensystem and ground state Ham factors between the extremities of coupling régime, i.e. from $G \otimes h$ to $G \otimes (g \oplus h)_{eq}$ through to $G \otimes g$. Once again, the parent $SO(4)$ symmetry is extensively utilized ($G \otimes (g \oplus h)_{eq} \equiv (\frac{1}{2}, \frac{1}{2}) \otimes (1,1)$ of $SO(4)$) [80]. Generation of eigenvalues is achieved by solving the Schrödinger equation on the equal coupling minimum hypersphere perturbed by a fourth-order icosahedral field term with appropriate extremal properties. Energy level diagrams and plots of the ground state Ham factors are constructed over the range of strengths of the field term. Expressions for these Ham factors

within this approximation are obtained and compared with equivalent expressions obtained at the coupling régime extremities. The numerically calculated properties of the system interpolate well between those appropriate to coupling to g and h modes separately. The limitations on the description of this approximate theory are also discussed by working back from the single mode models, $G \otimes g$ and $G \otimes h$. In the perturbative model the system is confined to motion in only three dimensions corresponding to the minimum energy hypersurface. By considering character contributions of the various configurations, the splitting of the first excited states may be obtained. This symmetry splitting is found to be in good agreement with the numerically calculated results.

Chapter 6 deals with the optical absoption line shapes generated by transitions from orbital singlet to G quartet states in an icosahedral environment [23]. The G state is subject to spin-orbit and Jahn-Teller interactions and the line shapes are numerically calculated by a classical Franck-Condon approximation and Monte Carlo integration for all possible combinations of interaction parameters. The limitations of the model are also discussed and a rough temperature dependence of the band shapes is estimated.

Concluding remarks are presented in Chapter 7. To assist in the reading of this thesis, the presentation of large arrays of equations and matrices which are not of immediate importance to the comprehension of the material, is reserved to the appendices which may be found at the end of Chapter 7.

Meanwhile, the remainder of this introductory chapter deals with the basic ideas involved in the study of Jahn-Teller systems. The emphasis is on techniques generally used to separate this complex molecular problem into tractable parts. The existence of review articles such as those of Judd [50], Ham [39], Longuet-Higgins [63], O'Brien and Chancey [75], and others [89, 28, 88] makes it unnecessary to give more than a brief résumé of techniques. This is separated into three main parts, the first of which, Section (1.3), discusses the adiabatic approximation and its application to Jahn-Teller systems. The second, Section (1.4), outlines important group theory concepts underlying the Jahn-Teller theorem itself, continuous symmetries of Jahn-Teller Hamiltonians, and the symmetry properties of adiabatic potential surfaces, which greatly simplify the analytical work in later Chapters. Finally, the third, Section (1.5), discusses Berry's phase as applied to Jahn-Teller theory [41].

1.3 The adiabatic approximation.

1.3.1 The Hamiltonian.

With the exception of very simple systems, most Jahn-Teller Hamiltonians possess interaction terms which cause a mixing of electronic states by nuclear displacements. Molecular systems considered in this thesis may be described by Hamiltonians of the form:

$$\mathcal{H} = T_Q + T_q + V(q,Q) \equiv T_Q + H_e(q,Q), \tag{1.1}$$

$$\text{with} \quad T_Q = \frac{-\hbar^2}{2M}\nabla_Q^2,$$

$$T_q = \frac{-\hbar^2}{2m}\nabla_q^2,$$

where q and Q represent repectively the electronic and nuclear coordinates with T_x for $x = q$ or Q, representing the kinetic energy associated with the coordinates x. V is the potential energy of the molecular system including the $q-Q$ coupling of the electronic and nuclear motions. m and M are the reduced masses associated with the electronic and nuclear motions repectively. Since $M \gg m$ implying that $T_Q \ll T_q$, a very crude first approximation would be to ignore the nuclear motion altogether and solve for the electronic motion at the fixed totally symmetric equilibrium configuration denoted Q_o. This is the *Born-Oppenheimer approximation*, and although it is quite well justified in non-degenerate systems as long as the energy is near the minimum, it is unsatisfactory in analysing Jahn-Teller systems where the variation of the electronic wave function over the field of distortion parameters becomes important. However, a modification of the *Born-Oppenheimer approximation* is applicable; by allowing the electronic motions to be sensitive to different nuclear configurations Q, whilst remaining indifferent to nuclear momenta in T_Q, a separation of the nuclear and electronic motions is achieved. A solution of the electronic Hamiltonian H_e over the field of the distortion parameters is then possible, yielding adiabatic potential energy sheets APESs (one for each of the electronic states degenerate at the Jahn-Teller origin, Q_o) upon which the nuclear motions take place. Finally, with the APESs acting as potential energies for the nuclear motions, the nuclear wave functions may be calculated and the resulting (nuclear)×(electronic) product wave functions are the *vibronic* states. Note however, that in the neighbourhood of a point of degeneracy on the adiabatic potential, the non-adiabaticity corrections are not sufficiently small and therefore the adiabatic potential loses its physical interpretation as the potential energy of the nuclei in the field of the electrons. At strong coupling however, this kind of approximation is permitted because the motions of the nuclei occur well away from such degeneracies.

The electronic degeneracy of Jahn-Teller systems complicates even these approximate solutions. Trial functions for Jahn-Teller Hamiltonians are usually of the form:

$$\Psi_i = \sum_j \chi_{i,j}(Q)\psi_j(Q)u_j(q,Q), \tag{1.2}$$

where ψ_j and u_j are solutions to the nuclear and electronic equations of motion respectively and the suscript j identifies the APES upon which this motion takes place. $\chi_{i,j}$ are elements of a square matrix which are in general functions of Q. This illustrates the fact that the number of *vibronic* states is the same as the original electronic degeneracy at Q_o and therefore that the overall degeneracy of a level cannot be reduced by the Jahn-Teller interaction; an important fact when considering the connection between the theoretical and experimental manifestations of the Jahn-Teller effect encapsulated in the concept of Ham factors [38, 37].

The study of the various icosahedral Jahn-Teller Hamiltonians of this thesis is concerned in particular with the ground state eigenfunctions in the régime of strong coupling. In this régime, the vibronic ground state eigenfunctions take the simplified form

$$\Psi_i = \psi_i(Q)u_i(q,Q), \tag{1.3}$$

where i designates the lowest APES and $u_i(q,Q)$ is the eigenstate of H_e accociated with motion on this sheet. $\psi_i(Q)$ is the solution of the nuclear equation of motion upon the lowest APES. It can be shown that both Equations (1.2) and (1.3) are accurate to order m/M [63, 66].

1.3.2 Effective modes.

Any real cluster of icosahedral symmetry is almost bound to be large enough to possess many different vibrations of each symmetry type. Therefore an analysis of an icosahedral Jahn-Teller system is extremely complicated in the first instance, since there are many active Jahn-Teller modes of each symmetry type capable of lifting the electronic degeneracy. However, the qualitative properties of the APESs may still be elucidated since the number of extremal points and their corresponding symmetries are independent of the number of interacting modes. This may be illustrated by making a scale transformation of each of the degrees of freedom and in doing so, transforming the harmonic potential of elastic distortions into an isotropic form. A rotation of these scaled coordinates will leave the harmonic potential unchanged but may be chosen so that it transforms the vibronic interaction term (the $q-Q$ coupling in $V(q,Q)$ of Equation (1.1)) into a form involving only one mode of each symmetry type.

The nuclear kinetic energy (T_Q in Equation (1.1)) under these rotations is transformed into a non-isotropic form with coupling terms bilinear in the momenta describing the interaction

between the new coordinates. This is due to the fact that these new coordinates are no longer normal modes. If, however, one is only concerned with the extremal properties of the APESs then the interaction between these effective modes does not affect the qualitative results and the problem is similar to the case of the one-mode Jahn-Teller effect.

Therefore, it is always possible to take a linear combination of the normal modes as an *effective mode* in such a way that coupling to this one mode is a best first approximation to the larger Hamiltonian [53, 71, 31]. The systems in this thesis are treated in accordance with this approximation.

1.4 Some important group theory concepts.

1.4.1 Conditions for a Jahn-Teller instability.

The task of a Jahn-Teller analysis is to determine whether the energy of degenerate molecular orbitals should depend linearly or not upon nuclear displacements. In the case of orbital degeneracy, the conditions for this are quite easily ascertained [47]. The $q-Q$ coupling part of the molecular potential, V, in Equation (1.1), may be expressed as a Taylor series in Q, about the Jahn-Teller origin, Q_o. The calculations of this thesis involve the inclusion of only the linear term in this expansion. There are two main reasons for doing this: Firstly, at the linear cut-off the single mode icosahedral systems of this thesis already exhibit the minimum symmetry that the Hamiltonian can have; that is, the symmetry of the Jahn-Teller origin. Inclusion of higher order terms cannot change the result *qualitatively*, although *quantitatively* these changes may be considerable. The calculations presented in this thesis produce some numerical results (Ham factors) which are in principle accessible to experimentation. However, these numbers are derived purely from the symmetry inherent in the system and in this sense are *qualitative* properties. Therefore, the inclusion of only linear terms in the V expansion, provides enough *qualitative* information to perform all such calculations presented in this thesis. Secondly, cutting the potential off at the linear term leads to the possibility of continuous invariance [79] in icosahedral systems involving more than one mode (see next Subsection for discussion of how this arises in general Jahn-Teller systems). This continuous invariance provides a convenient coordinate system which is used to parametrize the systems throughout this thesis.

The linear approximation leads to a potential term given by

$$V(q,Q) = V(q,Q_o) + \sum_i \Delta Q_i \left(\frac{\partial V(q,Q)}{\partial Q_i} \right)_{Q=Q_o} . \tag{1.4}$$

where the $\Delta Q_i = Q_i - Q_o$, are non-symmetric distortions of the totally symmetric molecular con-

figuration. It is both sensible and usual to use as distortion coordinates linear combinations of the ΔQ_i that diagonalize the quadratic terms in $V(Q)$ and T_Q and which transform irreducibly under the group of the Jahn-Teller origin. For the purposes of this discussion these linear combinations are designated $q\lambda_i$, where Λ is the irrep label (the lower case λ denotes the vibrational mode) and i labels the partners of the irrep. Note that from their definition these symmetry coordinates vanish at Q_o, hence the term Jahn-Teller origin, and that when dealing with the Hamiltonian of the whole system, they are the normal coordinates. The elementary group theory involved in these considerations may be found in the famous Wigner paper [93] on the subject.

Within the degenerate electronic state, perturbation theory shows that the perturbation energies are characteristic values of the perturbation matrix having the following elements:

$$M_{\sigma\rho} = \sum_i q\lambda_i \int u_\sigma^* \left(\frac{\partial V}{\partial q\lambda_i}\right)_{Q_o} u_\rho d\tau, \tag{1.5}$$

where $\{u\}$ is the electronic basis and $\{..\}$ is taken to mean "set of". In the case of orbital degeneracy only, the representation subtended by the $\{u\}$ may always be chosen real and the products, $u_\sigma \left(\frac{\partial V}{\partial q\lambda_i}\right)_{Q_o} u_\rho$, are linearly independent except that of course

$$u_\sigma \left(\frac{\partial V}{\partial q\lambda_i}\right)_{Q_o} u_\rho = u_\rho \left(\frac{\partial V}{\partial q\lambda_i}\right)_{Q_o} u_\sigma. \tag{1.6}$$

Since the potential in Equation (1.4) is an invariant of the group of the Jahn-Teller origin, $\left(\frac{\partial V}{\partial q\lambda_i}\right)_{Q_o}$ must transform as $q\lambda_i^*$, and since the products are of real representations only, this becomes $q\lambda_i$. Therefore, matrix elements involving products of the form (1.6) are non-zero if Λ, the irrep subtended by the $\{q\lambda\}$, appears in the symmetric square of the irrep subtended by the $\{u\}$. Jahn pointed out [48] that in the case of additional spin degeneracy, the above results apply without modification provided the molecule contains an even number of electrons. If the molecule were to contain an odd number of electrons, the irrep subtended by the $\{u\}$ would be an irrep of the corresponding double group of the Jahn-Teller origin. A character analysis of the representations subtended by the corresponding products of Equation (1.6), shows that in the case of an odd number of electrons the corresponding matrix elements are non-zero only if Λ appears in the anti-symmetric square of the irrep subtended by the $\{u\}$.

The Jahn-Teller "instability" outlined above, means that the single symmetric minimum of the non-degenerate case is replaced by several symmetry equivalent minima with an average symmetry that is the same as that of the Hamiltonian. These minima are a result of the inter-play between the linear perturbation term and the quadratic restoring force between the nuclei. It is only an individual minimum that corresponds to a distortion of a lower symmetry and it is in this sense that the Jahn-Teller interaction is sometimes termed "symmetry-breaking". In discussing

low energy nuclear motion, the nuclei may be considered as vibrating about these minima. This corresponds to the *static* régime in which the molecule appears distorted. If on the other hand, overlap is allowed via tunnelling between the states in the minima, the degenerate ground state made up of the oscillators localized within the minima becomes split by the tunnelling matrix elements. This is the beginning of what is termed the *dynamical* régime (see Chapter 3).

1.4.2 Continuous symmetry of Jahn-Teller Hamiltonians.

In order to show how a continuous symmetry may arise in a Jahn-Teller Hamiltonian, it is necessary to consider how the addition of the vibronic coupling affects the total symmetry group of the interaction [79]. To illustrate the theory, consider first a general interaction, making no reference to any specific group. In a group $\mathcal{G}$, the Hamiltonian for a linear $\Gamma \otimes \lambda$ interaction may be written

$$\hat{\mathrm{H}} = E_o\, \hat{\mathrm{I}} + \frac{1}{2}\sum_{i=1}^{|\Lambda|}(p\lambda_i^2 + \omega_\Lambda^2 q\lambda_i^2)\, \hat{\mathrm{I}} + V_\Lambda \sum_{i=1}^{|\Lambda|} \hat{\mathrm{C}}_i\; q\lambda_i, \tag{1.7}$$

where the $\{p\lambda\}$ are momenta conjugate to the $\{q\lambda\}$ and $\hat{\mathrm{I}}$ and $\{\hat{\mathrm{C}}\}$ are the identity operator and the Jahn-Teller active modes respectively, acting within the electronic Γ manifold (the $\hat{}$ indicates a matrix). The double vertical lines in $|\Lambda|$ should be read as *dimensionality of* Λ. E_o is the energy of the orbital $|\Gamma|$-tuplet, which is usually excluded from consideration by means of an appropriate choice of the zero of energy. V_Λ and ω_Λ are respectively the Jahn-Teller coupling constant and the frequency of vibration of the equivalent modes $\{q\lambda\}$. In the absence of the linear Jahn-Teller interaction, i.e. when $V_\Lambda = 0$, the Hamiltonian (1.7) consists of the two terms: $\hat{\mathrm{H}}_e = E_o\hat{\mathrm{I}}$, which corresponds to the energy of the degenerate state Γ, and $\hat{\mathrm{H}}_v = \frac{1}{2}\sum_{i=1}^{|\Lambda|}(p\lambda_i^2 + \omega_\Lambda^2 q\lambda_i^2)\, \hat{\mathrm{I}}$, which corresponds to the energy of the harmonic Λ-type vibrations. These two terms commute and the eigenfuctions of the Hamiltonian $\hat{\mathrm{H}}_e + \hat{\mathrm{H}}_v$ have a multiplicative form $\Psi = \psi\ |u>$, where $|u>$ and ψ are respectively the eigenfunctions of the Hamiltonians $\hat{\mathrm{H}}_e$ and $\hat{\mathrm{H}}_v$. Therefore, in the absence of Jahn-Teller interaction, the dynamical symmetry group of the Hamiltonian (1.7) is the direct product group $\mathcal{G}_e \otimes \mathcal{G}_v$, where $\mathcal{G}_e$ and $\mathcal{G}_v$ are the groups of symmetry of the Hamiltonians $\hat{\mathrm{H}}_e$ and $\hat{\mathrm{H}}_v$, respectively. The electronic Hamiltonian $\hat{\mathrm{H}}_e$ is a multiple of the $|\Gamma| \times |\Gamma|$ identity matrix which is invariant under any unitary transformation in the $|\Gamma|$-dimensional space of the electronic basis. Therefore, the group $\mathcal{G}_e$ is identical to the unitary group $U(|\Gamma|)$. The number of parameters that determine an arbitrary element of this group is $|\Gamma|^2$ corresponding to the $|\Gamma|^2$ generators. However, one of these parameters describes a trivial multiplication of the basis functions by a phase factor. Excluding from consideration these trivial operations, the symmetry of H_e is confined to the $(|\Gamma|^2 - 1)$-parameter subgroup $SU(|\Gamma|)$. An arbitrary element of this

group with parameters $\{\phi\}$ and generators $\{\hat{\mathrm{m}}\}$ may be written in the form

$$\hat{\mathrm{G}}(\{\phi\}) = \exp\{\, i\, (\sum_i \phi_i\, \hat{\mathrm{m}}_i)\, \}, \tag{1.8}$$

where the $\sum_i$ is over the $(|\Gamma|^2 - 1)$-non-trivial parameters. In a similar vein, the group $\mathcal{G}_v$ is just the group of a $|\Lambda|$-dimensional isotropic harmonic oscillator. The dynamical symmetry group of an n-dimensional isotropic harmonic oscillator is $SU(n)$ [51]. Therefore, the dynamical symmetry group of (1.7) in the absence of Jahn-Teller coupling is the direct product group $SU(|\Gamma|) \otimes SU(|\Lambda|)$. An arbitrary element of this direct product group is

$$\hat{\mathrm{G}}(\{\phi, \alpha\}) = \exp\{\, i\, (\sum_i \phi_i\, \hat{\mathrm{m}}_i) + i\, (\sum_j \alpha_j\, \hat{\mathrm{n}}_j)\}, \tag{1.9}$$

where the $\{\alpha\}$ and the $\{\hat{\mathrm{n}}\}$ are respectively the parameters and generators of the group $SU(|\Lambda|)$. Introducing the Jahn-Teller coupling into (1.7) lowers the initial symmetry of the problem so that the $|\Gamma|^2 + |\Lambda|^2 - 2$ parameters of the initial symmetry cease to be independent. The relations between them can be found from the condition that the operator (1.9) should commute with the full Hamiltonian and, in particular, with the operator of the Jahn-Teller interaction, i.e. if

$$\left[(\sum_i \phi_i\, \hat{\mathrm{m}}_i + \sum_j \alpha_j\, \hat{\mathrm{n}}_j)\, ,\, \sum_{k=1}^{|\Lambda|} \hat{\mathrm{C}}_k\, q\lambda_k \right] = 0. \tag{1.10}$$

Unless the continuous symmetry of the initial interaction is completely removed by the vibronic term, equations (1.10) will yield relationships between some of the continuous parameters and set others to zero. In these cases, the remaining parameters correspond to some residual symmetry. The Hamiltonian (1.7) will exhibit this residual symmetry as a continuous invariance under a subgroup of $SU(|\Gamma|) \otimes SU(|\Lambda|)$, determined by these remaining parameters.

Pooler [79] has obtained quite simple criteria for the appearance of continuous symmetries in linear Jahn-Teller models. His treatment begins by considering the operators that act within the electronic manifold. Since this thesis primarily deals within the icosahedral G state, a brief outline of Pooler's analysis for the G manifold [80] is presented below. On a G manifold, operators may be constructed belonging to the irreps in

$$G \otimes G = [A \oplus G \oplus H]_S \oplus \{T_1 \oplus T_2\}_A, \tag{1.11}$$

where the square brackets $[..]_S$ indicate the symmetric square and the curly brackets $\{..\}_A$ indicate the anti-symmetric square. From the general theory, Pooler [80] shows that the operators belonging to the irreps T_1 and T_2 together generate $SO(4)$. Subduction from $SO(4)$ to the icosahedral group shows that $(\frac{1}{2}, \frac{1}{2}) \rightarrow G$, where $(\frac{1}{2}, \frac{1}{2})$ is the four dimensional irrep of $SO(4)$.

Operators that act within the $(\frac{1}{2},\frac{1}{2})$ manifold in $SO(4)$ belong to the irreps. in

$$(\frac{1}{2},\frac{1}{2})\otimes(\frac{1}{2},\frac{1}{2}) = [(0,0)\oplus(1,1)]_S \oplus \{(1,0)\oplus(0,1)\}_A. \tag{1.12}$$

The branching rules from $SO(4) \rightarrow I$ for these irreps are then

$$(0,0) \rightarrow A, \quad (1,0) \rightarrow T_1, \quad (0,1) \rightarrow T_2, \quad (1,1) \rightarrow G \oplus H. \tag{1.13}$$

Since the operators belonging to $(1,0)$ and $(0,1)$ are generators of $SO(4)$, their action on the electronic basis $(\frac{1}{2},\frac{1}{2})$ transforms the electronic operators belonging to $(1,1)$ amongst themselves. Pooler [80] shows that this rotation can be reversed by the same type of operation acting directly upon the partners of the irrep $(1,1)$. Hence, the interaction $(\frac{1}{2},\frac{1}{2})\otimes(1,1) \equiv G \otimes (g \oplus h)_{eq}$ is $SO(4)$ invariant under the combined electronic-vibrational transformation described above. "Equal coupling" of the g and h-modes to the G state is therefore achieved when the coupling of the two modes are suitably adjusted so that the icosahedral representation $(g \oplus h)$ transforms as $(1,1)$ of $SO(4)$.

Much of the analysis presented in this thesis has its origins in the continuous invariance exihibited by $G\otimes(g\oplus h)_{eq}$. The parentage and parametrization of the continuous $SO(4)$ symmetry proves very useful even when describing discrete properties of $G \otimes (g \oplus h)$. This is discussed in more detail in Chapter 3.

1.4.3 Symmetry properties of APESs.

For Jahn-Teller systems which do not exhibit continuous symmetries, group theoretical considerations still lead to the deduction of many aspects of APES structure. In the parameter space of a non-continuous Jahn-Teller system, the adiabatic potential as a whole has to be an invariant of the group $\mathcal{G}_o$ of the reference nuclear configuration (the configuration at Q_o). In general however, not all the elements of $\mathcal{G}_o$ correspond to non-trivial transformations within the irrep of normal modes Λ. By inspecting the characters corresponding to Λ of $\mathcal{G}_o$, it is simple to deduce under which elements of $\mathcal{G}_o$, Λ is invariant. In group theory terminology, the subgroup of such elements is called the *kernel* $K(\mathcal{G}_o,\Lambda)$ of Λ in $\mathcal{G}_o$. This property means that $K(\mathcal{G}_o,\Lambda)$ is a *normal* subgroup of $\mathcal{G}_o$; that is to say that $K(\mathcal{G}_o,\Lambda)$ consists of complete classes of $\mathcal{G}_o$ [51]. The remaining elements of $\mathcal{G}_o$ including the identity element form a group which is identical to the group of the cosets of $K(\mathcal{G}_o,\Lambda)$ in $\mathcal{G}_o$ under coset multiplication. This is called the factor group $\mathcal{G}_o/K(\mathcal{G}_o,\Lambda)$ which is therefore the symmetry group of the adiabatic potential within the invariant subspace of the Λ irrep.

In principle, the symmetry types of the extremal points on the adiabatic potential are determined by the different subgroups of the factor group $\mathcal{G}_o/K(\mathcal{G}_o,\Lambda)$. These subgroups are called *epikernels* $E(\mathcal{G}_o,\Lambda)$ of $\mathcal{G}_o$, and this relationship between epikernels and the extrema of the adiabatic potential is encapsulated in the *epikernel principle* [15, 12, 16] which may be formulated as: *Extremal points of the adiabatic potential prefer to reside at epikernels rather than kernels, preferring epikernels of highest symmetry.* This preference for highest symmetry epikernels (or maximal epikernels) may be illustrated by considering the descent in symmetry away from $\mathcal{G}_o$ by the symmetry destroying Jahn-Teller active modes. One of the properties of an epikernel $E(\mathcal{G}_o,\Gamma)$ is that at least one of the partners $|x\rangle$ of Γ, is an invariant of $E(\mathcal{G}_o,\Gamma)$. If the system described by $|x\rangle$ is in a $E(\mathcal{G}_o,\Gamma)$ point then the force on the molecule in the direction of symmetry lowering coordinates (Jahn-Teller active modes) will be the slope of the adiabatic potential $\mathcal{E}(q)$ taken within the state $|x\rangle$:

$$\langle x|\frac{\partial\mathcal{E}(q)}{\partial q}|x\rangle. \tag{1.14}$$

Since at the point $E(\mathcal{G}_o,\Gamma)$, $|x\rangle$ transforms as an invariant, this expectation will only have a non-zero value if q also transforms totally symmetrically under $E(\mathcal{G}_o,\Gamma)$. Therefore, the molecular system at this point is only subject to forces that are totally symmetric under the operations of $E(\mathcal{G}_o,\Gamma)$. Although this therefore excludes the possibility of forces taking the molecular configuration to a lower symmetry epikernel, forces that might take the molecular configuration to a higher symmetry epikernel are in general non-zero and therefore the system exhibits a general preference for higher symmetry epikernels.

It should be stressed however, that the epikernel principle is only a mathematical artifice for verifying that the symmetries corresponding to calculated extremal points of the adiabatic potentials, are sensible with respect to the allowed symmetries predicted by the group theory. The epikernel principle by itself cannot, for example, identify the natures of these extrema which can only be provided by an analysis of the potential function at these points. Also, and maybe more importantly, the epikernel principle cannot identify which of the APESs these extrema reside upon. When considering strong coupling, this becomes important because the nuclear motion is restricted to only the lowest APES. This is not a problem in Jahn-Teller systems of lower groups, since extrema of these systems always occur on the lowest APES. In some icosahedral systems however, the APESs are sufficiently complicated for the upper sheets to exhibit extrema. In these cases, a full analysis of the all the APESs is required in order to be sure of which symmetry points of the lowest APES the extrema actually reside upon.

1.5 The Berry phase.

An adiabatic Hamiltonian does not change rapidly enough to induce transitions between the eigenstates. These eigenstates evolve independently of each other over the field of configuration parameters. However, if this evolution assumes a closed path or circuit, the phase acquired by the state on completion of the circuit may not be trivial. Herzberg and Longuet-Higgins [44] were the first to address this phenomenon in the context of molecular systems. Their analysis showed that conically self-intersecting potential surfaces demanded by symmetry, have a different topological character from a pair of distinct surfaces which happen to meet at a point. Indeed, if an adiabatic evolution of parameters around a circuit induces a sign change on the electronic state, one may conclude that somewhere within the circuit there must be a singular point at which the wave function is degenerate; that is to say, there must be a genuine conical intersection somewhere within the circuit. This non-trivial topology of molecular adiabatic potentials was recast in the form of the *Molecular Aharonov-Bohm effect* by Mead [64, 65]. In Mead's analysis, an effective vector potential must be inserted into the nuclear Born-Oppenheimer Hamiltonian whenever two or more electronic potential sheets experience a conical intersection. This arises from a proviso that the electronic wave function be single valued around a circuit enclosing the intersection.

These considerations are special cases of the more general "geometrical phase concept", introduced by Berry [9]. For the real symmetric matrices of a molecular system, the Berry phase factor is reduced to a simple sign change. As a consequence of this, Berry phase analyses for Jahn-Teller systems essentially follow a Mead approach [64, 65] as outlined above. Note that the Berry phase concept does not provide any new information appertaining to the Jahn-Teller system. However, as a mathematical artifice it is invaluable in analysing wave function continuity over complicated adiabatic potentials.

In the context of Jahn-Teller systems, the Berry phase refers to the sign change acquired by the electronic wave function, under adiabatic transport around a circuit in the space of Jahn-Teller active modes. Adiabatic transport in this case follows from the fact that the nuclear coordinates $\{Q\}$ vary slowly compared to the time scale for changes in the electronic coordinates $\{q\}$. Since the nuclei move slowly, the dynamical state of the electrons varies adiabatically with the gradual evolution of the nuclear configuration. The electronic states arising from a Jahn-Teller coupling may be obtained by limiting the Hamiltonian to the nuclear potential and Jahn-Teller interaction terms, treating the nuclear coodinates $\{Q\}$ as the parameters in the Hamiltonian. The Schrödinger equation governing the evolution of the total wave functions, $\Psi_n(t)$, may be

cast in the form

$$i\hbar\frac{\partial}{\partial t}\Psi_n(t) = H(q,Q(t))\ \Psi_n(t), \tag{1.15}$$

where the nuclear coordinates show a periodic behaviour, i.e. $Q(0) = Q(T)$, where T is the period of this motion. The instantaneous eigenfunctions $u_n(q,Q(t))$ are eigenfunctions of $H(q,Q(t))$ at each instant,

$$H(q,Q)\ u_n(q,Q) = E_n(Q)\ u_n(q,Q), \tag{1.16}$$

where Q is now treated as the parameter. In accordance with the Mead analysis [64, 65], the $u_n(q,Q)$ is constrained to be single-valued over the periodic Q-motion. For the purposes of this simple illustration, $u_n(q,Q)$ is also taken to be non-degenerate.

According to the adiabatic approximation, an electronic state $u_n(q,Q(0))$ at time $t = 0$ will evolve under the influence of H to a state $u_n(q,Q(t))$ at time t. The total eigenfunction $\Psi_n(t)$ may be written as

$$\Psi_n(t) = \exp\left(\frac{-i}{\hbar}\int_0^t dt' E_n(Q(t'))\right)\exp(i\gamma_n(t))\ u_n(q,Q(t))\psi_n(Q), \tag{1.17}$$

where $\psi_n(Q)$ is the solution to the nuclear Schrödinger equation, obtained by the adiabatic prescription discussed in Section (1.3). The first exponential is the familiar *dymanical* phase factor. In addition to this, the state acquires a *geometrical* phase factor $\exp(i\gamma_n(t))$, where γ_n is the Berry phase. The implications of this factor had been neglected by earlier authorities until Berry observed that it could be measured by allowing differently evolved wave functions to interfere [9].

Berry's original analysis recognized the "slow" variables $\{Q\}$ as being under experimental control, not themselves dynamical variables. Nevertheless, in molecular systems where the $\{Q\}$ are nuclear coodinates, the Berry phase manifests itself experimentally through its effect on the wave functions of the system. The Jahn-Teller effect couples the $\{Q\}$ and $\{q\}$ motions so that different parts of the total wave function Ψ_n change sign in a coordinated manner to preserve the overall cyclic single-valuedness of Ψ_n. In this way the Berry phase may be directly related to the degeneracy of the vibronic ground state [41].

An explicit expression for γ_n may be obtained by direct substitution of (1.17) into the Schrödinger equation (1.15). The adiabatic approximation simplifies the resulting differential equation leading to an expression for γ_n in terms of a line integral over the circuit C in $\{Q\}$ space:

$$\gamma_n = i\oint_C \langle n(Q)|\nabla_{\mathbf{Q}}|n(Q)\rangle \cdot d\mathbf{Q}, \tag{1.18}$$

where $|n\rangle$ is the abstract notation for the state $u_n(q,Q)$. Since the line integral is independent of how the circuit C is traversed, the *geometrical* nature of γ_n becomes evident in this expression.

For Jahn-Teller systems, the normalization of $|n\rangle$ ensures that γ_n will only take the values 0 or π. Thus the Berry phase factor in this case is

$$\begin{aligned} \exp(i\gamma_n(C)) &= -1, \text{ if } C \text{ encircles a degeneracy,} \\ &= +1, \text{ otherwise.} \end{aligned} \tag{1.19}$$

Direct evaluation of $|\nabla_{\mathbf{Q}} n(Q)\rangle$ requires a locally single-valued $|n\rangle$ which can be difficult to achieve. By an application of Stoke's theorem, Berry showed that the contour integral may be replaced by a surface integral, thereby relaxing the single-valuedness condition for systems in which the parameter space is three-dimensional or lower. $\gamma_n(C)$ then becomes

$$\gamma_n(C) = -\iint_S d\mathbf{S} \cdot \mathbf{V}_n(Q), \tag{1.20}$$

where

$$\mathbf{V}_n(Q) = \sum_{n \neq m} \frac{\langle n(Q)|\nabla_{\mathbf{Q}} H(q,Q)|m(Q)\rangle \times \langle m(Q)|\nabla_{\mathbf{Q}} H(q,Q)|n(Q)\rangle}{(E_m(Q) - E_n(Q))^2}. \tag{1.21}$$

This surface integral is evaluated over any surface bounded by the circuit C. The parameter spaces of icosahedral Jahn-Teller systems are at least four-dimensional; nevertheless, Equation (1.21) may still be applicable when the integration is restricted to the lower dimensional subspace of an APES.

The complexity of the APESs of some icosahedral Jahn-Teller systems, renders the derivation of a single-valued expression for $|n\rangle$ impossible. The lack of continuous symmetry in the minimum energy surfaces makes it necessary to introduce a method for numerically tracking phases (see Subsection (3.3.3)). In this way, the Berry phase proves to be a powerful tool in drawing conclusions about vibronic ground states of these systems without explicitly solving the complex motion on the minimum energy surface.

The above discussion assumes that the energies, $E_n(Q)$, are non-degenerate. A generalization of the Berry phase which includes the adiabatic evolution of degenerate states was due to Wilczek and Zee [92]. In this formulation the Berry phase γ is replaced by a matrix of dimension p, the order of the degeneracy. The off-diagonal terms of this matrix pertain to population variations between states in addition to phase changes in each of the state vectors. This formulation of Berry's phase is required to tackle the Kramer's degeneracy of spin-dependent Jahn-Teller systems [3]. However, the icosahedral systems presented in this thesis are spin-independent and therefore only require the non-degenerate formulation as described above.

1.6 Summary of Chapter 1.

A Jahn-Teller interaction is a complex coupling of nuclear and electronic motions which may be made tractable by the application of an adiabatic approximation. In Jahn-Teller systems, the variation of the electronic wave function over the field of distortion parameters becomes important, and a modification of the usual Born-Oppenheimer approximation is required. For strongly coupled systems, the adiabatic potential may then be interpreted as the potential energy of the nuclei in the field of the electrons.

Under the conditions of *equal coupling*, some linear Jahn-Teller systems exhibit a continuous symmetry which may be utilized to obtain a convenient group parentage for the discrete symmetries of single mode sub-systems. This parentage is used extensively in the later chapters of this thesis to provide parametrizations which aid in the analysis of the topography of the resulting APESs. The systems appearing in this thesis are all related to an $SO(4)$ parent symmetry and are parametrized and labelled accordingly.

The structure of the adiabatic potential in discrete systems is determined by the distribution of extrema which, according to the epikernel principle, prefer to reside at maximal epikernel symmetries. The epikernel principle provides a means of deducing the most likely directions in which a stabilization of the Jahn-Teller system occurs. The epikernel principle does not however, provide information pertaining to the natures of the extrema, nor does it specify the APES upon which these extrema may be found. Only an examination of the curvature at the extrema on the various APESs can provide information on these more specific details.

Adiabatic potentials of Jahn-Teller systems exhibit conical intersections at the high symmetry origin. In more complicated systems, conical intersections may also occur at other symmetry epikernels in the distortion parameter space. This complicated distribution of degeneracy points implies that adiabatic circuits tracked in parameter space are in general accompanied by geometrical phase changes. This geometrical phase or Berry phase proves to be a powerful tool in drawing conclusions about vibronic ground states of the Jahn-Teller system, without explicitly solving the complex motion on the minimum energy surface.

Chapter 2

Symmetry coupling in icosahedral systems.

2.1 The icosahedral group.

THE icosahedron and its face-vertex dual, the dodecahedron, are the most symmetric of the five platonic solids[1]. Consequently, the corresponding symmetry is the least *anisotropic*, whether *anisotropy* be defined by the maximum angular momentum that can be tolerated in a quantized state, or by the lowest order of a physical quantity with behaviour which distinguishes icosahedra and dodecahedra from spheres. Since the point groups of dual polyhedra must be identical, it follows that it is immaterial whether the group theory appertains to the icosahedron or the dodecahedron; the former is usually chosen for definiteness.

The icosahedron possesses twenty faces, each one an equilateral triangle. At every vertex five such triangles meet; this gives rise to six axes of five-fold symmetry, as can be seen from Figure 2.1. The character table of the icosahedral group I has been given by Butler [11] and is set out in Table (2.1). In this table the abbreviations $\mu = \frac{1}{2}(1+\sqrt{5})$ and $\nu = \frac{1}{2}(1-\sqrt{5})$ have been made. The elements in the classes C_1, C_2,...,C_5 correspond to rotations through angles 0, π, $\frac{2}{3}\pi$, $\frac{2}{5}\pi$ and $\frac{4}{5}\pi$ respectively.

The general method for determining how a J level of $SO(3)$ splits under the action of a crystal field of any point symmetry may be found in any standard group theory text [51, 27]. The procedure consists of finding values of the characters $\chi^J(\alpha) = \sin\frac{1}{2}(2J+1)\alpha / \sin\frac{1}{2}\alpha$ for the angles of rotation α associated with each of the classes, and then decomposing the sequence of numbers into combinations of the numbers given in the character table. As an example, for the

[1]The five platonic solids are the tetrahedron, the cube, the octahedron, the dodecahedron and the icosahedron.

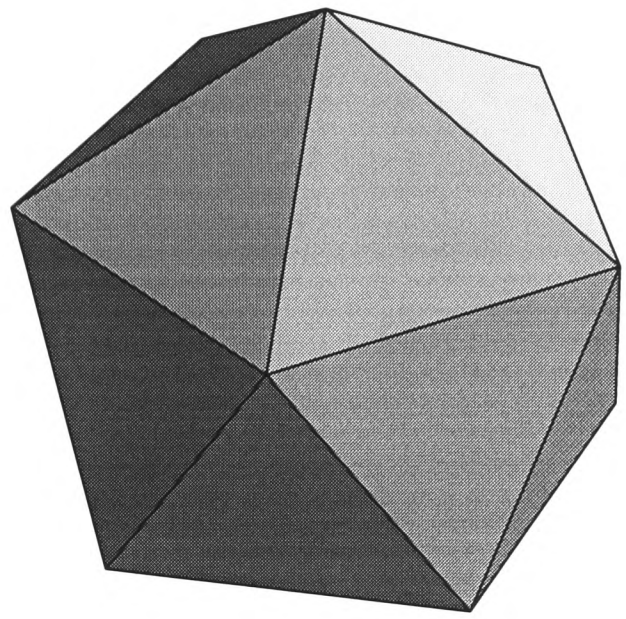

Figure 2.1: The icosahedron.

	C_1	C_2	C_3	C_4	C_5
A	1	1	1	1	1
T_1	3	-1	0	μ	ν
T_2	3	-1	0	ν	μ
G	4	0	1	-1	-1
H	5	1	-1	0	0

Table 2.1: Character table for I.

	C_1	C_1'	C_2	C_3	C_3'	C_4	C_4'	C_5	C_5'
A	1	1	1	1	1	1	1	1	1
T_1	3	3	-1	0	0	μ	μ	ν	ν
T_2	3	3	-1	0	0	ν	ν	μ	μ
G	4	4	0	1	1	-1	-1	-1	-1
H	5	5	1	-1	-1	0	0	0	0
Γ_6	2	-2	0	1	-1	μ	$-\mu$	$-\nu$	ν
Γ_7	2	-2	0	1	-1	ν	$-\nu$	$-\mu$	μ
Γ_8	4	-4	0	-1	1	1	-1	-1	-1
Γ_9	6	-6	0	0	0	-1	1	1	-1

Table 2.2: Character table for I'. The rotations associated with C_i' differ by 2π from those associated with C_i.

level $J = 4$ the characters are 9, 1, 0, -1, -1; and since this sequence can be obtained by selecting the combination $G \oplus H$, a level for which $J = 4$ will split under an icosahedral field into sub-levels corresponding to the two irreps G and H. This process is essentially the reduction of SO(3) into the irreps of I.

Levels possessing half-odd integral values of J may be split as above, into the irreps of the icosahedral double group (I') [8]. The character table for I' is given in Table (2.2). The $SO(3) \supset I$ reduction is set out in Table (2.3). for $J \leq 8$.

The icosahedral group is not "simply reducible" in the Wigner sense [94], and in this way differs fundamentally from the point groups of the other platonic solids. Essentially there are two criteria to be satisfied for the qualification "simply reducible"; these are:

(i) The symmetry elements of the group must belong to ambivalent classes, i.e. classes containing an element and its reciprocal.

(ii) The Kronecker square of any irrep does not contain any irrep more than once. N.B. This sort of multiplicity is referred to as a Kronecker multiplicity (see Table (2.4)) in contradistiction to the Reduction multiplicity appearing in the field splitting of J levels (see Table (2.3)).

The appearance of $2G$ and $2H$ irreps in the Kronecker square $H \oslash H$, means that I fails to meet the second of the two criteria and is therefore not simply reducible. The significance of criterion (ii) for simply reducible groups becomes evident if one reduces the Kronecker square of

J		J	
0	A	1/2	Γ_6
1	T_1	3/2	Γ_8
2	H	5/2	Γ_9
3	$T_2 \oplus G$	7/2	$\Gamma_7 \oplus \Gamma_9$
4	$G \oplus H$	9/2	$\Gamma_8 \oplus \Gamma_9$
5	$T_1 \oplus T_2 \oplus H$	11/2	$\Gamma_6 \oplus \Gamma_8 \oplus \Gamma_9$
6	$A \oplus T_1 \oplus G \oplus H$	13/2	$\Gamma_6 \oplus \Gamma_7 \oplus \Gamma_8 \oplus \Gamma_9$
7	$T_1 \oplus T_2 \oplus G \oplus H$	15/2	$\Gamma_8 \oplus 2\Gamma_9$
8	$T_2 \oplus G \oplus 2H$		

Table 2.3: $SO(3) \supset I$ reduction.

an irrep, i.e. transform it into a form in which it appears as a direct sum of irreps as shown in Table (2.4) for I. The elements of the matrix by which this transformation is carried out are the Clebsch-Gordan coefficients (C-G coefficients). These coefficients in the case of simply reducible groups are uniquely determined apart from a phase factor. For I this is not the case and the C-G coefficients are not unique. A convenient set of C-G coefficients for I may be realized by utilizing the symmetry descent $SO(3) \supset I$ (Table (2.3)), which facilitates a labelling of Kronecker multiplicities according to $SO(3)$ irrep labels. The coupling theory for I has been comprehensively studied using the symmetry descent method and the corresponding C-G coefficients are readily available in tabular form [81, 34]. The high dimensionality of the irreps and the numerous possible operators which act within the corresponding manifolds, makes a calculation of I coupling coefficients particularly laborious. In the following, a computational method is adopted which is very fast and easily implemented, and avoids what would otherwise be a laborious inspection of tables.

2.2 Icosahedral irreducible tensors.

2.2.1 General principles.

The generation of icosahedral tensors presented here, essentially follows the symmetry descent used by Golding and others [81, 34] to obtain icosahedral coupling coefficients. Analyses of Jahn-Teller systems require the construction of irreducible bases for the representation of electronic

Irrep.			Product with	
	T_1	T_2	G	H
A	T_1	T_2	G	H
T_1	$[A \oplus H]_S \oplus \{T_1\}_A$	$G \oplus H$	$T_2 \oplus G \oplus H$	$T_1 \oplus T_2 \oplus G \oplus H$
T_2		$[A \oplus H]_S \oplus \{T_2\}_A$	$T_1 \oplus G \oplus H$	$T_1 \oplus T_2 \oplus G \oplus H$
G			$[A \oplus G \oplus H]_S \oplus \{T_1 \oplus T_2\}_A$	$T_1 \oplus T_2 \oplus G \oplus 2H$
H				$[A \oplus G \oplus 2H]_S$ $\oplus\{T_1 \oplus T_2 \oplus G\}_A$

Table 2.4: The Kronecker products for the icosahedral single group.

states and Jahn-Teller active modes. The general method for finding bases for the different irreps of I is to construct them in terms of angular momentum eigenstates by diagonalizing an operator of icosahedral symmetry. All the necessary information for the construction of such an operator is given by Judd [49]. A suitable Cartesian tensor of icosahedral symmetry, with a five-fold axis of the icosahedron along Oz, is

$$V_{icos} = 231z^6 - 315r^2z^4 + 105r^4z^2 - 5r^6 + 42z(x^5 - 10x^3y^2 + 5xy^4). \tag{2.1}$$

Diagonalization of V_{icos} within a level J, yields linear combinations of angular momentum bases $\{|JM\rangle\}$ transforming according to the γ^{th} partner of the Γ irrep of I, resulting in a state basis of the form

$$|J\Gamma\gamma\rangle = \sum_M C(JM\Gamma\gamma)|JM\rangle, \tag{2.2}$$

where the C coefficients depend on J, M, Γ and γ, and are in general complex.

Operators transforming according to the Λ irrep of I may be constructed as linear combinations of spherical tensors Y^J_M yielding an operator basis

$$\mathcal{O}^{J\Lambda}_\lambda = \sum_M C(JM\Lambda\lambda)\, Y^J_M. \tag{2.3}$$

The transformation properties of the operator basis may be demonstrated by making a transformation $R \in I$ of the basis. For $R \in I$

$$\begin{aligned}
\exists \mathcal{O}_R: \quad \Lambda \quad &\rightarrow \Lambda \; \forall R \in I \Rightarrow \qquad (2.4)\\
\mathcal{O}_R \mathcal{O}^{J\Lambda}_{\lambda_i} \quad &= \quad \sum_{j=1}^{|\Lambda|} D^\Lambda_{ij}(R)\; \mathcal{O}^{J\Lambda}_{\lambda_j} = \sum_j \sum_M D^\Lambda_{ij}(R) C(JM\Lambda\lambda_j)\; Y^J_M \\
&= \quad \sum_M (\sum_j D^\Lambda_{ij}(R)\; C(JM\Lambda\lambda_j))\; Y^J_M = \sum_M C'(JM\Lambda\lambda_i)\; Y^J_M \\
&= \quad \mathcal{O}'^{J\Lambda}_{\lambda_i},
\end{aligned}$$

where $D^{\Lambda}_{ij}(R)$ is the (i,j) element of the matrix representation of $\mathcal{O}_R$ in Λ. The new primed basis $\{\mathcal{O}'^{J\Lambda}\}$ may therefore be obtained by finding the coefficients $C'(JM\Lambda\lambda_i)$ given by

$$C'(JM\Lambda\lambda_i) = \sum_{j=1}^{|\Lambda|} D^{\Lambda}_{ij}(R)\, C(JM\Lambda\lambda_j). \tag{2.5}$$

A similar expression connected with the transformation properties of the bases $\{|J\Gamma\rangle\}$ may be obtained by examinining the effect of $\mathcal{O}_R$ on Equation (2.2), yielding an expression which is identical to Equation (2.5) except that the (Λ,λ) are replaced by (Γ,γ).

Since these state bases and operators are required to represent a Jahn-Teller interaction in an orbital degeneracy, the irrep Λ is restricted to the symmetric square $[\Gamma\otimes\Gamma]_S$ and the C coefficients are chosen so that the state bases and operators are real. Therefore the resulting matrix representations of these operators acting within the Γ electronic manifold will be symmetric and real. A general matrix element of a partner $\mathcal{O}^{J'\Lambda}_{\lambda}$ of the operator basis within the $\{|J\Gamma\rangle\}$ state is then

$$\begin{aligned}\langle J\Gamma\gamma_i|\mathcal{O}^{J'\Lambda}_{\lambda}|J\Gamma\gamma_j\rangle &= \sum_{M,M',M''} C^*(JM\Gamma\gamma_i)C(J'M'\Lambda\lambda)C(JM''\Gamma\gamma_j)\,\langle JM|Y^{J'}_{M'}|JM''\rangle, \\ &= \sum_{M,M',M''} C^*(JM\Gamma\gamma_i)C(J'M'\Lambda\lambda)C(JM''\Gamma\gamma_j) \\ &\quad\times(-1)^{J-M}(J||Y^{J'}||J)\begin{pmatrix} J & J' & J \\ -M & M' & M''\end{pmatrix},\end{aligned} \tag{2.6}$$

where the $*$ denotes complex conjugation, $\begin{pmatrix} J & J' & J'' \\ M & M' & M''\end{pmatrix}$ is a standard $3{-}j$ symbol given by the Racah formula [85]

$$\begin{aligned}\begin{pmatrix} J & J' & J'' \\ M & M' & M''\end{pmatrix} &= (-1)^{J+J'-M''}\sqrt{(J+J'-J'')!(J-J'+J'')!(-J+J'+J'')!} \\ &\quad\times\sqrt{\frac{(J+M)!(J-M)!(J'+M')!(J'-M')!(J''+M'')!(J''-M'')!}{(J+J'+J''+1)!}} \\ &\quad\times\sum_k \frac{(-1)^k}{k!(J+J'-J''-k)!(J-M-k)!(J'+M'-k)!(J''-J'+M+k)!(J''-J-M'+k)!}.\end{aligned} \tag{2.7}$$

and $(J||Y^{J'}||J)$ is the reduced matrix element given by

$$(J||Y^{J'}||J) = (-1)^J\left[\frac{(2J+1)(2J'+1)(2J+1)}{4\pi}\right]^{1/2}\begin{pmatrix} J & J' & J \\ 0 & 0 & 0\end{pmatrix}. \tag{2.8}$$

The second expression in (2.6) is obtained by use of the expression for Gaunt coefficients [33] in reference [85]. The reduced matrix element, $(J||Y^{J'}||J)$, in (2.6) may be absorbed into a

multiplicative factor which represents the strength of the interaction pertaining to the operators $\{\mathcal{O}^{J'\Lambda}\}$. This is essentially the Wigner-Eckart theorem [51] which effectively factorizes the matrix element into a symmetry coefficient and a factor which embodies the strength of the interaction. The strength of the interaction may be introduced later as a coupling constant and any multiplicative factors which may arise may be absorbed into this effective coupling when these operators assume the rôle of observables. Note however, that care must be taken in determining whether or not the reduced matrix element is zero within a given triple (J, J', J), because this determines whether or not the matrix element in (2.6) is identically zero. The $3-j$ symbol within the reduced matrix element $\begin{pmatrix} J & J' & J \\ 0 & 0 & 0 \end{pmatrix}$ is non-zero only if $J + J' + J$ is even, and therefore the matrix element in (2.6) is only non-zero if the value J' is even, where J' labels the level from which the operator basis is derived. The operator basis may therefore be derived from any J level as long as J is even. However, it may be necessary to derive Λ from different even J levels if the operators are required to act within a manifold containing a multiplicity of Λ irreps. In this case, the convention is to derive the first Λ irrep from the lowest even J level which can tolerate Λ, and any subsequent Λ irreps from the next highest even J levels. The choice of J level from which the $\{|\Gamma\rangle\}$ bases are derived is essentially arbitrary. For definiteness, it is conventional to derive the $\{|\Gamma\rangle\}$ bases from the lowest J-level that can support a Γ irrep.

In view of the above considerations, the coupling coefficients defined in Equation (2.6) will be denoted hence forth by the symbol $(\Gamma\gamma_j; J'\Lambda\lambda|\Gamma\gamma_i)$ and standardised by requiring that they obey the orthonormality relation

$$\sum_{ij} (\Gamma\gamma_j; J'\Lambda\lambda|\Gamma\gamma_i)\,(\Gamma\gamma_j; J''\Lambda'\lambda'|\Gamma\gamma_i) = \delta_{J'J''}\delta_{\Lambda\Lambda'}\delta_{\lambda\lambda'}. \tag{2.9}$$

Note that the label J has been dropped from these symbols, since in accordance with convention, the $\{|\Gamma\rangle\}$ are always derived from the lowest J level which can tolerate a Γ irrep. The J' and J'' labels remain in place however, since they may be used to distinguish between a multiplicity of Λ irreps should more than one Λ irrep appear in $[\Gamma \otimes \Gamma]_S$. In the following, for cases where there is no such Kronecker multiplicity of Λ irreps, the J' and J'' labels are also dropped since in these cases the $\{|\Gamma\rangle\}$ bases will be unable to distinguish (except maybe in the overall sign of the symbols) between Λ irreps derived from different J' levels.

The symbols defined in Equation (2.9) exhibit two useful symmetries under exchange of indices within the symbol. Firstly, the symbol $(\Gamma\gamma_j; \Lambda\lambda|\Gamma\gamma_i)$ is clearly symmetric under the exchange of i and j, which is a consequence of the symmetrized nature of Λ. Secondly, the symbol $(\Gamma\gamma_j; \Lambda\lambda|\Gamma\gamma_i)$ is invariant under an interchange of the first two index entries $\Gamma\gamma_j$ and $\Lambda\lambda$,

which is a consequence of the property of the matrix elements defined by Equation (2.6):

$$\begin{aligned}\langle J\Gamma\gamma_i|\mathcal{O}^{J\Gamma}_{\gamma_i}|J'\Lambda\lambda\rangle &= \sum_{M,M',M''} C^*(JM\Gamma\gamma_i)C(JM'\Gamma\gamma_j)C(J'M''\Lambda\lambda) \\ &\quad \times(-1)^{J-M}(J||Y^J||J')\begin{pmatrix} J & J & J' \\ -M & M' & M'' \end{pmatrix} \\ &= \langle J\Gamma\gamma_i|\mathcal{O}^{J'\Lambda}_{\lambda}|J\Gamma\gamma_j\rangle,\end{aligned} \tag{2.10}$$

by the symmetry of the $3-j$ symbols under exchange of columns when $J+J'+J$ is even. These two exchange symmetries may be summarized as follows:

$$(\Gamma\gamma_j;\Lambda\lambda|\Gamma\gamma_i) = (\Gamma\gamma_i;\Lambda\lambda|\Gamma\gamma_j) \tag{2.11}$$

$$\text{and} \quad (\Gamma\gamma_j;\Lambda\lambda|\Gamma\gamma_i) = (\Lambda\lambda;\Gamma\gamma_j|\Gamma\gamma_i).$$

The two electronic manifolds which figure in this thesis, transform as the G and H irreps of I. By selection rule criteria for matrix elements (see Subsections 1.4.1, 1.4.2), the operators acting within a Γ manifold may be constructed belonging to the irreps in $\Gamma\otimes\Gamma$. An inspection of Table (2.4), reveals the symmetry properties of the possible operators which act within the G and H manifolds:

$$G\otimes G = [A\oplus G\oplus H]_S\oplus\{T_1\oplus T_2\}_A \text{ within the } G \text{ manifold,} \tag{2.12}$$

$$H\otimes H = [A\oplus G\oplus 2H]_S\oplus\{T_1\oplus T_2\oplus G\}_A \text{ within the } H \text{ manifold.} \tag{2.13}$$

2.2.2 Within the G manifold.

In accordance with the convention for the electronic bases (see Subsection (2.2.1)), the G irrep first appears in the splitting of the $J=3$ level (see Table (2.3)) and therefore the C coefficients for the G basis are obtained by the diagonalization of V_{icos} (Equation (2.1)) within $J=3$. V_{icos} within $J=3$ is a 7×7 square matrix and under normal circumstances the diagonalization of this matrix would involve laborious algebra. However, a routine written in *Mathematica* easily performs the diagonalization, the output of which is in a very convenient matrix form. The output for the C coefficients of a G basis, derived from $J=3$ is given in Table (2.5) and will be denoted $\hat{\mathrm{C}}^3_G$, where the partners $\{\alpha,\beta,\gamma,\delta\}$ transform under I as the Cartesian tensors

$$\begin{aligned}|G\alpha\rangle &= (3x^2y-y^2)+2(zy^2-zx^2), \\ |G\beta\rangle &= x^3-3xy^2-4xyz, \\ |G\gamma\rangle &= (x^2+y^2-4z^2)y, \\ |G\delta\rangle &= (x^2+y^2-4z^2)x.\end{aligned} \tag{2.14}$$

The array element (using a clearer notation) $\mathrm{C}^3_G[[a,M]] \equiv C(3MGa)$ for $a \in \{\alpha,\beta,\gamma,\delta\}$ and $M = -3,-2,-1,0,1,2,3$.

	$\|3-3\rangle$	$\|3-2\rangle$	$\|3-1\rangle$	$\|30\rangle$	$\|31\rangle$	$\|32\rangle$	$\|33\rangle$
$\langle G\alpha\|$	$\sqrt{\frac{3}{10}}$	$\frac{-i}{\sqrt{5}}$	0	0	0	$\frac{-i}{\sqrt{5}}$	$\sqrt{\frac{3}{10}}$
$\langle G\beta\|$	$i\sqrt{\frac{3}{10}}$	$\frac{-1}{\sqrt{5}}$	0	0	0	$\frac{1}{\sqrt{5}}$	$-i\sqrt{\frac{3}{10}}$
$\langle G\gamma\|$	0	0	$\frac{1}{\sqrt{2}}$	0	$\frac{1}{\sqrt{2}}$	0	0
$\langle G\delta\|$	0	0	$\frac{-i}{\sqrt{2}}$	0	$\frac{i}{\sqrt{2}}$	0	0

Table 2.5: $\hat{\mathrm{C}}^3_G$.

The Jahn-Teller operator basis acting within the G manifold may be derived in a similar fashion. From Equation (2.12), the operators corresponding to Jahn-Teller active modes transform as G and H. Since the operator basis must be derived from an even J level for a non-zero reduced matrix element, the lowest J level that the G-mode may be derived from is $J = 4$ (see Table 2.3.). The H-mode may also be derived from $J = 4$ and so diagonalizing V_{icos} within $J = 4$ yields all the necessary C coefficients to construct G and H Jahn-Teller modes. The resulting matrix of C coefficients is given in Table (2.6). and will be denoted $\hat{\mathrm{C}}^4_{G\oplus H}$. The transformation

	$\|4-4\rangle$	$\|4-3\rangle$	$\|4-2\rangle$	$\|4-1\rangle$	$\|40\rangle$	$\|41\rangle$	$\|42\rangle$	$\|43\rangle$	$\|44\rangle$
$\langle G\alpha\|$	0	$\frac{-1}{\sqrt{30}}$	$-i\sqrt{\frac{7}{15}}$	0	0	0	$i\sqrt{\frac{7}{15}}$	$\frac{1}{\sqrt{30}}$	0
$\langle G\beta\|$	0	$\frac{-i}{\sqrt{30}}$	$-\sqrt{\frac{7}{15}}$	0	0	0	$-\sqrt{\frac{7}{15}}$	$\frac{-i}{\sqrt{30}}$	0
$\langle G\gamma\|$	$\frac{2i}{\sqrt{15}}$	0	0	$-\sqrt{\frac{7}{30}}$	0	$\sqrt{\frac{7}{30}}$	0	0	$\frac{-2i}{\sqrt{15}}$
$\langle G\delta\|$	$\frac{-2}{\sqrt{15}}$	0	0	$i\sqrt{\frac{7}{30}}$	0	$i\sqrt{\frac{7}{30}}$	0	0	$\frac{-2}{\sqrt{15}}$
$\langle H\theta\|$	0	0	0	0	-1	0	0	0	0
$\langle H\epsilon\|$	0	$i\sqrt{\frac{7}{15}}$	$\frac{-1}{\sqrt{30}}$	0	0	0	$\frac{-1}{\sqrt{30}}$	$i\sqrt{\frac{7}{15}}$	0
$\langle Hx\|$	$\sqrt{\frac{7}{30}}$	0	0	$\frac{2i}{\sqrt{15}}$	0	$\frac{2i}{\sqrt{15}}$	0	0	$\sqrt{\frac{7}{30}}$
$\langle Hy\|$	$i\sqrt{\frac{7}{30}}$	0	0	$\frac{2}{\sqrt{15}}$	0	$\frac{-2}{\sqrt{15}}$	0	0	$-i\sqrt{\frac{7}{30}}$
$\langle Hz\|$	0	$\sqrt{\frac{7}{15}}$	$\frac{-i}{\sqrt{30}}$	0	0	0	$\frac{i}{\sqrt{30}}$	$-\sqrt{\frac{7}{15}}$	0

Table 2.6: $\hat{\mathrm{C}}^4_{G\oplus H}$.

properties of these G bases exactly correspond to those given in Equations (2.14). The transformation properties in terms of cartesians for the partners of H may be most easily derived from $J = 2$ (see Table 2.3.), these are

$$|H\theta\rangle \;=\; 2z^2 - x^2 - y^2, \tag{2.15}$$

where the $\{a\} \in \Re$ are the arbitrary components, and without loss of generality the $|G\rangle$ vector may be normalized such that

$$a_\alpha^2 + a_\beta^2 + a_\gamma^2 + a_\delta^2 = 1, \tag{2.19}$$

then the quadratic forms

$$\begin{aligned} \mathcal{Q}^G_{\Lambda\lambda} &= \sum_{ij} (G\ j; \Lambda\lambda | G\ i)\ a_i a_j, \\ &\quad (i,j) \in \{\alpha, \beta, \gamma, \delta\}, \\ &\quad \Lambda = G, H \text{ and } \lambda \text{ is the partner label,} \end{aligned} \tag{2.20}$$

may be seen to form a basis for the $G \oplus H$ representation of I and therefore provide a set of "coupling rules" for the coupling of $|G\rangle$ vector components to form components of G and H tensors. The coupling of $|H\rangle$ vector components to form components of G and H tensors is dealt with in the next Subsection (Within the H manifold). To show that the $\{\mathcal{Q}^G\}$ form a basis for $G \oplus H$, it is necessary to consider the transformation properties of the $\{\mathcal{Q}^G\}$ under an arbitrary rotation $R \in I$ defined in Equation (2.4) with $\Lambda = G$ or H. Under such a rotation of the Jahn-Teller active modes, the $\{\mathcal{Q}^G\}$ transform as follows

$$\begin{aligned} \mathcal{O}_R \mathcal{Q}^G_{\Lambda\lambda} &= \sum_{\lambda'}^{|\Lambda|} \sum_{ij} D^\Lambda_{\lambda\lambda'}(R) (G\ j; \Lambda\lambda' | G\ i)\ a_i a_j \\ &= \frac{1}{N} \sum_{i,j} a_i a_j \sum_{M,M',M"} (C^3_G[[i,M]])^* C^3_G[[j,M']] \sum_{\lambda'}^{|\Lambda|} D^\Lambda_{\lambda\lambda'}(R) C^4_\Lambda[[\lambda', M']] \\ &\qquad \times (-1)^{3-M} (3||Y^4||3) \begin{pmatrix} 3 & 4 & 3 \\ -M & M' & M'' \end{pmatrix} \\ &= \frac{1}{N} \sum_{i,j} a_i a_j \sum_{M,M',M"} (C^3_G[[i,M]])^* C^3_G[[j,M']] C'^4_\Lambda[[\lambda, M']] \\ &\qquad \times (-1)^{3-M} (3||Y^4||3) \begin{pmatrix} 3 & 4 & 3 \\ -M & M' & M'' \end{pmatrix} \\ &= \sum_{ij} (G\ j; \Lambda\lambda | G\ i)'\ a_i a_j \\ &= \mathcal{Q}'^G_{\Lambda\lambda}, \end{aligned} \tag{2.21}$$

which are exactly the transformation properties of the λ^{th} partner of the irrep $\Lambda(= G, H)$ under an arbitrary rotation $R \in I$. The second expression in (2.21) is obtained by applying Equation (2.16) for general $\Lambda(= G, H)$ with N a normalization constant such that $N(G\ j; \Lambda\lambda | G\ i) = \langle 3Gi | \mathcal{O}^{4\Lambda}_\lambda | 3Gj \rangle$. The third expression in (2.21) is obtained with the use of Equation (2.5) for $\Gamma = G$ and $\Lambda = G, H$. The explicit forms of these $\{\mathcal{Q}^G\}$ are given in Appendix (A.2).

As well as the Jahn-Teller active operators G and H, there are also T_1 and T_2 operators which act within the G electronic manifold (see Equation (2.12)). However, only the T_1 operators figure in this thesis (see Chapter 6) as they transform as the three components of orbital angular momentum $\mathbf{L}$ ($L_x \sim |T_1 x\rangle, L_y \sim |T_1 y\rangle, L_z \sim |T_1 z\rangle$) which is itself derived from the level $J = 1$. Diagonalization of V_{icos} within $J = 1$ yields the matrix of C coefficients given in Table (2.7).

	$\|1-1\rangle$	$\|10\rangle$	$\|11\rangle$
$\langle T_1 x\|$	$\frac{1}{\sqrt{2}}$	0	$\frac{-1}{\sqrt{2}}$
$\langle T_1 y\|$	$\frac{i}{\sqrt{2}}$	0	$\frac{i}{\sqrt{2}}$
$\langle T_1 z\|$	0	1	0

Table 2.7: $\hat{\mathrm{C}}^1_{T_1}$

A subtlety relating to the matrix representation of these T_1 operators should be remarked at this point. Since the components of orbital angular momentum transform as $J = 1$, Equation (2.6) cannot be used to calculate the matrix elements of these operators because the correponding reduced matrix element vanishes (the J label of the operator basis is odd). However, $\mathbf{L}$ is a pseudovector ($\mathbf{L} = \mathbf{r} \times \mathbf{p}$) and is therefore constructed according to a different rule to that of (2.6). Following the formulation of matrix elements of tensor operators in reference [85], the matrix elements of the components L_1, L_0, L_{-1} of $\mathbf{L}$ within the $|JM\rangle$ bases are then

$$\langle JM|L_\mu|J'M'\rangle = (-1)^{J-M}\,[J(J+1)(2J+1)]^{1/2} \begin{pmatrix} J & 1 & J' \\ -M & \mu & M' \end{pmatrix} \delta_{JJ'}. \tag{2.22}$$

The matrix elements of the T_1 operators obtained by the use of Equation (2.22) are found to be

$$\begin{aligned} \langle 3Gi|L_k|3Gj\rangle \;=\; & 2\sqrt{21} \sum_{M,M',M''} (C^3_G[[i,M]])^* C^1_{T_1}[[k,M']] C^3_G[[j,M'']] \\ & \times(-1)^{3-M} \begin{pmatrix} 3 & 1 & 3 \\ -M & M' & M'' \end{pmatrix}, \end{aligned} \tag{2.23}$$

where $k \in \{x, y, z\}$. A set of suitable operators acting within the G manifold and carrying the essential symmetry properties of the components of $\mathbf{L}$ is then

$$L_x = \begin{pmatrix} 0 & 0 & i & 0 \\ 0 & 0 & 0 & i \\ -i & 0 & 0 & 0 \\ 0 & -i & 0 & 0 \end{pmatrix}, \quad L_y = \begin{pmatrix} 0 & 0 & 0 & i \\ 0 & 0 & -i & 0 \\ 0 & i & 0 & 0 \\ -i & 0 & 0 & 0 \end{pmatrix}, \quad L_z = \begin{pmatrix} 0 & -i & 0 & 0 \\ i & 0 & 0 & 0 \\ 0 & 0 & 0 & i \\ 0 & 0 & -i & 0 \end{pmatrix}. \tag{2.24}$$

2.2.3 Within the H manifold.

The Jahn-Teller active modes within an H manifold may be constructed according to the symmetries contained within $[H \otimes H]_S$. The Kronecker multiplicity of two H irreps in $[H \otimes H]_S$, presents an added complication to these considerations. The symmetry descent method resolves this complication by deriving each of the two H irreps from different J levels, thereby obtaining two linearly independent H bases which may be used to construct any H basis within the subspace $H \oplus H$ of the H manifold. The C coefficients for one possible H operator basis are derived in the previous Subsection (see Table (2.6)) from the level $J = 4$. The second H operator basis may be derived from the level $J = 2$. Diagonalization of V_{icos} in $J = 2$ yields the C coefficient matrix $\hat{C}^2_H$ given in Table (2.8). Since the lowest J level that can support an H irrep is $J = 2$, by convention the H electronic basis is also derived from $J = 2$ (see Subsection (2.2.1)). The C coefficients for H from $J = 2$ are chosen in accordance with the transformation properties given in Equations (2.15). As before, the G operator basis must be derived from an even J level and

	$\|2-2\rangle$	$\|2-1\rangle$	$\|20\rangle$	$\|21\rangle$	$\|22\rangle$
$\langle H\theta\|$	0	0	-1	0	0
$\langle H\epsilon\|$	$\frac{-1}{\sqrt{2}}$	0	0	0	$\frac{-1}{\sqrt{2}}$
$\langle Hx\|$	0	$\frac{-i}{\sqrt{2}}$	0	$\frac{-i}{\sqrt{2}}$	0
$\langle Hy\|$	0	$\frac{-1}{\sqrt{2}}$	0	$\frac{1}{\sqrt{2}}$	0
$\langle Hz\|$	$\frac{-i}{\sqrt{2}}$	0	0	0	$\frac{i}{\sqrt{2}}$

Table 2.8: $\hat{C}^2_H$

this is conveniently given in Table (2.6) from $J = 4$.

A matrix representation of the Jahn-Teller active operators in the H manifold may now be constructed and the coupling symbols $(H\ j; G\ k|H\ i)$, $(H\ j; 2H\ l|H\ i)$ and $(H\ j; 4H\ l|H\ i)$, where $k \in \{\alpha, \beta, \gamma, \delta\}$ and $l \in \{\theta, \epsilon, x, y, z\}$, are the resulting normalized matrix elements which obey the orthonormality relation (see Equation (2.9).)

$$\sum_{i,j}(H\ j; \Lambda\lambda|H\ i)(H\ j; \Lambda'\lambda'|H\ i) = \delta_{\Lambda\Lambda'}\delta_{\lambda\lambda'}, \tag{2.25}$$

where $\Lambda, \Lambda' = G, 2H$ and $4H$ and $\lambda\lambda'$ are partner labels. The normalized matrix representations computed with Equations (2.6), (2.7) and (2.9) for G, $2H$ and $4H$ operators within $\{|H\rangle\}$ are given in Appendix (A.3).

By applying the procedures in the previous subsection, the "coupling rules" for the coupling of $|H\rangle$ vector components to form components of G, $2H$ and $4H$ tensors are found to be embodied

in the quadratic forms

$$\begin{aligned} \mathcal{Q}^H_{\Lambda\lambda} &= \sum_{ij}(H\ j;\Lambda\lambda|H\ i)\ a_i a_j, \\ & (i,j) \in \{\theta,\epsilon,x,y,z\}, \\ & \Lambda = G, 2H \text{ and } 4H \text{ and } \lambda \text{ is the partner label,} \end{aligned} \tag{2.26}$$

where these $\{a\} \in \Re$ are the arbitrary components of an $|H\rangle$ vector, and without loss of generality the $|H\rangle$ vector may be normalized such that

$$a_\theta^2 + a_\epsilon^2 + a_x^2 + a_y^2 + a_z^2 = 1. \tag{2.27}$$

The explicit forms of these $\{\mathcal{Q}^H\}$ are given in Appendix (A.4). The transformation properties of these quadratic forms may be examined by applying a similar procedure to that outlined in (2.21). The $\{\mathcal{Q}^H\}$ provide a basis for the icosahedral representation $G \oplus H \oplus H$.

2.2.4 Icosahedral invariants.

A preliminary study of icosahedral invariant quantities proves invaluable in the various analyses presented in this thesis. The invariants which arise from these analyses, are constructed from normal mode coordinates and are therefore obtained by the repeated application of "coupling rules" for the construction of *symmetric squares*. Coupling rules such as these are derived in the previous two subsections and are used extensively here. Invariants arising from the study of Jahn-Teller instability in a G manifold, are quadratic, cubic and quartic in the normal mode coordinates. The explicit expressions for the quartic invariants are too long for the main body of the thesis and are given in the appendices. The sets of normal modes which figure in this thesis transform according to the irreps G and H and the invariants constructed from these normal modes are termed quartet and quintet invariants respectively. Due to this distinction, these two types of invariant are treated separately. For clarity, a common notation will be used throughout. In the following, the construction of a symmetric quadratic form transforming according to an irrep $\Lambda \neq A$ from the components of a Γ tensor is denoted by the symbol $(\Gamma \times \Gamma)_\Lambda$. The scalar convolution of a tensor Γ with itself is denoted by $(\Gamma \cdot \Gamma)_A$.

- **Construction of quartet invariants.**

The G quartet of normal modes $\{q_\alpha, q_\beta, q_\gamma, q_\delta\}$ has transformation properties identical to those of the Cartesian tensors in Equations (2.14). The possible icosahedral invariants which may be constructed from $\{q_\alpha, q_\beta, q_\gamma, q_\delta\}$ may be determined by considering the symmetric square $[G \otimes G]_S = A \oplus G \oplus H$ (see (2.12)). There is only one trivial quadratic invariant constructed by

the scalar convolution $(G \cdot G)_A$, where

$$(G \cdot G)_A = q_\alpha^2 + q_\beta^2 + q_\gamma^2 + q_\delta^2. \tag{2.28}$$

Also there is only one cubic invariant constructed according to $((G \times G)_G \cdot G)_A$. By using the coupling rules for the quadratic forms $(G \times G)_G$ in Appendix (A.2), $((G \times G)_G \cdot G)_A$ may be shown to have the explicit form (without loss of generality, a common factor throughout the invariant is omitted).

$$\begin{aligned} ((G \times G)_G \cdot G)_A &= \sum_{ijk} (G\ j; G\ k | G\ i) q_i q_j q_k \quad \text{with } i,j,k \in \{\alpha,\beta,\gamma,\delta\} \\ &= -q_\alpha^2 q_\delta + q_\beta^2 q_\delta - q_\beta q_\delta^2 - 2q_\alpha q_\beta q_\gamma - 2q_\alpha q_\delta q_\gamma + q_\beta q_\gamma^2. \end{aligned} \tag{2.29}$$

There are five coupling rules which yield invariants quartic in the $\{q_\alpha, q_\beta, q_\gamma, q_\delta\}$. These are

$$\begin{gathered} ((G \times G)_G \cdot (G \times G)_G)_A, \\ (((G \times G)_G \times G)_G \cdot G)_A, \\ ((G \times G)_H \cdot (G \times G)_H)_A, \\ (((G \times G)_H \times G)_G \cdot G)_A, \\ ((G \cdot G)_A \cdot (G \cdot G)_A)_A. \end{gathered} \tag{2.30}$$

However, a closer inspection of the explicit forms of these invariants reveals that not all of them are different. For example, the invariant $(((G \times G)_H \times G)_G \cdot G)_A$ has the explicit form

$$\begin{aligned} (((G \times G)_H \times G)_G \cdot G)_A &= \sum_{ijklm} (G\ j; H\ k | G\ i)(H\ k; G\ l | G\ m) q_i q_j q_k q_l \\ &= \sum_{ijklm} (G\ j; H\ k | G\ i)(G\ l; H\ k | G\ m) q_i q_j q_k q_l \quad \text{by (2.11)} \\ &= ((G \times G)_H \cdot (G \times G)_H)_A, \end{aligned} \tag{2.31}$$

where $i,j,k,l,m \in \{\alpha,\beta,\gamma,\delta\}$. In a similar way, $((G \times G)_G \cdot (G \times G)_G)_A$ may be shown to be equal to $(((G \times G)_G \times G)_G \cdot G)_A$. Therefore there are only three different quartic invariants that may be constructed from $\{q_\alpha, q_\beta, q_\gamma, q_\delta\}$. The explicit forms of these are given in Appendix (B).

• Construction of quintet invariants.

This thesis primarily deals with only one type of H normal mode (the single H mode active in the G orbital). The invariants presented here are made up of H modes derived only from $J = 2$. The $J = 2$ level has been chosen only for definiteness. The theory would be the same if the H mode were to be derived from $J = 4$ since the G manifold cannot distinguish between H operators from different J levels, i.e. the C-G coefficients are unique up to a phase.

The quintet of normal modes $\{q_\theta, q_\epsilon, q_x, q_y, q_z\}$ have transformation properties identical to those of the Cartesian tensors of Equations (2.15). The possible icosahedral invariants which may be constructed from $\{q_\theta, q_\epsilon, q_x, q_y, q_z\}$ may be determined by considering the symmetric square $[H \otimes H]_S$ which in the symmetry descent formalism is $[H \otimes H]_S = A \oplus 2H \oplus 4H$, i.e. the multiple H irreps are distinguished by deriving them from different J levels. As before, there is only one trivial quadratic invariant constructed by the scalar convolution $(2H \cdot 2H)_A$, where

$$(2H \cdot 2H)_A = q_\theta^2 + q_\epsilon^2 + q_x^2 + q_y^2 + q_z^2. \tag{2.32}$$

There are two ways of constructing a cubic invariant corresponding to the two ways of constructing H tensors from H components. The corresponding coupling rules are $((2H \times 2H)_{2H} \cdot 2H)_A$ and $((2H \times 2H)_{4H} \cdot 2H)_A$. By using the quadratic forms $(2H \times 2H)_{2H}$ and $(2H \times 2H)_{4H}$ in Appendix (A.4), $((2H \times 2H)_{2H} \cdot 2H)_A$ and $((2H \times 2H)_{4H} \cdot 2H)_A$ may be shown to have the explicit forms (without loss of generality, common factors throughout the invariants are omitted).

$$\begin{aligned} ((2H \times 2H)_{2H} \cdot 2H)_A &= \sum_{ijk} (H\ j; 2H\ k | H\ i) q_i q_j q_k \qquad (2.33) \\ &\quad i, j, k \in \{\theta, \epsilon, x, y, z\} \\ &= -6q_\epsilon^2 q_\theta + 2q_\theta^3 - 3\sqrt{3} q_\epsilon q_x^2 + 3q_\theta q_x^2 + 3\sqrt{3} q_\epsilon q_y^2 \\ &\quad + 3q_\theta q_y^2 + 6\sqrt{3} q_x q_y q_z - 6q_\theta q_z^2, \end{aligned}$$

and

$$\begin{aligned} ((2H \times 2H)_{4H} \cdot 2H)_A &= \sum_{ijk} (H\ j; 4H\ k | H\ i) q_i q_j q_k \qquad (2.34) \\ &\quad i, j, k \in \{\theta, \epsilon, x, y, z\} \\ &= -3q_\epsilon^2 q_\theta - 6q_\theta^3 + 7\sqrt{3} q_\epsilon^2 q_x + 2\sqrt{3} q_\epsilon q_x^2 + 12 q_\theta q_x^2 \\ &\quad - 2\sqrt{3} q_\epsilon q_y^2 + 12 q_\theta q_y^2 + 14\sqrt{3} q_\epsilon q_y q_z - 4\sqrt{3} q_x q_y q_z \\ &\quad - 3q_\theta q_z^2 - 7\sqrt{3} q_x q_z^2. \end{aligned}$$

Note that $((2H \times 2H)_{2H} \cdot 2H)_A$ may also be written $((d \times d)_d \cdot d)_s$, where d and s are respectively the spectral labels for $J = 2$ and $J = 0$ of $SO(3)$. This means that $((2H \times 2H)_{2H} \cdot 2H)_A$ is actually an invariant of $SO(3)$.

There are nine coupling rules for the construction of quartic invariants from $2H$ modes, but the exchange symmetry of the coupling symbols reduces the number of different invariants to just five. The nine coupling rules are

$$\text{idem} \begin{cases} ((2H \times 2H)_G \cdot (2H \times 2H)_G)_A, \\ (((2H \times 2H)_G \times 2H)_{2H} \cdot 2H)_A, \end{cases} \tag{2.35}$$

$$\text{idem}\begin{cases}((2H\times 2H)_{2H}\cdot(2H\times 2H)_{2H})_A,\\(((2H\times 2H)_{2H}\times 2H)_{2H}\cdot 2H)_A,\end{cases}$$

$$\text{idem}\begin{cases}((2H\times 2H)_{2H}\cdot(2H\times 2H)_{4H})_A,\\(((2H\times 2H)_{2H}\times 2H)_{4H}\cdot 2H)_A,\end{cases}$$

$$\text{idem}\begin{cases}((2H\times 2H)_{4H}\cdot(2H\times 2H)_{4H})_A,\\(((2H\times 2H)_{4H}\times 2H)_{4H}\cdot 2H)_A,\end{cases}$$

$$((2H\cdot 2H)_A\cdot(2H\cdot 2H)_A)_A,$$

with those designated as "idem", producing the same invariants. The corresponding invariants may be found in Appendix (B).

2.3 Summary of Chapter 2.

The Kronecker multiplicity appearing in the square $H\otimes H$, means that I is not simply reducible and that a unique set of C-G coefficients cannot be established for I. A convenient set of C-G coefficients may be derived for I by a descent in symmetry $SO(3)\supset I$, which facilitates a labelling of the Kronecker multiplicity according to $SO(3)$ irrep labels. A routine written in *Mathematica* computes these C-G coupling coefficients and avoids what would otherwise be a laborious inspection of tables.

The quadratic forms derived from the matrix representation of the Jahn-Teller active operators, form a basis of "coupling rules" which may be used to construct icosahedral irreducible tensors. These icosahedral irreducible tensors may be coupled by repeated applications of the "coupling rules", to form icosahedral invariant quantities. A preliminary study of the resulting icosahedral invariant quantities proves invaluable in the various analyses presented in the latter parts of this thesis.

Chapter 3

$G \otimes (g \oplus h)$ and related subsystems.

3.1 Introduction.

UPON a G manifold, tensor operators may be constructed transforming according to the irreps contained in the Kronecker square $G \otimes G$ (see Table (2.4)). An application of the Jahn-Teller theorem reveals that the G manifold is Jahn-Teller active under the action of even operators belonging to the representation $G \oplus H$ (see Table (2.4)). The full general system pertaining to a G orbital degeneracy is therefore $G \otimes (g \oplus h)$. The full Hamiltonian for the $G \otimes (g \oplus h)$ linear coupling may be constructed from the matrix representations of Jahn-Teller modes active in G. These matrices are given in Appendix (A.1). The Hamiltonian is then

$$\begin{aligned} \hat{\mathrm{H}} = H_o \hat{\mathrm{i}} + V_H^G(Q_\theta \hat{\mathrm{h}}_\theta^G + Q_\epsilon \hat{\mathrm{h}}_\epsilon^G + Q_x \hat{\mathrm{h}}_x^G + Q_y \hat{\mathrm{h}}_y^G + Q_z \hat{\mathrm{h}}_z^G) \\ + V_G^G(Q_\alpha \hat{\mathrm{g}}_\alpha^G + Q_\beta \hat{\mathrm{g}}_\beta^G + Q_\gamma \hat{\mathrm{g}}_\gamma^G + Q_\delta \hat{\mathrm{g}}_\delta^G), \end{aligned} \tag{3.1}$$

where

$$\begin{aligned} H_o = (1/2\mu_H)(P_\theta^2 + P_\epsilon^2 + P_x^2 + P_y^2 + P_z^2 + \mu_H^2 \omega_H^2 (Q_\theta^2 + Q_\epsilon^2 + Q_x^2 + Q_y^2 + Q_z^2)) \\ + (1/2\mu_G)(P_\alpha^2 + P_\beta^2 + P_\gamma^2 + P_\delta^2 + \mu_G^2 \omega_G^2 (Q_\alpha^2 + Q_\beta^2 + Q_\gamma^2 + Q_\delta^2)). \end{aligned} \tag{3.2}$$

V_G^G and V_H^G are the Jahn-Teller coupling constants. The $\{Q\}$ and $\{P\}$ are respectively the adiabatic parameters and corresponding conjugate momenta labelled according to transformation properties, and the μ's and ω's are respectively the reduced masses and frequencies associated with the $\{Q\}$. $\hat{\mathrm{i}}$ is the unit matrix in G. In the adiabatic approximation (outlined in Section (1.3)), in which the nuclear kinetic energies (all the terms in $\{P\}$) are neglected, the lowest eigenvalue of the Hamiltonian is a function of the $\{Q\}$ and can be regarded as a potential energy function or the lowest APES in the nine dimensional Q-space. In the limit of infinitely large nuclear masses the equilibrium configuration of the complex is expected to correspond to the minimum

value of the lowest APES. The positions and natures of the turning points in the lowest APES were discussed by Ceulemans *et al.* [13], who showed that the hypersurface has three different structures depending on the relative magnitudes of V_G^G and V_H^G. The three different structures correspond to the subsystems $G \otimes (g \oplus h)_{eq}$, $G \otimes g$ and $G \otimes h$ and are sometimes referred to as "the extremities" of $G \otimes (g \oplus h)$. In the following, the *dynamical* properties of $G \otimes (g \oplus h)$ resulting from these three different structures are treated separately.

Within $G \otimes (g \oplus h)$, three main levels of symmetry may be recognised. These are:

(i) The continuous $SO(4)$ parent symmetry of the degeneracy space of the G manifold [80, 12].

(ii) The icosahedral point symmetry of the Jahn-Teller origin.

(iii) The point symmetries of the subgroups of the Jahn-Teller origin resulting from symmetry lowering distortions.

These three levels constitute a descent in symmetry which is prevalent in the following analysis of $G \otimes (g \oplus h)$ and allows for a simplified visualization of the interaction manifolds in terms of parameters appropriate to the continuous $SO(4)$ group.

3.2 $G \otimes (g \oplus h)_{eq}$.

In keeping with the idea of symmetry descent, a convenient starting point for this analysis is the $SO(4)$ invariance of $G \otimes (g \oplus h)_{eq}$. Subsection (1.4.2) outlines Pooler's [80] analysis of the G manifold which shows that at equal coupling $G \otimes (g \oplus h)$ coincides with the $SO(4)$ invariant system $(\frac{1}{2}, \frac{1}{2}) \otimes (1,1)$. The normalization of the matrices in Appendix (A.1) is such that the Hamiltonian in (3.1) becomes appropriate to $G \otimes (g \oplus h)_{eq}$ when $V_G^G = V_H^G$, $\mu_G = \mu_H$ and $\omega_G = \omega_H$. In this case the minimum energy surface of the lowest APES is a continuous hyperspherical trough embedded in the nine-dimensional parameter space. The representation in the projective electronic function space (f) is the $SO(4)$ irrep $(\frac{1}{2}, \frac{1}{2})$ and through the medium of a Jahn-Teller coupling, every antipodal pair of points on the unit hypersphere f corresponds to the same distortion in the vibrational coordinate space (v).

3.2.1 Biharmonics.

The task of parametrizing the $SO(4)$ group, though ancillary to these considerations, is nonetheless an important part of the analysis. There are two independent ways of doing this, corresponding to the two independent ways to parametrize four dimensions with angular coordinates.

If $\mathbf{r} = (x, y, z, w)$ denotes a point on a unit hypersphere, then the usual parametrization in polar angles yields scalar harmonic functions expressed in terms of the Gegenbauer polynomials. However, advances in the hyperspherical formulation of quantum gauge field models [24] has produced formulae for derivatives and integrals in terms of *biharmonics* [10], which prove to be extremely useful in the formulation of $G \otimes (g \oplus h)_{eq}$. The biharmonic parametrization of $\mathbf{r}$ is

$$\begin{aligned} \xi = x + iy = r\cos\theta e^{i\alpha}, \\ \zeta = z + iw = r\sin\theta e^{i\beta}, \end{aligned} \tag{3.3}$$

where $0 \leq \alpha, \beta < 2\pi$, $0 \leq \theta < \pi/2$ and $r = |\mathbf{r}| = 1$. A biharmonic parametrization coincides with a reconfiguring of the generators of $SO(4)$ into the components of two commuting angular momenta $\mathbf{L}_1$ and $\mathbf{L}_2$. The z-components of these angular momenta then take the coordinate forms

$$L_{1z} = -i\frac{\partial}{\partial\alpha}, \quad L_{2z} = -i\frac{\partial}{\partial\beta}. \tag{3.4}$$

Thus $SO(4)$ is locally isomorphic to $SO(3) \otimes SO(3)$ and its irreps may be labelled accordingly, i.e. (L_1, L_2). The traceless symmetric tensors of rank s constructed from the components of $\mathbf{r}$, form a basis for the irrep $(s/2, s/2)$. The dimensionality of this representation is $(s+1)^2$, and the value of the Laplacian is $-s(s+2)$. The basis functions of $(s/2, s/2)$ are referred to as S functions and take the explicit form

$$S_s^{s/2-a,s/2-b} = C_s[a!(s-a)!b!(s-b)!]^{1/2} \sum_k \frac{(\xi^*)^k \zeta^{b-k} (\zeta^*)^{a-k} (-\xi)^{l+k-a-b}}{k!(l+k-a-b)!(a-k)!(b-k)!}, \tag{3.5}$$

where $C_s^2 = (s+1)/2\pi^2$ and $a, b \in \{0, 1, .., s\}$.

The basis functions spanning the irreps $(\frac{1}{2}, \frac{1}{2})$ and $(1,1)$ are respectively, $S_1^{1/2-a,1/2-b}$, where $a, b \in \{0,1\}$, and $S_2^{1-a,1-b}$, where $a, b \in \{0,1,2\}$. By (3.5) with $s = 1$, the $\{S_1\}$ are given by

$$\begin{array}{c|cc} & b=0 & b=1 \\ \hline a=0 & -\frac{e^{i\alpha}\cos\theta}{\pi} & \frac{e^{i\beta}\sin\theta}{\pi} \\ a=1 & \frac{e^{-i\beta}\sin\theta}{\pi} & \frac{e^{-i\alpha}\cos\theta}{\pi} \end{array} \tag{3.6}$$

Similarly, the $\{S_2\}$ may be obtained by an application of (3.5) for $s = 2$ yielding

$$\begin{array}{c|ccc} & b=0 & b=1 & b=2 \\ \hline a=0 & \frac{\sqrt{3}\, e^{2i\alpha}\cos^2\theta}{\sqrt{2}\pi} & -\frac{\sqrt{3}\, e^{i(\alpha+\beta)}\sin 2\theta}{2\pi} & \frac{\sqrt{3}\, e^{2i\beta}\sin^2\theta}{\sqrt{2}\pi} \\ a=1 & -\frac{\sqrt{3}\, e^{-i(\beta-\alpha)}\sin 2\theta}{2\pi} & -\frac{\sqrt{3}\,\cos 2\theta}{\sqrt{2}\pi} & \frac{\sqrt{3}\, e^{i(\beta-\alpha)}\sin 2\theta}{2\pi} \\ a=2 & \frac{\sqrt{3}\, e^{-2i\beta}\sin^2\theta}{\sqrt{2}\pi} & \frac{\sqrt{3}\, e^{-i(\alpha+\beta)}\sin 2\theta}{2\pi} & \frac{\sqrt{3}\, e^{-2i\alpha}\cos^2\theta}{\sqrt{2}\pi} \end{array} \tag{3.7}$$

At equal coupling, $G \otimes (g \oplus h)$ coincides with the $SO(4)$ invariant system $(\frac{1}{2}, \frac{1}{2}) \otimes (1,1)$ and this equivalence of parent group irreps and finite group irreps of the first kind means that the irrep

spaces $(\frac{1}{2},\frac{1}{2})$ and $(1,1)$ may be taken to be real. The linear coupling matrices for $(\frac{1}{2},\frac{1}{2})\otimes(1,1)$ are easily obtained from the formulae for integrals involving S functions given in reference [24]. An arbitrary matrix element of an operator $S_2^{1-a,1-b}$, where $a,b\in\{0,1,2\}$, belonging to $(1,1)$ within the $(\frac{1}{2},\frac{1}{2})$ electronic manifold is found to be

$$\begin{aligned}\langle S_1^{il}|S_2^{jm}|S_1^{kn}\rangle &= (-1)^{(i+l)}\int S_1^{-i-l}S_2^{jm}S_1^{kn}\sin\theta\cos\theta d\alpha d\beta d\theta \\ &= (-1)^{(i+l)}R(1,2,1)\begin{pmatrix}\frac{1}{2} & 1 & \frac{1}{2}\\ -i & j & k\end{pmatrix}\begin{pmatrix}\frac{1}{2} & 1 & \frac{1}{2}\\ -l & m & n\end{pmatrix}, \\ & \quad i,k,l,n\in\{-\frac{1}{2},\frac{1}{2}\},\ \ j,m\in\{-1,0,1\},\end{aligned} \tag{3.8}$$

where

$$R(\lambda,\mu,\nu)=\frac{1}{\pi}\sqrt{(-1)^{\lambda+\mu+\nu}\left[\frac{(\lambda+1)(\mu+1)(\nu+1)}{2}\right]}=\frac{\sqrt{6}}{\pi}\quad\text{for }\lambda=1,\ \mu=2,\ \nu=1, \tag{3.9}$$

and $\begin{pmatrix}\frac{\lambda}{2} & \frac{\mu}{2} & \frac{\nu}{2}\\ i & j & k\end{pmatrix}$ is a standard $3j$ symbol (see Equation (2.7)). The linear coupling matrices resulting from (3.8) are hermitian. In order to relate these operators to those already calculated in Chapter 2, it is necessary to combine them into real symmetric combinations. This is done by rotations in v and f space. The matrix resulting from all these considerations is presented in Appendix (C). At equal coupling, the lowest APES exhibits an $SO(4)$ invariance which may be parametrized in terms of the biharmonic coordinates (q,θ,α,β). The parametrization is achieved by introducing the nine normal mode vibrations $q_i,\ i=1,..,9$, in terms of (q,θ,α,β) as follows

$$\begin{aligned}&q_1=\frac{q}{\sqrt{3}}\cos 2\theta,\quad q_2=\frac{q}{\sqrt{3}}\sin 2\theta\cos(\alpha+\beta),\quad q_3=\frac{q}{\sqrt{3}}\sin 2\theta\sin(\alpha+\beta),\\ &q_4=\frac{q}{\sqrt{3}}\sin 2\theta\cos(\beta-\alpha),\quad q_5=\frac{q}{\sqrt{3}}\sin 2\theta\sin(\beta-\alpha),\quad q_6=q\sqrt{\frac{2}{3}}\sin^2\theta\cos 2\beta,\\ &q_7=q\sqrt{\frac{2}{3}}\sin^2\theta\sin 2\beta,\quad q_8=q\sqrt{\frac{2}{3}}\cos^2\theta\cos 2\alpha,\quad q_9=q\sqrt{\frac{2}{3}}\cos^2\theta\sin 2\alpha,\end{aligned} \tag{3.10}$$

with $q^2=\sum_i q_i^2$. Introducing this parametrization into the linear coupling matrix for $(\frac{1}{2},\frac{1}{2})\otimes(1,1)$ (the full form of this matrix is presented in Appendix (C)), restricts the analysis to a continuum of concentric S^3 hyperspheres embedded in the nine dimensional parameter space. On diagonalizing $(\frac{1}{2},\frac{1}{2})\otimes(1,1)$ in the parametrization (3.10), the eigensystem is found to be a degenerate triplet at an energy $+qV_o/2\sqrt{3}$ above a singlet at an energy $-\sqrt{3}qV_o/2$, where $V_o=V_G=V_H$ is the effective linear Jahn-Teller coupling for $(\frac{1}{2},\frac{1}{2})\otimes(1,1)$. In terms of the biharmonic parametrization, the singlet is

$$|u(\theta,\alpha,\beta)\rangle=\cos\theta\cos\alpha|1\rangle+\cos\theta\sin\alpha|2\rangle+\sin\theta\cos\beta|3\rangle+\sin\theta\sin\beta|4\rangle\qquad\forall q. \tag{3.11}$$

Here the kets $|i\rangle$, $i = 1,2,3,4$, are the $(\frac{1}{2},\frac{1}{2}) \equiv G$ electronic unit vectors. The corresponding hyperspherical sub-spaces of the full nine dimensional APESs, are just the above eigenvalues added to the harmonic restoring potential $q^2/2$ (here $\mu_G\omega_G^2 = \mu_H\omega_H^2 = 1$). In terms of the coordinates (q,θ,α,β), these sub-spaces have the very simple form

$$\frac{q^2}{2} - qV_o\frac{\sqrt{3}}{2} \qquad \forall\theta,\alpha,\beta. \tag{3.12}$$

The minimum value of this potential is $-3V_o^2/8$ occuring at $q = V_o\sqrt{3}/2$. This represents a continuum of minima or "trough" forming an S^3 hypersphere embedded in the nine dimensional parameter space. The biharmonic parametrization emphasises the $SO(4)$ invariance of the parameter space and effectively factors out five of the nine degrees of freedom. To be satisfied that the continuum of minima is no more than three dimensional, it is necessary to examine the curvature of the lowest APES in directions perpendicular to the minimum energy hypersphere. Upon concentric hyperspheres, at a point defined by the biharmonic coordinates $\theta = 0$ and $\alpha = 0$, the vibration variables (3.10) reduce to simply

$$q_1 = \frac{q}{\sqrt{3}}, \quad q_8 = \frac{q\sqrt{2}}{\sqrt{3}}, \tag{3.13}$$

all the other q's are zero. The linear Jahn-Teller coupling matrix for $(\frac{1}{2},\frac{1}{2}) \otimes (1,1)$ is then found to be

$$V_o q \begin{pmatrix} -\frac{\sqrt{3}}{2} & 0 & 0 & 0 \\ 0 & \frac{1}{2\sqrt{3}} & 0 & 0 \\ 0 & 0 & \frac{1}{2\sqrt{3}} & 0 \\ 0 & 0 & 0 & \frac{1}{2\sqrt{3}} \end{pmatrix}. \tag{3.14}$$

Introducing the full Hamiltonian for $(\frac{1}{2},\frac{1}{2}) \otimes (1,1)$ (Equation (3.1) with $V_G^G = V_H^G = V_o$, $\mu_G = \mu_H = \mu_o$, $\omega_G^2 = \omega_H^2 = 1/\mu_o$) as a perturbation and working to second order, the energy of the ground state at this point is

$$-V_o\frac{q\sqrt{3}}{2} - V_o\frac{\delta q_1}{2} - \frac{V_o\delta q_8}{\sqrt{2}} - V_o^2\frac{(\frac{(\delta q_9)^2}{2} + \frac{(\delta q_a^+)^2}{2} + \frac{(\delta q_b^+)^2}{2})}{(\frac{2V_oq}{\sqrt{3}})} \tag{3.15}$$
$$+\frac{1}{2}((q_1+\delta q_1)^2 + (q_8+\delta q_8)^2 + \sum(\delta q_i)^2),$$

where $q_a^\pm = -(q_4 \pm q_2)/\sqrt{2}$ and $q_b^\pm = (q_3 \pm q_5)/\sqrt{2}$ and the sum is over all the other q's except q_1 and q_8. Setting $q = \sqrt{3}V_o/2$, i.e. at the minimum of the trough, yields

$$\frac{-q^2}{2} + \frac{1}{2}((\delta q_1)^2 + (\delta q_a^-)^2 + (\delta q_b^-)^2 + (\delta q_6)^2 + (\delta q_7)^2 + (\delta q_8)^2), \tag{3.16}$$

from which it is clear that only three of the nine parameters $q_1 ... q_9$ may be altered without increasing the potential energy, and that the curvatures of the lowest APES associated with the

changes in the other five directions are equal, and are equal to one in these units. The form of the lowest APES in Equation(3.12) means that this state of affairs will hold at all points on this four-dimensional surface, since any SO(4) rotation will take this special point into all the others.

3.2.2 The vibronic ground state at strong coupling.

Following the considerations outlined in section (1.3), the lowest APES at strong coupling is far away in energy from the other APESs and therefore the vibronic ground state will take the form

$$\Psi = \psi(q,\theta,\alpha,\beta)\; u(q,\theta,\alpha,\beta,\mathbf{r}), \tag{3.17}$$

where ψ is the wave function of nuclear motion to be calculated. u is the state given in Equation (3.11) with $\mathbf{r}$ representing all the electronic coordinates. If this Ψ is substituted into the Schrödinger equation of motion on the minimum energy trough, the result is found to be (in units for which $\mu_o = 1$)

$$-\frac{1}{2}(u\nabla^2\psi - 2\nabla\psi\cdot\nabla u + \psi\nabla^2 u) + \left(\frac{q^2}{2} - qV_o\frac{\sqrt{3}}{2}\right)\psi u = E\psi u, \tag{3.18}$$

where ∇ is the usual momentum operator in the coordinate representation. Applying closure with u to (3.18) yields

$$-\frac{1}{2}\nabla^2\psi - \nabla\psi\cdot\langle u|\nabla u\rangle - \frac{1}{2}\psi\langle u|\nabla^2 u\rangle + \left(\frac{q^2}{2} - qV_o\frac{\sqrt{3}}{2}\right)\psi = E\psi. \tag{3.19}$$

The components of ∇ in the biharmonic coordinate representation are

$$\left(\frac{\partial}{\partial q}, \frac{1}{q}\frac{\partial}{\partial\theta}, \frac{1}{q\sin\theta}\frac{\partial}{\partial\alpha}, \frac{1}{q\cos\theta}\frac{\partial}{\partial\beta}\right). \tag{3.20}$$

We may now calculate the terms in equation (3.19) and obtain as follows:

$$\langle u|\nabla u\rangle = \mathbf{0}, \tag{3.21}$$

as is always the case if $|u\rangle$ is real and normalized. The Laplace-Beltrami operator, ∇^2, in terms of the biharmonic coordinates is as follows:-

$$\frac{1}{q^3}\frac{\partial}{\partial q}q^3\frac{\partial}{\partial q} + \frac{1}{q^2\sin\theta\cos\theta}\frac{\partial}{\partial\theta}\sin\theta\cos\theta\frac{\partial}{\partial\theta} + \frac{1}{q^2\sin^2\theta}\frac{\partial^2}{\partial\alpha^2} + \frac{1}{q^2\cos^2\theta}\frac{\partial^2}{\partial\beta^2}. \tag{3.22}$$

The second term of Equation (3.19) may now be calculated yielding

$$\langle u|\bigtriangledown^2 u\rangle = -\frac{3}{q^2}. \tag{3.23}$$

Equation (3.19) then becomes

$$-\frac{1}{2}\frac{1}{q^3}\frac{\partial}{\partial q}q^3\frac{\partial}{\partial q}\psi - \frac{\triangle(\theta,\alpha,\beta)}{2q^2}\psi + \frac{3}{2q^2}\psi + \left(\frac{q^2}{2} - qV_o\frac{\sqrt{3}}{2}\right)\psi = E\psi. \tag{3.24}$$

where $\triangle(\theta, \alpha, \beta)$ is the angular part of the operator in (3.22) which is just the Laplacian in biharmonics. The hyperspherical trough upon which the motions take place, has a radius of $q = V_o\sqrt{3}/2$ and a depth of $-3V_o^2/8$. When the trough is deep (strong coupling, i.e V_o large) the wave function for the low-lying vibronic states will be concentrated on the hyperspherical continuum of minima, the distance from the next triply degenerate APES will be large V_o^2, and the conditions for application of an adiabatic approximation are satisfied. The appropriate concentration of wave function in the trough occurs when the variables are separated into radial and angular parts. Factorizing out the angular dependence by equating it to a constant K, leaves an equation in the radial coordinate q which describes nuclear motion in the directions perpendicular to the $SO(4)$ hyperspheres:

$$-\frac{1}{2q^3}\frac{d}{dq}q^3\frac{dg(q)}{dq} - \frac{(K+3)}{2q^2}g(q) + \left(\frac{q^2}{2} - qV_o\frac{\sqrt{3}}{2}\right)g(q) = Eg(q), \tag{3.25}$$

where $g(q)$ is the solution to this radial motion. By introducing a solution of the form $\chi(q)/(q\sqrt{q})$, (3.25) may be reduced to a the simpler form

$$\frac{3}{4}\chi'' - \frac{(4K+9)}{8q^2}\chi + \frac{(q - V_o\frac{\sqrt{3}}{2})^2}{2}\chi = (E + \frac{3}{8}V_o^2)\chi, \tag{3.26}$$

where the double primes indicate a second derivative with respect to q. According to the considerations leading to Equation (3.16), any motion away from the minimum energy hypersurface (in the direction of increasing or decreasing q), experiences a harmonic restoring force centred at $q = V_o\sqrt{3}$. At strong coupling this radial harmonic potential is deep and $(q - V_o\sqrt{3}/2) = \delta$ is small. Expanding the $1/q^2$ term in (3.26) about $q = V_o\sqrt{3}/2$ yields

$$\frac{1}{q^2} \approx \frac{4}{3V_o^2} - \frac{16}{V_o^3 3\sqrt{3}}\delta + O(\delta^2). \tag{3.27}$$

Introducing (3.27) into (3.26) results in an equation for χ to order $1/V_o^2$ of the form

$$\chi'' + \frac{2(q - V_o\frac{\sqrt{3}}{2})^2}{3}\chi = \frac{4}{3}\left(E + \frac{3}{8}V_o^2 + \frac{(4K+9)}{6V_o^2}\right)\chi, \tag{3.28}$$

which leads to solutions for χ of the form

$$\chi_n(q - V_o\frac{\sqrt{3}}{2}) = N_n \exp\left(\frac{\left(q - V_o\frac{\sqrt{3}}{2}\right)^2}{\sqrt{6}}\right)\mathcal{H}_n\left((\frac{2}{3})^{1/4}\left(q - V_o\frac{\sqrt{3}}{2}\right)\right), \tag{3.29}$$

which is just the solution to a radial harmonic oscillator centred about $q = V_o\sqrt{3}/2$ where N_n and $\mathcal{H}_n$ are respectively the normalization constant and Hermite polynomial of the n^{th} order. The ground state energy E_o to order $1/V_o^2$ is then

$$E_o = \sqrt{\frac{3}{8}} - \frac{3}{8}V_o^2 - \frac{(4K+9)}{6V_o^2}. \tag{3.30}$$

The equation of motion in the angular coordinates θ, α and β is of the form

$$\triangle(\theta,\alpha,\beta)f(\theta,\alpha,\beta) - Kf(\theta,\alpha,\beta) = 0, \tag{3.31}$$

where $f(\theta,\alpha,\beta)$ is the solution to this angular motion. Since $\triangle(\theta,\alpha,\beta)$ is just the biharmonic Laplacian, if K is set to the value $-s(s+2)$ then the corresponding eigenfunctions $f(\theta,\alpha,\beta)$ are just the basis states of the representation $(s/2, s/2)$.

The solutions of the nuclear equation of motion (3.24) at strong coupling are therefore products of a harmonic oscillator part centred at $q = V_o\sqrt{3}/2$ and an S function angular part. The corresponding ground states are pseudo-rotational and are of the form

$$\Psi_{o,s}^{s/2-a,s/2-b} \sim \frac{1}{q\sqrt{q}} \exp\left(\frac{\left(q - V_o\frac{\sqrt{3}}{2}\right)^2}{\sqrt{6}}\right) S_s^{s/2-a,s/2-b} |u(\theta,\alpha,\beta)\rangle, \quad a,b \in \{0,1,..,s\}, \tag{3.32}$$

corresponding to energies

$$E_o = \sqrt{\frac{3}{8}} - \frac{3}{2V_o^2} - \frac{3}{8}V_o^2 + \frac{2s(s+2)}{3V_o^2}. \tag{3.33}$$

This is still not the total energy, because the other five of the nine degrees of freedom have been left out in concentrating on the $SO(4)$ invariant sub-space. At equal coupling however, Equation (3.16) shows that none of these extra degrees of freedom couple linearly to the electronic states, so they only contribute a zero-point energy of $5/2$ to E_o.

3.2.3 Berry phase changes accompanying motion around the hyperspherical trough.

There is one final restriction that has to be applied to the wave functions in (3.32) before they can properly represent the ground state motion at strong coupling. In (3.32), the total wave function is the product of the nuclear wave function and a vector u of f-space. Physically, when the system is transported around an adiabatic circuit in parameter space, the total wave function must remain unchanged. The vector $|u\rangle$ however, suffers a phase change of π over the same circuit. More precisely, antipodal pairs of points $((\theta,\alpha,\beta)$ and $(\theta,\alpha+\pi,\beta+\pi))$ in f-space represent the same distortion in v space. Therefore, the ground state vibronic wave function will remain unchanged only if the nuclear factor suffers the same phase change as that of the $|u\rangle$ vector. This means that the pseudo-rotational part of (3.32) must come from the irreps $(s/2, s/2)$ for $s = 1, 3, 5, ...$ Since the degeneracy of these states is $(s+1)^2$, the lowest vibronic state has a four-fold degeneracy correponding to the nuclear motion state $(\frac{1}{2}, \frac{1}{2})$. A characteristic result of the Jahn-Teller effect is thus recovered: *When proper account of the Berry phase is taken, the*

properties of the vibronic ground state are formally identical, so far as symmetry considerations are concerned, with those of the uncoupled electronic orbital at the Jahn-Teller origin.

3.3 $G \oslash g$, $G \oslash h$ and $H \oslash g$.

Proceeding in accordance with the symmetry descent outlined at the beginning of this chapter, the next symmetries to be considered are the icosahedral symmetry of the origin and the point group symmetries resulting from the Jahn-Teller distortions. $G \oslash g$, $G \otimes h$ and $H \otimes g$ have lowest APESs which all exhibit icosahedral symmetry. This may be seen by examining the character table, Table (2.1), and deducing from it the kernels for the G and H irreps. The kernel for G and H is C_1, and therefore the APESs for the interactions $G \otimes g$, $G \otimes h$ and $H \otimes g$ will all exhibit a point symmetry which is isomorphic to the factor group $I/C_1 = I$ (see subsection (1.4.3)).

The dynamics of motion in the ground states depends upon the positions and natures of the turning points in the lowest APES. Ceulemans *et al.* [13] showed that in the case of $G \otimes (g \oplus h)$, the lowest APES has two different structures depending on which of the two modes, g or h, gives rise to the larger Jahn-Teller stabilization energy (depth of the minima). The corresponding APESs are very complex, spanning a nine dimensional parameter space when both g and h modes are present. In order to separate the treatment of the Berry phase and ground states into tractable parts, the following analysis of $G \otimes (g \oplus h)$ is divided into an analysis of $G \otimes g$ ($G \otimes (g \oplus h)$ when $V_H^G = 0$) and $G \otimes h$ ($G \otimes (g \oplus h)$ when $V_G^G = 0$), and an analysis of $G \otimes (g \oplus h)$ at all other relative couplings of the g and h modes ($G \otimes (g \oplus h)$ when $V_G^G \neq 0$ and $V_H^G \neq 0$). The method adopted here for the examination of the extremal properties of these systems is that due to Öpik and Pryce [77]. Ceulemans [12] showed the equivalence of the Öpik and Pryce method to his use of an isostationary function and the *epikernel principle* (see subsection (1.4.3)). The Öpik and Pryce method has been chosen here for convenience; firstly because as a routine written in *Mathematica*, this method is particularly fast and easily implemented, and secondly because the tensorial properties of the equations arising from this method are readily available from the analysis of icosahedral tensors in Chapter 2.

In the f-space representation of $G \otimes g$, the minima and saddles occur at points corresponding to the maximal[1] and lower ranking epikernels. The same is true of the v-space representation of this scheme, except that in v-space the extrema are distributed in phase space on concentric hypersurfaces, each hypersurface corresponding to one type of extremum. The angular distributions of the extrema over these hypersurfaces are the same as those of the f-space representation.

[1] A maximal epikernel is an epikernel of highest symmetry, lower ranking means "of lower symmetry".

In a similar way, the following analyses show that $G \oslash h$ and $H \oslash g$ share a common maximal epikernel symmetry for minima (see the genealogy in figure 2 of [13]). The f-space representation of $G \otimes h$ minima is therefore just a projective version of the v representation of $H \otimes g$ minima and vice versa. Bearing in mind these considerations, $G \otimes g$ will be referred to as *self-dual* and $G \otimes h$ and $H \otimes g$ will be referred to as *dual* with respect to mimima.

3.3.1 The method of Öpik and Pryce.

$G \otimes g$ and $G \otimes h$.

The method of Öpik and Pryce [77] requires the solution of a set of non-linear equations constructed and solved according to the following prescription:

(i) If the matrix representing the linear Jahn-Teller interaction in (3.1) is denoted $\hat{\mathrm{H}}_{JT}$, then the distortion coordinates corresponding to extremal points on the APESs are found to be

$$Q_i = -\left(\frac{1}{\omega_\Lambda^2}\right) \times \mathbf{a}^T \cdot \left(\frac{\partial \hat{\mathrm{H}}_{JT}}{\partial Q_i}\right) \cdot \mathbf{a}, \tag{3.34}$$

where $i \in \{\alpha, \beta, \gamma, \delta\}$ when $\Lambda = G$ or $i \in \{\theta, \epsilon, x, y, z\}$ when $\Lambda = H$, and $\mathbf{a}$ is the normalized column vector in the G manifold with components $(a_\alpha, a_\beta, a_\gamma, a_\delta)$. T is the transpose operation so $\mathbf{a}^T$ is a row vector and $\mathbf{a}^T \cdot \mathbf{a} = 1$. The quadratic form resulting from (3.34), is identical (except for a multiplicative factor of $V_\Lambda^G/\omega_\Lambda^2$) to $-\mathcal{Q}_{\Lambda i}^G$ which is derived in Chapter 2 (the explicit forms of the $\mathcal{Q}_{\Lambda i}^G$ are given in Appendix (A.2)), therefore

$$Q_i = -\left(\frac{V_\Lambda^G}{\omega_\Lambda^2}\right) \mathcal{Q}_{\Lambda i}^G. \tag{3.35}$$

Here the $\{a\}$ are the extremal coordinates in the f-space representation of the interaction and via the operation (3.34), this f-space representation is mapped into v-space. The extremal coordinates in v-space are then just the $\{Q\}$ given by Equation (3.35).

(ii) The distortion coordinates in terms of the $\{a\}$ given in (3.35) are reintroduced into the matrix $\hat{\mathrm{H}}_{JT}$ and the set of non-linear equations

$$\hat{\mathrm{H}}_{JT} \cdot \mathbf{a} = E\mathbf{a}, \tag{3.36}$$

are solved using a routine written in *Mathematica*, for the solution array $(E, a_\alpha, a_\beta, a_\gamma, a_\delta)$.

(iii) The distortion coordinates corresponding to the solution array $(E, a_\alpha, a_\beta, a_\gamma, a_\delta)$ are calculated by introducing the $\{a\}$ of the solution array into (3.35). The value of the adiabatic

potential at these extremal points is then found to be

$$\frac{1}{2}\omega_\Lambda^2 \sum_i Q_i^2 + E = \frac{1}{2}\left(\frac{V_\Lambda^G}{\omega_\Lambda}\right)^2 \sum_i (\mathcal{Q}_{\Lambda i}^G)^2 + E, \tag{3.37}$$

where as before, $i \in \{\alpha, \beta, \gamma, \delta\}$ when $\Lambda = G$ or $i \in \{\theta, \epsilon, x, y, z\}$ when $\Lambda = H$.

The Öpik and Pryce procedure finds the eigenvector **a** and corresponding eigenvalue $E.$ of the Jahn-Teller matrix $\hat{\mathrm{H}}_{JT}$ that corresponds to a turning point on the appropriate APES. The results obtained from an Öpik and Pryce analysis for $G \oslash g$ and $G \otimes h$ reveal that there are four types of extremum present in the corresponding APESs. These results are presented in Table (3.1). The extremal coordinates appear as positions on the f-space hypersphere, parametrized by the coordinates (θ, α, β). The antipodal equivalent of the point $(\theta_o, \alpha_o, \beta_o)$ is at $(\theta_o, \bar{\alpha_o}, \bar{\beta_o})$ where $\bar{\alpha_o}, \bar{\beta_o}$ is taken to mean $\alpha_o + \pi, \beta_o + \pi$. The θ values which appear in Table (3.1) are as follows

$$\begin{aligned} \theta_1^{(1)} &= \Omega_\mathrm{I}/2, & \theta_1^{(2)} &= \pi/4 - \Omega_\mathrm{I}/2, & \theta_1^{(3)} &= \Omega_\mathrm{D}, \\ \theta_2^{(1)} &= \pi/2 - \Omega_\mathrm{I}/2, & \theta_2^{(2)} &= \pi/4 + \Omega_\mathrm{I}/2, & \theta_2^{(3)} &= \pi/2 - \Omega_\mathrm{D}, \end{aligned}$$

where Ω_I is the icosahedral angle between two neighbouring five-fold axes: $\tan\Omega_\mathrm{I} = 2$; and Ω_D is the dodecahedral angle between two neighbouring three-fold axes: $\cos\Omega_\mathrm{D} = (\sqrt{5}-1)/2\sqrt{3})$. The eigenstates corresponding to the f-space points appearing in Table (3.1) are given by Equation (3.11). In Table (3.1), the columns marked $E(\mathrm{G} \otimes g)$ and $E(\mathrm{G} \otimes h)$ show the energy at the particular extremum type.

There are two subtle points appertaining to $G \otimes g$ which are not immediately obvious from the Öpik and Pryce solutions: Firstly, an inspection of the v-space points of $G \otimes g$ pertaining to Type (II) extrema, shows that not all of the corresponding distortions are different when constructed from g-modes. There are only five different distortions in $G \otimes g$ corresponding to Type (II) extrema. The Type (II) entries in Table (3.1) are labelled with subscripts to show which of the points become physically indistinguishable when viewed in the context of $G \otimes g$. Secondly, the Type(III) extrema in $G \otimes g$ do not occcur on the lowest APES and the energy entry for these extrema is underlined to emphasise this. All other points resulting from the Öpik and Pryce analysis for both $G \otimes g$ and $G \otimes h$, reside upon the lowest APESs.

To deduce the nature of a particular extremum. Öpik and Pryce [77] suggested an examination of the energy increment, to second order, accompanying an incremental displacement from the extremum. By considering the sign of the coefficients of quadratic terms, this Öpik and Pryce method effectively calculates the curvature near the extremum. Computational symbolic algebra makes the direct calculation of the curvature at any point on the lowest APES very simple. If

Type	$E(\mathrm{G}\otimes g)$	$E(\mathrm{G}\otimes h)$	$(\theta,\alpha/(\pi/10),\beta/(\pi/10))$
(I)	$-\frac{(V_G^G)^2}{2\omega_G^2}$	$-\frac{(V_H^G)^2}{4\omega_H^2}$	$(\theta_1^{(1)},\bar{0},\bar{0}),\ (\theta_1^{(1)},\bar{2},\bar{6}),\ (\theta_1^{(1)},\bar{4},2),\ (\theta_1^{(1)},\bar{6},8),\ (\theta_1^{(1)},\bar{8},\bar{4})$ $(\theta_2^{(1)},0,\bar{0}),\ (\theta_2^{(1)},\bar{2},6),\ (\theta_2^{(1)},\bar{4},\bar{2}),\ (\theta_2^{(1)},\bar{6},\bar{8}),\ (\theta_2^{(1)},\bar{8},4)$
(II)	$-\frac{(V_G^G)^2}{12\omega_G^2}$	$-\frac{2(V_H^G)^2}{3\omega_H^2}$	$(\theta_1^{(2)},\bar{0},0)_1,\ (\theta_1^{(2)},\bar{2},6)_2,\ (\theta_1^{(2)},\bar{4},\bar{2})_3,\ (\theta_1^{(2)},6,8)_4,\ (\theta_1^{(2)},8,\bar{4})_5$ $(\theta_2^{(2)},0,0)_1,\ (\theta_2^{(2)},\bar{2},\bar{6})_2,\ (\theta_2^{(2)},4,\bar{2})_3,\ (\theta_2^{(2)},6,\bar{8})_4,\ (\theta_2^{(2)},8,4)_5$ $(\frac{\pi}{4},5,5)_1,\ (\frac{\pi}{4},7,\bar{1})_2,\ (\frac{\pi}{4},\bar{9},7)_3,\ (\frac{\pi}{4},1,\bar{3})_4,\ (\frac{\pi}{4},3,\bar{9})_5$
(III)	$-\frac{(V_G^G)^2}{18\omega_G^2}$	$-\frac{25(V_H^G)^2}{36\omega_H^2}$	$(\theta_1^{(3)},5,5)_1,\ (\theta_1^{(3)},\bar{7},1)_2,\ (\theta_1^{(3)},9,\bar{7})_3,\ (\theta_1^{(3)},1,\bar{3})_4,\ (\theta_1^{(3)},\bar{3},9)_5$ $(\theta_2^{(3)},7,\bar{1})_6,\ (\theta_2^{(3)},\bar{9},7)_7,\ (\theta_2^{(3)},\bar{1},3)_8,\ (\theta_2^{(3)},3,\bar{9})_9,\ (\theta_2^{(3)},\bar{5},\bar{5})_{10}$
(IV)	$-\frac{3(V_G^G)^2}{4\omega_G^2}$	0	$(\frac{\pi}{4},5,\bar{5})_1,\ (\frac{\pi}{4},9,7)_2,\ (\frac{\pi}{4},1,3)_3,\ (\frac{\pi}{4},\bar{7},\bar{1})_4,\ (\frac{\pi}{4},\bar{3},\bar{9})_5$

Table 3.1: Results of the Öpik and Pryce analysis for $G\otimes g$ and $G\otimes h$.

the lowest APES has a functional form

$$\mathcal{E}(\{q\}) = \frac{1}{2}\sum_i q_i^2 + E(\{q\}), \tag{3.38}$$

where $E(\{q\})$ is the lowest root of

$$d = \det(\hat{\mathrm{H}}_{JT} - E(\{q\})\,\hat{\mathrm{i}}) = 0, \tag{3.39}$$

then the extremal conditions for $\mathcal{E}(\{q\})$ lead to:

$$\frac{\partial E}{\partial q_i} = -q_i \quad \forall\ i. \tag{3.40}$$

The curvature tensor of $\mathcal{E}(\{q\})$ is found by differentiating (3.38) twice yielding

$$\frac{\partial^2 \mathcal{E}}{\partial q_i \partial q_j} = \frac{\partial^2 E}{\partial q_i \partial q_j} + \delta_{ij}. \tag{3.41}$$

The expression for the curvature tensor of E may be obtained by differentiating (3.39) twice leading to an expression for $\frac{\partial^2 E}{\partial q_i \partial q_j}$ of the form

$$\frac{\partial^2 E}{\partial q_i \partial q_j} = \frac{\left(q_i \frac{\partial^2 d}{\partial E \partial q_j} + q_j \frac{\partial^2 d}{\partial E \partial q_i} - q_i q_j \frac{\partial^2 d}{\partial E^2} - \frac{\partial^2 d}{\partial q_i \partial q_j}\right)}{\frac{\partial d}{\partial E}}. \tag{3.42}$$

Equation (3.41) is the Hessian of the function $\mathcal{E}$ and an inspection of the eigenvalues of this matrix at an extremum yields the nature of that extremum. Note that all these considerations fail at a point where the root $E(\{q\})$ is degenerate with one or more of the upper sheets since an incremental displacement from this point may be upon any of these sheets. The eigenvalues of the Hessian (3.41) corresponding to the extrema appearing in Table (3.1) are given in Table (3.2).

Type	Hessian eigenvalues in $G \otimes g$	Hessian eigenvalues in $G \oslash h$
(I)	$(-2, 1, 1, 1)$	$(-5, 1, 1, -5, 1)$
(II)	Degeneracy	$(-\frac{1}{4}, 1, 1, \frac{5}{6}, \frac{5}{6})$
(III)	$(-\frac{5}{3}, 10, 1, -\frac{5}{3})$	$(1, \frac{1}{3}, 1, \frac{1}{3}, 1)$
(IV)	$(1, \frac{5}{6}, \frac{5}{6}, \frac{5}{6})$	Degeneracy

Table 3.2: Hessian eigenvalues for $G \otimes g$ and $G \otimes h$.

According to the Hessian eigenvalues (Table (3.2)), the natures of the four types of extremum are found to be:

Type (I): are low energy saddles in $G \otimes g$, and high energy saddles in $G \otimes h$.

Type (II): are degeneracies in $G \otimes g$, and low energy saddles in $G \otimes h$.

Type (III): are high energy saddles in $G \otimes g$, and minima in $G \otimes h$.

Type (IV): are minima in $G \otimes g$, and degeneracies in $G \otimes h$.

In Table (3.1), the extrema which correspond to the stable minima of $G \otimes g$ or $G \otimes h$, are numbered so that in subsequent calculations individual minima may be easily identified.

Each of the four types of extremum correspond to a symmetry lowering distortion of the icosahedron. The v-space representation of these distortions may be modelled directly onto computer generated icosahedra. This makes a visual identification of the symmetry lowering distortions possible. The distortions corresponding to the four types of solution are shown in the Figures (3.1), (3.2), (3.3), (3.4), (3.5); the dark circles represent outward distortions whilst the grey cubes represent inward distortions of the same magnitude. The figures corresponding to extrema of Types (I) and (III) are most conveniently derived from the v-space representation of $G \otimes h$, because the rotation matrices for the v-coordinates are exactly those appropriate to a d-tensor, i.e. derived from $J = 2$, which are easily calculated (with the use of Table(2.8)) and

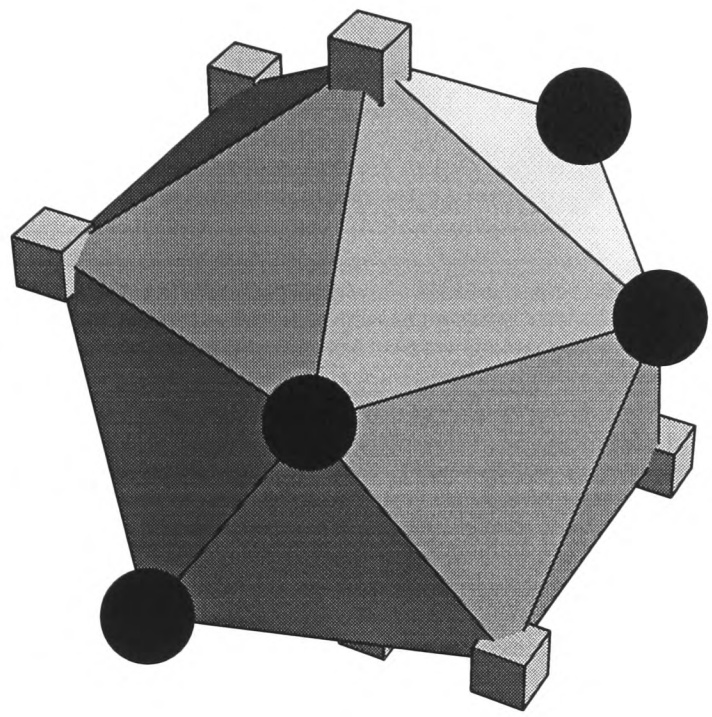

Figure 3.1: Type (I): $\mathcal{D}_3$ distortion in $G \otimes h$.

may be used to obtain an aspect for the figures which best reveals the salient features. Type (II) distortions are depicted in forms pertaining to both $G \otimes g$ and $G \otimes h$. The figure corresponding to Type (IV) extrema may only be derived from the v-space representation of $G \otimes g$, since this particular distortion cannot be constructed by h-modes. From these figures it is simple to deduce that:

Type (I): extrema reside at $\mathcal{D}_3$ epikernels in both $G \otimes g$ and $G \otimes h$.

Type (II): extrema reside at $\mathcal{T}$ epikernels in $G \otimes g$ and $\mathcal{D}_2$ epikernels in $G \otimes h$.

Type (III): extrema reside at $\mathcal{D}_3$ epikernels in both $G \otimes g$ and $G \otimes h$.

Type (IV): extrema reside at $\mathcal{T}$ epikernels in $G \otimes g$ and are zero distortions in $G \otimes h$.

From these considerations the extrema presented in Table (3.1) may be identified with those found by Ceulemans *et al.* [13] via: (I)$\rightarrow \gamma$, (II)$\rightarrow \delta$, (III)$\rightarrow \beta$, (IV)$\rightarrow \alpha$.

$H \otimes g$.

The method of Öpik and Pryce is difficult to use for $H \otimes g$ since there are five a_i to be found. *Mathematica* has difficulty reducing such complicated equations and no minimal or intermediate

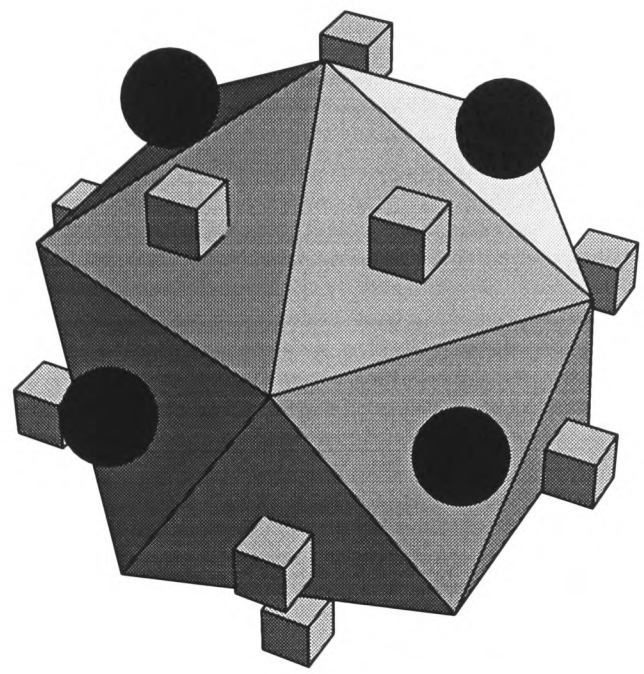

Figure 3.2: Type (II): $\mathcal{T}$ distortion in $G \otimes g$.

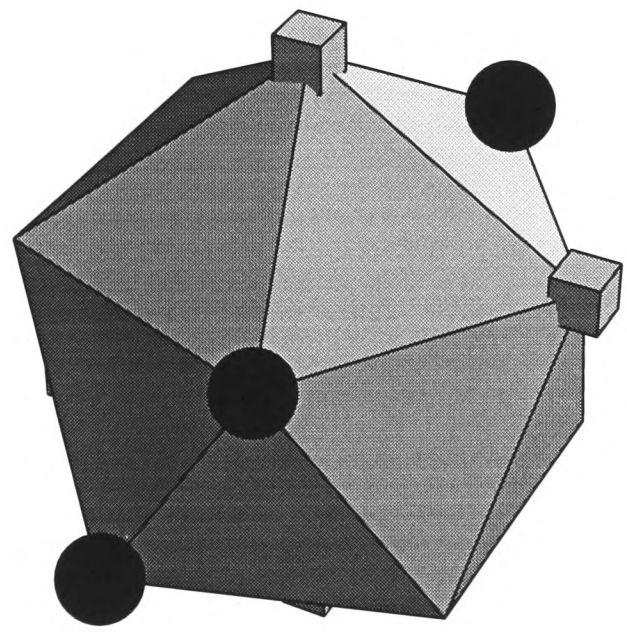

Figure 3.3: Type (II): $\mathcal{D}_2$ distortion in $G \otimes h$.

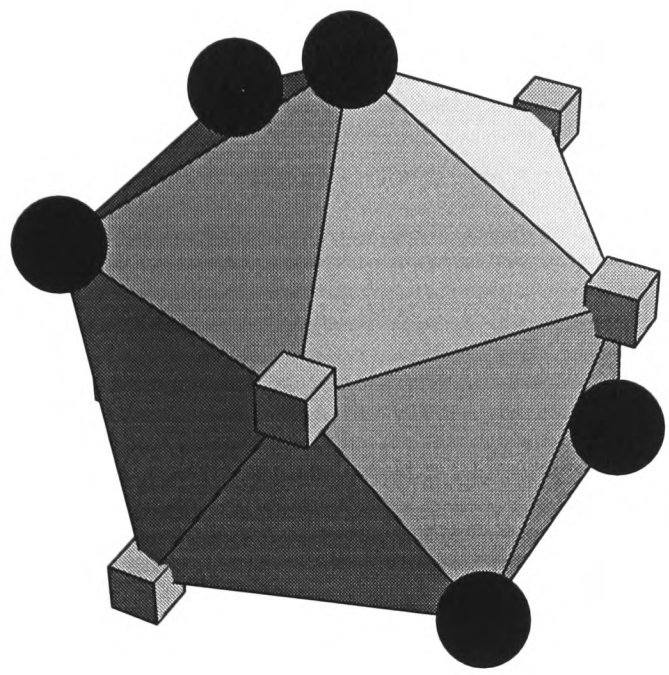

Figure 3.4: Type (III): $\mathcal{D}_3$ in $G \otimes h$.

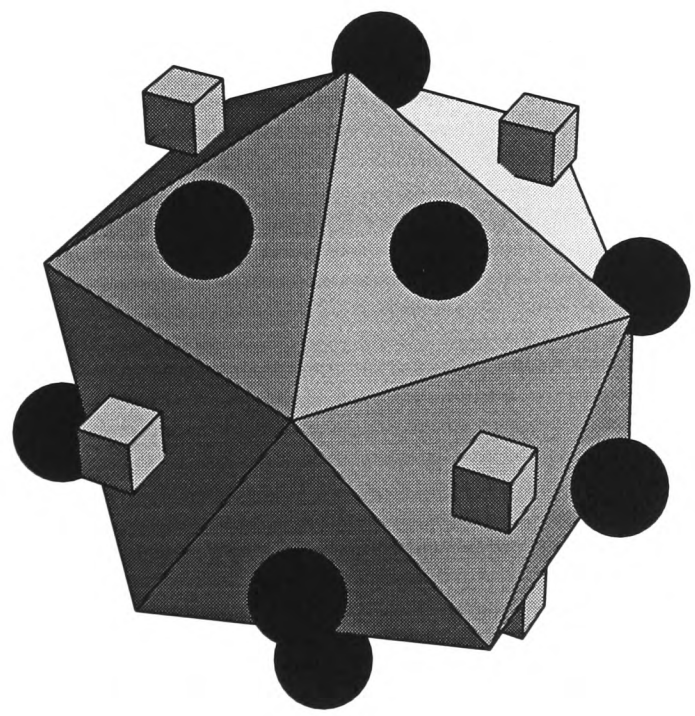

Figure 3.5: Type (IV): $\mathcal{T}$ in $G \otimes g$.

extremal coordinates for $H \otimes g$ are produced by this method. Only some points at T epikernels result from an Öpik and Pryce analysis of $H \otimes g$, which on closer inspection are shown to be degeneracies.

The epikernel symmetry under which at least one of the partners of both G and H transforms totally symmetrically, is that of $\mathcal{D}_3$. Therefore, according to the epikernel principle [15. 12. 16] (see Subsection (1.4.3)), the stable minima of $H \oslash g$ are most likely to reside at the $\mathcal{D}_3$ epikernels. The coordinates of the $\mathcal{D}_3$ points on the H electronic manifold may be derived from the v-coordinates of the same points in $G \oslash h$. For a given point m in $G \otimes h$ v-space, the corresponding vector in $H \otimes g$ f-space is just the projection of m onto a five-dimensional unit sphere. Introducing these f-space coordinates into the quadratic forms $\mathcal{Q}_{gi}^{H}$ (see Appendix (A.4)), where $i \in \{\alpha, \beta, \gamma, \delta\}$, yields the v-space coordinates of the $\mathcal{D}_3$ points in $H \otimes g$. The remainder of the Öpik and Pryce prescription outlined in Equations (3.36) and (3.37), reveals that these $\mathcal{D}_3$ points are extrema and correspond to an energy $-16(V_G^H)^2/45\omega_G^2$, where V_G^H and ω_G are respectively the coupling of g-modes to the H electronic state, and the frequency of these g-modes. The eigenvalues of the Hessian for $H \otimes g$ ((3.41) modified for $H \otimes g$) at these $\mathcal{D}_3$ points are $(1, 1/3, 1/3, 1)$, so the stable minima of $H \otimes g$ do indeed reside at $\mathcal{D}_3$ epikernels. This is the duality mentioned earlier between $G \otimes h$ and $H \otimes g$.

3.3.2 Reduction of the static vibronic ground state into icosahedral irreducible spaces.

The static vibronic ground states of $G \otimes g$, $G \otimes h$ and $H \otimes g$, by definition, occur at strong coupling (V_G^G, V_H^G, V_G^H are large) when the wells in the corresponding lowest APESs are deep and the nuclear motion is strongly confined to the minima. Under conditions such as these, the solution to the ground state nuclear motion may be represented by linear combinations of ground state harmonic oscillators centred at the minima of the lowest APES. The static ground state of nuclear motion is therefore N-fold degenerate, where N is the number of equivalent minima on the lowest APES. If tunnelling occurs between these minima, the N-fold degenerate static ground states will be linearly combined into icosahedral irreducible bases by the tunnelling matrix elements. The tunnelling effectively reduces the N-fold degenerate static ground state into icosahedral irreducible spaces.

The transformation that reduces the static ground state into icosahedral irreducible spaces, may be obtained as a "by-product" of the Öpik and Pryce analysis. This may be most easily illustrated in the context of $G \otimes g$. The v-representation of $G \otimes g$ is just a state space of all possible distortions which may be reached by the g-modes. The distortion state at a minimum

m of the lowest APES may be represented as a linear combination of the basis g-modes. The coefficient of the i^{th} g-mode in this linear combination, is just the value of the i^{th} vibration coordinate at m given by the Öpik and Pryce equation

$$Q_i(m) = -\left(\frac{1}{\omega_G^2}\right) \times \mathbf{a}^T(m) \cdot \left(\frac{\partial \hat{\mathrm{H}}_{JT}}{\partial Q_i}\right) \cdot \mathbf{a}(m), \qquad \begin{array}{l} i \in \{\alpha, \beta, \gamma, \delta\}. \\ m \in \{1, 2, 3, 4, 5\} \end{array} \tag{3.43}$$

A matrix $\hat{\mathbf{Q}}^{Gg}$ of elements $Q_i(m)$, with column index i and row index m, is a 4×5 matrix which describes how to construct a tetrahedral $\mathcal{T}$ distortion out of g-modes. This matrix, when column-normalized, forms part of the full orthogonal transformation which transforms the 5-fold degenerate $\mathcal{T}$ distortions into irreducible spaces of the icosahedral group. The full orthogonal transformation is then a 5×5 matrix with a 4×5 section containing the elements of the column-normalized $\hat{\mathbf{Q}}^{Gg}$. The remaining 1×5 section is the normalized column vector $\sqrt{1/5}(1, 1, 1, 1, 1)$. The resulting orthogonal transformation is denoted $\hat{\mathrm{T}}(\mathcal{T})$, and reduces the space of the five $\mathcal{T}$ distortions corresponding to the minima in $G \otimes g$, into irreducible spaces A and G of the icosahedral group. The explicit form of $\hat{\mathbf{Q}}^{Gg}$ is presented in Appendix (C).

Similar considerations may be applied to $G \otimes h$ and $H \otimes g$. The matrices of coordinates for the $\mathcal{D}_3$ minima in $G \otimes h$ and $H \otimes g$ are respectively $\hat{\mathbf{Q}}^{Gh}$ and $\hat{\mathbf{Q}}^{Hg}$. The orthogonal transformation which reduces the degenerate space of $\mathcal{D}_3$ distortions into icosahedral irreducible spaces is a 10×10 matrix with a 5×10 section containing the elements of the column-normalized $\hat{\mathbf{Q}}^{Gh}$ and a 4×10 section containing the elements of the column-normalized $\hat{\mathbf{Q}}^{Hg}$. The remaining 1×10 section is taken up by the normalized column vector $\sqrt{1/10}(1, 1, 1, 1, 1, 1, 1, 1, 1, 1)$. The resulting transformation is denoted $\hat{\mathrm{T}}(\mathcal{D}_3)$ and reduces the space of the ten $\mathcal{D}_3$ distortions corresponding to the minima in $G \otimes h$ and $H \otimes g$, into irreducible spaces A, G and H of the icosahedral group. The explicit forms of both $\hat{\mathbf{Q}}^{Gh}$ and $\hat{\mathbf{Q}}^{Hg}$ are presented in Appendix (C).

$\hat{\mathrm{T}}(\mathcal{T})$ and $\hat{\mathrm{T}}(\mathcal{D}_3)$ are transformations which describe the effect of tunnel splitting in the static ground states of $G \otimes g$, $G \otimes h$ and $H \otimes g$. However, these transformations do not possess information pertaining to the ordering of this splitting. Once again, this information may be obtained by considering the wave fuction boundary conditions via an analysis of the Berry phase on the lowest APES.

3.3.3 The Berry phase on the lowest APES and tunnel splitting of the Jahn-Teller ground states.

The many extrema and degeneracies present in the lowest APESs of $G \otimes g$, $G \otimes h$ and $H \otimes g$, make an analysis of Berry phases induced over adiabatic circuits in these surfaces a very complicated

task. Tracking the phase of the electronic state upon these surfaces is further complicated by the fact that there is no intrinsic way of relating the phase of states calculated at two neighbouring points on the lowest APES. A computational method overcomes these problems by calculating the electronic eigenstate numerically over a circuit, adjusting the overall sign of the eigenstates at each point on the circuit so that the first component is always positive. This produces continuity except where the first component would naturally pass through zero. The number of discontinuities are then counted, which should of course occur at the same points for each component. If this number is odd, then the eigenstate will have changed sign an odd number of times implying an overall Berry phase change of π on completion of the adiabatic circuit. An Example of this phase tracking for a path on the lowest APES of G$\oslash h$ is given in Figure 3.6. The phase tracking analyses for $G \otimes g$, $G \otimes h$ and $H \otimes g$ are treated separately below:

(A) G$\otimes g$.

The g-modes may be parametrized in the same way as the G bases (see Equation (3.11)):

$$\begin{aligned} q_\alpha &= q\cos\theta\cos\alpha \\ q_\beta &= q\cos\theta\sin\alpha \\ q_\gamma &= q\sin\theta\cos\beta \\ q_\delta &= q\sin\theta\sin\beta. \end{aligned} \tag{3.44}$$

The energy eigenvalues may then be plotted in the sub-space q =constant. The minima all occur at $\theta = \pi/4$, so that this sub-surface may be taken as defining a base plane and α and β may be plotted along cartesian axes in this plane. Due to the periodicity in α and β, this has the effect of plotting this subspace onto a unit cell of a two-dimensional cubic lattice.

This base plane also contains points where the lowest APES is triply degenerate. These points correspond to tetrahedral $\mathcal{T}$ distortions of opposite sign to those giving minima (see Type (II) entries for $G \otimes g$ in Table (3.1)). On the base plane, these degeneracies appear at the face-centres of the lattice of minima. In order to obtain the rest of the subspace, the θ coordinate is plotted along the vertical axis perpendicular to the base plane. In Figure 3.7 the gap between the two lowest eigenvalues of $G \otimes g$ is plotted across this base plane, and the minima and threefold degeneracy points are clearly visible. The nature of the three-fold degeneracies may be studied by considering the subduction of G irreps at these points. The three-fold degeneracies correspond to $\mathcal{T}$ epikernels, and in an environment of $\mathcal{T}$ symmetry, the G irrep transforms as $A \oplus T$ of $\mathcal{T}$. Since the T modes (from $G \rightarrow A \oplus T$) at a triple degeneracy are available for further distortion, a $\mathcal{T}$ epikernel of $G \otimes g$ is subject to a $T \otimes \tau$ Jahn-Teller instability. Therefore, the $\mathcal{T}$ epikernels

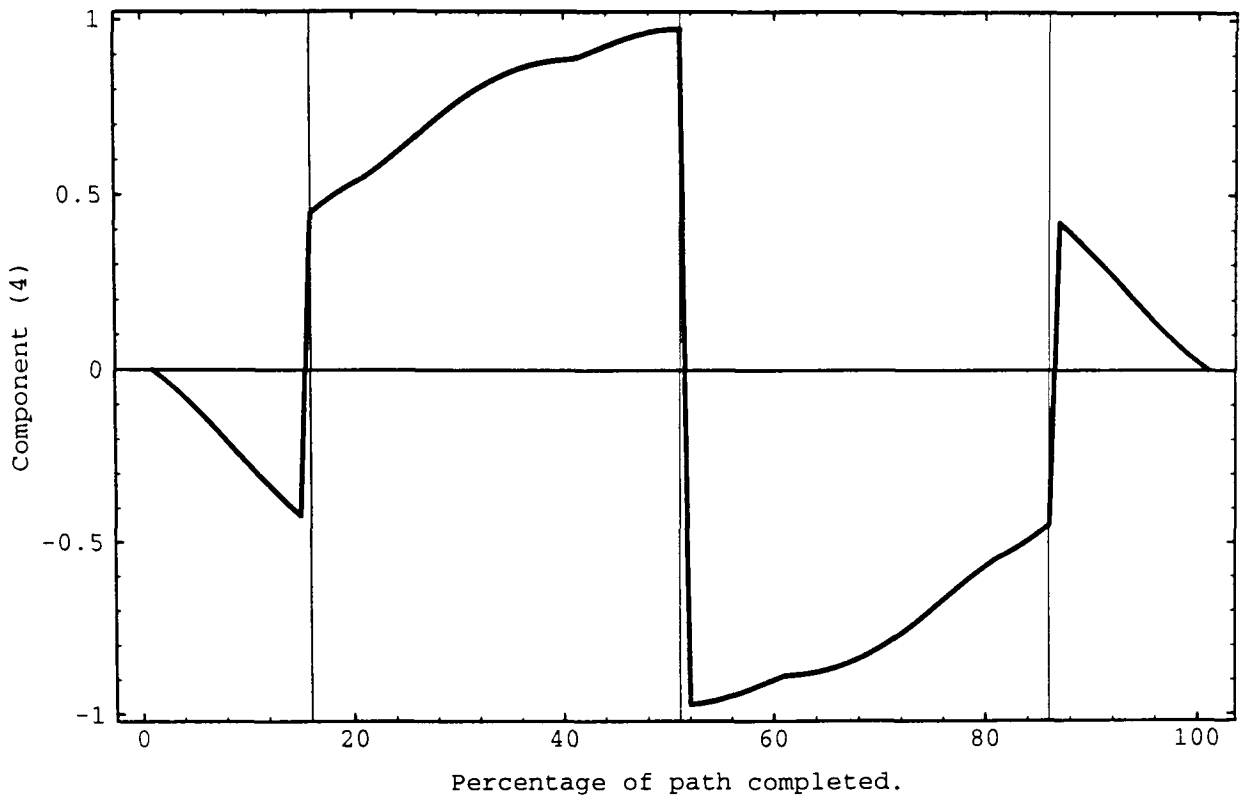

Figure 3.6: This plot shows the tracking of the fourth component of an electronic eigenstate around a closed path in the v-space of G$\otimes h$. On this path, the plot makes it obvious that three sign changes will ensure continuity, so there is a phase change of π around the complete path.

in $G \otimes g$ have four lines of two-fold degeneracy radiating from them towards the vertices of a tetrahedron; two lines above the base plane and two lines below it [74]. The degeneracies may be tracked throughout phase space by taking "slices" along the θ coordinate axis. The lines of degeneracy are found to pass from one three-fold degeneracy to the next, half of them looping above the base plane and half of them looping below the base plane. A numerical scan of the difference between the two lowest eigenvalues of $G \otimes g$ across planes above and below the base plane, picks up these lines of degeneracy again and shows where they terminate (Figure 3.8).

The saddle points on the lowest APES (Type (I) extrema) are located at the same value of $|\theta - \pi/4|$, half with $\theta > \pi/4$ and half with $\theta < \pi/4$,and with values of α and β that correspond to points on the base plane that are halfway between neighbouring minima as well as being halfway between neighbouring threefold degeneracy points.

Using the phase tracking method described in Subsection (3.3.3), the various adiabatic circuits that produce Berry phase changes in the eigenvector may be analysed. One set of such circuits pass from minimum to minimum, starting and terminating at two copies of the same minimum. To understand how this type of path induces such a sign change, it is necessary to imagine "rolling up" the unit cell, and counting the number of lines of degeneracy that are enclosed by the resulting cylinder. For real states in a many dimensional phase space, tracking the phase

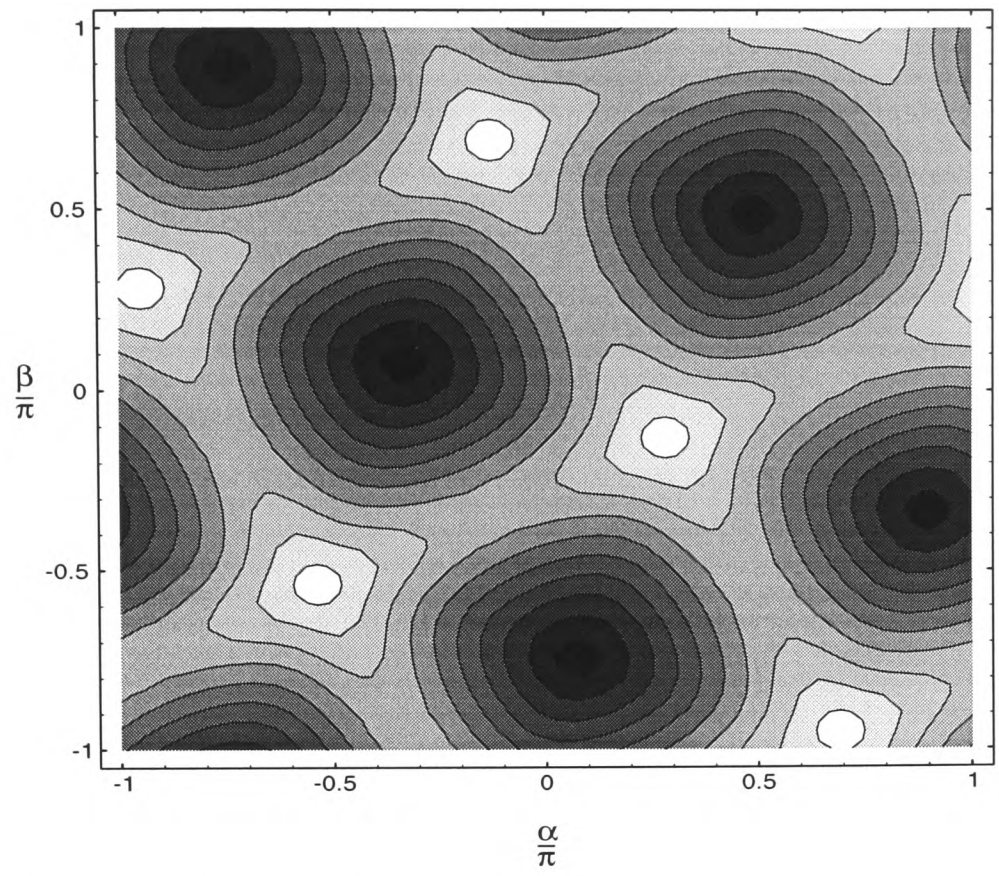

Figure 3.7: A contour plot of the difference in energy between the two lowest APES's for G$\otimes g$. The minima appear as circular wells and the three-fold degeneracies as squarish peaks.

around a closed loop produces a phase change of π for every line of degeneracies that intersects the loop [9, 1] (see Section (1.5)). Since the cylinder corresponding to a circuit between two copies of the same minimum is found to encircle an odd number of degeneracy lines, the overall phase change in the eigenstate on completing such a loop must be π.

The two real eigenvectors of opposite sign corresponding to each of the minima in v-space appear as a pair of antipodal eigenstates in f-space. The eigenstate at the i^{th} minimum is denoted $|m_i\rangle$ and its antipodal equivalent is denoted $|\bar{m}_i\rangle$. From the conclusions of the phase studies a consistent account of the relative phases may be produced if the following rule is implemented: If an eigenstate is transported on the G$\otimes g$ lowest APES from the i^{th} to j^{th} to k^{th} to etc.. minima, the eigenstate passes from $|m_i\rangle$ to $|\bar{m}_j\rangle$ to $|m_k\rangle$ to etc... eigenstates.

(B) $G \otimes h$.

For this case, the lowest APES may be parametrized in terms of the coordinates $\{Q, \alpha, \gamma, \theta, \phi\}$ [72] as follows:

$$\begin{aligned} q_\theta &= Q((1/2)(3\cos^2\theta - 1)\cos\alpha + (1/2)\sqrt{3}\sin^2\theta\sin\alpha\cos 2\gamma), \qquad (3.45) \\ q_\epsilon &= Q((1/2)\sqrt{3}\sin^2\theta\cos 2\phi\cos\alpha + (1/2)(1+\cos^2\theta)\cos 2\phi\sin\alpha\cos 2\gamma \end{aligned}$$

$$
\begin{aligned}
& - \cos\theta \sin 2\phi \sin\alpha \sin 2\gamma), \\
q_x &= Q((1/2)\sqrt{3}\sin 2\theta \sin\phi \cos\alpha - (1/2)\sin 2\theta \sin\phi \sin\alpha \cos 2\gamma \\
& - \sin\theta \cos\phi \sin\alpha \sin 2\gamma), \\
q_y &= Q((1/2)\sqrt{3}\sin 2\theta \cos\phi \cos\alpha - (1/2)\sin 2\theta \cos\phi \sin\alpha \cos 2\gamma \\
& + \sin\theta \sin\phi \sin\alpha \sin 2\gamma), \\
q_z &= Q((1/2)\sqrt{3}\sin^2\theta \sin 2\phi \cos\alpha + (1/2)(1+\cos^2\theta)\sin 2\phi \sin\alpha \cos 2\gamma \\
& + \cos\theta \cos 2\phi \sin\alpha \sin 2\gamma),
\end{aligned}
$$

where $0 \leq Q < \infty$, $0 \leq \alpha < \pi/3$, $0 \leq \gamma < \pi$, $0 \leq \theta < \pi/2$, $0 \leq \phi < 2\pi$, so that all possible distortions in the five dimensional phase space are covered. In Subsection (2.2.4), a third order $SO(3)$ invariant, $((2H \times 2H)_{2H} \cdot 2H)_A \equiv ((d \times d)_d \cdot d)_s$ (see Equation (2.33)), is constructed in terms of the $\{qh_i\}$ and is greatly simplified in terms of the parameterization in (3.45):

$$
\begin{aligned}
((2H \times 2H)_{2H} \cdot 2H)_A &= \sum_{ijk} (H\ j; 2H\ k | H\ i) q_i q_j q_k \qquad (3.46) \\
& \quad i,j,k \in \{\theta, \epsilon, x, y, z\} \\
&= -6q_\epsilon^2 q_\theta + 2q_\theta^3 - 3\sqrt{3}q_\epsilon q_x^2 + 3q_\theta q_x^2 + 3\sqrt{3}q_\epsilon q_y^2 \\
& \quad +3q_\theta q_y^2 + 6\sqrt{3}q_x q_y q_z - 6q_\theta q_z^2 \\
&= Q^3 \cos 3\alpha.
\end{aligned}
$$

The α value for all the minima is found to be zero which means that the positions of the minima only have a θ, ϕ dependence. If the θ range is doubled, the θ, ϕ dependence is consistent with placing two copies of the same minima at the vertices of a dodecahedron embedded in the full five dimensional parameter space. A plot of this subspace of the lowest APES (the $\alpha = 0$ surface) is shown in Figure 3.9.

This geometry simplifies greatly the phase tracking since the proximity of minima to neighbouring minima is immediately obvious in terms of an easily visualized structure. For the Type (II) saddle points we find $\cos 3\alpha = \sqrt{27/32}$, and although they do not lie on the same α-surface as the minima, a calculation of the distances between Type (II) extrema shows that these saddle points may be considered as occupying the centres of the edges of the dodecahedron. The centres of the faces of the dodecahedron in the $\alpha = 0$ surface are two-fold degeneracies on the lowest APES. Tracking the phase numerically along paths between neighbouring minima via the saddle points between them shows that there are sign changes in the eigenstate corresponding to two specific types of path. First, a circuit around a pentagonal face of the dodecahedral surface in (Q, θ, ϕ)-space results in a path enclosing a degeneracy (path I Figure 3.10). Taking path II in

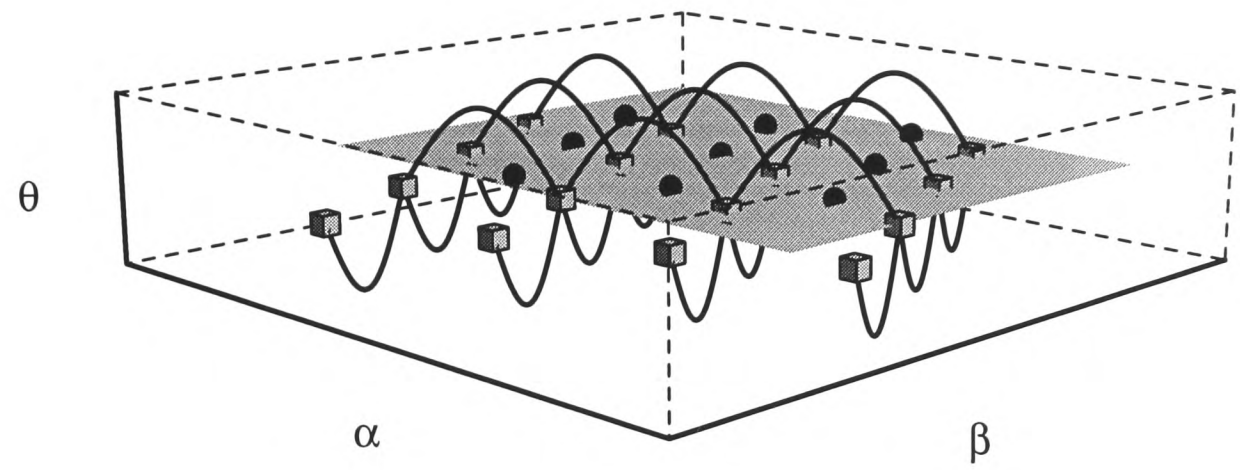

Figure 3.8: This figure shows, schematically, the lines of degeneracy above and below the plane $\theta = \pi/4$ for G$\otimes g$. Cubes mark points of threefold degeneracy and dots mark positions of minima.

Figure 3.10 also induces a phase change of π in the eigenstate, though in this representation it is not obvious that the path encloses a degeneracy. A simple re-labelling of the dodecahedron, making sure that nearest neighbour minima remain the same, shows that when viewed on Figure 3.11, path II does indeed enclose a degeneracy. Similarly, paths that induce sign changes but do not seem to enclose degeneracies in Figure 3.11 are seen to enclose degeneracies in Figure 3.10. It is therefore necessary to view any circuit on the lowest APES in terms of the two dodecahedra in order to see whether or not a degeneracy has been enclosed. The Berry phase properties of the eigenstates are found to be correctly reproduced by implementing the rule introduced in (A); that is, if an eigenstate is transported on the G$\otimes h$ lowest APES from the i^{th} to j^{th} to k^{th} to etc.. minima, the eigenstate passes from $|m_i\rangle$ to $|\bar{m}_j\rangle$ to $|m_k\rangle$ to etc... eigenstates.

(C) $H \otimes g$.

The ten equivalent minima in H$\otimes g$ correspond to $\mathcal{D}_3$ distortions of the icosahedron. The co-ordinates of these points in phase space are just the rows of the matrix $\hat{\mathrm{Q}}^{Hg}$ in Appendix (C). Other special points on the lowest APES are as follows: A set of points of $\mathcal{D}_3$ symmetry that are not minima are degeneracies. Points in phase space corresponding to $\mathcal{T}$ distortions are either two-fold or three-fold degenerate. The three-fold degeneracies have lines of degeneracy running between them, and passing through those points of trigonal symmetry that are not minima. Thus the lines of degeneracy make a pattern in (θ, α, β) space that is not unlike that of the lines of degeneracy in G$\otimes g$. These properties have also been established by means of various numerical

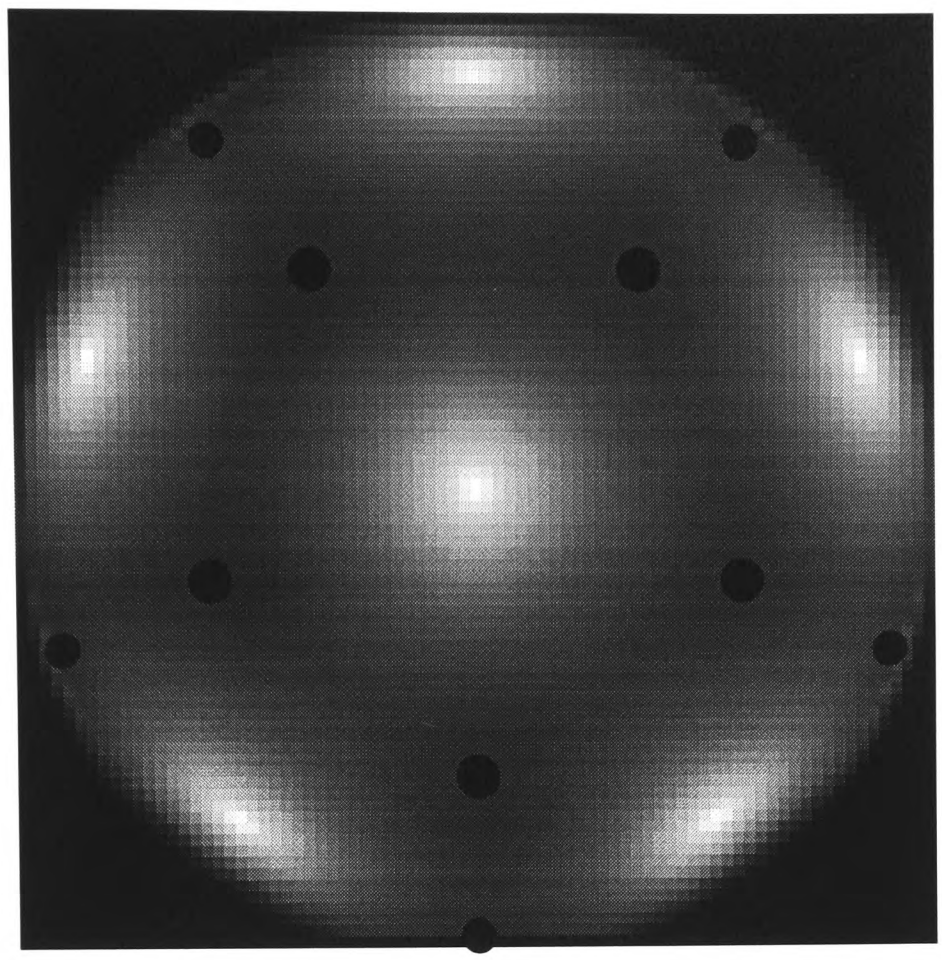

Figure 3.9: A density plot of the lowest APES for the G$\otimes h$ interaction projected onto spherical geometry. Dark areas indicate lower energy, black discs mark minima. Peaks in the energy, which appear white, are also degeneracies and occur at points of fivefold symmetry.

scans. Phase tracking for H$\otimes g$ is slightly more complicated. The simplest paths are between adjacent minima. When the distances between minima in phase space are calculated, each of the minima on the lowest APES of H$\otimes g$ has six others as equally near neighbours. The phases are traced along closed paths passing via neighbouring minima. Wherever such paths traverse an odd number of minima there is a Berry phase change of π, whereas an even number of minima gives no phase change. This is consistent with the rule in (A) which is also applied to this system to take proper account the Berry phase of the transported eigenstate.

The tunnel splitting of vibronic ground states in G$\otimes g$, G$\otimes h$ and H$\otimes g$ at strong coupling.

In the following a WKB approximation is used which allows a small amount of tunnelling between minima and nearest neighbour minima only. The Jahn-Teller system is now *dynamical* and the lowest states, as given by this WKB approximation, will be linear combinations of wave functions corresponding to ground state harmonic oscillators (GSHO) in each minimum of the lowest APES. These linear combinations must be invariant under the operations of the symmetry

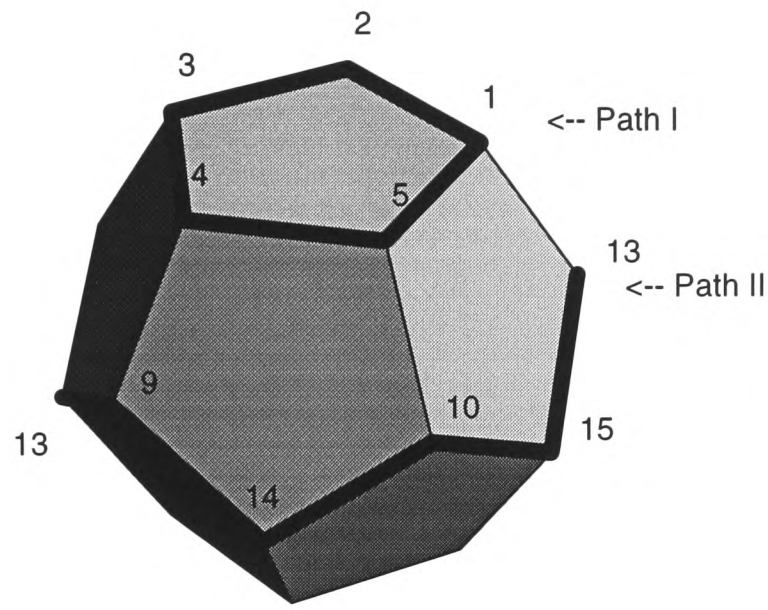

Figure 3.10: The two paths shown both induce Berry phase changes of π on the eigenstate.

group of the Jahn-Teller centre. This amounts to saying that a translation that takes a point from one minimum to another copy of itself must leave the full vibronic wave function invariant. Therefore, wherever this translation changes the sign of the electronic basis, the change of sign must be compensated for by a corresponding change of sign in the vibrational wave function so that the full vibronic wave function is unchanged. The GSHOs in the minima must therefore obey a similar rule to that imposed on the electronic eigenstates on transportation from minimum to minimum (see (A)). Let the GSHO in the i^{th} minimum be Φ_i so that its antipodal equivalent be $-\Phi_i$. The full vibronic wave function in the i^{th} minimum is then $\Phi_i|m_i\rangle$ which equals $-\Phi_i|\bar{m}_i\rangle$. This is the required invariance of the vibronic state under a translation from one minimum to another copy of itself.

The distribution of nearest neighbour minima for a system $\Gamma \otimes \lambda$, may be represented in the form of a matrix $\hat{\mathrm{S}}^{\Gamma\lambda}$, the bases of which are the kets that correspond to the minima in v-space listed as rows of the matrix $\hat{\mathrm{Q}}^{\Gamma\lambda}$. $\hat{\mathrm{S}}^{\Gamma\lambda}$ is a matrix of overlaps between nearest neighbour minima on the lowest APES of $\Gamma \otimes \lambda$. The elements $S_{i,j}^{\Gamma\lambda}$, of $\hat{\mathrm{S}}^{\Gamma\lambda}$, are $-S$, where S is the value of the overlap integral between two neighbouring GSHOs, if minimum i and minimum j are nearest neighbour minima and zero if minimum i and j are not. The negative value of the overlap is a consequence of the sign change of the GSHOs as one translates from minimum to minimum.

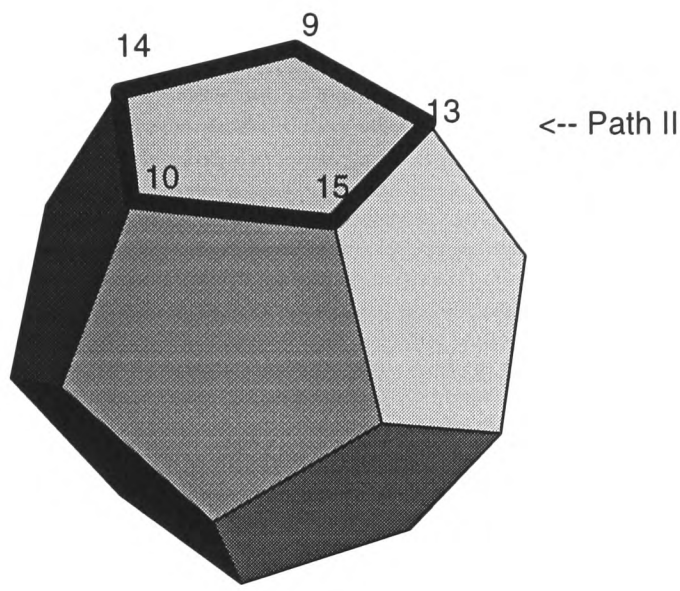

Figure 3.11: The path shown encloses a degeneracy after the relabelling of the dodecahedral vertices.

In the case of $G \otimes g$, the overlap matrix $\hat{\mathrm{S}}^{Gg}$ has a relatively simple form given in Table (3.3), which may be easily diagonalized yielding an eigensystem which is four-fold degenerate at an overlap of $+S$ and singlet at an overlap of $-4S$.

The linear combinations of GSHOs which diagonalize $\hat{\mathrm{S}}^{Gg}$ are just the columns of the matrix $\hat{\mathrm{T}}(\mathcal{T})$ which reduces the space of $\mathcal{T}$ minima into irreducible spaces A and G. When properly normalized to account for the overlap between nearest neighbour minima, these linear combinations may be used to obtain expectation values of the nuclear motion Hamiltonian in the WKB approximation. These expectations are found to be:

$$\begin{aligned} \langle \phi_A | H | \phi_A \rangle &= E_A = \frac{H_{11} - 4H_{12}}{1 - 4S}, \\ \langle \phi_G | H | \phi_G \rangle &= E_G = \frac{H_{11} + H_{12}}{1 + S}, \end{aligned} \tag{3.47}$$

where ϕ_A and ϕ_G are linear combinations of GSHOs transforming as A and G respectively. $H_{11} = E$ is the expectation value of the nuclear motion Hamiltonian, H, in the GSHO at any one of the minima, and H_{12} is a matrix element of H between two GSHOs in nearest neighbour minima. The tunnel splitting in this strong coupling approximation is found to be

$$E_A - E_G \approx 5(ES - H_{12}) = \frac{5}{\sqrt{4\pi}} \exp\left(-I_T - 1/2\right), \tag{3.48}$$

	min 1	min 2	min 3	min 4	min 5
min 1	0	$-S$	$-S$	$-S$	$-S$
min 2	$-S$	0	$-S$	$-S$	$-S$
min 3	$-S$	$-S$	0	$-S$	$-S$
min 4	$-S$	$-S$	$-S$	0	$-S$
min 5	$-S$	$-S$	$-S$	$-S$	0

Table 3.3: Overlap matrix $\hat{\mathrm{S}}^{Gg}$

where I_T is a tunnelling integral. The second expression in (3.48) is obtained by using the O'Brien expression for H_{12} given in [74]. The value of the tunnel splitting in (3.48) is positive which implies that the ground state is the G quartet below a tunnelling A singlet. This is consistent with the nature of the overlaps since one may show by considering the curvature of the wave function, that maximum overlap leads to minimum energy.

The corresponding calculation for $G \otimes h$ and $H \otimes g$ involves the two overlap matrices $\hat{\mathrm{S}}^{Gh}$ and $\hat{\mathrm{S}}^{Hg}$ respectively. These two matrices are constructed in the same way as $\hat{\mathrm{S}}^{Gg}$. The 10×10 matrix $\hat{\mathrm{S}}^{Gh}$, given in Table (3.4), has three off-diagonal non-zero elements in each row corresponding to an overlap of $-S$ between nearest neighbour minima.

The 10×10 matrix $\hat{\mathrm{S}}^{Hg}$, given in Table (3.5), has the other six off-diagonal elements in each row non-zero, corresponding to an overlap of $-S$ between nearest neighbour minima. The transformation that diagonalizes $\hat{\mathrm{S}}^{Gh}$ and $\hat{\mathrm{S}}^{Hg}$ is then just $\hat{\mathrm{T}}(\mathcal{D}_3)$ (defined in 3.3.2) which reduces the space of $\mathcal{D}_3$ minima in both $G \otimes h$ and $H \otimes g$ to the irreducible spaces A, G and H of the icosahedral group. For G$\otimes h$, the diagonalization yields a G quartet, an H quintet and an A singlet of states corresponding to the overlap eigenvalues $2S$, $-S$ and $-3S$ respectively. By the same argument as before [74], $G \otimes h$ is found to exhibit a G ground state below an H quintet and A singlet in that order. The energies of the low lying states in $G \otimes h$ at strong coupling are

$$\begin{aligned} E_A &= \frac{H_{11} - 3H_{12}}{1 - 3S}, \\ E_H &= \frac{H_{11} - H_{12}}{1 - S}, \\ E_G &= \frac{H_{11} + 2H_{12}}{1 + 2S}. \end{aligned} \tag{3.49}$$

For H$\otimes g$, the diagonalization yields an H quintet, a G quartet and an A singlet of states corresponding to the overlap eigenvalues $2S$, $-S$ and $-6S$ respectively. By the same argument as

	min 1	min 2	min 3	min 4	min 5	min 6	min 7	min 8	min 9	min 10
min 1	0	0	$-S$	$-S$	0	0	0	0	0	$-S$
min 2	0	0	0	$-S$	$-S$	$-S$	0	0	0	0
min 3	$-S$	0	0	0	$-S$	0	$-S$	0	0	0
min 4	$-S$	$-S$	0	0	0	0	0	$-S$	0	0
min 5	0	$-S$	$-S$	0	0	0	0	0	$-S$	0
min 6	0	$-S$	0	0	0	0	$-S$	0	0	$-S$
min 7	0	0	$-S$	0	0	$-S$	0	$-S$	0	0
min 8	0	0	0	$-S$	0	0	$-S$	0	$-S$	0
min 9	0	0	0	0	$-S$	0	0	$-S$	0	$-S$
min 10	$-S$	0	0	0	0	$-S$	0	0	$-S$	0

Table 3.4: Overlap matrix $\hat{\mathrm{S}}^{Gh}$

before [74], H$\otimes g$ is found to exhibit an H ground state below a G quartet and A singlet in that order. The energies of the low lying states of $H \otimes g$ at strong coupling are

$$\begin{aligned} E_A &= \frac{H_{11} - 6H_{12}}{1 - 6S}, \\ E_G &= \frac{H_{11} - H_{12}}{1 - S}, \\ E_H &= \frac{H_{11} + 2H_{12}}{1 + 2S}. \end{aligned} \tag{3.50}$$

In both G$\otimes h$ and H$\otimes g$, the linear combinations of GSHOs corresponding to the overlap eigenvalues are therefore just the columns of the matrix $\hat{\mathrm{T}}(\mathcal{D}_3)$.

3.4 The Berry phase and ground states in G$\otimes(g \oplus h)$ at other relative couplings of g and h.

The lowest APES of G$\otimes(g \oplus h)$ has two different structures depending on which of the two modes, g or h, gives rise to the larger Jahn-Teller stabilization energy. If the coupling to both sets of modes is included in the Öpik and Pryce equations (3.3.1), then the solutions are the same as for the two modes separately, so all the solutions are as listed in Table (3.1). The turning point energies may be plotted accordingly against the relative coupling strength, as is done in Figure 3.12. On Figure 3.12 it is very obvious that only three situations arise. Whenever the g coupling

	min 1	min 2	min 3	min 4	min 5	min 6	min 7	min 8	min 9	min 10
min 1	0	$-S$	0	0	$-S$	$-S$	$-S$	$-S$	$-S$	0
min 2	$-S$	0	$-S$	0	0	0	$-S$	$-S$	$-S$	$-S$
min 3	0	$-S$	0	$-S$	0	$-S$	0	$-S$	$-S$	$-S$
min 4	0	0	$-S$	0	$-S$	$-S$	$-S$	0	$-S$	$-S$
min 5	$-S$	0	0	$-S$	0	$-S$	$-S$	$-S$	0	$-S$
min 6	$-S$	0	$-S$	$-S$	$-S$	0	0	$-S$	$-S$	0
min 7	$-S$	$-S$	0	$-S$	$-S$	0	0	0	$-S$	$-S$
min 8	$-S$	$-S$	$-S$	0	$-S$	$-S$	0	0	0	$-S$
min 9	$-S$	$-S$	$-S$	$-S$	0	$-S$	$-S$	0	0	0
min 10	0	$-S$	$-S$	$-S$	$-S$	0	$-S$	$-S$	0	0

Table 3.5: Overlap matrix $\hat{\mathrm{S}}^{Hg}$

predominates the minima are of Type (IV) and the path of lowest energy between them goes via the Type (I) saddle points. Conversely if the h coupling is strongest, the minima are of Type (III) and the intermediate saddle points are of Type (II). In the case of equal coupling all the above points coincide in energy and lie on the minimum energy hypersphere of $G \otimes (g \oplus h)_{eq}$ (see 3.2).

To discuss the complete structure of degeneracies and Berry phases over the full nine dimensional phase space of G$\otimes(g \oplus h)$ would be a mammoth task. Indeed, it is a task that has not been completed for even the four and five dimensional phase spaces of the subsystems G$\otimes g$ and G$\otimes h$. What has been done and what is needed now is to understand how the phases change over the minimum energy tunnelling paths between minima. Figure 3.12 shows that at all relative coupling strengths the minima and the minimum energy paths connecting them are either the same or closely related to those calculated for the g and h mode régimes separately. This means that if the coupling to one phonon type alone is modified by increasing the influence of the other phonon type, the topology of the minima, the tunnelling paths that connect them, the phases and the ground states will be constructed in just the same way as before.

In the case where the g modes dominate, the five minima are of Type (IV), with $q_i = 0$, $i \in \{\theta, \epsilon, x, y, z\}$, and the minimum energy path available for tunnelling is via the Type (I) saddles. The difference now is that the coupling to the h modes reduces the energy of the saddles, but

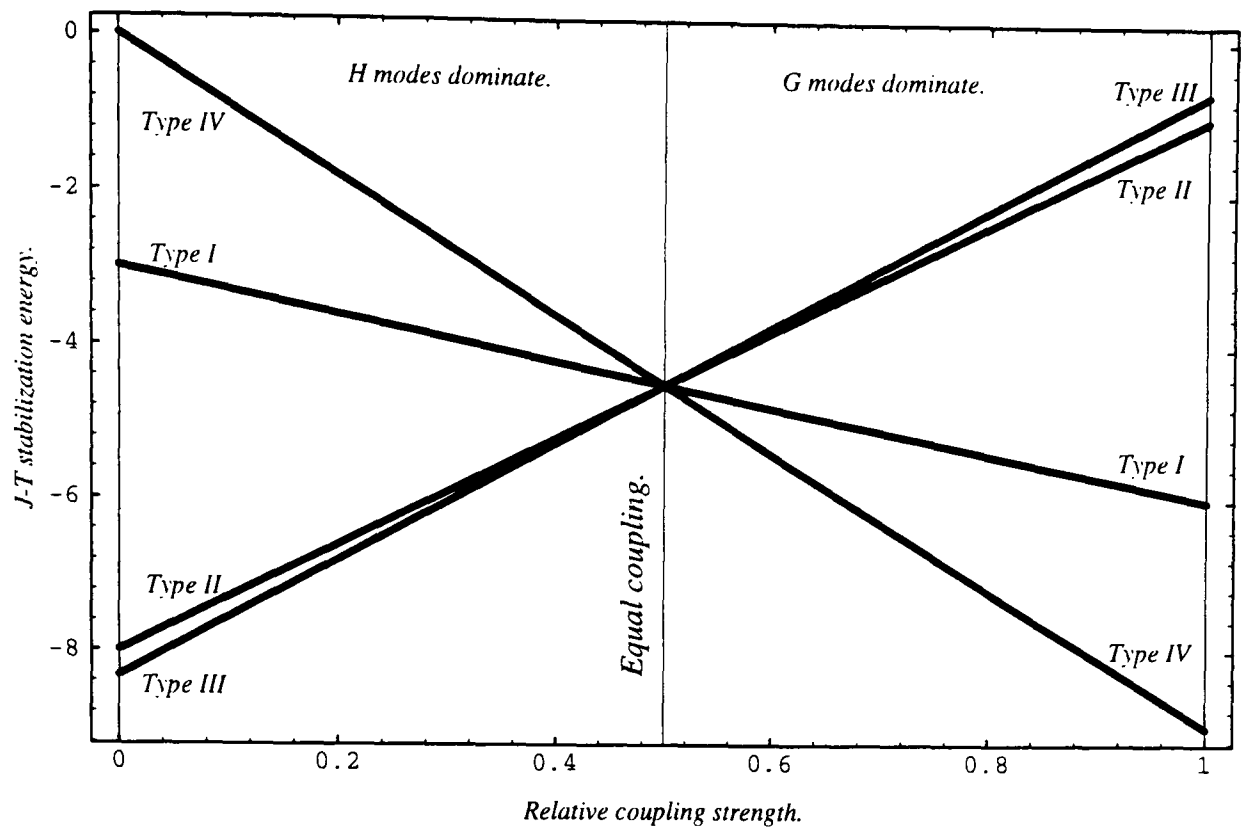

Figure 3.12: The energies of the Öpik and Pryce extremal points in $G \otimes (g \oplus h)$, showing how they vary with relative coupling strength. The energies in this figure are given in arbitrary units for the three different régimes.

increases the length of the minimum energy tunnelling paths. The path that dominates the tunnelling energy will be a compromise between these two effects, but as long as the old path can be continuously distorted into the new one without crossing a degeneracy on the lowest APES, the phase relationships will be preserved. As the system approaches $G \otimes (g \oplus h)_{eq}$, the coordinates of the Type (IV) $\mathcal{T}$ minima on hypersphere remain as given in Table (3.1). All these points lie on hypersphere at a θ value of $\pi/4$. forming a lattice of these points and their antipodal equivalents on the (α, β) surface. The phase relationships between these points (and their antipodal equivalents) are found to be consistent with the phase changes of the $G \otimes (g \oplus h)_{eq}$ eigenstate (equation(3.11)), so the argument for identifying the vibronic ground states may be carried through from $G \otimes g$ coupling to equal coupling at $G \otimes (g \oplus h)_{eq}$.

In a similar vein, the system may be examined as it approaches $G \otimes (g \oplus h)_{eq}$ from $G \otimes h$. The f-space coordinates of the $G \otimes h$ minima are given in Table (3.1). In this case as the strength of the g distortions are increased, the points corresponding to $\mathcal{D}_3$ symmetry remain mutually equidistant. As the system approaches $G \otimes (g \oplus h)_{eq}$, the tunnelling between the $\mathcal{D}_3$ points is still via the Type (II) saddles. The coupling to the g modes reduces the energy of these saddles, but

increases the length of the minimum energy tunnelling paths. The form of the overlap matrix between the $\mathcal{D}_3$ points remains unchanged until the system reaches the equal coupling régime. so the argument for identifying the vibronic ground states may be carried through from G$\oslash h$ coupling, to equal coupling at G$\otimes(g \oplus h)_{eq}$.

3.5 Summary of Chapter 3.

An analysis of $G \otimes (g \oplus h)$ may be facilitated by a three level descent in symmetry originating in the $SO(4)$ parent symmetry. The "highest" of these three levels corresponds to $G \oslash (g \oplus h)_{eq}$, and may be analysed in terms of a biharmonic parametrization. This parametrization simplifies the visualization of the electronic manifold and assists the analysis of Berry phases accompanying adiabatic transport over circuits in the parameter space. The minimum energy hypersurface of $G \otimes (g \oplus h)_{eq}$ is a "trough" embedded in the full nine dimensional parameter space. The solutions of the Schrödinger equation of motion in this trough are pseudo-rotational with a displaced (from the origin of coordinates) harmonic oscillation as the radial motion. The correct ground state degeneracy of four, may be recovered by appealing to the Berry phase analysis which only selects those solutions which exhibit the correct cyclic boundary conditions.

The interactions $G \otimes g$, $G \otimes h$ and $H \otimes g$, reside in the next levels of the symmetry descent corresponding to I and the lower point groups resulting from symmetry lowering distortions. In all three systems, there are more equivalent distortions corresponding to the static ground states than the multiplicity of the original electronic state. Tunnelling matrix elements linearly combine the static ground states into irreducible representations of the icosahedral origin. The transformations $\hat{\mathrm{T}}(\mathcal{T})$ and $\hat{\mathrm{T}}(\mathcal{D}_3)$ which describe this tunnel splitting are easily obtained as a "by product"of the Öpik and Pryce analysis of the extrema. A numerical scan of the Berry phase properties on the lowest APESs, leads to a rule for the relative phases in adjacent minima which reproduces the Berry phase changes accompanying adiabatic transport from one minimum to a copy of the same minimum. This Berry phase information, when used in conjunction with the transformations $\hat{\mathrm{T}}(\mathcal{T})$ and $\hat{\mathrm{T}}(\mathcal{D}_3)$, reduces the overlap matrices for the lowest APESs and yields the ordering of the tunnel splitting and the energies of the corresponding levels.

At all other relative mode couplings in $G \otimes (g \ominus h)$, the solutions to the Öpik and Pryce equations are the same as when the two modes are included separately. When the turning point energies are plotted against relative coupling strength, three distinct situations are seen to arise. In the region where g-modes dominate, the overlap matrix between $\mathcal{T}$ points remains unchanged until the system reaches the equal coupling régime, so the argument for identifying vibronic

ground states may be carried through from pure $G \oslash g$ to $G \otimes (g \oplus h)_{eq}$. Similarly, the overlap matrix between $\mathcal{D}_3$ points in the region where h-modes dominate is unchanged until the system reaches $G \otimes (g \oplus h)_{eq}$, so the argument for identifying vibronic ground states may also be carried through from pure $G \oslash h$ to $G \otimes (g \oplus h)_{eq}$.

Chapter 4

Ground state Ham factors.

4.1 Introduction.

THE Hamiltonian for a Jahn-Teller system has the full symmetry of the Jahn-Teller origin under the simultaneous transformation of *both* electronic and vibrational coordinates. The exact eigenstates of the Hamiltonian must therefore belong to the irreps of the Jahn-Teller origin and must possess the corresponding degeneracies. In particular, the ground state is always found to be a vibronic multiplet with the same degeneracy as the original uncoupled electronic basis, whatever the strength of the Jahn-Teller coupling. Thus, so long as excited vibronic states are far away in energy from the ground state relative to the size of any perturbation that may be applied, the properties of the vibronic ground state are formally identical, so far as symmetry considerations are concerned, with those of the uncoupled electronic orbital at the Jahn-Teller origin. This continuity of the symmetry properties is encapsulated in the definition and use of reduction or Ham factors [37, 38] which are simply defined as the ratio of the effect of a perturbation, such as external stress or spin-orbit coupling, within the ground vibronic state relative to its effect in the original uncoupled electronic state. Essentially, these Ham factors are a set of symmetry-related parameters which facilitate a summary of the effect of a perturbation in terms of an effective Hamiltonian.

Of the strongly coupled systems examined in this thesis, only $G \otimes (g \oplus h)_{eq}$ exhibits the state of affairs mentioned above, where the low-lying vibronic ground states are always separated by at least a pseudo-rotational energy. A generalization of the standard definition of the Ham factor is required to cover some icosahedral systems that do not quite satisfy the above assumptions. The principal generalisation presented in this chapter deals with the lowest vibronic state when it is so closely approached by others that the effect of a perturbation in coupling these states to each

other cannot be neglected compared with its effect within the ground state itself. One way that such a situation can occur is when, under strong Jahn-Teller coupling, there are more equivalent Jahn-Teller distortions than the multiplicity of the parent state. The icosahedral subsystems $G \otimes g$, $G \oslash h$ and $H \otimes g$ all exhibit this kind of behaviour (see Chapter 3). In these systems. the vibronic ground states at strong coupling are in close proximity in energy to low-lying excited states belonging to singlet and non-singlet irreps. This may be demonstrated by following a similar argument to that of [74]: For all three systems, tunnelling between the stable minima of the lowest APESs splits the static ground states into icosahedral irreducible spaces separated in energy by tunnel splittings, Δ, of the form

$$\Delta = \text{constant} \times V \exp(-IV^2), \tag{4.1}$$

where V is the corresponding linear J-T coupling and I is a tunnelling integral. The exact value of I has been the subject of much debate and is a problem that has still not been satisfactorily resolved for dimensions higher than one [83, 52, 82, 46, 4]. However, the form of Δ is independent of the choice of definition of I. Since I is always positive, at strong coupling (i.e. large V) the splitting between the ground and excited levels is small. In this case, the excited vibronic states of $G \otimes g$, $G \otimes h$ and $H \otimes g$ are no longer far away in energy from the ground states relative to the size of any perturbation that may be applied.

The purpose of this chapter is to examine the ground state Ham factors in strongly coupled $G \otimes (g \oplus h)_{eq}$, $G \otimes g$, $G \otimes h$ and $H \otimes g$. In the light of the above considerations, it becomes evident that matrix elements of operators within the vibronic ground states of these systems, either involve a continuous integral (as in the case of $G \otimes (g \oplus h)_{eq}$), or a discrete matrix manipulation (as in the case of $G \otimes g$, $G \otimes h$ and $H \otimes g$). Bearing this in mind, the following analysis divides naturally into two parts. The first deals with the ground state Ham factors of $G \otimes (g \oplus h)_{eq}$ which do not require a generalization of the Ham factor definition and may be calculated in the standard way as a ratio of integrals. The second, deals with the calculation of the ground state Ham factors for $G \otimes g$, $G \oslash h$ and $H \oslash g$. This requires some new definitions which classify the resulting Ham factors as *standard* or *extended* depending upon which of the low-lying vibronic states are connected by the operators. A matrix method facilitates the calculation of the matrix operators within *all* the nuclear motion states subduced from the static ground state by tunnel splitting.

4.2 $G \otimes (g \oplus h)_{eq}$.

$G \otimes (g \oplus h)_{eq}$ exhibits a four dimensional trough of minimum energy in the lowest APES. At strong coupling, the nuclear motion is restricted to this trough and the ground state corresponds to the pseudo-rotational state $(\frac{1}{2}, \frac{1}{2})$. Operators which act within the $(\frac{1}{2}, \frac{1}{2})$ manifold belong to the irreps in

$$(\frac{1}{2}, \frac{1}{2}) \otimes (\frac{1}{2}, \frac{1}{2}) = [(0,0) \oplus (1,1)]_S \oplus \{(1,0) \oplus (0,1)\}_A. \tag{4.2}$$

The Ham factors of these operators within the $(\frac{1}{2}, \frac{1}{2})$ vibronic ground state are calculated by first taking the expectation of the operator within the electronic state $|u(\theta, \alpha, \beta)\rangle$ (Equation (3.11)) and then taking the expectation of the resulting function within the nuclear motion state $(\frac{1}{2}, \frac{1}{2})$. By virtue of their antisymmetric nature, the operators belonging to both $(1,0)$ and $(0,1)$ all yield zero expectations within $|u(\theta, \alpha, \beta)\rangle$ and therefore have vanishing Ham factors within the vibronic ground state.

The operators belonging to $(1,1)$ are the functions $S_2^{1-a,1-b}$ $a, b \in \{0,1,2\}$. Since a Ham factor is essentially a reduced matrix element, any of the partners of $(1,1)$ may be chosen to calculate the ground state Ham factor for the $(1,1)$ operators. For simplicity, S_2^{00} is chosen yielding an expectation value within $|u(\theta, \alpha, \beta)\rangle$ of the form

$$-\frac{1}{\pi\sqrt{6}} \cos 2\theta. \tag{4.3}$$

The Ham factor for $(1,1)$ operators, which is denoted K^{eq}, is therefore

$$\begin{aligned} K^{eq} &= \left(\frac{1}{\pi\sqrt{6}}\right) \frac{\langle S_1^{ij}| - \cos 2\theta |S_1^{kl}\rangle}{\langle S_1^{ij}|S_2^{00}|S_1^{kl}\rangle} = \left(\frac{1}{\pi\sqrt{6}}\right) \frac{\langle S_1^{ij}|\frac{\pi\sqrt{2}}{\sqrt{3}} S_2^{00}|S_1^{kl}\rangle}{\langle S_1^{ij}|S_2^{00}|S_1^{kl}\rangle} \\ &= \left(\frac{1}{3}\right) \frac{\langle S_1^{ij}|S_2^{00}|S_1^{kl}\rangle}{\langle S_1^{ij}|S_2^{00}|S_1^{kl}\rangle} = \frac{1}{3}. \end{aligned} \tag{4.4}$$

The second expression in (4.4) is obtained by applying the definitions in (3.7). The matrix elements of the scalar operator in $(0,0)$ is unaffected by the Jahn-Teller coupling.

4.3 $G \otimes g$, $G \otimes h$ and $H \otimes g$.

The vibronic ground states of strongly coupled $G \otimes g$, $G \otimes h$ and $H \otimes g$ are product wave functions of the form: $\Phi|u\rangle$, where $|u\rangle$ is the electronic state corresponding to the lowest APES and Φ is the nuclear motion wave function, which is a linear combination of GSHOs localized at the minima of the lowest APES. The Ham factor of a perturbation within these ground states may be calculated by first taking the expectation of the perturbation within $|u\rangle$ at the minima of the lowest APES.

and then taking the expectation of the resulting matrix within the GSHOs of the ground state nuclear motion. The coefficients of the linear combinations of GSHOs for the ground states of $G \otimes g$, $G \otimes h$ and $H \otimes g$ are the columns of the column normalized matrices $\hat{\mathrm{Q}}^{Gg}$, $\hat{\mathrm{Q}}^{Gh}$ and $\hat{\mathrm{Q}}^{Hg}$, respectively. How the Ham factor of a perturbation may be derived from these considerations. is best illustrated by considering a simple example:

Example: The ground state Ham factor for $\hat{\mathrm{g}}_\alpha$ in strongly coupled $G \otimes g$.

Let the perturbation under consideration transform as the α component of the irrep G. The expectation of this perturbation within $|u\rangle$ at the minima of the lowest APES of $G \otimes g$ is a 5×5 diagonal matrix, the elements of which are the values of the expectation of $\hat{\mathrm{g}}_\alpha$ (see Appendix (A.1) for the explicit form of $\hat{\mathrm{g}}_\alpha$) at the five minima. Let this matrix be denoted $\hat{\mathrm{X}}^G_\alpha$. Then the matrix representation of the perturbation within the vibronic ground state of $G \otimes g$ at strong coupling is then given by:

$$\frac{16}{15}\left(\hat{\mathrm{Q}}^{Gg}\right)^T \cdot \hat{\mathrm{X}}^G_\alpha \cdot \hat{\mathrm{Q}}^{Gg} = \frac{3}{4}\,\hat{\mathrm{g}}_\alpha, \tag{4.5}$$

where the fraction 16/15 is from the column normalization of $\hat{\mathrm{Q}}^{Gg}$. Consequently, it is evident from (4.5) that the Ham factor for G operators acting within the ground state of $G \otimes g$ at strong coupling is 3/4.

At strong coupling, the close energy proximity of the singlet tunnelling sublevel in $G \otimes g$ means that the G ground state and A tunnelling sublevels may be mixed by the perturbation. This need to consider the tunnelling singlet means that the matrix in (4.5) is only part of the matrix of the perturbation acting within the low-lying vibronic states. Indeed, the full matrix must therefore be:

$$\left(\hat{\mathrm{T}}(\mathcal{T})\right)^T \cdot \hat{\mathrm{X}}^G_\alpha \cdot \hat{\mathrm{T}}(\mathcal{T}), \tag{4.6}$$

where $\hat{\mathrm{T}}(\mathcal{T})$ is the transformation which reduces the five degenerate $\mathcal{T}$ distortions of an icosahedron into irreps A and G (see Subsection (3.3.2)). The matrix (4.5) is the section of the matrix (4.6) between the G vibronic states. The elements describing the mixing at strong coupling of A and G sublevels appear as off-diagonal elements between A and G bases.

Corresponding considerations in $G \otimes h$ and $H \otimes g$ involve the matrix $\hat{\mathrm{T}}(\mathcal{D}_3)$ which reduces the space of degenerate $\mathcal{D}_3$ distortions into irreps A, G and H. Perturbations within the low-lying states of these interactions are represented by complicated 10×10 matrices. The various sections

of these matrices correspond to the action of the perturbation within and between the sublevels $A \oplus G \oplus H$.

It is clear from the above considerations that the close energy proximity of the tunnelling sublevels, complicates the effect of a perturbation within low-lying vibronic states. As shown above, the effect of a perturbation within a vibronic ground state is described as a multiple of the matrix of the perturbation within the uncoupled electronic state, the multiplying factor being the Ham factor. Within a tunnelling sublevel however, the effect of a perturbation cannot be described by a Ham factor as such, because the symmetry properties of the tunnelling sublevel do not coincide with those of the uncoupled electronic state. Nevertheless, by means of an *extended* reduction factor it is convenient to represent the resulting matrices in terms of the matrices appearing in Appendices (A.1) and (A.3).

A substantial simplification of the matrix algebra may be made by considering more closely matrix equations of the form (4.6). This is most easily illustrated by considering a general system $\Gamma \otimes \Lambda$ (where $\Gamma \otimes \Lambda$ could be $G \otimes g$, $G \otimes h$ or $H \otimes g$) exhibiting N minimal distortions of symmetry $\mathcal{G}$, where $N > |\Gamma|$ and $\mathcal{G} \subset I$. At strong coupling the static ground state of N degenerate distortions is split by the matrix $\hat{\mathrm{T}}(\mathcal{G})$ into irreps of I. This splitting takes the form $\Gamma \oplus \Gamma' \oplus A$ (except in the case of $G \otimes g$ where there is no Γ'), where the vibronic gound state transforms as Γ and the low-lying tunnelling sublevels are Γ' below an A singlet. Let us now consider the action of a perturbation transforming as the k^{th} component of $\Upsilon \subset \Gamma \otimes \Gamma$ within these low-lying vibronic states. The effect of this perturbation may be studied by considering the individual sections of the matrix

$$\left(\hat{\mathrm{T}}(\mathcal{G})\right)^T \cdot \hat{\mathrm{X}}_k^{\Upsilon} \cdot \hat{\mathrm{T}}(\mathcal{G}), \tag{4.7}$$

where $\hat{\mathrm{X}}_k^{\Upsilon}$ is the diagonal $N \times N$ matrix of electronic expectations for the perturbation evaluated at the N minima. Below, these individual sections are examined separately:

(A) **Within the vibronic ground state** Γ: The $(i,j)^{th}$ element of the matrix (4.7) within the vibronic state Γ is designated in the following by the symbol $\langle \Gamma i | \Upsilon k | \Gamma j \rangle$. By means of a set of Ham factors $K_{\Gamma}^{JJ'\Upsilon}(\mathcal{G})$, the matrix elements $\langle \Gamma i | \Upsilon k | \Gamma j \rangle$ may be constructed in terms of the coupling symbols $(\Gamma i; J \Upsilon k | \Gamma j)$. This yields the following set of equations

$$\begin{aligned} \langle \Gamma i | \Upsilon k | \Gamma j \rangle &= \sum_J K_{\Gamma}^{JJ'\Upsilon}(\mathcal{G}) \, (\Gamma i; J \Upsilon k | \Gamma j) \\ &= \sum_m T_{mi}(\mathcal{G}) \, T_{mj}(\mathcal{G}) \sum_{pq} a_p^{\Gamma}(m) \, a_q^{\Gamma}(m) \, (\Gamma p; J' \Upsilon k | \Gamma q), \end{aligned} \tag{4.8}$$

where the index m runs through the N stable minima, $T_{mi}(\mathcal{G})$ is the $(m,i)^{th}$ element of $\hat{\mathrm{T}}(\mathcal{G})$, and $a_p^{\Gamma}(m)$ is the p^{th} component of the f-space coordinates of the m^{th} minimum. J

and J' are J-labels that are used to distinguish between a multiplicity of Υ irreps in $\Gamma \oslash \Gamma$. The symbols $(\Gamma i; J\Upsilon k|\Gamma j)$ are defined in Subsection (2.2.1) and obey the orthonormality relation (2.9). By using the orthonormality of the symbols and making the observation that

$$T_{mi}(\mathcal{G}) = \sqrt{\frac{|\Gamma|}{N}}\, a_i^{\Gamma}(m), \tag{4.9}$$

where N is the number of stable minima, Equation (4.8) may be reduced to:

$$K_{\Gamma}^{JJ'\Upsilon}(\mathcal{G}) = \frac{|\Gamma|}{|\Upsilon|}\, \mathcal{I}_{\Gamma}^{JJ'\Upsilon}(\mathcal{G}), \tag{4.10}$$

where

$$\begin{aligned} \mathcal{I}_{\Gamma}^{JJ'\Upsilon}(\mathcal{G}) &= \sum_k \sum_{ijpq} a_i^{\Gamma}(m)\, a_j^{\Gamma}(m)\, a_p^{\Gamma}(m)\, a_q^{\Gamma}(m)\, (\Gamma i; J\Upsilon k|\Gamma j)\, (\Gamma p; J'\Upsilon k|\Gamma q) \qquad (4.11) \\ &= ((\Gamma \times \Gamma)_{J\Upsilon} \cdot (\Gamma \times \Gamma)_{J'\Upsilon})_A \text{ evaluated at any of the } N \text{ minima.} \end{aligned}$$

$\mathcal{I}_{\Gamma}^{JJ'\Upsilon}(\mathcal{G})$ is therefore an icosahedral invariant constructed from the coupling rules outlined in Subsection (2.2.4), evaluated at any of the N minima.

(B) **Within the tunnelling sublevel Γ':** The $(i,j)^{th}$ element of the matrix (4.7) within the tunnelling sublevel Γ' is designated by the symbol $\langle \Gamma' i|\Upsilon k|\Gamma' j\rangle$ and is found to be

$$\begin{aligned} \langle \Gamma' i|\Upsilon k|\Gamma' j\rangle &= \sum_J K_{\Gamma\Gamma'}^{JJ'\Upsilon}(\mathcal{G})\, (\Gamma' i; J\Upsilon k|\Gamma' j) \qquad (4.12) \\ &= \sum_m T_{mi}(\mathcal{G})\, T_{mj}(\mathcal{G}) \sum_{pq} a_p^{\Gamma}(m)\, a_q^{\Gamma}(m)\, (\Gamma p; J'\Upsilon k|\Gamma q), \end{aligned}$$

where $K_{\Gamma\Gamma'}^{JJ'\Upsilon}(\mathcal{G})$ are extended Ham factors and are distinguished from standard Ham factors by the extra Γ' subscript. The designations for the other indices and in (4.12) coincide with those given in (A) above. The $T_{mi}(\mathcal{G})$ are matrix elements belonging to the Γ' columns of $\hat{\mathrm{T}}(\mathcal{G})$, so

$$T_{mi}(\mathcal{G}) = \sqrt{\frac{|\Gamma'|}{N}}\, a_i^{\Gamma'}(m). \tag{4.13}$$

By introducing (4.13) into (4.12) and using the orthonormality of the symbols $(\Gamma' i; J\Upsilon k|\Gamma' j)$, (4.12) may be reduced to:

$$K_{\Gamma\Gamma'}^{JJ'\Upsilon}(\mathcal{G}) = \frac{|\Gamma'|}{|\Upsilon|}\, \mathcal{I}_{\Gamma\Gamma'}^{JJ'\Upsilon}(\mathcal{G}), \tag{4.14}$$

where

$$\begin{aligned} \mathcal{I}_{\Gamma\Gamma'}^{JJ'\Upsilon}(\mathcal{G}) &= \sum_k \sum_{ijpq} a_i^{\Gamma'}(m)\, a_j^{\Gamma'}(m)\, a_p^{\Gamma}(m)\, a_q^{\Gamma}(m)\, (\Gamma' i; J\Upsilon k|\Gamma' j)\, (\Gamma p; J'\Upsilon k|\Gamma q) \qquad (4.15) \\ &= ((\Gamma' \times \Gamma')_{J\Upsilon} \cdot (\Gamma \times \Gamma)_{J'\Upsilon})_A \text{ evaluated at any of the } N \text{ minima.} \end{aligned}$$

$\mathcal{I}_{\Gamma\Gamma'}^{JJ'\Upsilon}(\mathcal{G})$ is therefore an icosahedral invariant constructed from the coupling rules outlined in Subsection (2.2.4), evaluated at any of the N minima.

(C) **Mixing between the vibronic levels:** The mixing of vibronic levels by the perturbation, is described by the off-diagonal matrix elements between Γ and Γ', Γ and A, and Γ' and A. The designations for these matrix elements are given below along with formulae for calculating them:

Matrix elements $\langle \Gamma | J\Upsilon | \Gamma' \rangle$ between Γ and Γ':

$$\langle \Gamma i | J\Upsilon k | \Gamma' j \rangle = \frac{\sqrt{|\Gamma||\Gamma'|}}{N} \sum_{mpq} a_i^{\Gamma}(m)\, a_j^{\Gamma'}(m)\, a_p^{\Gamma}(m)\, a_q^{\Gamma}(m)\, (\Gamma p; J\Upsilon k | \Gamma q). \tag{4.16}$$

Matrix elements $\langle \Gamma | J\Upsilon | A \rangle$ and $\langle \Gamma' | J\Upsilon | A \rangle$ between Γ/Γ' and A:

$$\langle \Gamma i | J\Upsilon k | A \rangle = \delta_{\Gamma\Upsilon}\delta_{ik} \frac{\sqrt{|\Gamma|}}{N} \sum_{mpq} a_i^{\Gamma}(m)\, a_p^{\Gamma}(m)\, a_q^{\Gamma}(m)\, (\Gamma p; J\Upsilon k | \Gamma q), \tag{4.17}$$

where the corresponding matrix element for $\langle \Gamma' | J\Upsilon | A \rangle$ may be obtained from (4.17) by replacing Γ with Γ'.

The simplifications outlined above, mean that the effect of a perturbation within $\Gamma \oplus \Gamma' \oplus A$ may be reduced to a description involving only two reduction factors (standard and extended Ham factors) and a set of mixing elements.

The general gist of the above considerations is not new. Indeed, the need to consider mixing between vibronic levels also occurs in $T \otimes \tau$ of cubic symmetry, where the vibronic ground state is a triplet with a tunnelling singlet close above it. In some icosahedral systems however, the effect of a perturbation within the low-lying states is further complicated by the appearance of a non-singlet tunnelling sublevel. This does not occur in Jahn-Teller systems of lower symmetry than that of the icosahedron. The extended Ham factor is therefore exactly what its name suggests; an extention of Ham's powerful concept of vibronic reduction factors, to describe the effect of non-singlet tunnelling sublevels within low-lying vibronic states of icosahedral systems.

4.4 Results for $G \otimes g$, $G \otimes h$ and $H \otimes g$.

The results of applying the above considerations specifically to the cases $G \otimes g$, $G \otimes h$ and $H \otimes g$, are presented below. Due to the complicated nature of the matrices involved, the results for the perturbations of each symmetry type are accompanied by a matrix operator corresponding to one of the partners. The matrices appearing in these results are "sectioned-off" to emphasise the various vibronic levels under consideration.

4.4.1 $G \otimes g$.

Within the low-lying vibronic levels of $G \otimes g$ at strong coupling, the matrix elements of anti-symmetric operators vanish because their expectation within the electronic part of the vibronic states is necessarily zero. Under the same conditions. the matrices of symmetric operators do not necessarily vanish unless the corresponding Ham factor is zero. Therefore the operators to be investigated here, appear in the symmetric square $[G \otimes G]_S = A \oplus G \oplus H$. The vibronic coupling has no effect on the scalar operator A. The effect of G and H perturbations within the $A \oplus G$ vibronic levels of $G \otimes g$ may be studied by applying the formulae (4.10) and (4.17). There is no need for the formulae (4.12) and (4.16) since there is no non-singlet tunnelling sublevel in $G \otimes g$. The results of applying (4.10) and (4.17) for G and H perturbations are as follows:

• **Within the G ground state:**

$$\begin{aligned} \mathcal{I}_G^G(\mathcal{T}) &= ((G \times G)_G \cdot (G \times G)_G)_A|_{\mathcal{T}} = \frac{3}{4}, \\ \mathcal{I}_G^H(\mathcal{T}) &= ((G \times G)_H \cdot (G \times G)_H)_A|_{\mathcal{T}} = 0, \end{aligned} \tag{4.18}$$

where "$|_{\mathcal{G}}$" denotes evaluation at the $\mathcal{G} = \mathcal{T}, \mathcal{D}_3$ epikernels corresponding to stable minima. Therefore the ground state Ham factors for G and H perturbations are:

$$\begin{aligned} K_G^G(\mathcal{T}) &= \frac{4}{4}\mathcal{I}_G^G(\mathcal{T}) = \frac{3}{4} \\ \text{and} \quad K_G^H(\mathcal{T}) &= \frac{4}{5}\mathcal{I}_G^H(\mathcal{T}) = 0. \end{aligned} \tag{4.19}$$

Note that, since there is no Kronecker multiplicity in $[G \otimes G]_S$, the J and J' labels of (4.10) have been dropped.

• **Between A and G sublevels:** Using the expression for mixing between A and G ((4.17) with $\Gamma = G$) and choosing the α^{th} component of G to be the perturbation (although the value would be the same for any of the components of G), the mixing element is found to be

$$\langle A|G_\alpha|G_\alpha\rangle = -\frac{3}{4}\frac{1}{\sqrt{3}}. \tag{4.20}$$

An H perturbation cannot connect $|A\rangle$ and $|G\rangle$ vibronic states.

Consequently, in the strong coupling limit, the matrix of a G_α perturbation within the low-lying vibronic states of $G \otimes g$ is given by (4.6) yielding the matrix in Table (4.1). In Table (4.1) the kets $|\Psi^A>$ and $|\Psi_i^G>$, $i \in \{\alpha, \beta, \gamma, \delta\}$ are nuclear motion states transforming as A and G respectively. The matrix of any H perturbation within the same states is a null matrix.

	$\|\Psi^A>$	$\|\Psi^G_\alpha>$	$\|\Psi^G_\beta>$	$\|\Psi^G_\gamma>$	$\|\Psi^G_\delta>$
$<\Psi^A\|$	0	$-\frac{3}{4}\frac{1}{\sqrt{3}}$	0	0	0
$<\Psi^G_\alpha\|$	$-\frac{3}{4}\frac{1}{\sqrt{3}}$	0	0	0	$-\frac{3}{4}\frac{1}{\sqrt{6}}$
$<\Psi^G_\beta\|$	0	0	0	$-\frac{3}{4}\frac{1}{\sqrt{6}}$	0
$<\Psi^G_\gamma\|$	0	0	$-\frac{3}{4}\frac{1}{\sqrt{6}}$	0	$-\frac{3}{4}\frac{1}{\sqrt{6}}$
$<\Psi^G_\delta\|$	0	$-\frac{3}{4}\frac{1}{\sqrt{6}}$	0	$-\frac{3}{4}\frac{1}{\sqrt{6}}$	0

Table 4.1: Matrix of G_α in $G \otimes g$.

4.4.2 $G \otimes h$.

In $G \otimes h$, the low-lying vibronic states at strong coupling are a G ground state below H and then A tunnelling sublevels, all of which are in close energy proximity to each other. All the formulae (4.10), (4.12), (4.16) and (4.17) are required to describe the effect of a perturbation within the $A \oplus G \oplus H$ vibronic levels, and once again it is only the symmetric operators which have non-zero matrices within these levels. Applying the formulae (4.10), (4.12), (4.16) and (4.17) to the $A \oplus G \oplus H$ vibronic levels for G and H perturbations yields:

- **Within the G ground state:**

$$\begin{aligned} \mathcal{I}^G_G(\mathcal{D}_3) &= ((G\times G)_G \cdot (G\times G)_G)_A|_{\mathcal{D}_3} = \frac{1}{18}, \\ \mathcal{I}^H_G(\mathcal{D}_3) &= ((G\times G)_H \cdot (G\times G)_H)_A|_{\mathcal{D}_3} \frac{25}{36}, \end{aligned} \tag{4.21}$$

therefore the ground state Ham factors for G and H perturbations are:

$$\begin{aligned} K^G_G(\mathcal{D}_3) &= \frac{4}{4}\mathcal{I}^G_G(\mathcal{D}_3) = \frac{1}{18} \\ \text{and } K^H_G(\mathcal{D}_3) &= \frac{4}{5}\mathcal{I}^H_G(\mathcal{D}_3) = \frac{5}{9}. \end{aligned} \tag{4.22}$$

Once again, there is no multiplicity and the J and J' labels of (4.10) have been dropped.

- **Within the H tunnelling sublevel:**

$$\begin{aligned} \mathcal{I}^G_{GH}(\mathcal{D}_3) &= ((G\times G)_G \cdot (H\times H)_G)_A|_{\mathcal{D}_3} = \frac{2}{9}\sqrt{\frac{2}{5}}, \\ \mathcal{I}^{2H}_{GH}(\mathcal{D}_3) &= ((G\times G)_H \cdot (H\times H)_{2H})_A|_{\mathcal{D}_3} = \frac{5}{3}\sqrt{\frac{1}{14}}, \\ \mathcal{I}^{4H}_{GH}(\mathcal{D}_3) &= ((G\times G)_H \cdot (H\times H)_{4H})_A|_{\mathcal{D}_3} = \frac{5}{9}\sqrt{\frac{5}{14}}, \end{aligned} \tag{4.23}$$

therefore the extended Ham factors for G and H perturbations are:

$$\begin{aligned} K^{G}_{GH}(\mathcal{D}_3) &= \frac{5}{4}\mathcal{I}^{G}_{GH}(\mathcal{D}_3) = \frac{1}{9}\sqrt{\frac{5}{2}}, \\ K^{2H}_{GH}(\mathcal{D}_3) &= \frac{5}{5}\mathcal{I}^{2H}_{GH}(\mathcal{D}_3) = \frac{5}{3}\sqrt{\frac{1}{14}}, \\ \text{and } K^{4H}_{GH}(\mathcal{D}_3) &= \frac{5}{5}\mathcal{I}^{4H}_{GH}(\mathcal{D}_3) = \frac{5}{9}\sqrt{\frac{5}{14}}. \end{aligned} \tag{4.24}$$

Here, the multiplicity of H irreps acting within the H nuclear motion state has lead to two extended Ham factors for an H perturbation. Therefore, the section of the H perturbation matrix between the H nuclear motion states will be a matrix of the form

$$\frac{5}{3}\sqrt{\frac{1}{14}}\,\hat{\mathrm{h}}^{H}_{2i} + \frac{5}{9}\sqrt{\frac{5}{14}}\,\hat{\mathrm{h}}^{H}_{4i} \quad \forall i \in \{\theta, \epsilon, x, y, z\}, \tag{4.25}$$

where $\hat{\mathrm{h}}^{H}_{2i}$ and $\hat{\mathrm{h}}^{H}_{4i}$ are matrices given in Appendix (A.3).

• **Between A and G sublevels:** The only non-zero mixing between A and G is by a G perturbation. Using the expression for mixing between A and G (4.17 with $\Gamma = G$), these matrix elements are found to be

$$\langle A|G_i|G_i\rangle = -\frac{1}{3\sqrt{8}} \quad \forall i \in \{\alpha, \beta, \gamma, \delta\}. \tag{4.26}$$

• **Between A and H sublevels:** The only non-zero mixing between A and H is by an H perturbation. Using the expression for mixing between A and H (4.17 with $\Gamma = H$), these matrix elements are found to be

$$\langle A|H_i|H_i\rangle = -\frac{\sqrt{5}}{6} \quad \forall i \in \{\theta, \epsilon, x, y, z\}. \tag{4.27}$$

• **Between G and H sublevels:** The matrices of mixing between G and H sublevels by G and H perturbations are listed in Appendix (D).

• **Matrices of G and H perturbations within the low-lying vibronic states of $G \otimes h$ at strong coupling:** With the above results, matrices of G and H perturbations may be constructed and examples of this for an α component of G and θ component of H are given in Tables (4.2) and (4.3).

4.5 $H \otimes g$.

As in $G \otimes h$, $H \otimes g$ at strong coupling exhibits tunnel split low-lying vibronic levels $A \oplus G \oplus H$. However in $H \otimes g$, these low-lying vibronic states are ordered with an H ground state below G and then A tunnelling sublevels, all of which are in close energy proximity to each other. Once again, all the formulae (4.10), (4.12), (4.16) and (4.17) are required to describe the effect

	$\|\Psi^A>$	$\|\Psi^G_\alpha>$	$\|\Psi^G_\beta>$	$\|\Psi^G_\gamma>$	$\|\Psi^G_\delta>$	$\|\Psi^H_\theta>$	$\|\Psi^H_\epsilon>$	$\|\Psi^H_x>$	$\|\Psi^H_y>$	$\|\Psi^H_z>$
$<\Psi^A\|$	0	$-\frac{1}{3\sqrt{8}}$	0	0	0	0	0	0	0	0
$<\Psi^G_\alpha\|$	$-\frac{1}{3\sqrt{8}}$	0	0	0	$-\frac{1}{18}\frac{1}{\sqrt{6}}$	$\frac{5}{18\sqrt{10}}$	0	$-\frac{5}{9\sqrt{30}}$	0	0
$<\Psi^G_\beta\|$	0	0	0	$-\frac{1}{18}\frac{1}{\sqrt{6}}$	0	0	0	0	$\frac{5}{9\sqrt{30}}$	0
$<\Psi^G_\gamma\|$	0	0	$-\frac{1}{18}\frac{1}{\sqrt{6}}$	0	$-\frac{1}{18}\frac{1}{\sqrt{6}}$	0	$\frac{5}{18\sqrt{30}}$	$\frac{5}{18\sqrt{30}}$	0	0
$<\Psi^G_\delta\|$	0	$-\frac{1}{18}\frac{1}{\sqrt{6}}$	0	$-\frac{1}{18}\frac{1}{\sqrt{6}}$	0	0	0	0	$-\frac{5}{18\sqrt{30}}$	$\frac{5}{18\sqrt{30}}$
$<\Psi^H_\theta\|$	0	$\frac{5}{18\sqrt{10}}$	0	0	0	0	0	0	0	$-\frac{1}{9\sqrt{2}}$
$<\Psi^H_\epsilon\|$	0	0	0	$\frac{5}{18\sqrt{30}}$	0	0	0	0	$-\frac{1}{18\sqrt{6}}$	0
$<\Psi^H_x\|$	0	$-\frac{5}{9\sqrt{30}}$	0	$\frac{5}{18\sqrt{30}}$	0	0	0	0	$-\frac{2}{9\sqrt{6}}$	$\frac{1}{18\sqrt{6}}$
$<\Psi^H_y\|$	0	0	$\frac{5}{9\sqrt{30}}$	0	$-\frac{5}{18\sqrt{30}}$	0	$-\frac{1}{18\sqrt{6}}$	$-\frac{2}{9\sqrt{6}}$	0	0
$<\Psi^H_z\|$	0	0	0	0	$\frac{5}{18\sqrt{30}}$	$-\frac{1}{9\sqrt{2}}$	0	$\frac{1}{18\sqrt{6}}$	0	0

Table 4.2: Matrix for G_α in $G \otimes h$.

	$\|\Psi^A>$	$\|\Psi^G_\alpha>$	$\|\Psi^G_\beta>$	$\|\Psi^G_\gamma>$	$\|\Psi^G_\delta>$	$\|\Psi^H_\theta>$	$\|\Psi^H_\epsilon>$	$\|\Psi^H_x>$	$\|\Psi^H_y>$	$\|\Psi^H_z>$
$<\Psi^A\|$	0	0	0	0	0	$-\frac{\sqrt{5}}{6}$	0	0	0	0
$<\Psi^G_\alpha\|$	0	$\frac{5}{9}\frac{1}{2}$	0	0	0	0	0	0	0	$-\frac{\sqrt{5}}{9}$
$<\Psi^G_\beta\|$	0	0	$\frac{5}{9}\frac{1}{2}$	0	0	0	$-\frac{\sqrt{5}}{9}$	0	0	0
$<\Psi^G_\gamma\|$	0	0	0	$-\frac{5}{9}\frac{1}{2}$	0	0	0	0	$-\frac{\sqrt{5}}{9}$	0
$<\Psi^G_\delta\|$	0	0	0	0	$-\frac{5}{9}\frac{1}{2}$	0	0	$\frac{\sqrt{5}}{9}$	0	0
$<\Psi^H_\theta\|$	$-\frac{\sqrt{5}}{6}$	0	0	0	0	0	0	0	0	0
$<\Psi^H_\epsilon\|$	0	0	$-\frac{\sqrt{5}}{9}$	0	0	0	$-\frac{5}{18}$	0	0	0
$<\Psi^H_x\|$	0	0	0	0	$\frac{\sqrt{5}}{9}$	0	0	$\frac{5}{18}$	0	0
$<\Psi^H_y\|$	0	0	$-\frac{\sqrt{5}}{9}$	0	0	0	0	0	$\frac{5}{18}$	0
$<\Psi^H_z\|$	0	$-\frac{\sqrt{5}}{9}$	0	0	0	0	0	0	0	$-\frac{5}{18}$

Table 4.3: Matrix for H_θ in $G \otimes h$.

of a perturbation within the $A \oplus G \oplus H$ vibronic levels, and it is only the symmetric operators which have non-zero matrices within these levels. Applying the formulae (4.10), (4.12), (4.16) and (4.17) to the $A \oplus G \oplus H$ vibronic levels for G and H perturbations yields:

• **Within the H ground state:**

$$\begin{aligned}
\mathcal{I}_H^G(\mathcal{D}_3) &= ((2H \times 2H)_G \cdot (2H \times 2H)_G)_A|_{\mathcal{D}_3} = \frac{16}{45}, \\
\mathcal{I}_H^{22H}(\mathcal{D}_3) &= ((2H \times 2H)_{2H} \cdot (2H \times 2H)_{2H})_A|_{\mathcal{D}_3} = \frac{2}{7}, \\
\mathcal{I}_H^{24H}(\mathcal{D}_3) &= \mathcal{I}_H^{42H}(\mathcal{D}_3) = ((2H \times 2H)_{2H} \cdot (2H \times 2H)_{4H})_A|_{\mathcal{D}_3} = \frac{2\sqrt{5}}{21}, \\
\mathcal{I}_H^{44H}(\mathcal{D}_3) &= ((2H \times 2H)_{4H} \cdot (2H \times 2H)_{4H})_A|_{\mathcal{D}_3} = \frac{10}{63}.
\end{aligned} \tag{4.28}$$

The ground state Ham factors for a G perturbation may be easily obtained by applying (4.10) yielding:

$$K_H^G(\mathcal{D}_3) = \frac{5}{4}\mathcal{I}_H^G(\mathcal{D}_3) = \frac{4}{9}. \tag{4.29}$$

The effect of H perturbations is complicated by the fact that there is a multiplicity of H irreps which act within both the electronic and nuclear manifolds. The effect of an H perturbation must therefore be described by a 2×2 matrix of Ham factors which relates matrix elements within the vibronic ground state with those of the uncoupled electronic basis. The elements of this matrix of Ham factors are then

$$\begin{aligned}
K_H^{22H}(\mathcal{D}_3) &= \frac{5}{5}\mathcal{I}_H^{22H}(\mathcal{D}_3) = \frac{2}{7}, \\
K_H^{24H}(\mathcal{D}_3) &= K_H^{42H}(\mathcal{D}_3) = \frac{5}{5}\mathcal{I}_H^{24H}(\mathcal{D}_3) = \frac{2\sqrt{5}}{21}, \\
\text{and } K_H^{44H}(\mathcal{D}_3) &= \frac{5}{5}\mathcal{I}_H^{44H}(\mathcal{D}_3) = \frac{10}{63}.
\end{aligned} \tag{4.30}$$

The explicit form of this matrix and how it relates vibronic and uncoupled electronic matrix elements is as follows:

$$\begin{pmatrix} \langle Hi|2Hk|Hj\rangle \\ \langle Hi|4Hk|Hj\rangle \end{pmatrix} = \begin{pmatrix} K_H^{22H}(\mathcal{D}_3) & K_H^{24H}(\mathcal{D}_3) \\ K_H^{42H}(\mathcal{D}_3) & K_H^{44H}(\mathcal{D}_3) \end{pmatrix} \begin{pmatrix} (Hi;2Hk|Hj) \\ (Hi;4Hk|Hj) \end{pmatrix}, \tag{4.31}$$

$\forall i, j, k \in \{\theta, \epsilon, x, y, z\}$.

• **Within the G tunnelling sublevel:**

$$\begin{aligned}
\mathcal{I}_{HG}^G(\mathcal{D}_3) &= ((2H \times 2H)_G \cdot (G \times G)_G)_A|_{\mathcal{D}_3} = \frac{2}{9}\sqrt{\frac{2}{5}}, \\
\mathcal{I}_{HG}^{2H}(\mathcal{D}_3) &= ((2H \times 2H)_{2H} \cdot (G \times G)_H)_A|_{\mathcal{D}_3} = \frac{5}{3}\sqrt{\frac{1}{14}}, \\
\mathcal{I}_{HG}^{4H}(\mathcal{D}_3) &= ((2H \times 2H)_{4H} \cdot (G \times G)_H)_A|_{\mathcal{D}_3} = \frac{5}{9}\sqrt{\frac{5}{14}},
\end{aligned} \tag{4.32}$$

therefore the extended Ham factors for G and H perturbations are:

$$\begin{aligned} K^{G}_{HG}(\mathcal{D}_3) &= \frac{4}{4}\mathcal{I}^{G}_{HG}(\mathcal{D}_3) = \frac{2}{9}\sqrt{\frac{2}{5}}, \\ K^{2H}_{HG}(\mathcal{D}_3) &= \frac{4}{5}\mathcal{I}^{2H}_{HG}(\mathcal{D}_3) = \frac{4}{3}\sqrt{\frac{1}{14}}, \\ \text{and } K^{4H}_{HG}(\mathcal{D}_3) &= \frac{4}{5}\mathcal{I}^{4H}_{HG}(\mathcal{D}_3) = \frac{4}{9}\sqrt{\frac{5}{14}}. \end{aligned} \tag{4.33}$$

Here, the multiplicity of H irreps acting within the H electronic manifold has lead to two extended Ham factors for an H perturbation. Therefore, the section of the H perturbation matrix between the G nuclear motion states may take on two possible forms corresponding to the two possible H operators which act in the H electronic manifold.

• **Between A and G sublevels:** The only non-zero mixing between A and G is by a G perturbation. Using the expression for mixing between A and G ((4.17) with $\Gamma = G$), these matrix elements are found to be

$$\langle A|G_i|G_i\rangle = -\frac{2}{3\sqrt{5}} \quad \forall i \in \{\alpha, \beta, \gamma, \delta\}. \tag{4.34}$$

• **Between A and H sublevels:** There are two possible mixing elements between A and H corresponding to the two types of H perturbation acting in the H manifold. Using the expression for mixing between A and H (4.17 with $\Gamma = 2H, 4H$), these matrix elements are found to be

$$\begin{aligned} \langle A|2H_i|H_i\rangle &= -\sqrt{\frac{2}{35}}, \\ \langle A|4H_i|H_i\rangle &= -\frac{1}{3}\sqrt{\frac{2}{7}}, \end{aligned} \tag{4.35}$$

$\forall i \in \{\theta, \epsilon, x, y, z\}$.

• **Between G and H sublevels:** The matrices of mixing between G and H sublevels by G, $2H$ and $4H$ perturbations are listed in Appendix (D).

• **Matrices of G, $2H$ and $4H$ perturbations within the low-lying vibronic states of $G \otimes h$ at strong coupling:** With the above results, matrices of G, $2H$ and $4H$ perturbations may be constructed and examples of this for an α component of G and θ components of $2H$ and $4H$ are given in Tables (4.4), (4.5) and (4.6).

4.6 Summary of Chapter 4.

The symmetry properties of the vibronic ground state of a Jahn-Teller system, are formally identical to those of the uncoupled electronic orbital at the Jahn-Teller origin. The most general form of an effective Hamiltonian for a perturbation within the vibronic ground state, may be

	$\|\Psi^A>$	$\|\Psi^G_\alpha>$	$\|\Psi^G_\beta>$	$\|\Psi^G_\gamma>$	$\|\Psi^G_\delta>$	$\|\Psi^H_\theta>$	$\|\Psi^H_\epsilon>$	$\|\Psi^H_x>$	$\|\Psi^H_y>$	$\|\Psi^H_z>$
$<\Psi^A\|$	0	$-\frac{2}{3\sqrt{5}}$	0	0	0	0	0	0	0	0
$<\Psi^G_\alpha\|$	$-\frac{2}{3\sqrt{5}}$	0	0	0	$-\frac{2}{9}\frac{1}{\sqrt{15}}$	$\frac{2}{9}$	0	$-\frac{4}{9\sqrt{3}}$	0	0
$<\Psi^G_\beta\|$	0	0	0	$-\frac{2}{9}\frac{1}{\sqrt{15}}$	0	0	0	0	$\frac{4}{9\sqrt{3}}$	0
$<\Psi^G_\gamma\|$	0	0	$-\frac{2}{9}\frac{1}{\sqrt{15}}$	0	$-\frac{2}{9}\frac{1}{\sqrt{15}}$	0	$\frac{2}{9\sqrt{3}}$	$\frac{2}{9\sqrt{3}}$	0	0
$<\Psi^G_\delta\|$	0	$-\frac{2}{9}\frac{1}{\sqrt{15}}$	0	$-\frac{2}{9}\frac{1}{\sqrt{15}}$	0	0	0	0	$-\frac{2}{9\sqrt{3}}$	$\frac{2}{9\sqrt{3}}$
$<\Psi^H_\theta\|$	0	$\frac{2}{9}$	0	0	0	0	0	0	0	$-\frac{4}{9}\frac{1}{\sqrt{5}}$
$<\Psi^H_\epsilon\|$	0	0	0	$\frac{2}{9\sqrt{3}}$	0	0	0	0	$-\frac{4}{9}\frac{1}{2\sqrt{15}}$	0
$<\Psi^H_x\|$	0	$-\frac{4}{9\sqrt{3}}$	0	$\frac{2}{9\sqrt{3}}$	0	0	0	0	$-\frac{4}{9}\frac{1}{\sqrt{15}}$	$\frac{4}{9}\frac{1}{2\sqrt{15}}$
$<\Psi^H_y\|$	0	0	$\frac{4}{9\sqrt{3}}$	0	$-\frac{2}{9\sqrt{3}}$	0	$-\frac{4}{9}\frac{1}{2\sqrt{15}}$	$-\frac{4}{9}\frac{2}{\sqrt{15}}$	0	0
$<\Psi^H_z\|$	0	0	0	0	$\frac{2}{18\sqrt{3}}$	$-\frac{4}{9}\frac{1}{\sqrt{5}}$	0	$\frac{4}{9}\frac{1}{2\sqrt{15}}$	0	0

Table 4.4: Matrix for G_α in $H \otimes g$.

	$\|\Psi^A>$	$\|\Psi^G_\alpha>$	$\|\Psi^G_\beta>$	$\|\Psi^G_\gamma>$	$\|\Psi^G_\delta>$	$\|\Psi^H_\theta>$	$\|\Psi^H_\epsilon>$	$\|\Psi^H_x>$	$\|\Psi^H_y>$	$\|\Psi^H_z>$
$<\Psi^A\|$	0	0	0	0	0	$-\sqrt{\frac{2}{35}}$	0	0	0	0
$<\Psi^G_\alpha\|$	0	$\frac{1}{3}\sqrt{\frac{2}{7}}$	0	0	0	0	0	0	0	$-\frac{4}{3\sqrt{70}}$
$<\Psi^G_\beta\|$	0	0	$\frac{1}{3}\sqrt{\frac{2}{7}}$	0	0	0	$-\frac{4}{3\sqrt{70}}$	0	0	0
$<\Psi^G_\gamma\|$	0	0	0	$-\frac{1}{3}\sqrt{\frac{2}{7}}$	0	0	0	0	$-\frac{4}{3\sqrt{70}}$	0
$<\Psi^G_\delta\|$	0	0	0	0	$-\frac{1}{3}\sqrt{\frac{2}{7}}$	0	0	$\frac{4}{3\sqrt{70}}$	0	0
$<\Psi^H_\theta\|$	$-\sqrt{\frac{2}{35}}$	0	0	0	0	0	0	0	0	0
$<\Psi^H_\epsilon\|$	0	0	$-\frac{4}{3\sqrt{70}}$	0	0	0	$-\frac{1}{3}\sqrt{\frac{2}{7}}$	0	0	0
$<\Psi^H_x\|$	0	0	0	0	$\frac{4}{3\sqrt{70}}$	0	0	$\frac{1}{3}\sqrt{\frac{2}{7}}$	0	0
$<\Psi^H_y\|$	0	0	0	$-\frac{4}{3\sqrt{70}}$	0	0	0	0	$\frac{1}{3}\sqrt{\frac{2}{7}}$	0
$<\Psi^H_z\|$	0	$-\frac{4}{3\sqrt{70}}$	0	0	0	0	0	0	0	$-\frac{1}{3}\sqrt{\frac{2}{7}}$

Table 4.5: Matrix for $2H_\theta$ in $H \otimes g$.

	$\|\Psi^A>$	$\|\Psi^G_\alpha>$	$\|\Psi^G_\beta>$	$\|\Psi^G_\gamma>$	$\|\Psi^G_\delta>$	$\|\Psi^H_\theta>$	$\|\Psi^H_\epsilon>$	$\|\Psi^H_x>$	$\|\Psi^H_y>$	$\|\Psi^H_z>$
$<\Psi^A\|$	0	0	0	0	0	$-\frac{1}{3}\sqrt{\frac{2}{7}}$	0	0	0	0
$<\Psi^G_\alpha\|$	0	$\frac{2}{9}\sqrt{\frac{5}{14}}$	0	0	0	0	0	0	0	$-\frac{4}{9\sqrt{14}}$
$<\Psi^G_\beta\|$	0	0	$\frac{2}{9}\sqrt{\frac{5}{14}}$	0	0	0	$-\frac{4}{9\sqrt{14}}$	0	0	0
$<\Psi^G_\gamma\|$	0	0	0	$-\frac{2}{9}\sqrt{\frac{5}{14}}$	0	0	0	0	$-\frac{4}{9\sqrt{14}}$	0
$<\Psi^G_\delta\|$	0	0	0	0	$-\frac{2}{9}\sqrt{\frac{5}{14}}$	0	0	$\frac{4}{9\sqrt{14}}$	0	0
$<\Psi^H_\theta\|$	$-\frac{1}{3}\sqrt{\frac{2}{7}}$	0	0	0	0	0	0	0	0	0
$<\Psi^H_\epsilon\|$	0	0	$-\frac{4}{9\sqrt{14}}$	0	0	0	$-\frac{2}{9}\sqrt{\frac{5}{14}}$	0	0	0
$<\Psi^H_x\|$	0	0	0	0	$\frac{4}{9\sqrt{14}}$	0	0	$\frac{2}{9}\sqrt{\frac{5}{14}}$	0	0
$<\Psi^H_y\|$	0	0	0	$-\frac{4}{9\sqrt{14}}$	0	0	0	0	$\frac{2}{9}\sqrt{\frac{5}{14}}$	0
$<\Psi^H_z\|$	0	$-\frac{4}{9\sqrt{14}}$	0	0	0	0	0	0	0	$-\frac{2}{9}\sqrt{\frac{5}{14}}$

Table 4.6: Matrix for $4H_\theta$ in $H \otimes g$.

expressed in terms of a limited set of symmetry-related parameters. These parameters or Ham factors are simply defined as the ratio of the effect of the perturbation within the vibronic ground state relative to its effect in the original uncoupled electronic state.

The effect of a perturbation within the vibronic ground state of strongly coupled $G \otimes (g \oplus h)_{eq}$, may be examined in the standard way, yielding only one non-zero ground state Ham factor corresponding to the symmetric $(1,1)$ operators. The antisymmetric operators belonging to $(1,0)$ and $(0,1)$ are null matrices within this vibronic ground state.

The calculation of Ham factors for the strongly coupled $G \otimes g$, $G \otimes h$ and $H \otimes g$, requires an extention beyond the standard definitions. This is to allow for the fact that at strong coupling, several vibronic multiplets become close in energy and the effect of a perturbation between these multiplets cannot be neglected compared with its effect within the ground state itself. The definition of the Ham factor as a single number also requires an extention to cover the case when one particular irrep appears more than once in a symmetric square, i.e. H operators in $H \otimes H$. For this more complicated situation a matrix of Ham factors is required to correctly describe the effect of the perturbation within the vibronic ground state. To facilitate an analysis of these more complicated discussions, it is necessary to make extensive use of formulae derived

from matrix manipulations within the low-lying vibronic states. One may conclude from these formulae, that the complicated effect of a symmetric perturbation within the low-lying vibronic states may be reduced to a description involving up to only two reduction factors (standard and extended Ham factors) and a set of mixing elements. Antisymmetric operators have null matrices within low-lying vibronic states of strongly coupled $G \oslash g$, $G \otimes h$ and $H \oslash g$.

Chapter 5

The $G \otimes (g \oplus h)$ eigenvalue problem near the equal coupling limit.

5.1 Introduction.

Essentially, it is only the extremities of $G \otimes (g \oplus h)$ that have been studied thus far. Apart from the calculations leading to Figure 3.12, the previous two chapters make no allusion towards the behaviour of the system as one varies the relative coupling strength of g and h-modes from one extremity to another. In this chapter, a simple model is set up to study the properties of strongly coupled $G \otimes (g \oplus h)$ across the régimes of coupling which yield the three different structures that may be assumed by the lowest APES. The model used is the eigenvalue problem of $G \otimes (g \oplus h)$ near the limit of equal coupling $G \otimes (g \oplus h)_{eq}$, and is studied by appealing to the parent $SO(4)$ symmetry. The eigenvalues are generated numerically by solving the Schrödinger equation of motion at equal coupling, perturbed by a fourth order icosahedral field term with appropriate extremal properties. This line of attack first assumes that the coupling is about equally strong to both types of mode, and that the frequencies are equal. The difference in the coupling to the modes is then used as a parameter, and the energy levels and ground state Ham factors over a range of values of the parameter may be calculated.

5.2 Hamiltonian and conditions for the appearance of a dynamical Jahn-Teller effect.

The Hamiltonian under consideration here is given in Equation (3.1). To simplify the following considerations, which involve the variation of the relative coupling of g and h-modes, a change

of variables is made in the Hamiltonian (3.1). This change of variables facilitates the extraction of an overall coupling factor so that only a relative coupling factor remains which quantifies the extent to which the two couplings differ. This change of variables in the Hamiltonian is as follows:

$$\begin{aligned} q_\alpha &= (\omega_G\sqrt{\mu_G})Q_\alpha, \quad q_\theta = (\omega_H\sqrt{\mu_H})Q_\theta, \\ q_\beta &= (\omega_G\sqrt{\mu_G})Q_\beta, \quad q_\epsilon = (\omega_H\sqrt{\mu_H})Q_\epsilon, \\ q_\gamma &= (\omega_G\sqrt{\mu_G})Q_\gamma, \quad q_x = (\omega_H\sqrt{\mu_H})Q_x, \\ q_\delta &= (\omega_G\sqrt{\mu_G})Q_\delta, \quad q_y = (\omega_H\sqrt{\mu_H})Q_y, \\ & \qquad\qquad q_z = (\omega_H\sqrt{\mu_H})Q_z. \end{aligned} \tag{5.1}$$

The overall coupling constant extracted is $K = (V_G/\omega_G\sqrt{\mu_G})$ and

$$\lambda = (V_H/\omega_H\sqrt{\mu_H})/(V_G/\omega_G\sqrt{\mu_G}), \tag{5.2}$$

is the remaining relative coupling constant. The condition for equal coupling is then just $\lambda = 1$.

In the adiabatic approximation, outlined in Section (1.3), the lowest eigenvalue of the Hamiltonian is a function of the Q's and is regarded as the potential energy function or lowest APES for the nuclear motion in the nine dimensional Q-space. In the limit of infinitely large nuclear masses, the equilibrium configurations of the complex correspond to the minimum values of the lowest APES. The positions and natures of the turning points in the lowest APES are analysed in Chapter 3, and the hypersurface is seen to exhibit three different structures depending upon the relative coupling strengths of the two modes. According to Figure 3.12, when g-modes predominate ($\lambda < 1$) the configurations of minimal energy correspond to Type (IV) tetrahedral or $\mathcal{T}$ epikernels. The paths of lowest energy between these minima pass via Type (I) saddles which reside at $\mathcal{D}_3$ epikernels. Conversely, if h-modes dominate ($\lambda > 1$) the minima reside at Type (III) points which correspond to $\mathcal{D}_3$ epikernels and the intermediate saddles reside at Type (II) points or $\mathcal{D}_2$ epikernels. In the limit of equal coupling, when $G \otimes (g \oplus h)$ of I becomes $(\frac{1}{2}, \frac{1}{2}) \otimes (1, 1)$ of $SO(4)$ [80], all the above points coincide in energy.

Dynamical Jahn-Teller effects may be obtained by considering paths between minima of the lowest APES along which the potential energy changes are small. It is obvious that this occurs near the limit of equal coupling when, as is shown in Subsection (3.2.1), there exists a three-dimensional region of Q-space connecting these points upon which the energy remains constant. In Chapter 3, the Schrödinger equation of nuclear motion upon this surface is solved and with additional information from a Berry Phase analysis, the nuclear motion states are found to belong to the $SO(4)$ irreps $(s/2, s/2)$ where $s = 1, 3, 5, ...$ with a degeneracy of $(s + 1)^2$. The corresponding energy eigenvalues are given to order $(1/V_o)^2$ in Equation (3.33).

5.3 The eigenvalue problem when $\mathcal{T}$ and $\mathcal{D}_3$ energies are different.

When $\lambda - 1$ is different from zero, the $SO(4)$ symmetry of the equipotential surface $(q_o, \theta, \alpha, \beta)$ in the nine dimensional Q-space is reduced. An analysis of the strong coupling nuclear motion involves finding the lowest root of a quartic equation. which is then used to represent the potential function for the nuclear Schrödinger equation. Even when $\lambda - 1$ is small, an analytic expression for the lowest root of the quartic equation is extremely difficult to obtain, and hence the form of the lowest APES as a function of the Q's is in general not known. It is however, reasonable to assume that there is no drastic change in the lowest APES as $\lambda - 1$ becomes different from zero. As long as the difference between the energies of $\mathcal{T}$ and $\mathcal{D}_3$ distortions is small compared with the Jahn-Teller stabilization energy, the potential energy on the hypersphere in the nine-dimensional Q-space is still much lower than anywhere else, though it is no longer constant.

In the following, the system is assumed to be constrained to move on the $(q_o, \theta, \alpha, \beta)$ sphere. A term $V(\theta, \alpha, \beta)$ is added to the nuclear motion Hamiltonian, to represent the differences of potential on this surface. Since $V(\theta, \alpha, \beta)$ is to represent these differences in potential over the three different coupling régimes, it must be able to exhibit the same extremal properties as those of the lowest APESs for both $G \otimes g$ and $G \oslash h$, and therefore must be an icosahedral invariant. The lowest order invariants that $V(\theta, \alpha, \beta)$ may be constructed from are of order four, since $V(\theta, \alpha, \beta)$ is also required to possess non-zero reduced matrix elements between the nuclear motion states $(s/2, s/2)$ where $s = 1, 3, 5, ...$ Suitable fourth order invariants may be constructed from the quartet invariants calculated in Section (2.2.4). In this way, the introduction of the biharmonic parametrization into the explicit form of the invariant may be achieved by the variable designations in Equations (3.44). An invariant possessing a very simple biharmonic form is the fourth-order scalar appearing in the characteristic equation appertaining to the $G \otimes g$ interaction. In terms of the biharmonic coordinates this scalar is found to be

$$(1 + 3\cos 4\theta) - 16\cos(\alpha - 3\beta)\cos^3\theta \sin\theta + 16\cos(3\alpha + \beta)\cos\theta \sin^3\theta. \qquad (5.3)$$

This scalar exhibits all the extremal properties required of $V(\theta, \alpha, \beta)$[1] and is also easily written in terms of S functions. Using Cutkosky's [24] designations for the S functions of $(2, 2)$, a suitable form for the operator $V(\theta, \alpha, \beta)$ is found to be

$$V(\theta, \alpha, \beta) = \Delta[S_4^{00}(\theta, \alpha, \beta) - S_4^{-1-2}(\theta, \alpha, \beta) + S_4^{12}(\theta, \alpha, \beta) - S_4^{2-1}(\theta, \alpha, \beta) + S_4^{-21}(\theta, \alpha, \beta)]. \quad (5.4)$$

[1]The fourth-order scalar appearing in the characteristic equation for $G \otimes g$, is the product of the four APESs of $G \otimes g$ and therefore must possess all the extrema listed in Table (3.1).

An analysis of the extremal properties of this V is presented in Table (5.1). In Table (5.1),

Symmetry Type	Value of V	Hessian Eigenvalues	Extremum Type
Type(I)	-4Δ	$(80\Delta, -64\Delta, 80\Delta)$	Saddle
Type(II)	6Δ	$(-80\Delta, -80\Delta, 16\Delta)$	Saddle
Type(III)	$\frac{20}{3}\Delta$	$(-\frac{80}{3}\Delta, -\frac{80}{3}\Delta, -\frac{320}{3}\Delta)$	Maximum for $+ve\ \Delta$
Type(IV)	-10Δ	$(80\Delta, 80\Delta, 80\Delta)$	Minimum for $+ve\ \Delta$

Table 5.1: Analysis of extremal properties of V.

the values in the column marked "Hessian eigenvalues", are calculated using the Hessian in the (θ, α, β) coordinate representation. The explicit form of this Hessian is presented in Table (5.2). The sign of the parameter Δ determines the symmetry type of the minima in $V(\theta, \alpha, \beta)$. If Δ is

$$\begin{pmatrix} \frac{\partial^2}{\partial\theta^2} & \frac{\partial}{\partial\theta}\frac{1}{\sin\theta}\frac{\partial}{\partial\alpha} & \frac{\partial}{\partial\theta}\frac{1}{\cos\theta}\frac{\partial}{\partial\beta} \\ \frac{1}{\sin\theta}\frac{\partial^2}{\partial\alpha\partial\theta} & \frac{1}{\sin^2\theta}\frac{\partial^2}{\partial\alpha^2} & \frac{2}{\sin 2\theta}\frac{\partial^2}{\partial\alpha\partial\beta} \\ \frac{1}{\cos\theta}\frac{\partial^2}{\partial\beta\partial\theta} & \frac{2}{\sin 2\theta}\frac{\partial^2}{\partial\beta\partial\alpha} & \frac{1}{\cos^2\theta}\frac{\partial^2}{\partial\beta^2} \end{pmatrix}$$

Table 5.2: Hessian operator in the (θ, α, β) coordinate representation

positive, it is the Type (IV) $\mathcal{T}$ distortions which reside at the points of minimal $V(\theta, \alpha, \beta)$, with Type (I) $\mathcal{D}_3$ saddles at the intermediate turning points. If Δ is negative however, it is the Type (III) $\mathcal{D}_3$ distortions which are the minima in $V(\theta, \alpha, \beta)$, with Type (II) $\mathcal{D}_2$ at the intermediate turning points.

For variations in (θ, α, β) alone, the line element is found to be

$$ds^2 = \sum_{i=1}^{9} dq_i^2 = \frac{8}{3}(d\theta^2 + \sin^2\theta d\alpha^2 + \cos^2\theta d\beta^2), \tag{5.5}$$

where the $\{q_i\}$, $i = 1, ..., 9$, are the functions in Equations (3.10). The Schrödinger equation for the nuclear motion near the limit of equal coupling is then

$$-\frac{3\hbar^2\omega^2}{16q^2}(\frac{1}{\sin\theta\cos\theta}\frac{\partial}{\partial\theta}\sin\theta\cos\theta\frac{\partial}{\partial\theta} + \frac{1}{\sin^2\theta}\frac{\partial^2}{\partial\alpha^2} + \frac{1}{\cos^2\theta}\frac{\partial^2}{\partial\beta^2})\psi + V(\theta, \alpha, \beta)\psi = E\psi, \tag{5.6}$$

where $q^2 = \sum_{i=1}^{9} q_i^2$, ω is the frequency of the equally coupled modes and ψ is the nuclear motion wave function. Since this is an approximation that is expected to hold when V is small, the zeroth order eigenstates are chosen to be eigenstates of (5.6) with $V = 0$. These eigenstates

belong to the $SO(4)$ irreps $(s/2, s/2)$ where $s = 1, 3, 5, ...$ which describe the nuclear motion upon the equal coupling hypersphere.

A criterion for the validity of this approximation may be found by comparing the energy levels associated with motion orthogonal to and within the minimum energy hypersphere. The spacing of energy levels associated with motion in the hypersphere $(q_o, \theta, \alpha, \beta)$, is of the order of $\hbar^2\omega^2/q^2$ (see Equation (5.6)). For motion orthogonal to this surface the potential is harmonic (see Subsection (3.2.1)), with a restoring force associated with the frequency ω. Therefore, the characteristic separation of energy levels for this kind of motion is $\hbar\omega$. Consequently, one may consider the motion on the hyperspherical surface on its own as long as the energies concerned are much less than $\hbar\omega$; that is, as long as

$$\frac{\hbar^2\omega^2}{q^2} \ll \hbar\omega \tag{5.7}$$

or

$$E_{JT} \gg \frac{1}{2}\hbar\omega, \tag{5.8}$$

where $E_{JT} = q^2/2$, $q = V_o\sqrt{3}/2$. These are just the conditions for strong coupling in $G \otimes (g \oplus h)$ (see Subsection (3.2.1)). Therefore this perturbative model is well suited to studying the pseudo-rotational behaviour of $G \otimes (g \oplus h)$ in the strong coupling régime.

When $V \neq 0$, zeroth order levels may be linked by the perturbation yielding matrix elements of the form (see Equation (3.8)):

$$\begin{aligned}
\langle S_\lambda^{il} | S_4^{jm} | S_\nu^{kn} \rangle &= (-1)^{(i+l)} \int S_\lambda^{-i-l} S_4^{jm} S_\nu^{kn} \sin\theta \cos\theta d\alpha d\beta d\theta \qquad (5.9)\\
&= (-1)^{(i+l)} R(\lambda, 4, \nu) \begin{pmatrix} \frac{\lambda}{2} & 2 & \frac{\nu}{2} \\ -i & j & k \end{pmatrix} \begin{pmatrix} \frac{\lambda}{2} & 2 & \frac{\nu}{2} \\ -l & m & n \end{pmatrix}\\
&\quad i, k \in \{-\frac{\lambda}{2}, .., \frac{\lambda}{2}\},\\
&\quad l, n \in \{-\frac{\nu}{2}, .., \frac{\nu}{2}\},\\
&\quad (j, m) = (0,0), (-1,-2), (1,2), (2,-1), (-1,2),
\end{aligned}$$

where

$$R(\lambda, 4, \nu) = \frac{1}{\pi}\sqrt{(-1)^{\lambda+4+\nu}\left[\frac{5(\lambda+1)(\nu+1)}{2}\right]}. \tag{5.10}$$

The form of the resulting V matrix leads to two further complications:

(i) From the selection rules for the $3j$ symbols in (5.9), a level corresponding to $s = \lambda$, where $\lambda = 2p + 1$, $p = 0, 1, 2, ..$, may be linked by the perturbation V to levels $s = \nu$ where $|3/2 - p| \leq \nu/2 \leq 5/2 + p$. Therefore the $n \times n$ matrix of V operating within the n lowest eigenstates is not very sparse, and certainly not tridiagonal.

(ii) The construction of the matrix for V within the n lowest eigenstates is complicated by the fact that each zeroth order basis state corresponding to a particular s-level is identified by two indices. The weight space for these states is therefore two-dimensional and the degeneracy of the levels is effectively an "area" of this weight space (c.f. degeneracy= $(s+1)^2$). Therefore, even for a relatively small cutoff for s, the size of the matrix of V is very large, the dimensionality of this matrix taking the form:

$$\sum_{s=1}^{c}(s+1)^2, \tag{5.11}$$

where c is the cutoff for s-levels.

The first of these complications means that the tridiagonal diagonalization algorithms which are normally used for these kinds of problems are not immediately applicable. In fact, JACOBI and QR algorithms [69] are found to be more appropriate. The second of these complications leads

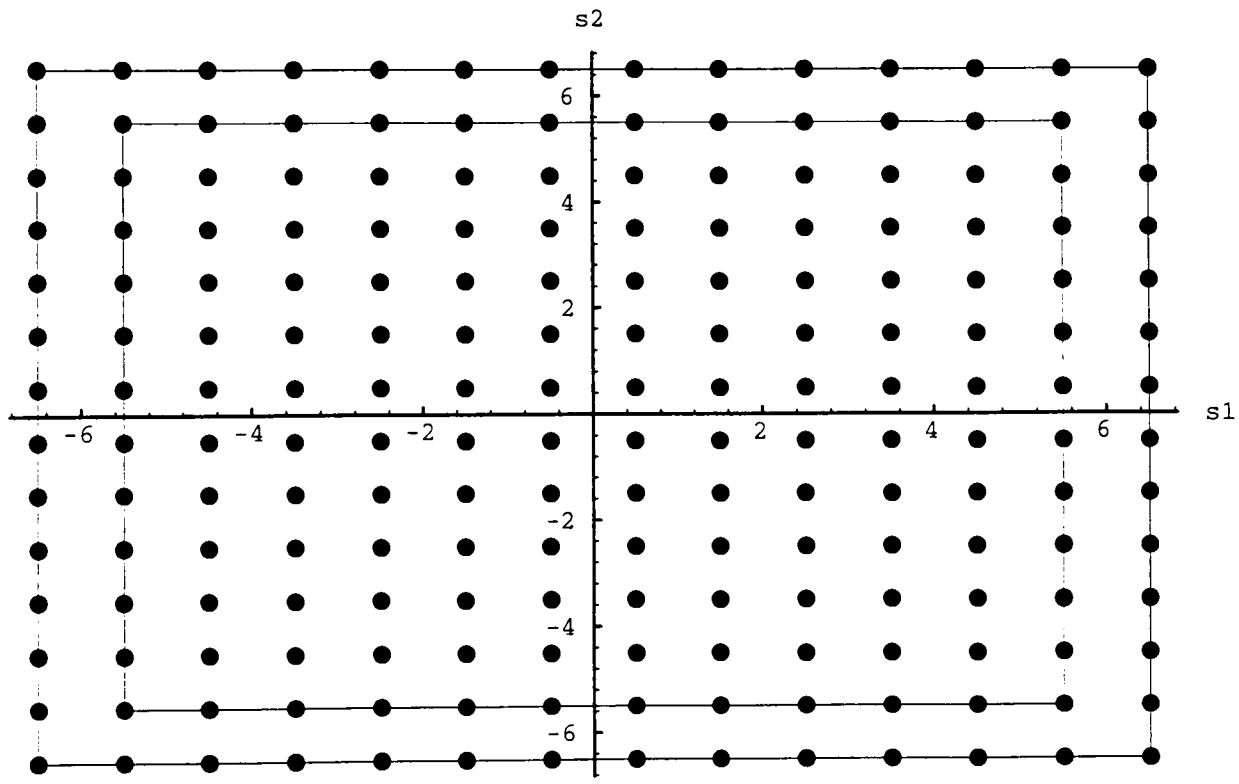

Figure 5.1: The weight space of zeroth order eigenstates up to $s = 13$. The dark points represent a pair of indices $(s1, s2)$. The inner and outer-most boxes are the extent to which the $(s1, s2)$ pairs are included within $s = 11$ and $s = 13$ levels respectively.

to quite involved organizational considerations for the matrix elements. These considerations, and the subsequent construction of the V matrix, may be illustrated by considering the weight space for levels up to a cutoff. The weight space for zeroth order eigenstates may be represented

$i=$	1	2	3	4	5	6.....20	21.....36 *etc*
$A(1,i)$	1	1	1	1	3	3.....	5.....*etc*
$A(2,i)$	1/2	1/2	−1/2	−1/2	3/2	3/2.....	.....*etc*
$A(3,i)$	1/2	−1/2	1/2	−1/2	3/2	1/2.....	.....*etc*

Table 5.3: The array A.

as a lattice of points $(s1, s2)$, where $s1$ and $s2$ are S function indices corresponding to the indices i, k, l, n in (5.9). Figure 5.1 shows this weight space up to $s = 13$. Referring to Figure 5.1, the inner and outer-most boxes enclose all the $(s1, s2)$ pairs included in the levels corresponding to $s = 11$ and $s = 13$ respectively.

For the calculation presented here, the zeroth order bases are taken up to $s = 13$ and the results are depicted for levels originating from states up to $s = 5$, which should be relatively free from the effects of the cutoff at $s = 13$. Figure 5.1 shows exactly which states are under consideration here, and the construction of the matrix for V depends on how the sets of indices depicted in Figure 5.1 are ordered. The matrix for V is calculated according to the following prescription: The points in Figure 5.1 are sampled and the indices corresponding to each point are allocated to a set of arrays, each array corresponding to one of the seven concentric boxes. If the point sampled is within two concentric boxes, then the coordinates of the point are allocated to arrays corresponding to both boxes. This is done until all the points depicted in Figure 5.1 are allocated to the array corresponding to $s = 13$. This will mean that all the points on and within the box corresponding to $s = 11$ are allocated to the array corresponding to $s = 11$ etc.. These arrays store the indices necessary for the implementation of formulae of the form Equation (5.9), which calculate the matrix of V within the zeroth order states up to $s = 13$. Rearrangement of these arrays leads to a single array denoted here A, of which a small section is depicted in Table (5.3). The array A has dimensions 3×560, where 560 comes from the sum of the "areas" of the seven concentric boxes in Figure 5.1.

In terms of the array elements in Table (5.3), the matrix elements of V may be computed by the following formula (c.f. (5.9)):

$$\langle S^{A(2,p),A(3,p)}_{A(1,p)} | S^{jm}_{4} | S^{A(2,q),A(3,q)}_{A(1,q)} \rangle = (-1)^{A(2,p)+A(3,p)} R(A(1,p), 4, A(1,q)) \times \begin{pmatrix} \frac{A(1,p)}{2} & 2 & \frac{A(1,q)}{2} \\ -A(2,p) & j & A(2,q) \end{pmatrix} \begin{pmatrix} \frac{A(1,p)}{2} & 2 & \frac{A(1,q)}{2} \\ -A(3,p) & m & A(3,q) \end{pmatrix}, \tag{5.12}$$

$$p, q \in \{1, 2, 3, ..., 560\},$$

$$(j, m) = (0, 0), (-1, -2), (1, 2), (2, -1), (-1, 2),$$

where

$$R(A(1,p), 4, A(1,q)) = \frac{1}{\pi}\sqrt{(-1)^{A(1,p)+4+A(1,q)}\left[\frac{5(A(1,p)+1)(A(1,q)+1)}{2}\right]} \qquad (5.13)$$

5.3.1 Results.

The matrix resulting from Equations (5.12) and (5.13) may be diagonalized with the JACOBI algorithm, and the variation with respect to Δ of the energy eigenvalues originating from $s = 1$, $s = 3$ and $s = 5$ may be plotted. This is done for positive Δ in Figure 5.2.

In Figure 5.2, the lowest two lines are a G ground state and an A tunnelling sublevel which eventually coincide in energy as the magnitude of Δ increases. In the limit of large Δ, the potential wells on the hypersurface are deep compared to the saddles joining them, and the five $\mathcal{T}$ wells form the five-fold degenerate static ground state of the $G \otimes g$ interaction. The letters labelling the lines are the symmetry designations for those lines at $\Delta/E_o = 8$ units, the energy being measured in units of E_o where $E_o = 3\hbar^2\omega^2/16q^2$. The corresponding results for negative Δ are plotted in Figure 5.3.

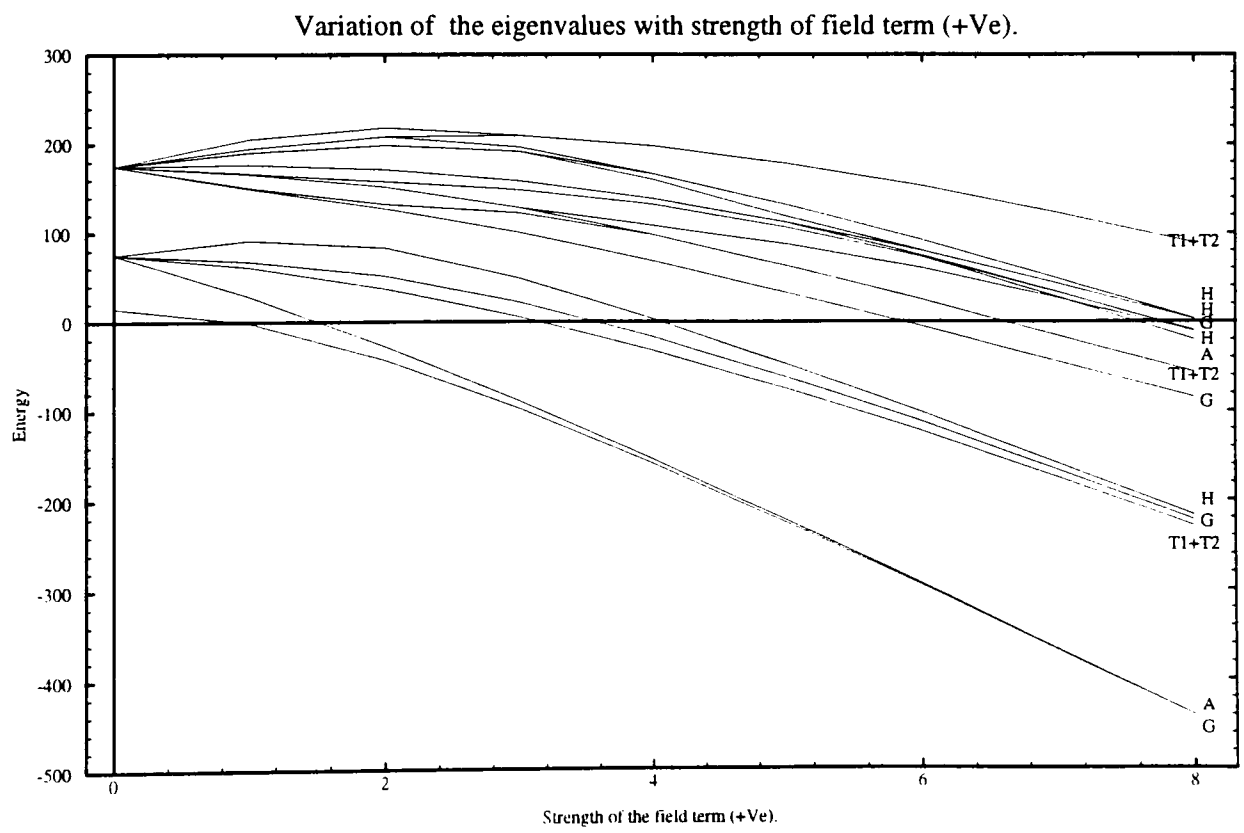

Figure 5.2:

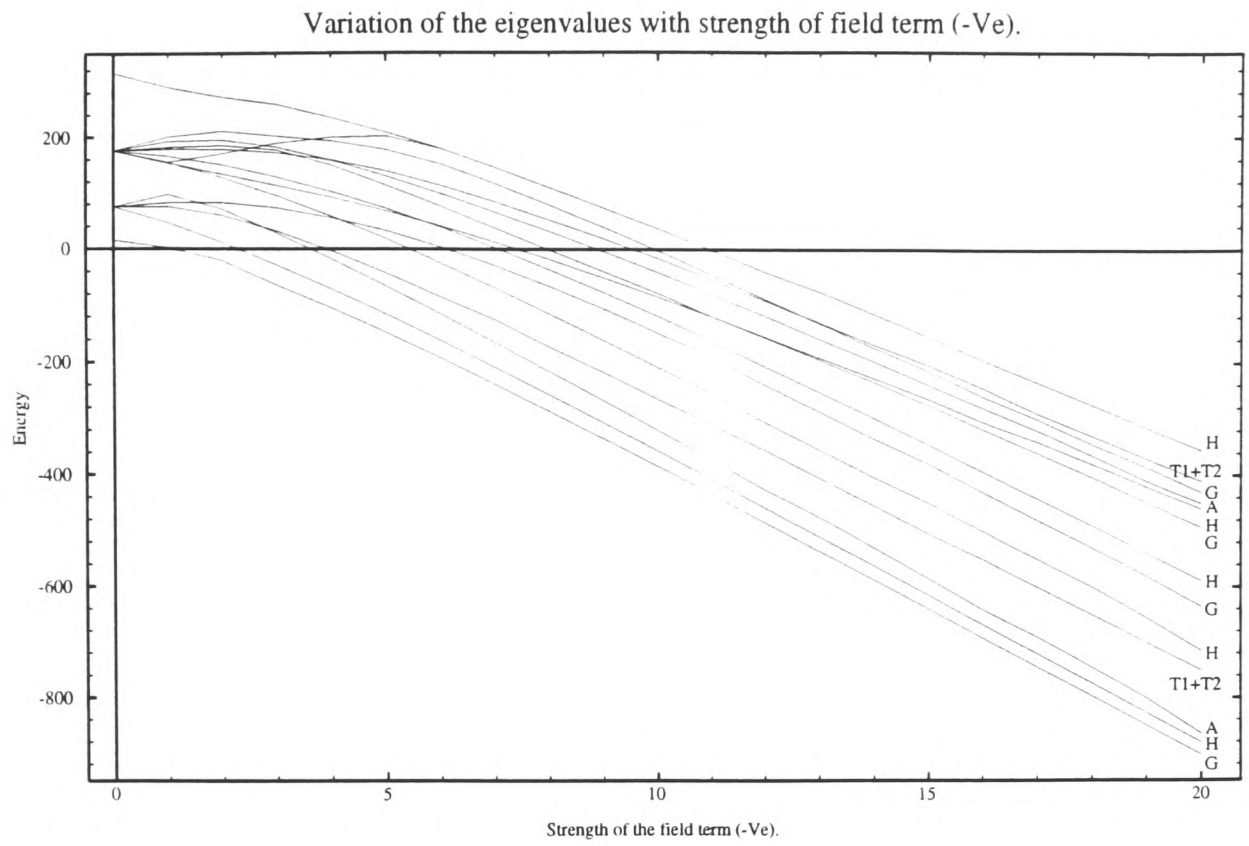

Figure 5.3:

In Figure 5.3, the lowest three lines correspond to a G ground state being approached by H and A tunnelling sublevels in that order. The letters labelling the lines are the symmetry designations for those lines at $|\Delta/E_o| = 20$ units, where Δ here is negative. The ten lowest states (corresponding to the lowest three lines) eventually coincide for very large $|\Delta/E_o|$. Compared with the positive Δ region, the convergence to the static ground state of the lowest ten states in the negative Δ region is relatively slow. This is a consequence of the discrepency in the barrier heights between the wells of the chosen potential in the two regions. For $+ve$ Δ, the height of a potential barrier (the energy distance between a well and an intermediate saddle) is 6Δ (see Table (5.1)), for $-ve$ Δ it is only $2\Delta/3$. This discrepency in the barrier heights means that the conditions for the convergence of the ground levels in the positive Δ region, are only attained in the negative Δ region for a much larger value of Δ. in fact for $\Delta/E_o \approx -72$ units corresponding to an energy of the G ground state of -4135 units. The energy eigenvalues in Figure 5.3 are depicted up to a field strength of $\Delta/E_o = -20$ units. because this value of Δ/E_o is large enough to display the eventual coincidence of the lowest three levels, and yet close enough to the equal coupling limit to display the salient features of the level splittings.

The above results may be summarized as follows: As the magnitude of Δ is increased, the nuclear wave function is increasingly confined to areas on the hypersphere which have common

(θ, α, β) coordinates with those of minima in $G \otimes g$, for $+ve\ \Delta$, or minima in $G \otimes h$, for $-ve\ \Delta$. In the $+ve\ \Delta$ region the barrier heights are relatively large and the ground state of the system already resembles the static régime for $G \otimes g$ (see Figure 5.2) at a Δ/E_o value of $+8$ units. For $-ve\ \Delta$, the static régime occurs at a much larger value of Δ/E_o. For a given value of Δ, the barrier heights between the potential wells in $-ve\ \Delta$ region are a factor of nine shallower than the corresponding heights in the $+ve\ \Delta$ region. The static behaviour of the ground state in the $-ve\ \Delta$ region is recovered at $\Delta/E_o \approx -72$ units.

It is satisfactory that this perturbative model is able to reproduce results obtained in Chapter 3 for the extremities of $G \otimes (g \oplus h)$. From Figures (5.2) and (5.3) it is evident that the ground state remains a G quartet throughout the range of the parameter Δ. The properties of the ground state over the range of Δ are therefore formally identical, so far as symmetry considerations are concerned, to those of the uncoupled electronic state G. The variation in the effect of a perturbation within the ground state may therefore be described by a ground state Ham factor which in this case is a function of Δ. By extracting the eigenvectors corresponding to the lowest energy eigenvalue depicted in Figures (5.2) and (5.3), the strong coupling vibronic ground state may be constructed over the range of Δ. The G vibronic ground state may be written in the form:

$$\begin{aligned} \psi_{g\alpha} &= f_\alpha(\theta, \alpha, \beta, \Delta)|\theta, \alpha, \beta\rangle, \\ \psi_{g\beta} &= f_\beta(\theta, \alpha, \beta, \Delta)|\theta, \alpha, \beta\rangle, \\ \psi_{g\gamma} &= f_\gamma(\theta, \alpha, \beta, \Delta)|\theta, \alpha, \beta\rangle, \\ \psi_{g\delta} &= f_\delta(\theta, \alpha, \beta, \Delta)|\theta, \alpha, \beta\rangle, \end{aligned} \tag{5.14}$$

where $|\theta, \alpha, \beta\rangle$ is the ket in Equation (3.11) and the functions $f_i(\theta, \alpha, \beta, \Delta)$ are linear combinations of S functions of the form

$$f_i(\theta, \alpha, \beta, \Delta) = \sum_{\lambda,j,k} \mathcal{F}_i^{\lambda,j,k} S_\lambda^{jk}(\theta, \alpha, \beta), \tag{5.15}$$

where the coefficient $\mathcal{F}_i^{\lambda,j,k}$ for $i \in \{\alpha, \beta, \gamma, \delta\}$, $\lambda \in \{1, 3, 5, .., 13\}$ and $j, k \in \{-\frac{\lambda}{2}, .., \frac{\lambda}{2}\}$, is a function of Δ and at any given value of Δ it is given by the overlap integral

$$(-1)^{j+k} \int S_\lambda^{-j-k}(\theta, \alpha, \beta) f_i(\theta, \alpha, \beta, \Delta) d\Omega, \tag{5.16}$$

where $d\Omega$ is the volume element $d\alpha d\beta \sin\theta \cos\theta d\theta$, c.f. the integrals in Equations (3.8) and (5.9). Perturbations which do not necessarily have null matrices within the strongly coupled ground state, belong to G and H. The matrix elements of G and H operators between the states in

(5.14) may be constructed using the matrices in Appendices (A.1) and (A.3). Choosing only the δ^{th} and θ^{th} partners of G and H respectively for the calculation of Ham factors, one obtains matrix elements of the form:

$$\langle\psi_{gi}|\hat{\mathrm{g}}_{\delta}^{G}|\psi_{gj}\rangle = -\frac{1}{\sqrt{6}}\int f_i^*(\theta,\alpha,\beta)f_j(\theta,\alpha,\beta)(\sin 2\theta\cos(\alpha-\beta)+\cos^2\theta\cos 2\alpha)d\Omega. \tag{5.17}$$

and

$$\langle\psi_{gi}|\hat{\mathrm{h}}_{\theta}^{G}|\psi_{gj}\rangle = -\frac{1}{2}\int f_i^*(\theta,\alpha,\beta)f_j(\theta,\alpha,\beta)\cos 2\theta d\Omega. \tag{5.18}$$

By using the variable designations for $(1,1)$ in (3.7), Equations (5.17) and (5.18) may be recast into the form of products of $3j$ symbols. Using (3.8) and (5.15), and considering only the (α,α) elements, expressions for the Ham factors $K(G)$ and $K(H)$ are found to be

$$K(G) = \frac{\pi}{\sqrt{6}}\sum_{\lambda,a,b}\sum_{\nu,a',b'}\sum_{p,q}(-1)^{a+b}\mathcal{F}_{\alpha}^{\lambda,a,b}\mathcal{F}_{\alpha}^{\nu,a',b'}R(\lambda,2,\nu) \tag{5.19}$$
$$\times\left(pq+(p-q)\sqrt{2}\right)\begin{pmatrix}\frac{\lambda}{2} & 1 & \frac{\nu}{2}\\ -a & p & a'\end{pmatrix}\begin{pmatrix}\frac{\lambda}{2} & 1 & \frac{\nu}{2}\\ -b & q & b'\end{pmatrix},$$

$$\text{with}\quad (p,q) = (0,-1),(0,1),(1,1),(-1,-1),$$

$$K(H) = \sqrt{\frac{2\pi^2}{3}}\sum_{\lambda,a,b}\sum_{\nu,a',b'}(-1)^{a+b}\mathcal{F}_{\alpha}^{\lambda,a,b}\mathcal{F}_{\alpha}^{\nu,a',b'}R(\lambda,2,\nu)$$
$$\times\begin{pmatrix}\frac{\lambda}{2} & 1 & \frac{\nu}{2}\\ -a & 0 & a'\end{pmatrix}\begin{pmatrix}\frac{\lambda}{2} & 1 & \frac{\nu}{2}\\ -b & 0 & b'\end{pmatrix}.$$

The variations of these expressions over the range of the parameter Δ are calculated numerically and the results of this are presented in Figures 5.4 and 5.5. These numerically calculated results agree extremely well with the analytical results at the extremities of $G\otimes(g\oplus h)$ calculated in Chapter 4. In Figure 5.4, the Ham factor $K(G)$ approaches an asymptotic value of $1/18$ for large negative Δ, varies through a value of $1/3$ at $\Delta=0$, and approaches an asymptotic value of $3/4$ at large positive Δ. Therefore, at the three extremities of the numerically calculated $K(G)$ in Figure 5.4, there is agreement with the three analytical solutions $K_G^G(\mathcal{D}_3)=1/18$, $K^{eq}=1/3$ and $K_G^G(\mathcal{T})=3/4$, which are calculated in Chapter 4. Similarly, referring to Figure 5.5, the Ham factor $K(H)$ approaches an asymptotic value of $5/9$ for large negative Δ, varies through a value of $1/3$ at $\Delta=0$, and approaches an asymptotic value of 0 at large positive Δ. These three extremities agree very well with the three analytical solutions $K_G^H(\mathcal{D}_3)=5/9$, $K^{eq}=1/3$ and $K_G^H(\mathcal{T})=0$, of Chapter 4.

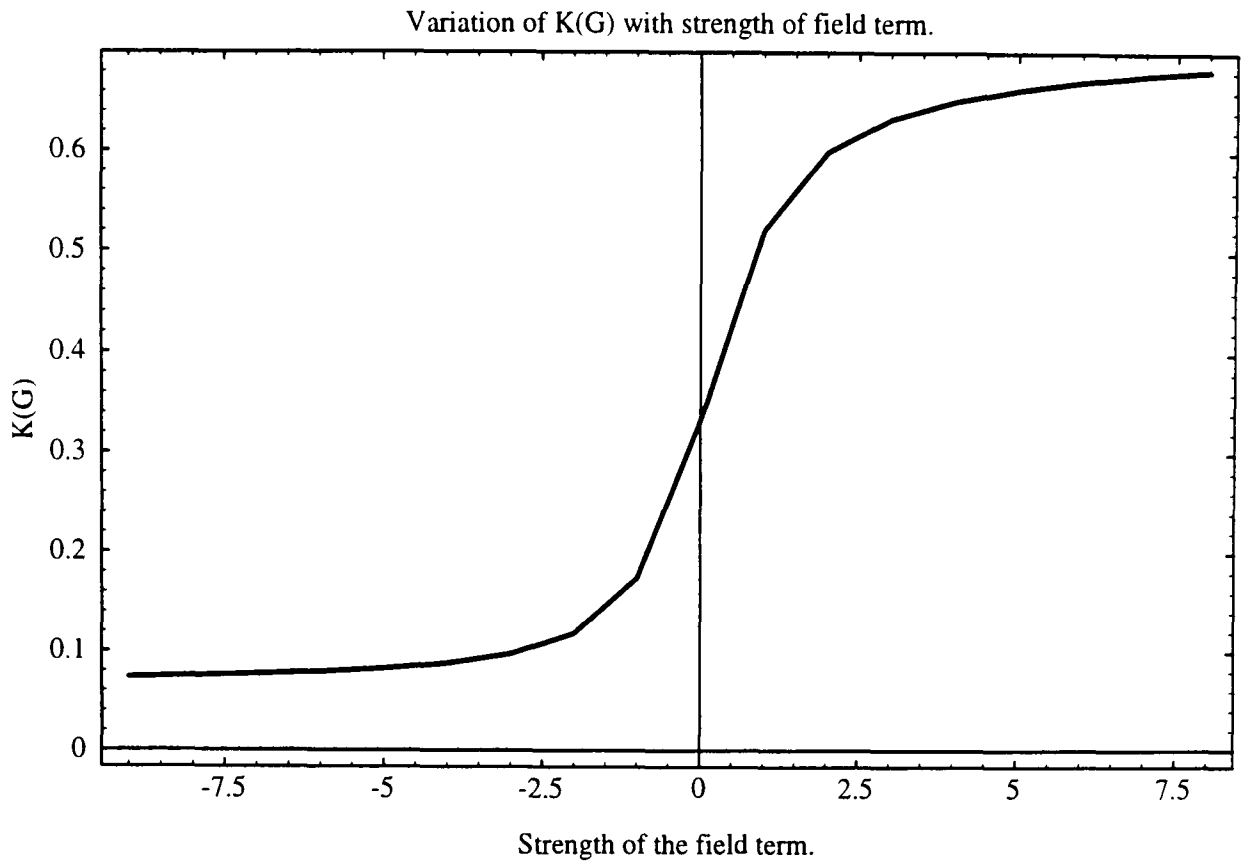

Figure 5.4:

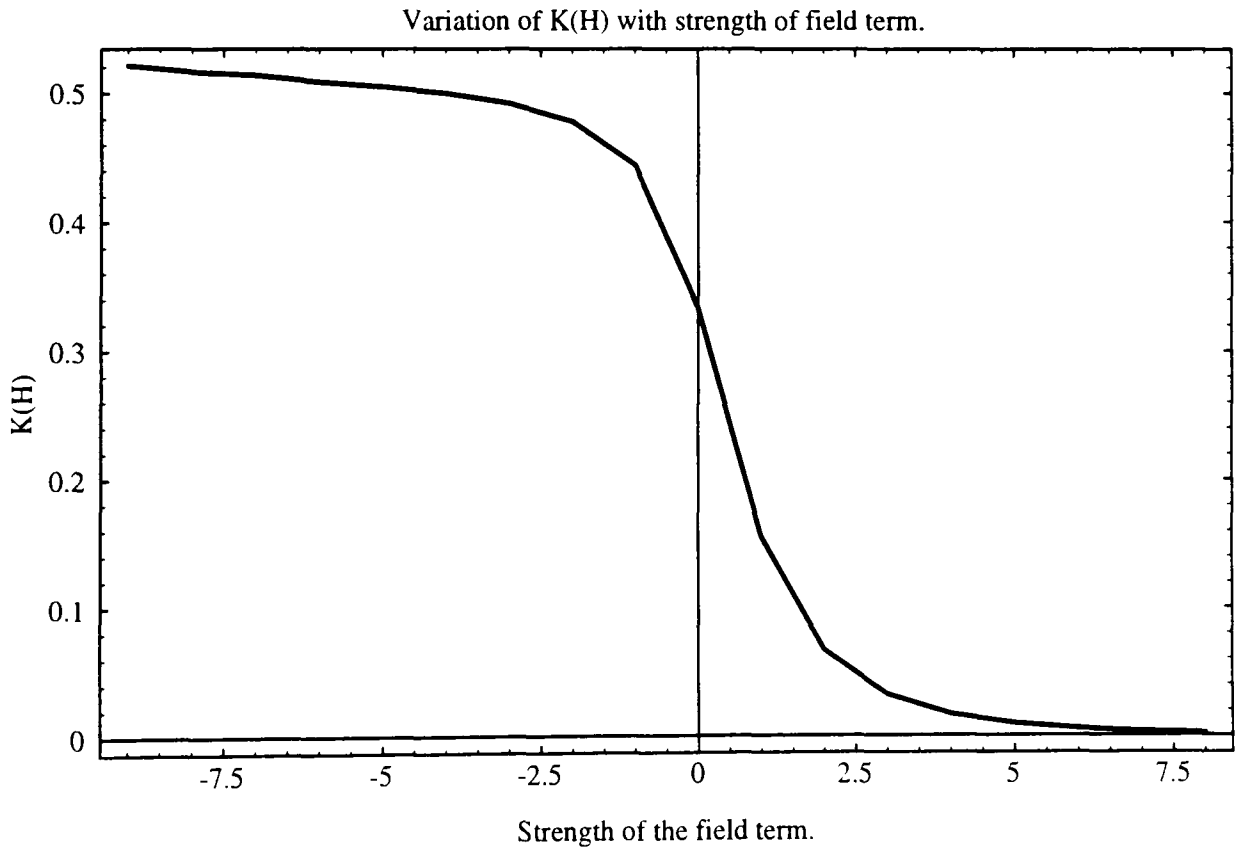

Figure 5.5:

5.4 Limitations of the model.

The most striking limitation of this perturbative model becomes apparent when one attempts to predict the splittings of the first excited states of $G \otimes (g \oplus h)$ for varying Δ. This shortfall of the model is most easily illustrated by considering the positive Δ region depicted in Figure 5.2. According to these results, the first excited state appears to be made up of the irreps $T_1 \oplus T_2 \ominus G \oplus H$ and therefore has a multiplicity of fifteen. For $G \otimes g$ however, the first excited state must have a multiplicity of twenty, corresponding to the four single oscillations that may be excited in each of the five $\mathcal{T}$ wells. This discrepency of five in the two multiplicities arises from the fact that the perturbative model is confined to move upon the hypersphere $(q_o, \theta, \alpha, \beta)$. The nuclear motion therefore only "explores" a three dimensional subspace of the full nine dimensional parameter space which is why the model only predicts a multiplicity of fifteen (three single oscillations in each of the five $\mathcal{T}$ wells) for the first excited state of large positive Δ.

To demonstrate that the model is nevertheless working correctly within its limitations, one may appeal to an analysis of character contributions from the five $\mathcal{T}$ distortions under icosahedral rotations (operations of I). Each $\mathcal{T}$ distortion of an icosahedron possesses three $\mathcal{D}_2$ axes, just as for every Type (II) $\mathcal{T}$ distortion in $G \otimes g$, there are three Type (II) $\mathcal{D}_2$ distortions in $G \otimes h$ (see Table (3.1)). Therefore at each $\mathcal{T}$ distortion of the icosahedron in the perturbative model, the three single oscillations are conveniently represented by three $\mathcal{D}_2$ axes. The effect of icosahedral rotations on these five $\mathcal{T}$ distortions may be analysed class-wise as follows:

Class C_1: This is the class of the identity operation. The three axes of each of the five $\mathcal{T}$ wells, remain fixed under the identity operation and so the character contribution is $5 \times 3 = 15$.

Class C_2: This is the class of rotations by π. Under this operation only one of the five $\mathcal{T}$ distortions will be transformed into a rotated version of itself, contributing a character of -1 (the π rotation about one of the three axes, say z, leads to $(x, y, z) \rightarrow (-x, -y, z) \Rightarrow$ character contribution $-1 - 1 + 1 = -1$). The other $\mathcal{T}$ distortions are rotated into each other and therefore they contribute nothing to the character.

Classes C_3, C_4 and C_5: Classes C_3, C_4 and C_5 correspond respectively to rotations through angles $\frac{2}{3}\pi$, $\frac{2}{5}\pi$ and $\frac{4}{5}\pi$. Operations belonging to these three classes transform all five $\mathcal{T}$ distortions into each other and therefore contribute nothing to the character.

The sequence of characters resulting from the above analysis is therefore:

$$15,\ -1,\ 0,\ 0,\ 0.$$

By referring to the character table for I, Table (2.1), it is simple to see that this sequence may be obtained by selecting the combination of irreps $T_1 \oplus T_2 \oplus G \oplus H$. Therefore, the perturbative result for the first excited state within the positive Δ region, is consistent with the predictions of group theory.

Similar considerations arise in the negative Δ region depicted in Figure 5.3. In this region, if one attributes three single excitations to each of the ten $\mathcal{D}_3$ wells (nuclear motion remains in a three-dimensional subspace) then a multiplicity of thirty is immediately obvious. The first thirty excited states in Figure 5.3, appear to be made up of the irreps $T_1 \oplus T_2 \oplus H \oplus G \oplus H \oplus G \oplus H \oplus A$. In $G \otimes h$ the multiplicity of the first excited state within the ten $\mathcal{D}_3$ minima is fifty. This discrepency in the multiplicities is due to the confinement of the perturbative model to the $(q_o, \theta, \alpha, \beta)$ hypersphere. Once again, this splitting of the first excited states in the perturbative model may be verified by appealing to character theory.

In Chapter 3, the distribution of $\mathcal{D}_3$ minimal distortions over the parameter space of $G \otimes h$ is recast into an easily visualized structure. Two copies of the $\mathcal{D}_3$ minima may be visualized as residing at the vertices of a dodecahedron embedded in the five dimensional parameter space. A representation of a system in which there are three single excitations at each $\mathcal{D}_3$ minimum, may be achieved by placing a vector at each vertex of the dodecahedron. The analysis of the character contribution of such a figure under icosahedral rotations may be done class-wise as follows:

Class C_1: This is the class of the identity operation. The three vector componenets at each of the twenty dodecahedral vertices, remain fixed under the identity operation and so the character contribution is $20 \times 3 = 60$.

Class C_3: This is the class of rotations by $\frac{2}{3}\pi$. Under this operation two of the vertices of the dodecahedron remain fixed (the axis of rotation passes through them) and contribute a character

$$2 + 4\cos\frac{2\pi}{3} = 0.$$

Classes C_2, C_4 and C_5: Classes C_3, C_4 and C_5 correspond respectively to rotations through angles π, $\frac{2}{5}\pi$ and $\frac{4}{5}\pi$. Operations belonging to these three classes transform all ten $\mathcal{D}_3$ vertices into each other and therefore contribute nothing to the character.

The sequence of characters resulting from the above analysis is therefore:

$$60,\ 0,\ 0,\ 0,\ 0.$$

This sequence of characters corresponds to the *regular representation* Γ_{reg} of I [51] and therefore

decomposes into irreps of I according to the direct sum

$$\Gamma_{reg} = A \oplus 3T_1 \oplus 3T_2 \oplus 4G \oplus 5H. \tag{5.20}$$

In order to make use of the symmetry properties of the dodecahedron, the above calculation considers two copies of the same $\mathcal{D}_3$ minima. Therefore, of all the irreps in the regular representation, only those which exhibit an invariance under the inversion symmetry correctly describe the system of $\mathcal{D}_3$ minima. In order to see which of the irreps of the regular representation of I (5.20) fall under this category, one may appeal to the symmetry descent $SO(3) \supset I$. In an icosahedral crystal field, the regular representation of I (5.20) may be constructed in terms of the irreps $D^{(J)}$ of $SO(3)$ (see Table (2.3)):

$$\Gamma_{reg} = D^{(5)} \oplus D^{(6)} \oplus D^{(8)} \oplus D^{(9)}. \tag{5.21}$$

States of even J are symmetric under inversion so the the system of $\mathcal{D}_3$ minima is correctly described by the irreps in $D^{(6)} \oplus D^{(8)}$ which are

$$T_1 \oplus T_2 \oplus H \oplus G \oplus H \oplus A \oplus H \oplus G. \tag{5.22}$$

This is exactly the set of irreps predicted by the perturbative model for the first thirty excited states within the negative Δ region.

The perturbative approach therefore recovers the types of irreps expected by the group theory in the ground states and first excited states for both the $+ve$ and $-ve$ Δ regions. It should be mentioned however, that the truncation of the zeroth order states at $s = 13$ is a source of error which affects the level spacing. By the variational principle, the errors introduced into the energy eigenvalues by truncating the infinite matrix are always positive; that is, the energy calculated by the perturbative method will always be higher than the actual energy.

Therefore as a model of qualitative behaviour, the perturbative approach within its limitations agrees very well with the results expected by group theory (in Chapters 3 and 4, and the character analysis of this section). However, the truncation of the infinite matrix, which allows this problem to be tractable, means that the quantitative results have limited meaning.

5.5 Experimental manifestations of the results.

Although strong manifestations of the icosahedral $G \otimes (g \oplus h)$ interaction have yet to appear in the experimental record, there are some interesting remarks to be made regarding the relationship between these theoretical results and experiment. From Figures (5.4) and (5.5), the main point

to note is that the Ham factors $K(G)$ and $K(H)$ change rather rapidly from their equal coupling ($\Delta = 0$) values of $1/3$ and approach very closely the values appropriate to pure $\mathcal{T}$ (large $+ve$ Δ) and $\mathcal{D}_3$ (large $-ve$ Δ) distortions, even when $|\Delta|$ is not particularly large. The fact that the values of $K(G)$ and $K(H)$ coincide so well with the pure distortion values at the extremes of the coupling régime (i.e. at pure $G \otimes g$, pure $G \otimes h$ and $G \otimes (g \oplus h)_{eq}$), would suggest that enough eigenstates of the perturbed equal coupling Hamiltonian (5.6) were accounted for to accurately model the behaviour of the ground state. Since the results of experiments on such a system will frequently depend on $K(G)$ and $K(H)$, this suggests that one may deduce from the experiments that the system is in a state of $\mathcal{T}$ or $\mathcal{D}_3$ distortion, even when the system is near the equal coupling limit. To illustrate this, one may consider the effect of stress on such a system. Under icosahedral symmetry, the strain tensor

$$e_{i,j} = \frac{1}{2}\left[\left(\frac{\partial u}{\partial x_j}\right) + \left(\frac{\partial u}{\partial x_j}\right)\right], \quad i,j \in \{x,y,z\}, \tag{5.23}$$

transforms as the representation $A \oplus H$, where A-type strain is just $e_A = e_{xx} + e_{yy} + e_{zz}$, and the components of H-type strain are

$$\begin{aligned} e_\theta &= 2e_{zz} - (e_{xx} + e_{yy}), \\ e_\epsilon &= \sqrt{3}(e_{xx} - e_{yy}), \\ e_x &= e_{yz}, \quad e_y = e_{zx}, \quad e_z = e_{xy}. \end{aligned} \tag{5.24}$$

The response of the vibronic system to external stress is characterized by the Ham factor $K(H)$ (the action of an A-type strain in the vibronic ground state is unaffected by the vibronic coupling). A very strong quenching of the effect of H-type strains would indicate a very small or even vanishing $K(H)$. This is exactly the state of affairs appearing in the $+ve$ Δ region of Figure 5.5, which would indicate a g-mode predominance in the Jahn-Teller coupling. Whether or not this g-mode predominance is large is difficult to say because of the very strong decay of $K(H)$ in the $+ve$ Δ region. Nevertheless, in terms of the model used in this chapter, the ground or zero-phonon state in the orbital quartet should therefore correspond to a situation of $\mathcal{T}$ type distortion.

5.6 Summary of Chapter 5.

The Jahn-Teller coupling of a G quartet to both g and h-modes of vibration, can lead to a vibronic ground state that includes both $\mathcal{T}$ and $\mathcal{D}_3$ distortions if the energy difference between the static distortions is small. A simple perturbative model may be set up to study the properties of this

ground state, assuming the Jahn-Teller coupling is strong, so that the adiabatic approximation may be used. This perturbative model involves the solution of the $G \otimes (g \oplus h)$ eigenvalue problem near the limit of equal coupling. The eigenvalues are generated numerically by appealing to the $SO(4)$ parent symmetry and solving the resulting Schrödinger equation at equal coupling perturbed by a fourth-order icosahedral field term with appropriate extremal properties. The resulting ground state is found to be a quartet belonging to the same irrep as the original electronic quartet throughout the range of the field term. Therefore the variation of the ground state Ham factors for G and H operators, $K(H)$ and $K(G)$, may also be studied over this range. The properties of $K(H)$ and $K(G)$ interpolate very well between those appropriate to coupling to g and h-modes separately. The results of experiments on such a system will frequently depend on $K(H)$ and $K(G)$, and one may deduce from the magnitude of these factors that the system is in a state of $\mathcal{T}$ or $\mathcal{D}_3$ distortion, even when the system is near the equal coupling limit. In particular, the variation of $K(H)$ over the Δ range suggests that any strong quenching of H-type strain would indicate a g-mode predominance in the Jahn-Teller coupling and hence a $\mathcal{T}$ type distortion state.

The perturbative model agrees very well with the analytical results for the ground states calculated in Chapters 3 and 4. The static ground states for $G \otimes g$ and $G \otimes h$, and the Ham factors of G and H operators within these ground states may be recovered at the extremities of the perturbative model. As a model of qualitative behaviour, the perturbative approach is able to recover results predicted by the group theory not only in the ground state but also within the qualitative limitations of the first excited state. However, in order to render the problem tractable, a truncation of the infinite interaction matrix is necessary, and therefore the quantitative data resulting from this analysis has limited meaning.

Chapter 6

Optical absorption line shapes for transitions from orbital singlet to G quartet states.

6.1 Introduction.

The optical transition of electrons from a non-degenerate ground state to a degenerate excited state, is usually analysed by considering the effect of the energy splitting of the excited state in the neighbourhood of the equilibrium configuration for the ground state. The dynamical coupling problem between electronic and nuclear motions is very complex, since one cannot assume that the nuclear motions are slow compared to the frequency difference between the electronic levels. Longuet-Higgins *et al.* [62] treated the vibronic problem numerically in the case of $E \otimes \epsilon$ in cubic symmetry. For more complicated systems, the problem becomes intractable because of the complexity of the corresponding APESs. In these cases one may approach an investigation of the line shapes of the optical absorption band, by applying the Franck-Condon approximation. Within this approximation, the effect of the dynamical Jahn-Teller coupling is quite tractable in these more complicated systems. The analyses of this chapter investigate the various possible patterns of classical splitting (i.e. within the framework of the Franck-Condon approximation) of the absorption band corresponding to transitions from an orbital singlet to a G quartet state which is subject to spin-orbit and $G \otimes (g \oplus h)$ dynamical Jahn-Teller interactions.

Much theoretical and experimental work has gone into the interpretation of the spectroscopy of the icosahedral C_{60} molecule [2, 26, 29, 30, 36, 42, 57, 58, 56, 68, 78, 91]. Due to the high symmetry of C_{60}, excited states are degenerate and subject to Jahn-Teller distortion. This would

give rise to the appearance of Jahn-Teller active modes along with Franck-Condon active modes in the spectra. Leach *et al.* [59] discuss how orbitally forbidden bands can appear for the isolated molecule by Herzberg-Teller interactions in which excitation of a vibration of suitable symmetry enables the forbidden transitions to "borrow" intensity from allowed transitions. In the case of C_{60}, the false origins thus created should be capable of acting as origin bands for exitation not only of totally symmetric modes but also of non-totally symmetric Jahn-Teller active vibrations. Apart from the relatively few A_g and A_u states, the electronic states of C_{60} are triply or higher-order orbitally degenerate. These states should exhibit Jahn-Teller distortions in which the degeneracy is removed by exitation of vibrations of suitable symmetry. The detailed vibronic analyses of Leach *et al.* [59] for the $1^1T_{1u} \leftarrow 1^1A_g$ and $2^1T_{1u} \leftarrow 1^1A_g$ allowed transitions, illustrate the rôle of the Jahn-Teller couplings. Regarding orbitally forbidden transitions from the 1^1A_g ground state to G and H levels, Leach *et al.* [59] assign the ζ and η bands in the 2.90-3.02 eV region, to the $2^1H_u \leftarrow 1^1A_g$ and $2^1G_u \leftarrow 1^1A_g$ transitions. On symmetry grounds the Jahn-Teller inducing vibration can be h_g or g_g for these two transitions and Leach *et al.* [59] assign $h_g(8)$ as the mediating mode on the basis of the observed intervals (297 and 247 cm^{-1} respectively [68]). The g_g vibration of lowest frequency in the ground state having a value of about 500 cm^{-1} [68]. In spite of all this, very little structure in the ζ and η bands can be resolved. Other possible icosahedral systems which may exhibit manifestations of the $G\otimes(g\oplus h)$ Jahn-Teller interaction in their optical spectra are those reported in references [86, 18, 84]. One system in particular seems quite a promising candidate; the work of Gu *et al.* [35] on the electronic structure of icosahedral silicon clusters finds that the icosahedral Si_{13}^+ cluster has a highest occupied molecular orbital of symmetry G_g but with only one electron occupation. Therefore, icosahedral Si_{13}^+ will be subject to Jahn-Teller distortions appropriate to G_g electronic state. This work on Si_{13}^+ has been largely theoretical with only a little experimental work vindicating the icosahedral structure of the Si_{13}^+ cluster [18].

Strong manifestations of the $G \otimes (g \oplus h)$ dynamical Jahn-Teller effect have yet to appear in the experimental record. However with modern computing power, theoretical investigations of band shapes resulting from strongly coupled $G \otimes (g \oplus h)$ are possible. The shapes of the absorption bands are very rich in structure, and it is well worth studying these structures even before possible evidence of some of them appear in experimental investigations.

6.2 Vibration induced splitting and band shapes.

In analysing the optical transition from an orbital singlet ground state to a degenerate excited state, one must take into account the splitting of the transition energy due to the excitation of Jahn-Teller active modes. If the degenerate excited state is a G icosahedral quartet, then the operator for angular momentum (the components of $\mathbf{L}$ transform as the partners of the irrep T_1) possesses non-zero matrix elements within the excited state (see Equations (2.24)). Therefore, an optical transition from a singlet to a G icosahedral quartet, will in general be subject to both Jahn-Teller and spin-orbit interactions.

It is difficult to infer anything about the variation of the spectra from the structure of the APESs resulting from the combination of Jahn-Teller and spin-orbit interactions. For $G \otimes (g \oplus h)$ with the inclusion of spin-orbit coupling, a transition from a singlet ground state may occur to any of the four two-fold degenerate multi-dimensional energy surfaces. How these surfaces vary over the field of distortion parameters is not trivial to say the least, and problems of this level of complexity are usually made tractable only by numerical Monte Carlo integration. However, by considering more closely the spin-orbit basis in the G excited state, some structure in the optical spectra may be ascertained without having to perform a numerical integration. The spin-orbit basis for the G excited state reduces to a direct sum of irreps of the icosahedral double group (see Tables (2.2) and (2.3)) according to the symbolic equation

$$G \otimes \Gamma_6 = \Gamma_6 \oplus \Gamma_9, \tag{6.1}$$

where Γ_6 is the spin-$(1/2)$ representation and Γ_9 is the six-fold degenerate spin representation derived from the $SO(3)$ irrep $J = 5/2$. The Kramers degeneracy of Γ_6 cannot be lifted by Jahn-Teller distortions. However, both G and H modes are present within the anti-symmetric square (see Subsection (1.4.1) for the conditions of a Jahn-Teller instability for a spin dependent system).

$$\{\Gamma_9 \otimes \Gamma_9\}_A = 2T_1 \oplus 2T_2 \oplus G \oplus H, \tag{6.2}$$

and therefore the six-fold degeneracy of Γ_9 is in general reduced by Jahn-Teller interaction to three two-fold Kramers degenerate states. Thus, when the spin-orbit interaction is predominant, one would expect an asymmetric absorption band with four intensity maxima, one corresponding to the Γ_6 Kramers degeneracy and the other three corresponding to the symmetry reduced Γ_9, split by the Jahn-Teller interaction. Spectra of this type are usually referred to as "spin-orbit type", referring to the predominance of the spin-orbit coupling over the Jahn-Teller interaction. As the influence of the Jahn-Teller interactions increases, the asymmetry of the absorption band

becomes increasingly "washed away" and the Jahn-Teller effect begins to mix the spin-orbit basis. The energy eigenvalues corresponding to a positive Jahn-Teller distortion differ only by a sign to the energy eigenvalues of the corresponding negative distortion. Therefore, one would expect the optical spectra corresponding to a Jahn-Teller predominance to be symmetric about the average transition energy. The spectra resulting from a predominantly Jahn-Teller system are usually referred to as "x type", where x labels the Jahn-Teller active mode.

It should also be noted that instantaneous splittings in the absorption band of any real system may be almost smoothed away by the complex molecular vibrations in the system. A molecular vibration of one symmetry type is really a superposition of a number of normal modes of the same symmetry but with differing frequency. When averaged over this complicated motion, an instantaneous splitting would be smoothed out. To resolve this problem, *effective modes* (see Section (1.3.2)) are introduced in the place of normal modes. The introduction of effective modes is justified here because the calculations performed in this chapter are confined to the classical Franck-Condon approximation where the nuclear kinetic energy is effectively neglected.

6.3 The Franck-Condon principle.

The Franck-Condon principle asserts that, within a molecular system, an electronic transition takes place more rapidly than the nuclei can respond. This rather intuitive physical consideration is the basis of a relatively simple method for obtaining the electronic transition intensities to different vibrational levels of the electronically excited molecule. The gist of this method is most easily illustrated by considering a very simple system depicted schematically in Figure 6.1. Before the absorption the system is in the ground vibrational state of its ground electronic state, the probability density of which is represented by the Gaussian in the lower curve. Therefore, the transition is most likely to take place when the system is in a configuration $q = 0$, and the likelihood of the transition occuring when $q \neq 0$ varies as a Gaussian in q centred at $q = 0$. When the transition occurs, the system is excited into a state represented by the upper curve. According to the Franck-Condon principle, the nuclear framework remains constant during this excitation, and so one may imagine the transition as being represented by a vertical line $q = q_o$. This is the origin of the expression *vertical transition* which is used to denote an electronic transition which occurs without change of nuclear geometry.

In Figure 6.1, a vertical transition at $q = 0$ cuts through several vibrational levels of the upper electronic state. The level corresponding to the classical turning point in the upper curve is the one in which the system is most likely be at the initial configuration $q = 0$, and therefore

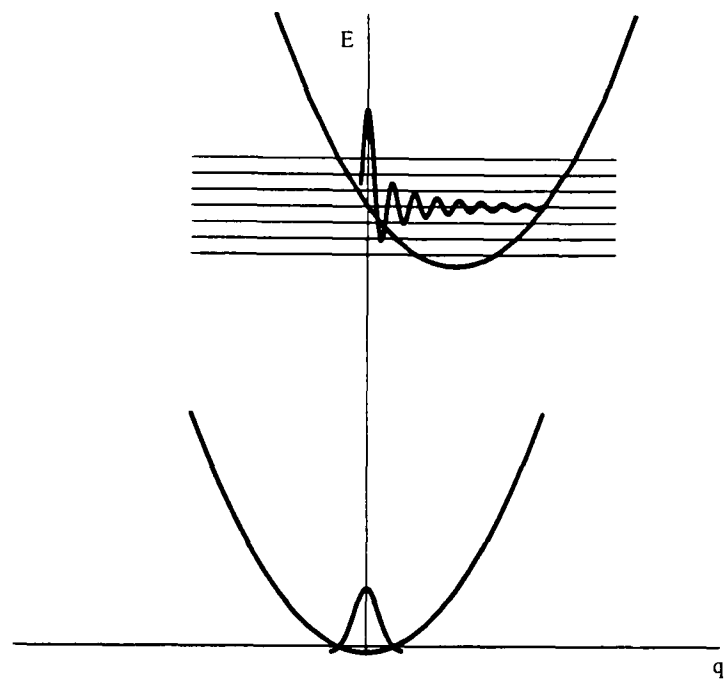

Figure 6.1: Sketch of the potential energy curves in two states between which optical absorption takes place, showing the upper curve on which a vertical transition can arrive. In the lower curve is plotted the square of the ground state wave function, upon which the probability of a vertical transition depends.

is the most probable level for the termination of the transition. If the kinetic energy of the nuclei is ignored, the nuclear wave function at this point may be approximated as a δ-function spike centred at $q = 0$. Therefore, within this approximation, the transition intensity is effectively a *projection* of the ground state probability distribution onto the energy space of the upper state, via whatever interaction that exists in the upper state which produces the displacement of the potential energy curves.

The vibrational structure of the spectrum depends upon the relative displacement of the two potential energy curves, and a lot of vibrational structure is stimulated if the two states are appreciably displaced. However, taking the δ-function approximation for the nuclear wave function of the upper sheet has the effect of smoothing this detail out. For real systems, the great number of normal modes means that the molecular vibrations are not usually manifested as quantum structures in the optical absorption spectrum. A broadening of the spectrum gives rise to a smooth band which is effectively an envelope of unresolved quantum structures. Under these circumstances, the approximation described above can lead to quite a good prediction of

the band shape [90, 19].

For a system in which the excited state is subject to a strong Jahn-Teller interaction, one may imagine a schematic representation similar to that depicted in Figure 6.1. The parameter q in this case is replaced by a set of parameters corresponding to the Jahn-Teller active modes, and the excited state resides upon a set of multi-dimensional APESs. A strongly coupled Jahn-Teller system possesses APESs with minima which are appreciably displaced from the Jahn-Teller origin. Therefore in such systems, a vertical transition takes the system to a state which has a displacement from the origin which is very small compared with the equilibrium Jahn-Teller displacement. Apart from these differences, the procedure for the determination of transition intensities in the Jahn-Teller case is essentially the same as the procedure already outlined above; that is, the transition intensity is effectively a *projection* of the ground state probability distribution onto the adiabatic potential surfaces of the excited state, via a Jahn-Teller (and/or spin-orbit) interaction in the excited state.

These considerations allude to a formulation of the problem which is accessible by computational methods. The following computational prescription, which mimics the above considerations, may be used to calculate the absorption band shapes for a $A \rightarrow \Gamma$ transition, where Γ exemplifies strong Jahn-Teller and spin-orbit interactions:

(i) An energy axis is set up which is divided into N equally spaced slots. The centre of the axis is chosen to correspond to the average transition energy, i.e. the energy at the Jahn-Teller origin. This energy axis represents the energy space upon which the probability distribution of the ground state will ultimately be projected to yield the transition intensities for the various energies.

(ii) The values of the Jahn-Teller active modes are chosen from a Gaussian distribution; that is, the probability of choosing a value x between x and $x + dx$ for a mode value is given by

$$P(x, x + dx) = \frac{1}{\sigma\sqrt{2\pi}} \exp\left(\frac{-x^2}{2\sigma^2}\right) dx, \tag{6.3}$$

where σ^2 is the variance of the distribution. These Gaussian deviates may be generated by the GASDEV routine which has a zero mean and unit variance, using a RAN1 routine as the source of uniform deviates. Both the above mentioned routines may be found in "Numerical recipes for FORTRAN" [69].

(iii) The values of the Jahn-Teller modes generated in (ii) are introduced into the interaction matrix (Jahn-Teller and spin-orbit, see next Section), and the resulting matrix is diagonal-

ized by JACOBI [69]. This yields a set of energy eigenvalues which are then allocated to the energy slots prepared in (i).

(iv) Steps (ii) and (iii) are repeated over many iterations so that a histogram of the occurance of energy eigenvalues may be built up.

The classical Franck-Condon approximation [43], may be formulated in terms of the Fermi "golden rule" yielding a line shape function

$$f(E) = \sum_e |\langle e|P|g\rangle|^2 \delta(E - E_e + E_g), \tag{6.4}$$

where $|g\rangle$ is the ground state and $|e\rangle$ are the excited states. E_g, E_e and E are the energies of the ground state, excited states and the light respectively. P is the dipole moment of the system which interacts with the incident light. $f(E)$ in (6.4) is effectively the sum of the overlaps of the wave function $P|g\rangle$ with the excited states $|e\rangle$, and may be rewritten in terms of an integral of the form

$$f(E) = \left(\frac{1}{2\pi\sigma^2}\right)^{N/2} \sum_j^K \int \ldots \int dQ_1 dQ_2 \ldots dQ_N \exp\left(\frac{-\sum_i^N Q_i^2}{2\sigma^2}\right) \delta(E - E_j(\{Q\})), \tag{6.5}$$

where K is the number of adiabatic potential sheets $E_j(\{Q\})$, upon which the transition can terminate, N is the number of normal modes and σ is the standard deviation of the ground state probability distribution. Equation (6.5), may be further reduced to a convolution of a Gaussian with a band shape function g

$$\begin{aligned} f(E) &= \frac{1}{\sqrt{2\pi\sigma^2}} \int dQ_1 \exp\left(\frac{-Q_1^2}{2\sigma^2}\right) g(E - \kappa_1 Q_1), \\ &= \frac{1}{|\kappa_1|\sqrt{2\pi\sigma^2}} \int dE' \exp\left(\frac{-(E - E')^2}{2\sigma^2\kappa_1^2}\right) g(E'), \end{aligned} \tag{6.6}$$

where Q_1 and κ_1 are respectively the adiabatic parameter and its corresponding coupling coefficient for the A breathing mode and

$$g(E) = \left(\frac{1}{2\pi\sigma^2}\right)^{N/2-1} \sum_j^K \int \ldots \int dQ_2 dQ_3 \ldots dQ_N \exp\left(\frac{-\sum_{i=2}^N Q_i^2}{2\sigma^2}\right) \delta(E - E_j(\{Q\})). \tag{6.7}$$

The introduction of the A mode therefore leads to a broadening and smoothing of the band shape function g.

The computational prescription presented in steps (i) to (iv), describes a numerical Monte Carlo integration. This method effectively calculates complicated integrals of the form (6.7), which arise in the general line shape formula for $A \rightarrow \Gamma$ transition (6.6), where the Γ exemplifies strong Jahn-Teller and spin-orbit coupling.

6.4 The interaction matrix.

The calculation of absorption band shapes for $A \rightarrow G$ where the G exemplifies strong $G \otimes (g \oplus h)$ and spin-orbit coupling, is quite involved and the Monte Carlo method is required to carry out the complicated integral arising from the very large interaction matrix. Using interaction mode coordinates, and choosing $|\alpha+\rangle$, $|\beta+\rangle$, $|\gamma+\rangle$, $|\delta+\rangle$, $|\alpha-\rangle$, $|\beta-\rangle$, $|\gamma-\rangle$, $|\delta-\rangle$, as the electronic basis with spin assignments for the excited states of the icosahedral complex, the 8×8 Jahn-Teller interaction Hamiltonian for the excited states may be written as

$$\hat{\mathrm{H}}_{JT} = \begin{pmatrix} \hat{\mathrm{H}} & 0 \\ 0 & \hat{\mathrm{H}} \end{pmatrix}, \tag{6.8}$$

where the first and second columns appertain to up and down spin states respectively, and $\hat{\mathrm{H}}$ is the 4×4 interaction matrix

$$\begin{aligned} \hat{\mathrm{H}} \;=\; & \kappa_1 Q_a \hat{\mathrm{i}} + \kappa_2 \sum_i Q_i \hat{\mathrm{h}}_i^G + \kappa_3 \sum_j Q_j \hat{\mathrm{g}}_j^G \\ & i \in \{\theta, \epsilon, x, y, z\} \\ & j \in \{\alpha, \beta, \gamma, \delta\}, \end{aligned} \tag{6.9}$$

where $\hat{\mathrm{i}}$ is the unit operator in G and the constants κ_1, κ_2 and κ_3 describe the effective coupling of the G state to the breathing mode A and the Jahn-Teller active modes H and G respectively. The matrices $\{\hat{\mathrm{h}}_i^G\}$ and $\{\hat{\mathrm{g}}_j^G\}$ are given in Appendices (A.3) and (A.1) respectively. The spin-orbit coupling may be introduced by adding to $\hat{\mathrm{H}}_{JT}$ the term

$$\hat{\mathrm{H}}_{so} = \lambda \, (S_x L_x + S_y L_y + S_z L_z), \tag{6.10}$$

the matrix representation of which is constructed from the Pauli matrices and the matrices for L_x, L_y and L_z in (2.24):

$$\hat{\mathrm{H}}_{so} = \frac{\lambda}{2} \begin{pmatrix} 0 & -i & 0 & 0 & 0 & 0 & i & 1 \\ i & 0 & 0 & 0 & 0 & 0 & -1 & i \\ 0 & 0 & 0 & i & -i & 1 & 0 & 0 \\ 0 & 0 & -i & 0 & -1 & -i & 0 & 0 \\ 0 & 0 & i & -1 & 0 & i & 0 & 0 \\ 0 & 0 & 1 & i & -i & 0 & 0 & 0 \\ -i & -1 & 0 & 0 & 0 & 0 & 0 & -i \\ 1 & -i & 0 & 0 & 0 & 0 & i & 0 \end{pmatrix} \tag{6.11}$$

where λ is the effective spin-orbit interaction constant for the excited states of the system. The adiabatic potentials appearing in the general line shape integral are given by the eigenvalues of the interaction matrix [1]

$$\hat{\mathrm{H}}_{int} = \hat{\mathrm{H}}_{JT} + \hat{\mathrm{H}}_{so}, \tag{6.12}$$

over the field of the adiabatic parameters $\{Q_i\}$, $i \in \{a, \theta, \epsilon, x, y, z, \alpha, \beta, \gamma, \delta\}$.

6.5 Results.

There are two important invariances of the band shapes which are worth mentioning before commencing a discussion of the results. These are:

(i) A sign change of the parameters κ_1, κ_2 and κ_3 does not affect the band shape.

(ii) A simultaneous sign change of E and λ leaves the band shape invariant.

In the following calculations, the numerical values of κ_1, κ_2, κ_3 and λ are taken to be positive so that photon energy and the abscissa of the resulting histograms are in the same direction of magnitude.

For the band shapes calculated in the following, it has been necessary to normalize the abscissa as

$$x = \frac{\hbar\omega - \epsilon_o}{\sqrt{\langle M_2 \rangle}}, \tag{6.13}$$

where $\hbar\omega$ is the incident photon energy, ϵ_o is the transition energy for $\kappa_1 = \kappa_2 = \kappa_3 = \lambda = 0$, and $\langle M_2 \rangle$ is the average of the second moment of the interaction Hamiltonian H_{int},

$$\langle \mathrm{Trace}[H_{int}^2] \rangle = 24\lambda^2 + 2\sigma^2(\kappa_1^2 + 5\kappa_2^2 + 4\kappa_3^2), \tag{6.14}$$

where σ is the standard deviation of the distribution from which the values of the adiabatic parameters are derived. For the following results, the Gaussian deviates are derived from GASDEV with a source RAN1, which have a mean of zero and unit standard deviation. The histograms are constructed using 500000 iterations.

The results presented here correspond to the line spectra calculated for the following combinations of the parameters λ, κ_1, κ_2 and κ_3:

$$(1).\ \lambda \neq 0,\ \ \kappa_2 \neq 0,\ \ \kappa_3 = 0.$$

$$(2).\ \lambda \neq 0,\ \ \kappa_2 = 0,\ \ \kappa_3 \neq 0.$$

[1] $\hat{\mathrm{H}}_{int}$ is Hermitian, and its eigenvalues are computed by turning the 8×8 complex problem into a 16×16 real problem.

$$_1 = 0 \text{ and } \kappa_1 \neq 0.$$

$$\kappa_2 \neq 0, \quad \kappa_3 \neq 0.$$

$$\text{for } \kappa_1 \neq 0.$$

$$(4). \quad \lambda \neq 0, \quad \kappa_2 \neq 0, \quad \kappa_3 \neq 0.$$

$$\text{for } \kappa_1 \neq 0.$$

The abscissae of the corresponding figures have been offset along the ordinate axes. This assists the inspection of progressive variations in the band shapes due to the varying of the parameters.

(1). Figures 6.2 and 6.3 show the variation of the line shape with the change in the ratio of λ and κ_2. Since the H mode is Jahn-Teller active in the presence of the spin-orbit interaction, four peaks are generally seen corresponding to Kramers degenerate pairs, three derived from Γ_9, and one derived from Γ_6 (see Section (6.2)). As the influence of the H mode increases, the band shape becomes increasingly symmetric and spread-out with the peaks decreasing in prominence, see Figure 6.2. The peak corresponding to the spin-orbit type Γ_6 doublet, merges with the rest of the band at around $\lambda/\kappa_2 = 0.75$ and seems to become a shoulder of the broad H type band at around $\lambda/\kappa_2 = 0.25$. The three peaks corresponding to the three Kramers doublets derived from Γ_9, seem to eventually form a shoulder and central maxima. For $\lambda/\kappa_2 = 0.00$, the band becomes broad with three "mini" maxima flanked by high shoulders, see Figure 6.3.

The results for the inclusion of the A breathing mode into H/spin-orbit type spectra, are presented in Figures 6.4, 6.5, 6.6 and 6.7. In Section (6.3), the line shape formula is shown to be a convolution of a Gaussian function in the A mode and a band shape function g, leading to a smoothing effect on g. The plots in Figures 6.4, 6.5, 6.6 and 6.7, exemplify the kind of smoothing behaviour expected for these combinations of parameters. The spin-orbit coupling is large compared to the H Jahn-Teller coupling and so asymmetry is always present. The effect of the A mode is to smooth-out the peaks corresponding to the Kramers doublets from Γ_6 and Γ_9, but a distinction between these two kinds of doublet is still present. As the H mode increases in strength, peaks corresponding to the three Kramers doublets of Γ_9 once again become visible at about $\lambda = 1.00$, $\kappa_1 = 0.25$, $\kappa_2 = 0.50$, see Figure 6.5.

(2). Spectra for G/Spin-orbit type are presented in Figures 6.8, 6.9, 6.10, 6.11, 6.12, and 6.13. The structures in these spectra closely resemble structures appearing in the spectra of (1). In Figures 6.8 and 6.9, the behaviour of the band shape as λ/κ_3 decreases is very similar

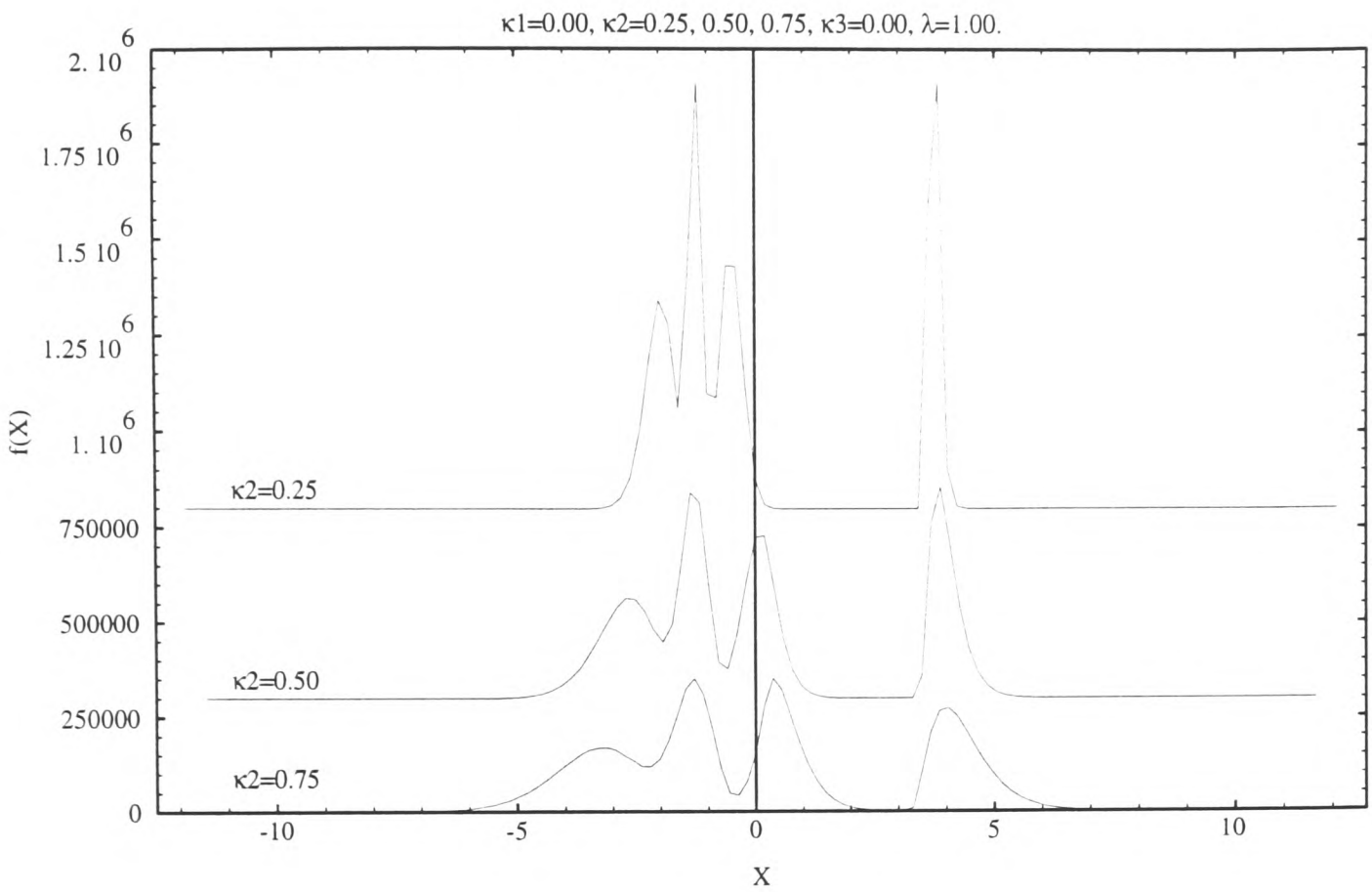

Figure 6.2: Spin-orbit type > H type.

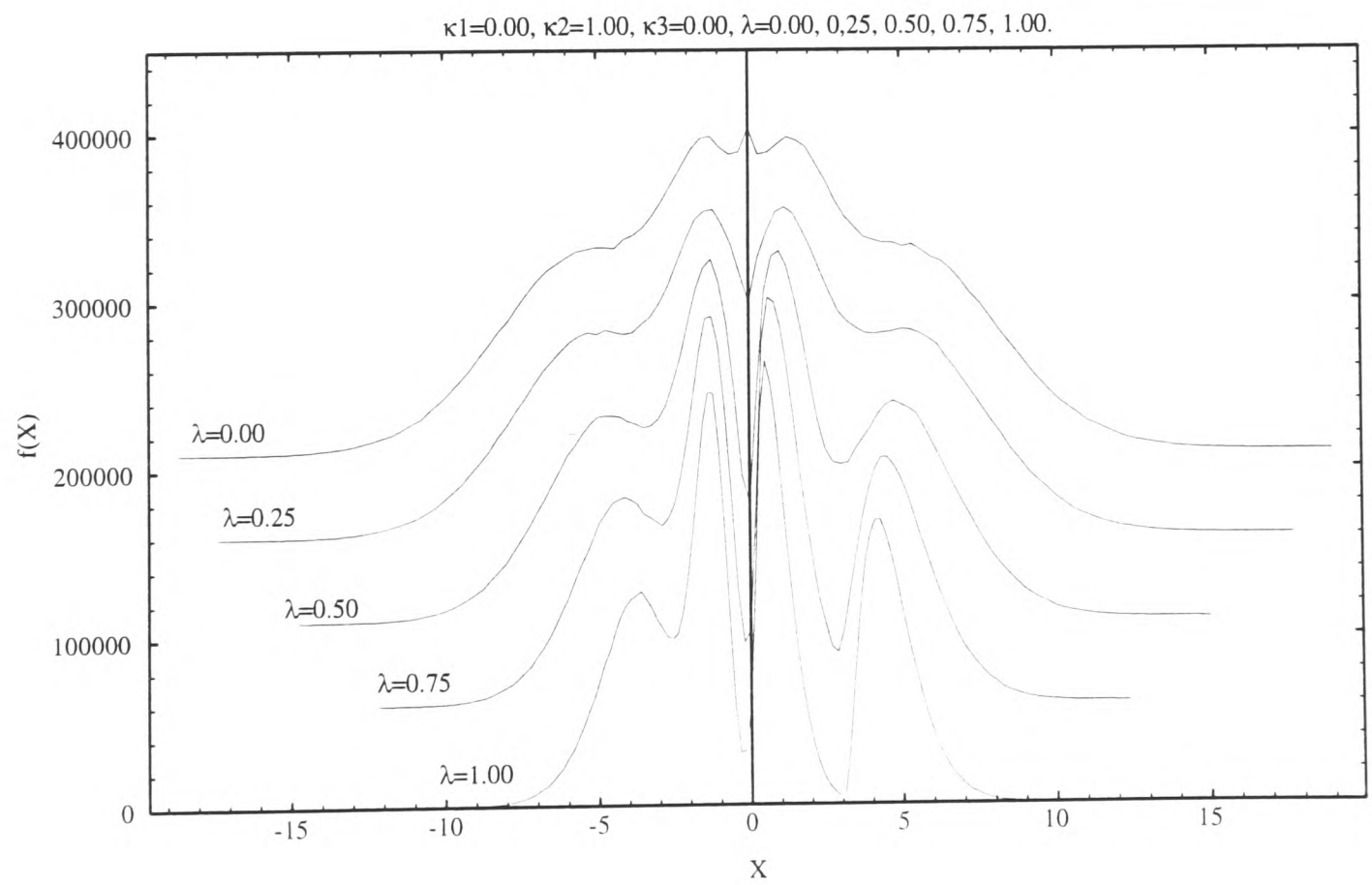

Figure 6.3: H type > Spin-orbit type.

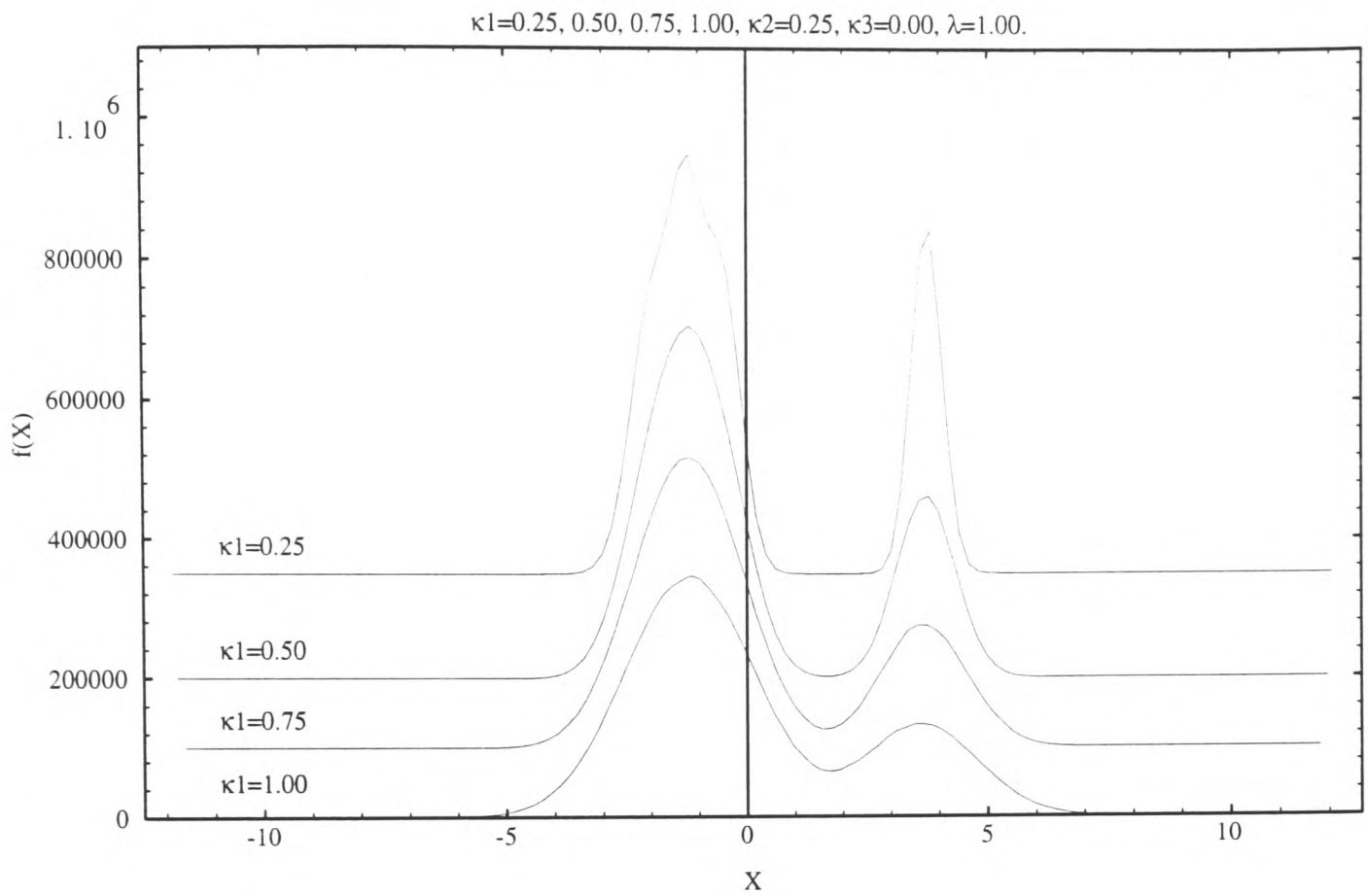

Figure 6.4: H/Spin-orbit type with A breathing mode (a).

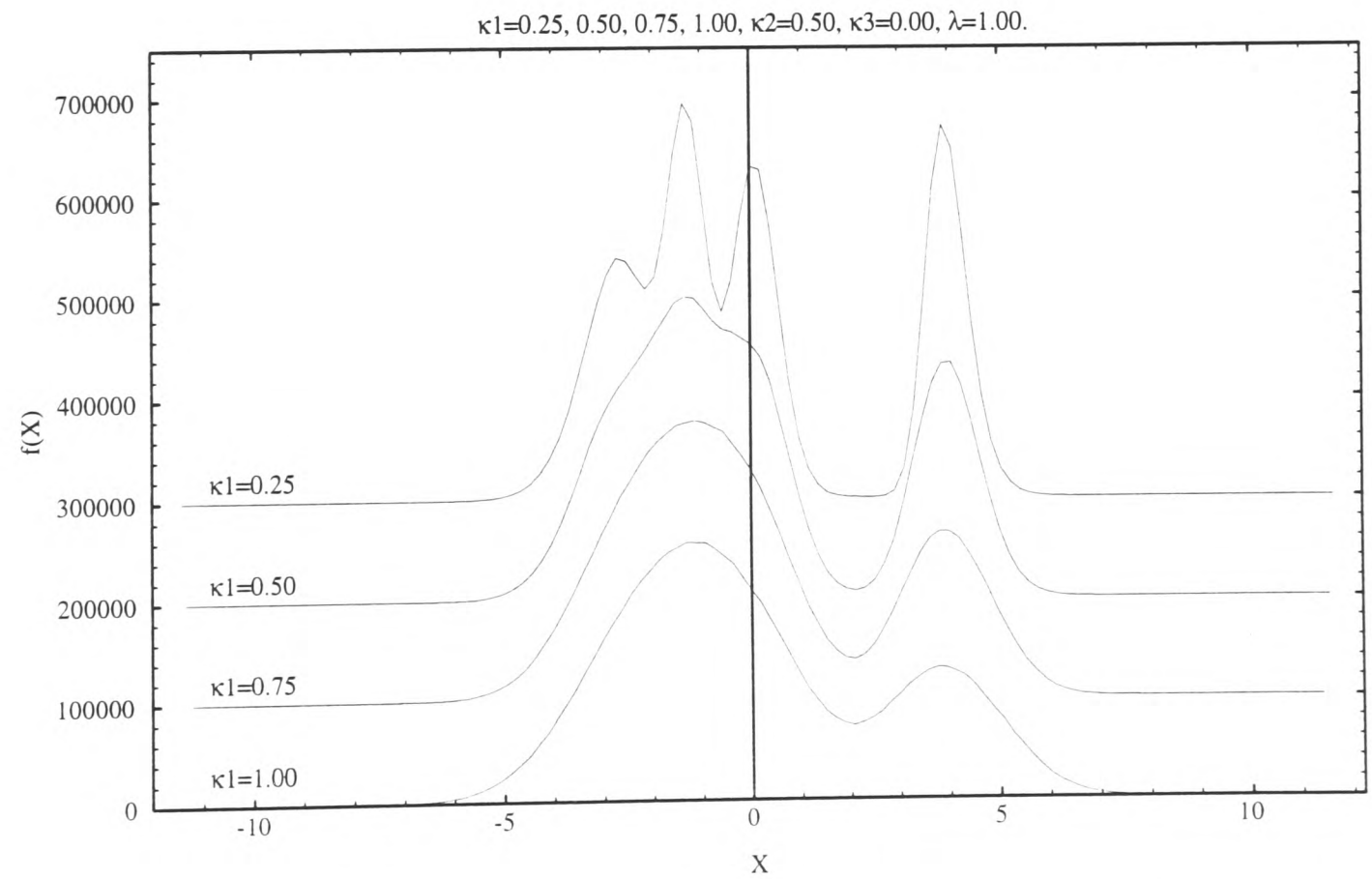

Figure 6.5: H/Spin-orbit type with A breathing mode (b).

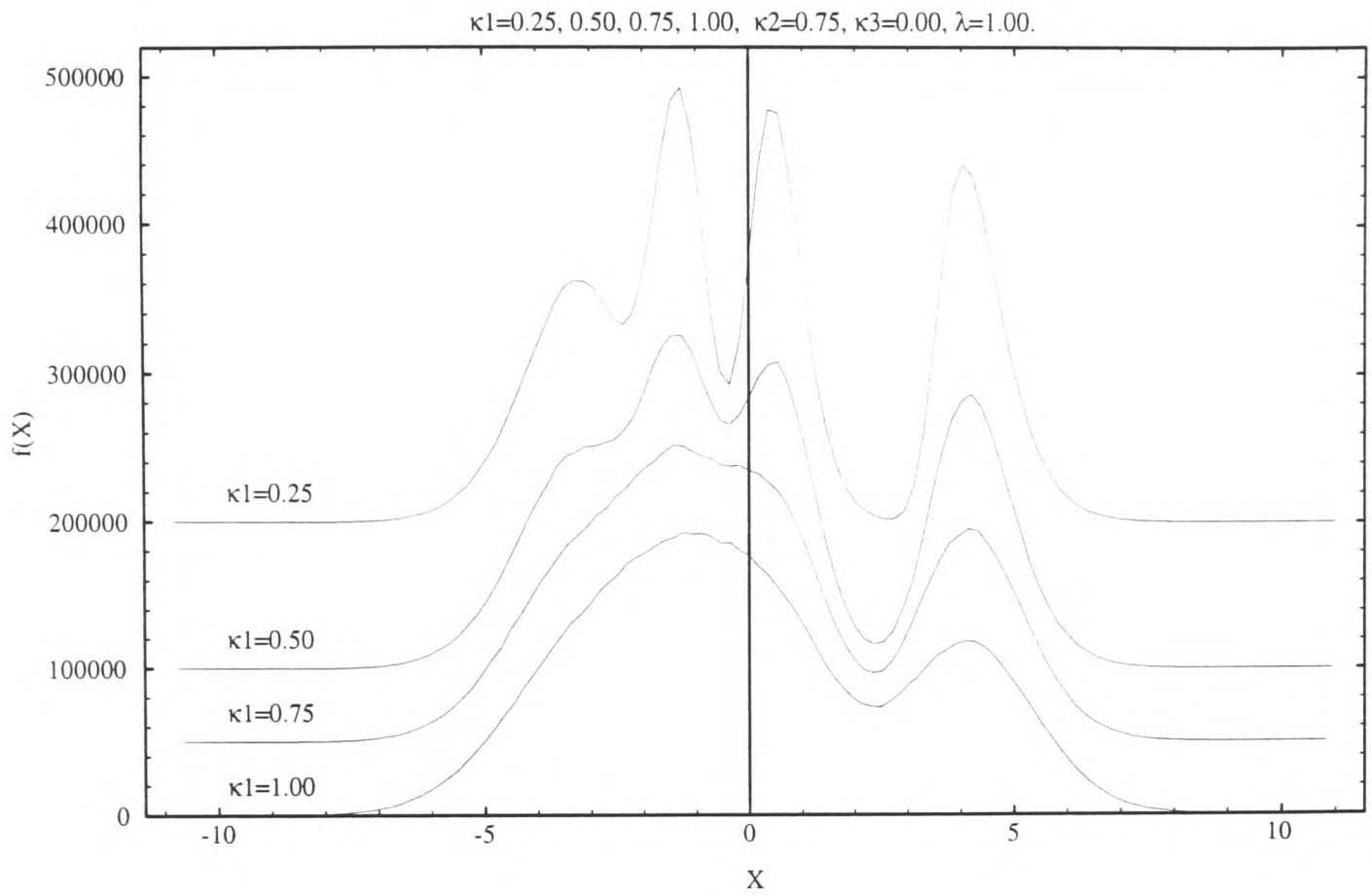

Figure 6.6: H/Spin-orbit type with A breathing mode (c).

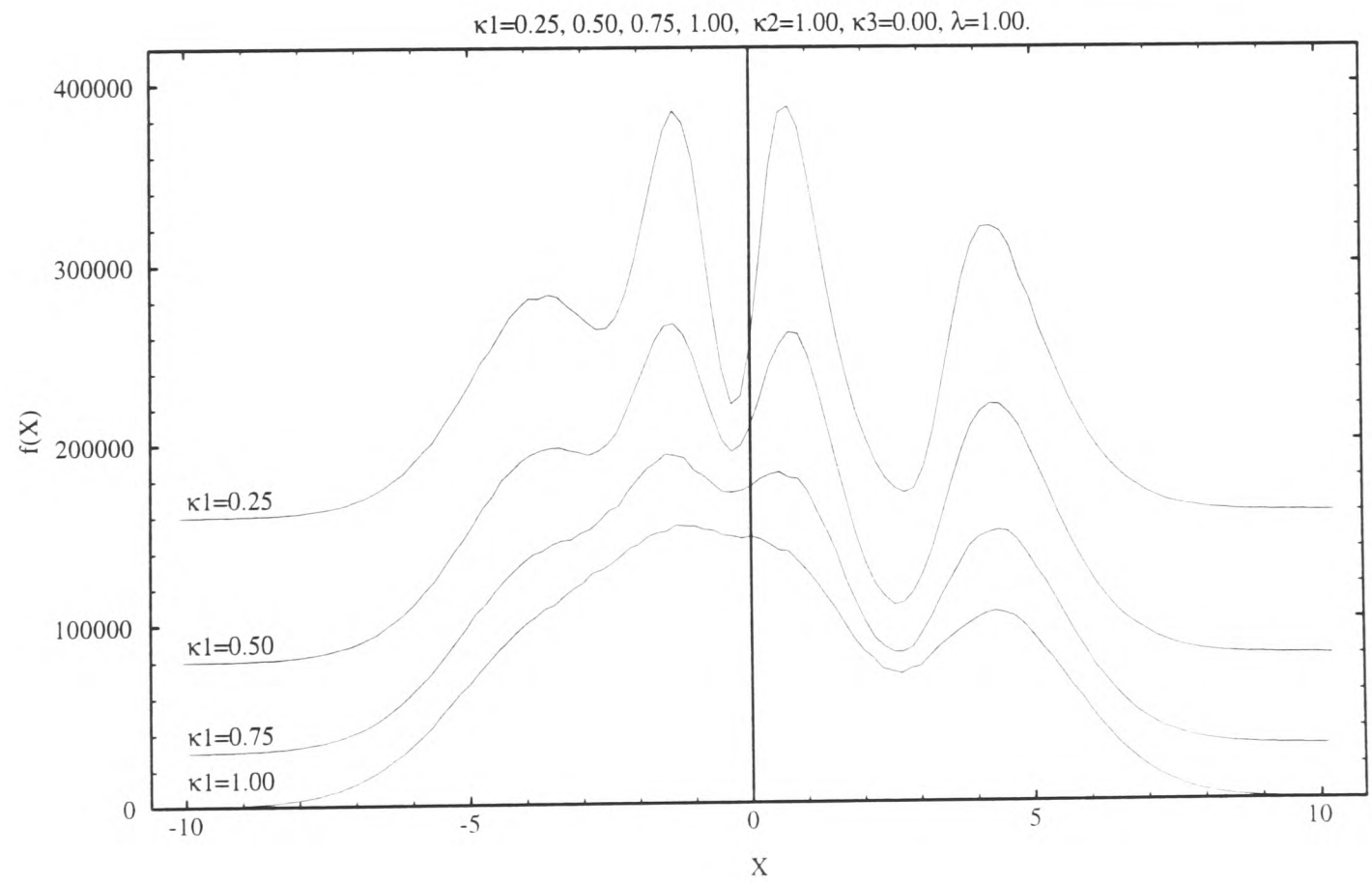

Figure 6.7: H/Spin-orbit type with A breathing mode (d).

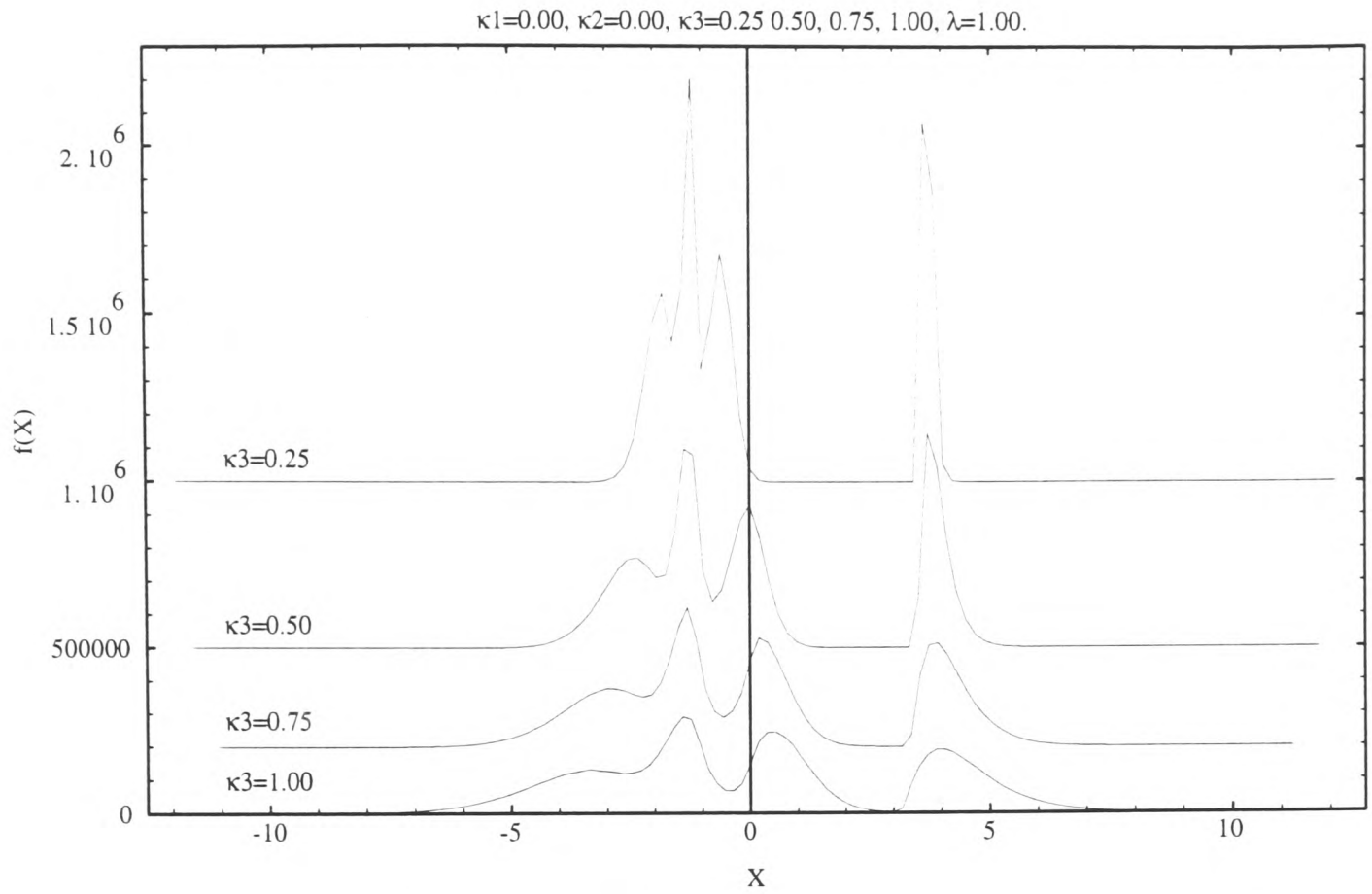

Figure 6.8: Spin-orbit type > G type.

to the behaviour exhibited by the H/Spin-orbit type spectra for decreasing λ/κ_2, except that for $\lambda/\kappa_3 = 0.00$ the band exhibits two relatively prominent maxima. The Figures 6.10, 6.11, 6.12, and 6.13, show the smoothing effect of the A mode on G/Spin-orbit type spectra.

(3). H/G type: For these spectra $\lambda = 0$ and the results are presented in Figures 6.14, 6.15 and 6.16, for varying A mode influence. Figures 6.14 and 6.16 respectively depict the results for $\kappa_2 > \kappa_3$ and $\kappa_3 > \kappa_2$. Figure 6.15 shows the behaviour of the "Equal coupling" band shape under the influence of an A mode of increasing strength. The equal coupling band is well spread out and exhibits four almost equally prominent maxima for $\kappa_1 \rightarrow 0$.

(4). Some results for the most general cases are given in Figures 6.17, 6.18, 6.19, 6.20 and 6.21. In order not to repeat bands of very similar structure, only four cases for which $\kappa_3 \geq \kappa_2$ and one case for which $\kappa_3 < \kappa_2$, are presented. The structures in Figures 6.17, 6.18 and 6.19, are very similar in both $\kappa_3 \geq \kappa_2$ and $\kappa_3 < \kappa_2$ régimes. The structures in Figures 6.20 and 6.21 differ slightly in that for $\kappa_3 \geq \kappa_2$ the second maximum from the left is the most prominent, whereas for $\kappa_3 < \kappa_2$ it is the third which is the most prominent.

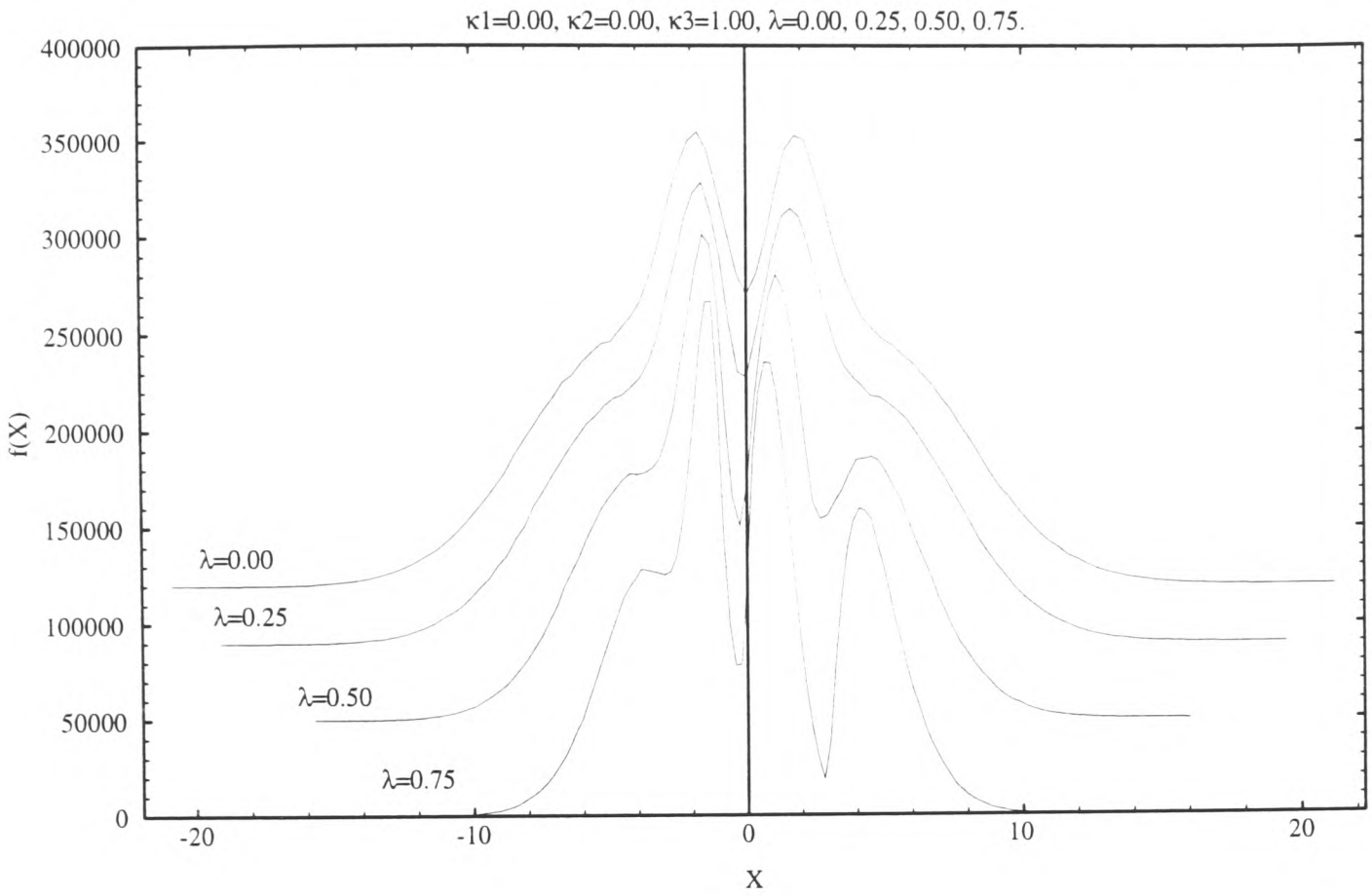

Figure 6.9: G type > Spin-orbit type.

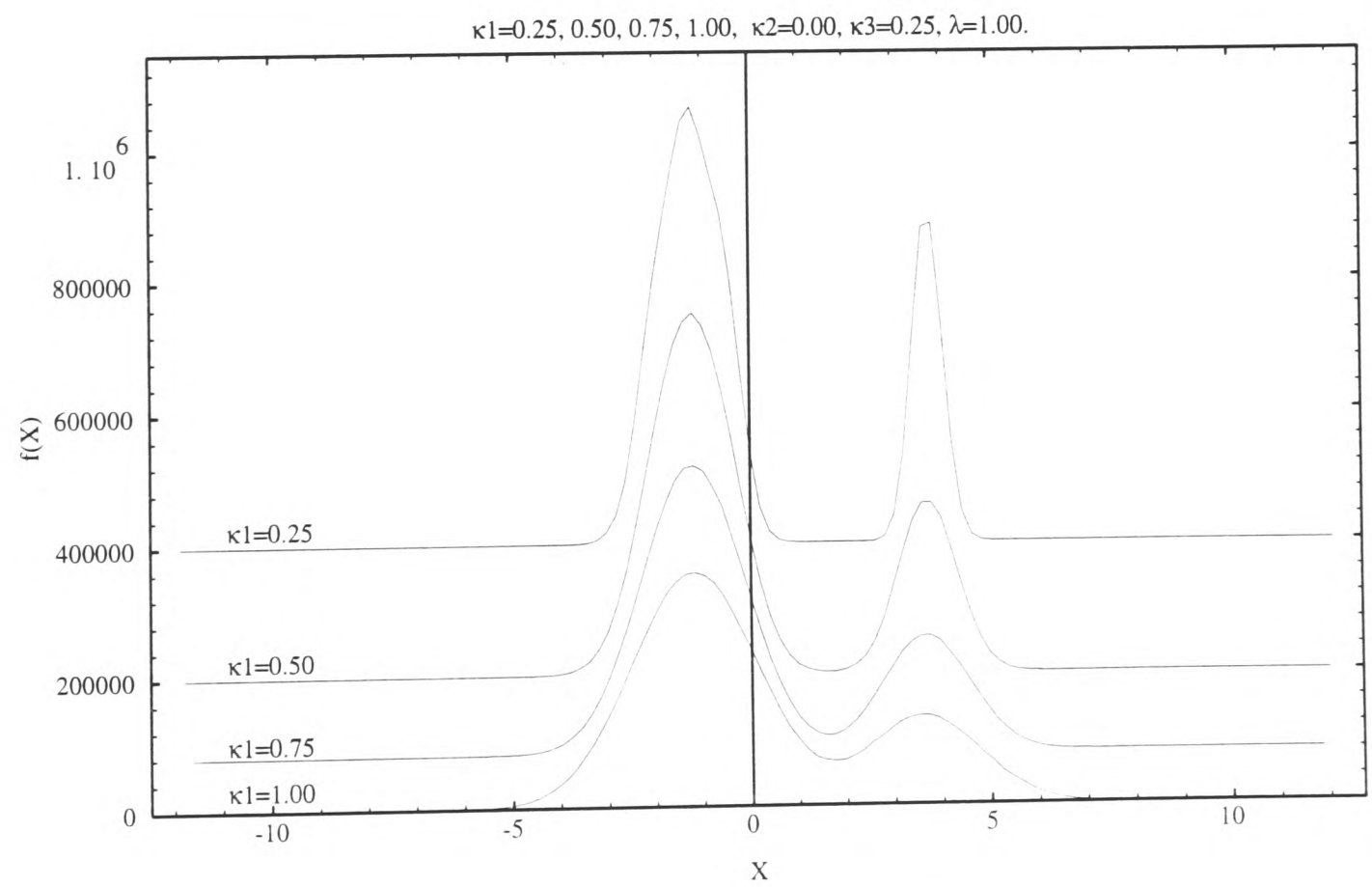

Figure 6.10: G/Spin-orbit type with A breathing mode (a).

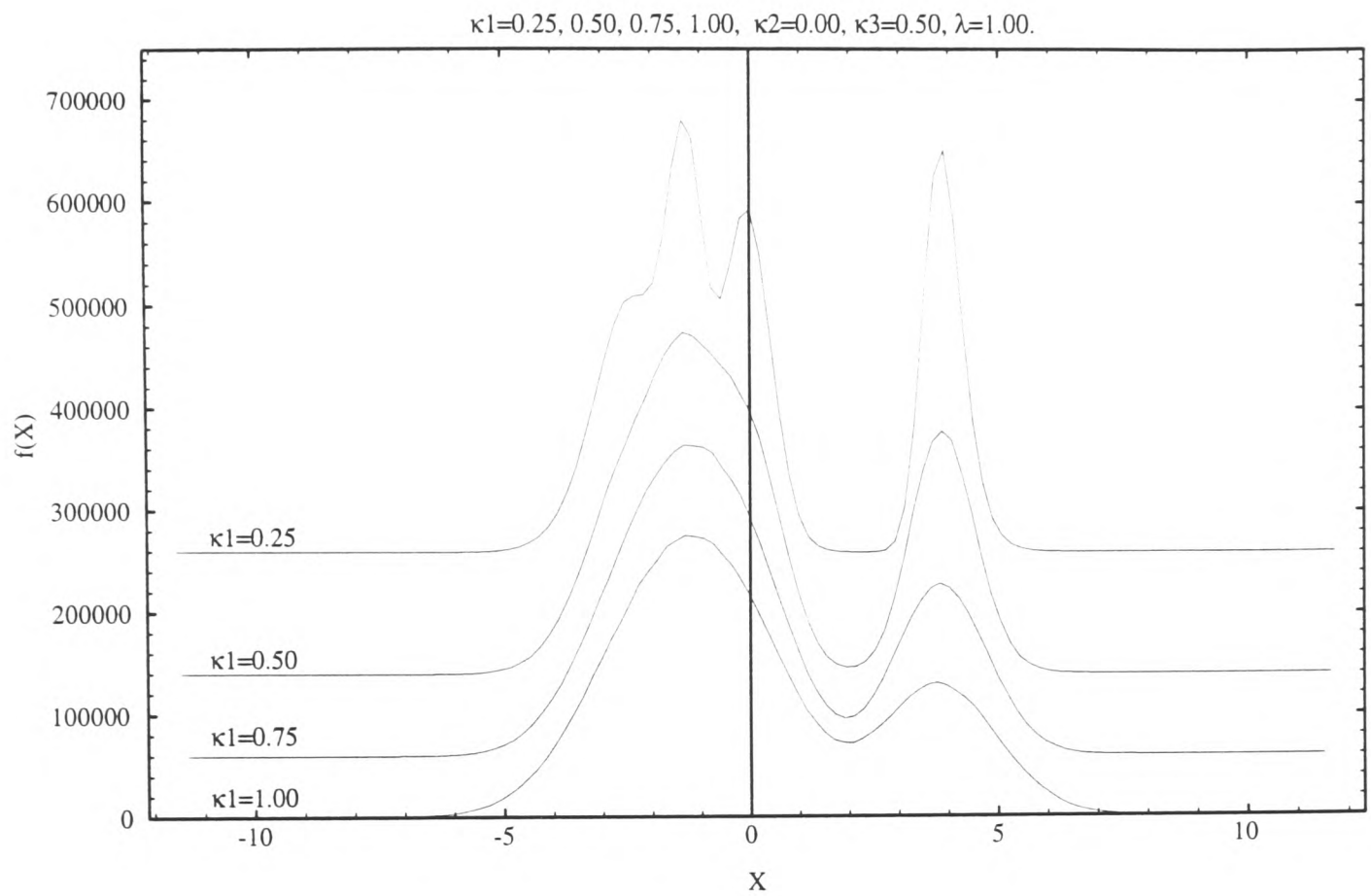

Figure 6.11: G/Spin-orbit type with A breathing mode (b).

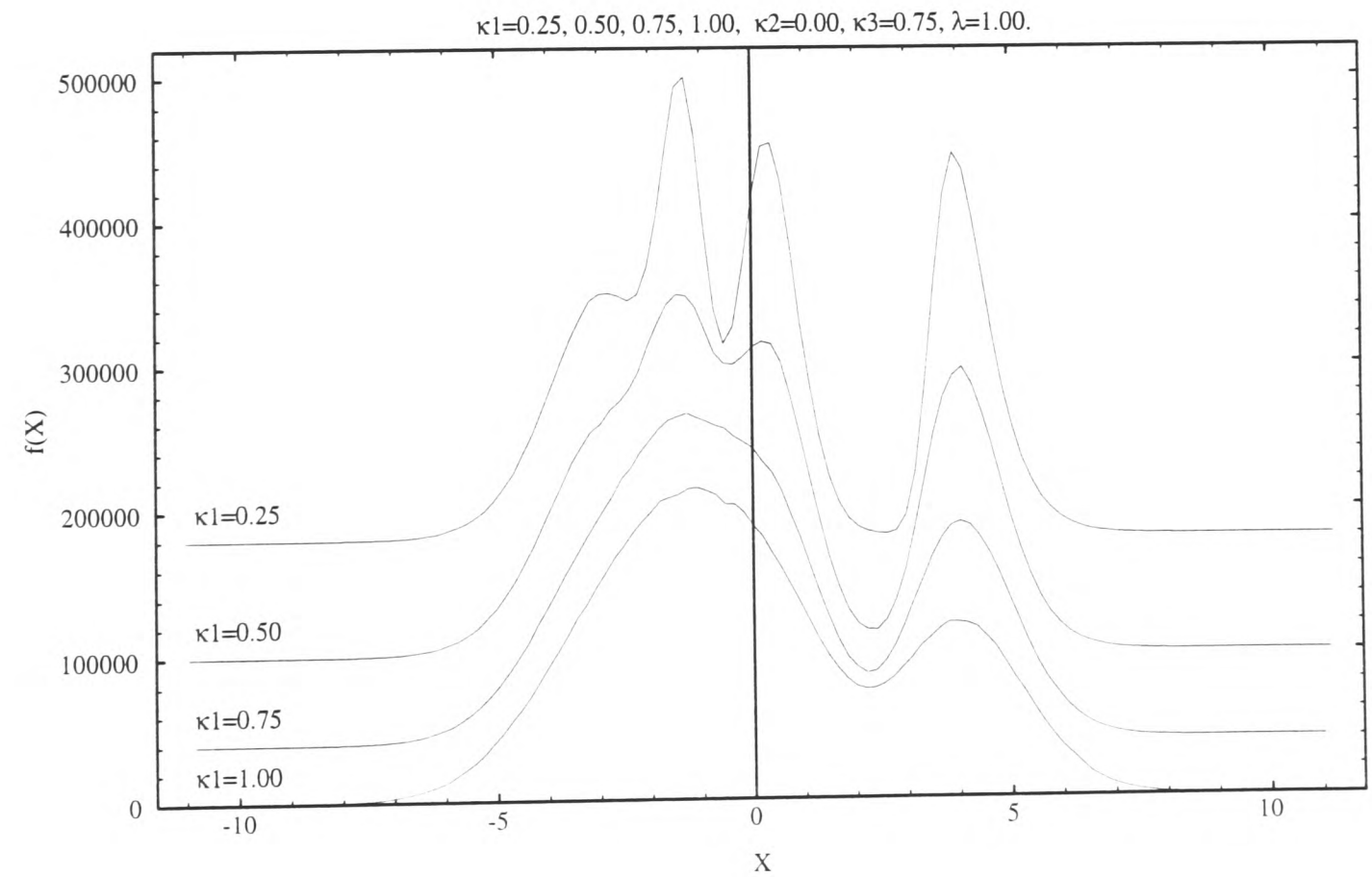

Figure 6.12: G/Spin-orbit type with A breathing mode (c).

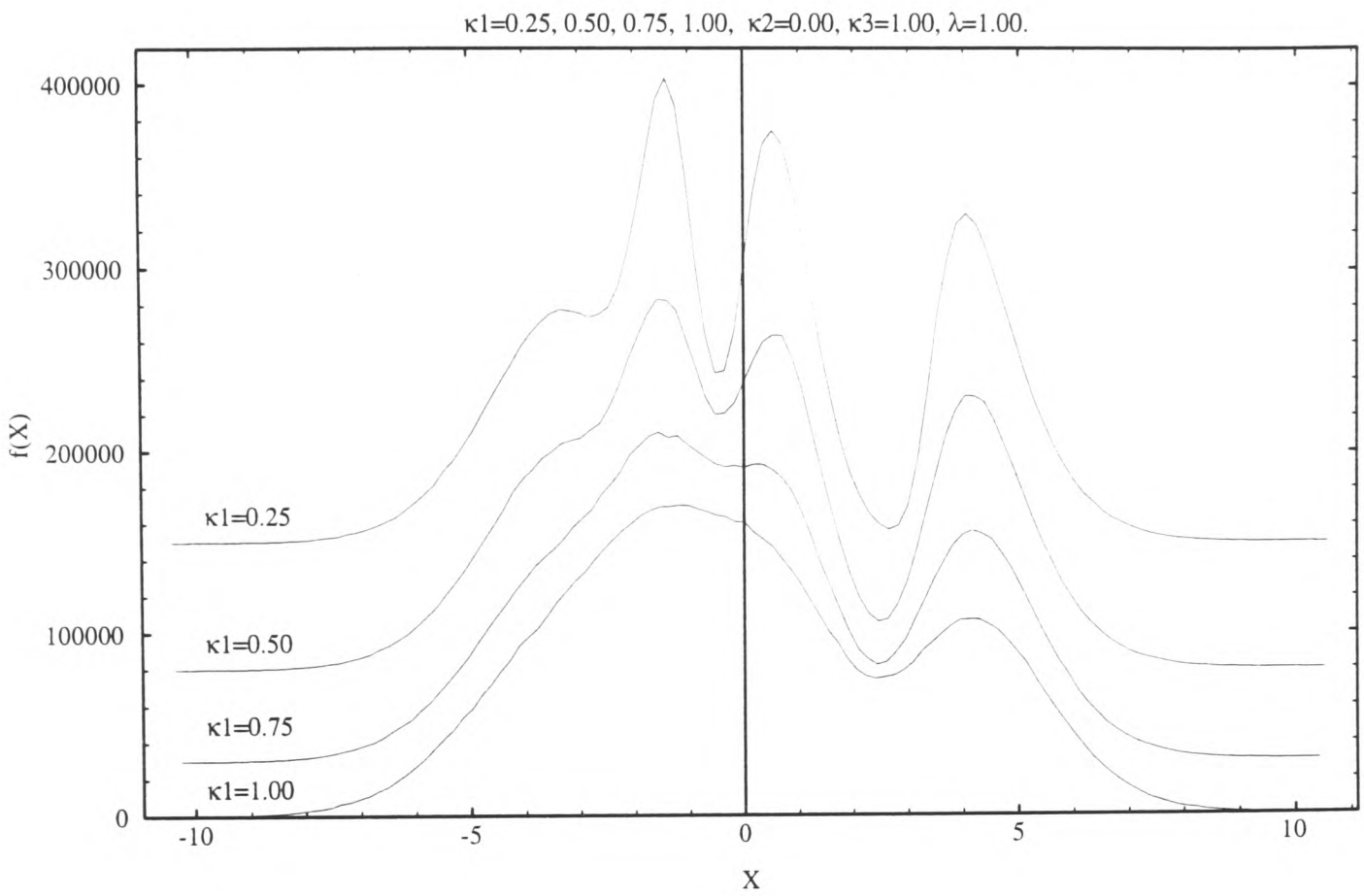

Figure 6.13: G/Spin-orbit type with A breathing mode (d).

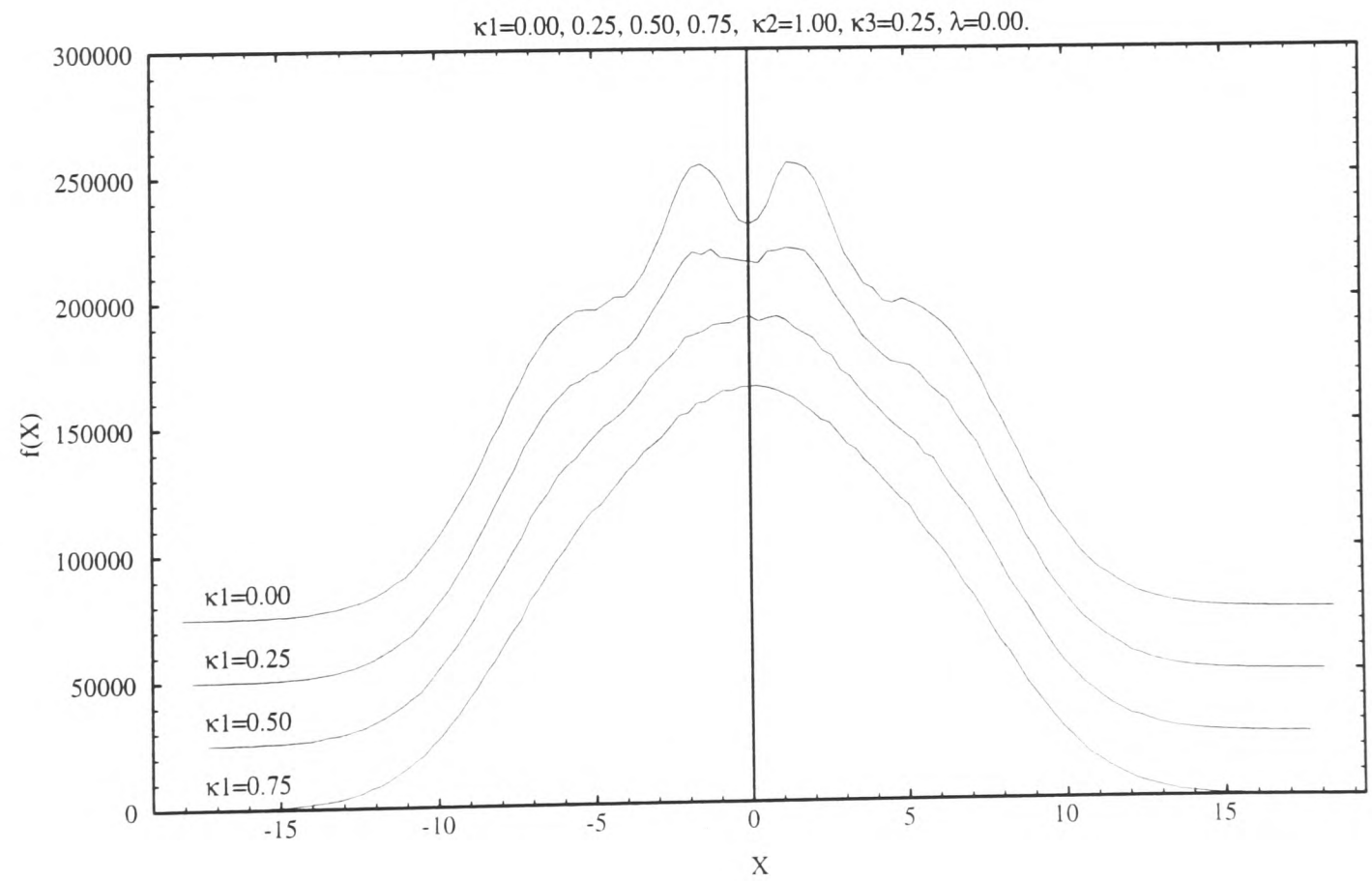

Figure 6.14: $H > G$ type with A breathing mode.

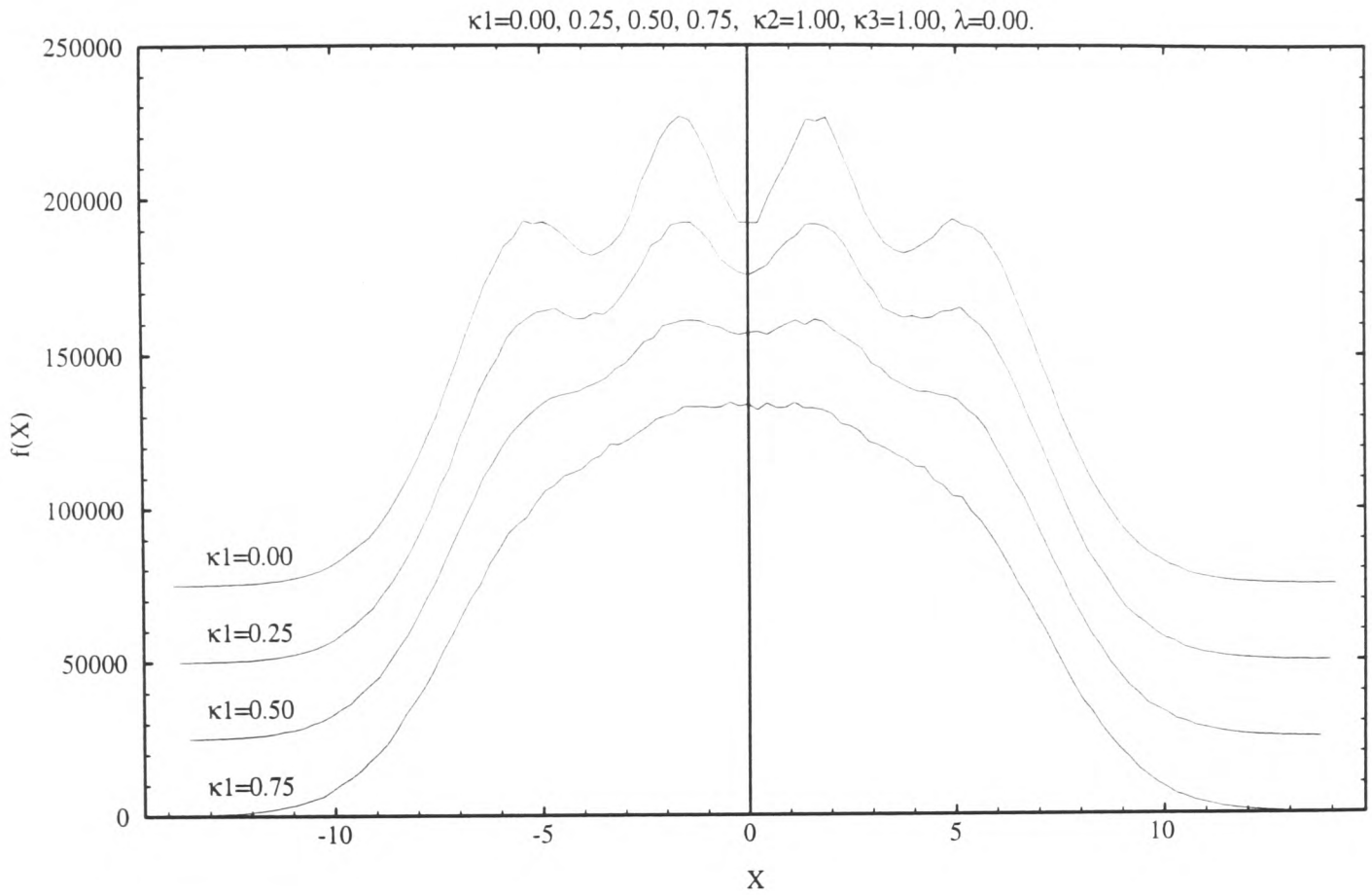

Figure 6.15: $H = G$ type with A breathing mode.

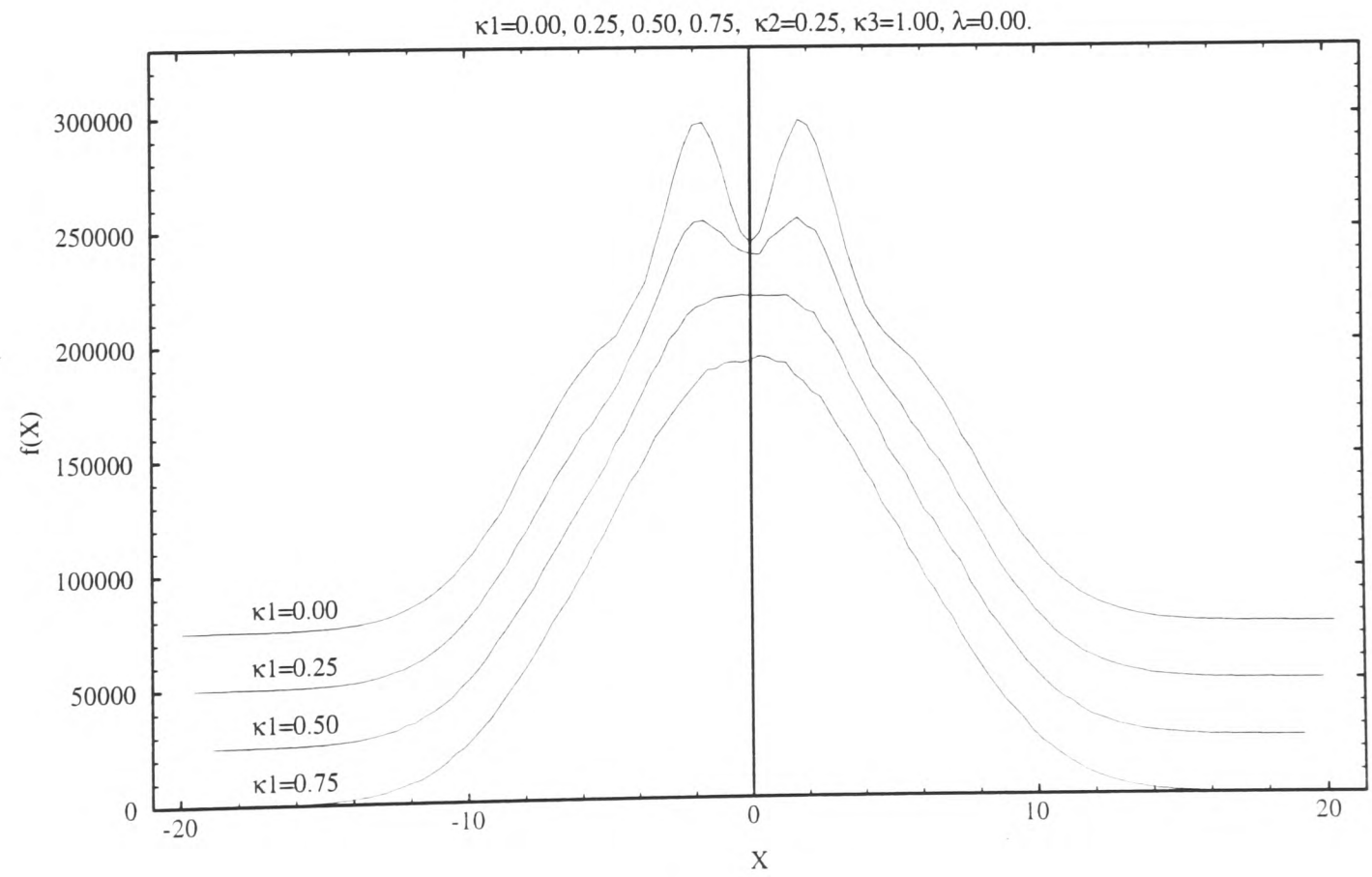

Figure 6.16: $G > H$ type with A breathing mode.

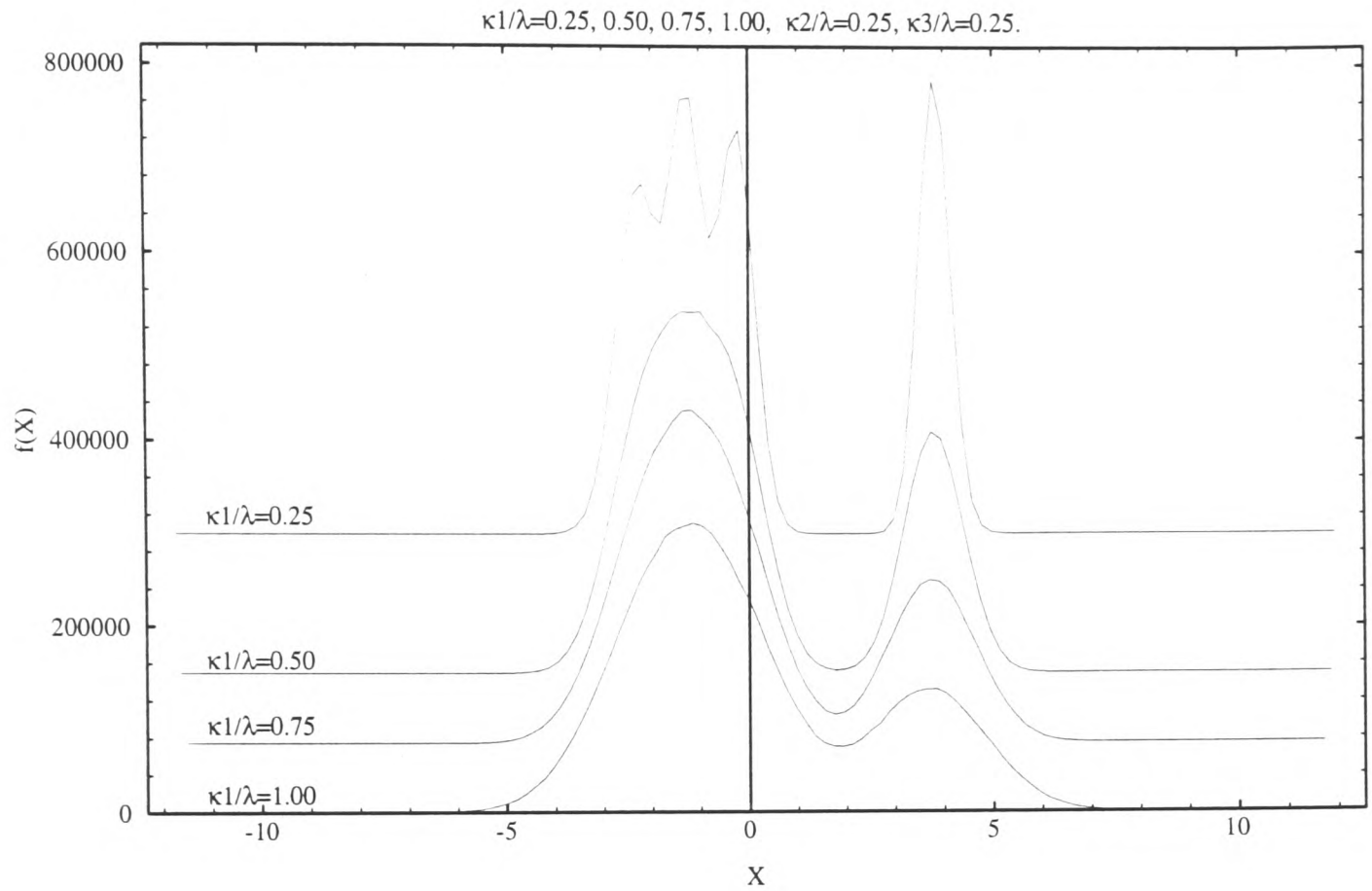

Figure 6.17: General cases (a).

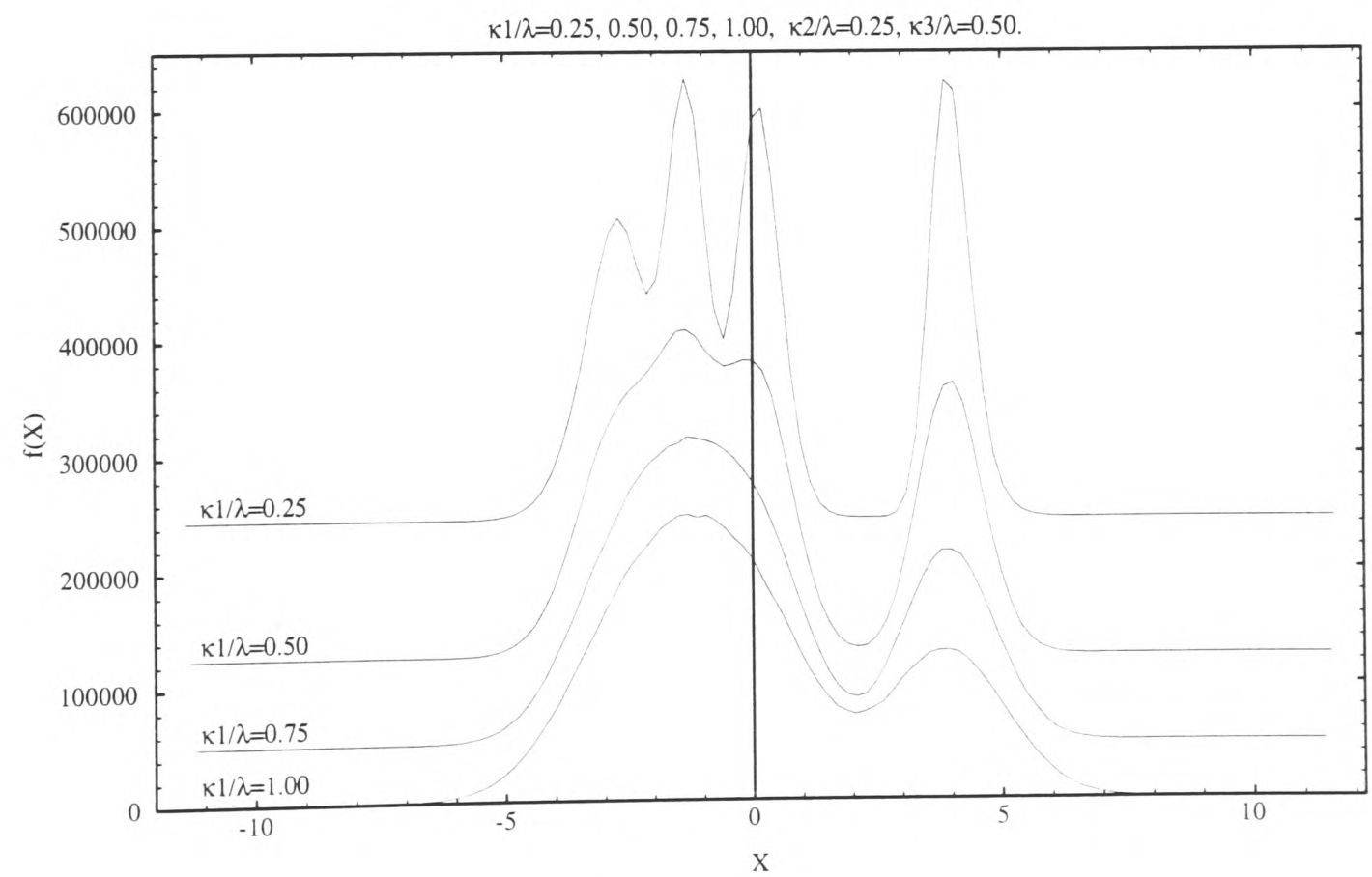

Figure 6.18: General cases (b).

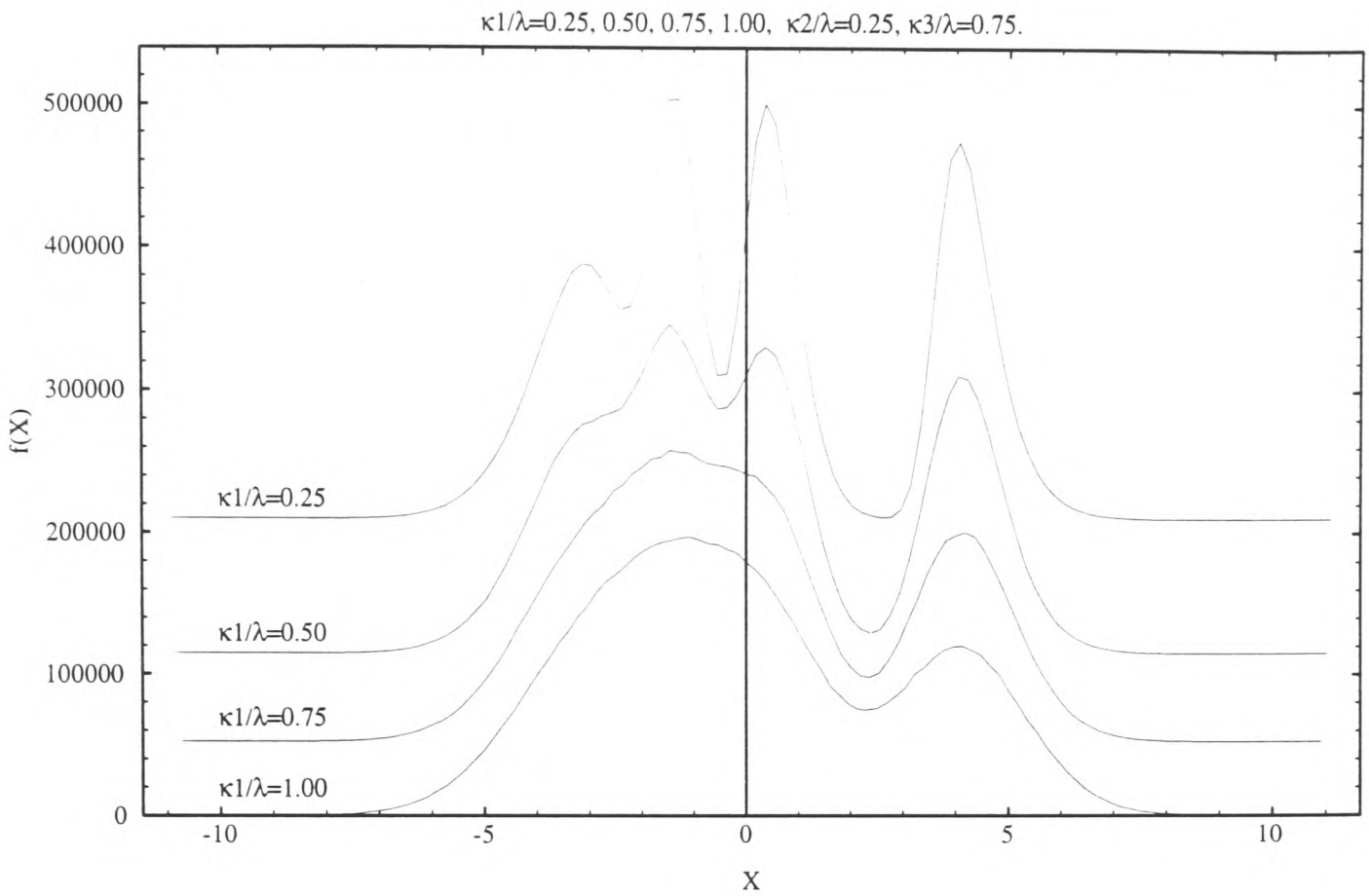

Figure 6.19: General cases (c).

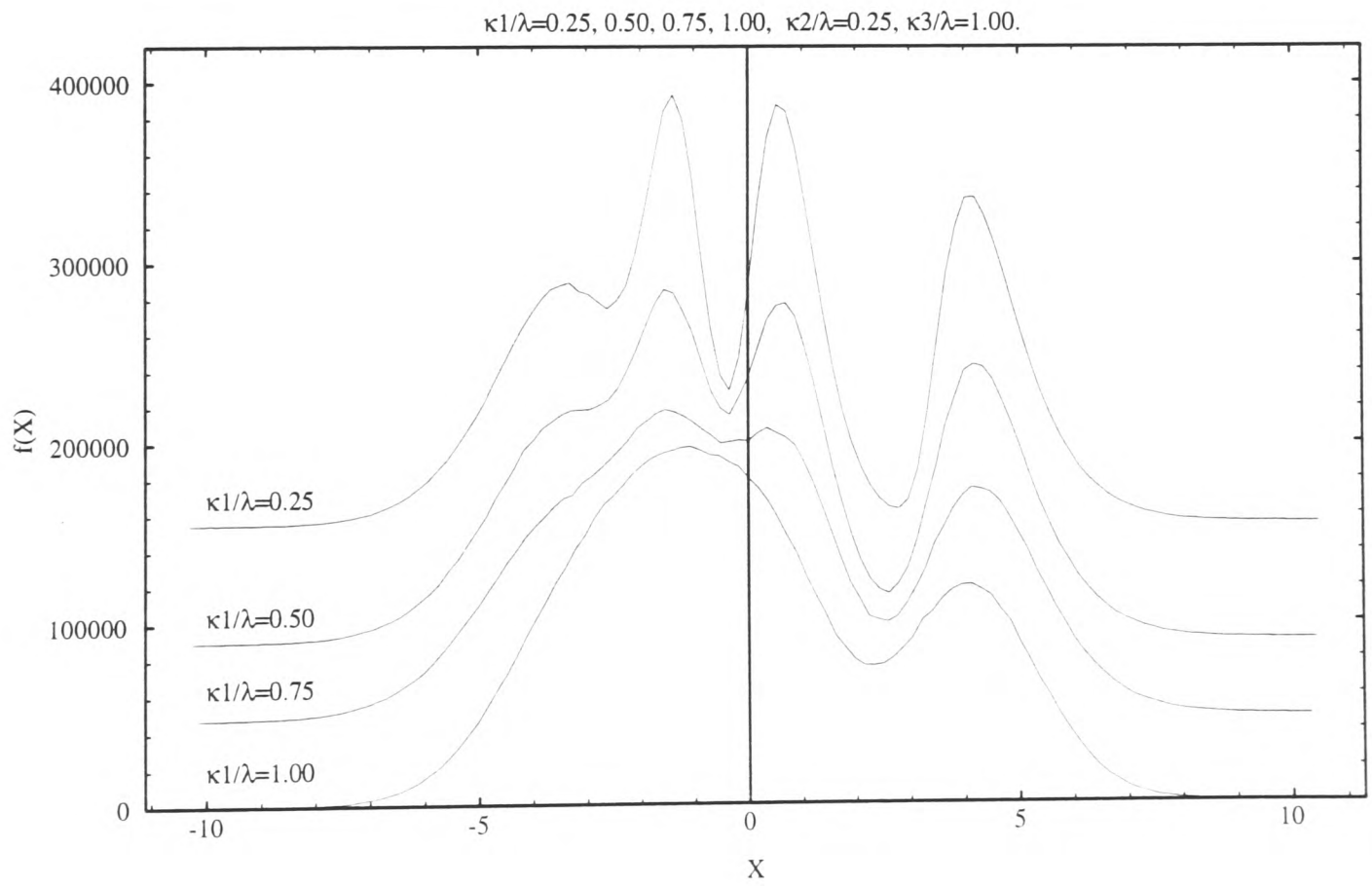

Figure 6.20: General cases (d).

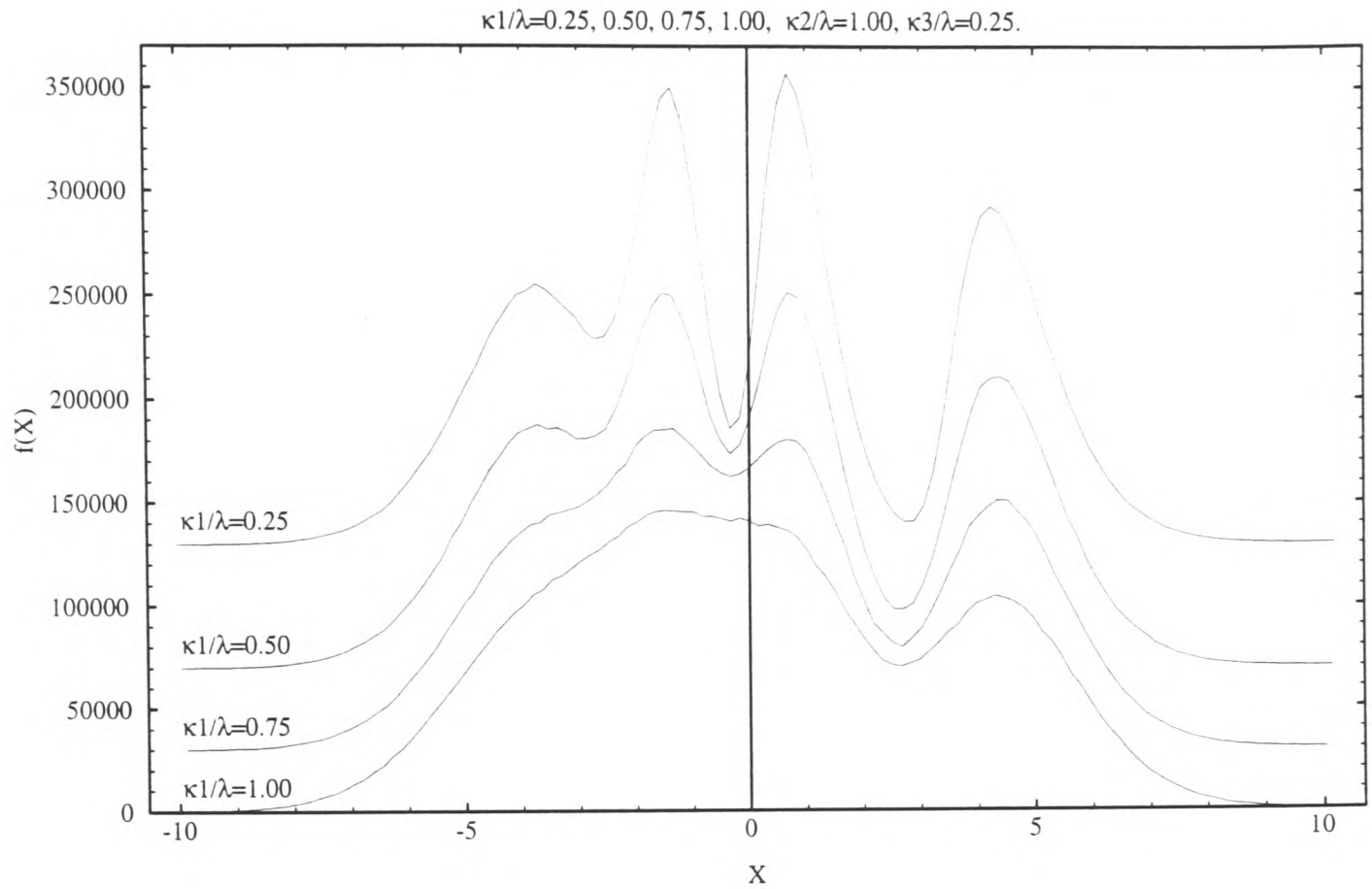

Figure 6.21: General cases (e).

6.6 Discusssion of the results.

In the previous section, for given sets of adiabatic parameters, the corresponding absorption line shapes are produced relatively easily by numerical Monte-Carlo integration. The spectra show very clearly features pertaining to strongly competing spin-orbit and $G \otimes (g \oplus h)$ Jahn-Teller interactions.

The inverse problem, i.e. the determination of unknown parameters by comparing theoretical and experimental spectra, is somewhat more difficult. There are three main limitations of this model which one must bear in mind when considering the relationship between the theory and experiment:

(1) Different combinations and magnitudes of the parameters can result in very similar band shapes, even when there is quite a lot of structure (e.g. (6.6)/(6.7) and (6.12)/(6.13)). Therefore, in many cases, there are very few distinguishing features which could facilitate a unique assignment of parameter values from a comparison of theory and experiment. A distinction between various similar spectra is possible by comparing higher order moments of the bands. However, such an analysis is beyond the scope of this classical model.

(2) The calculations of the band shapes in the previous section, apply only at the absolute zero

of temperature, as they assume that all the oscillations of the system are initially in their ground state. At higher temperatures the excited states are populated and the mean of the square radius, $\langle Q^2 \rangle = \sigma^2$ for each coordinate, increases. The line shape function from the classical Franck-Condon approximation, Equation (6.4), is modified to

$$f(E) = \mathrm{Av}_i \sum_f |\langle f|P|i\rangle|^2 \delta(E - E_f + E_i), \tag{6.15}$$

where i and f label initial and final states respectively, and Av_i is a thermal average over the initial states. Within the classical Franck-Condon approximation [90] [19], the integral form of this function is then found to be

$$f(E) = \frac{1}{4}\left(\frac{1}{\pi kT}\right)^{N/2} \sum_j^K \int \ldots \int dQ_1 dQ_2 \ldots dQ_N \exp\left(\frac{-\sum_i^N Q_i^2}{kT}\right) \delta(E - E_j(\{Q\})), \tag{6.16}$$

which is obtained by replacing the variance, σ^2, in Equation (6.5) by its classical equipartition value, i.e. $\sigma^2 = kT/2$. One should thus be able to obtain a rough estimate of the effect of changes of temperature on the line shapes by replacing the σ^2 in the computational prescription (GASDEV see [69]) by a linear temperature dependence. An example of this is given below in Figure 6.22, for the parameter combination $\lambda = \kappa_1 = \kappa_2 = 0$, $\kappa_3 = 1$ and $\theta = kT/2\sigma^2 = 0.25, 0.50, 0.75, 1.00$, where θ is a dimensionless temperature parameter.

(3) The model only considers the effect of a linear Jahn-Teller interaction, and non-linear electron-lattice interactions have not been accounted for. These non-linear interactions may manifest themselves as they do in other systems (e.g. $T \otimes (\epsilon \oplus \tau)$ see [19]), as an asymmetry in the band shapes at higher temperatures.

6.7 Summary of Chapter 6.

The optical transition from an orbital singlet ground state to a G excited state, is in general subject to both Jahn-Teller and spin-orbit interactions. The resulting APESs are very complicated and it is difficult to infer anything from their structure about the variation of the corresponding spectra. However, some structure may be initially ascertained by considering more closely the spin-orbit basis in the G excited state. The spin-orbit basis under consideration is $G \otimes \Gamma_6 = \Gamma_6 \oplus \Gamma_9$, where Γ_6 is the spin-$(1/2)$ representation and Γ_9 is the six-fold degenerate spin representation derived from the $SO(3)$ irrep $J = 5/2$. Since Kramers degeneracy cannot be lifted by Jahn-Teller interactions, the spin-orbit type spectra are in general expected to exemplify four maxima, three derived from Γ_9 and one from Γ_6.

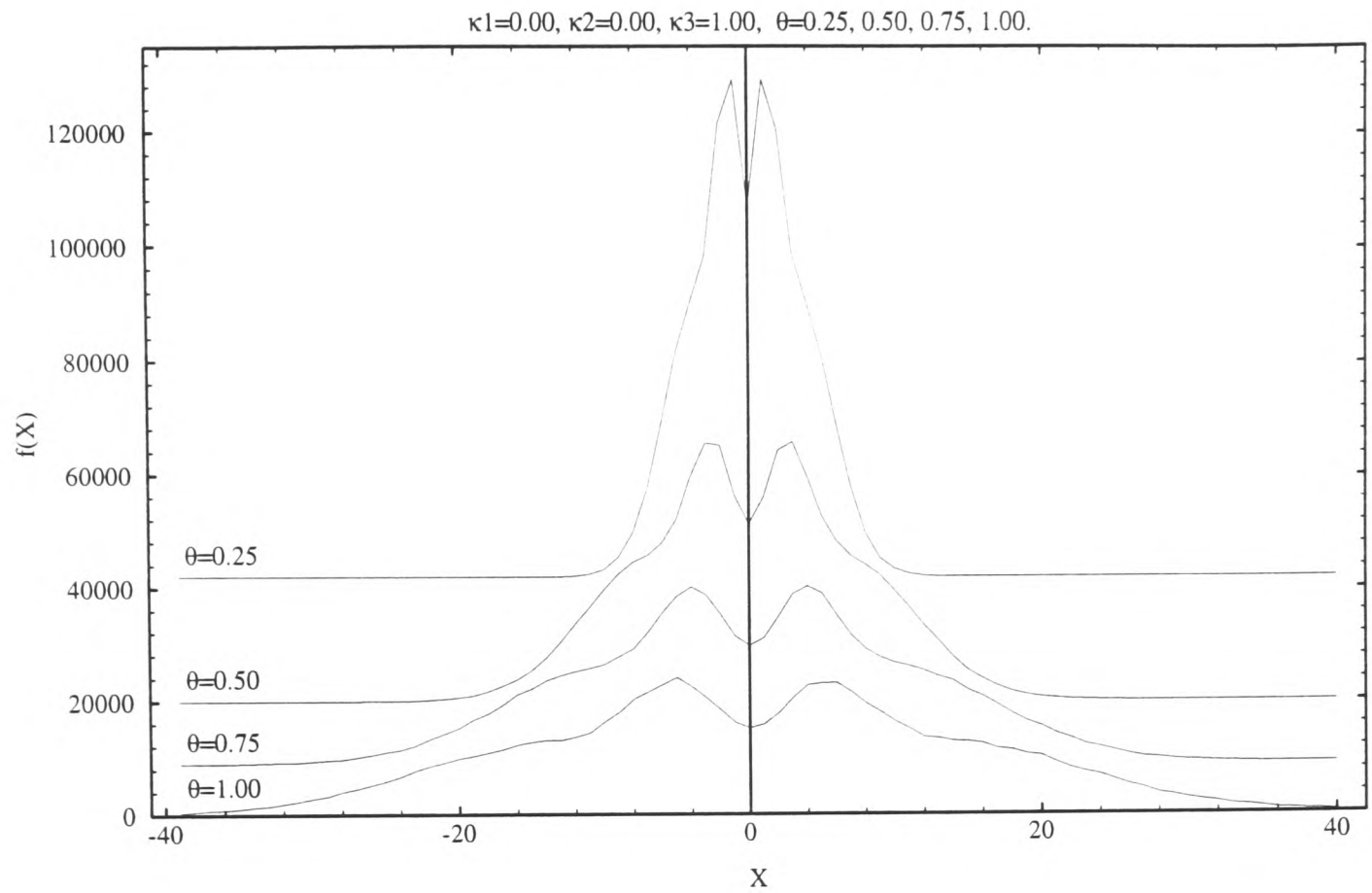

Figure 6.22: Rough estimate of temperature dependence.

The spectra are computed by numerical Monte Carlo integration and the results of this procedure for various combinations of the adiabatic parameters are presented. There are however, three main limitations of the model which one should bear in mind when considering the relationship between the theory and experiment:

(1) Different combinations of the adiabatic parameters seem to result in spectra of very similar aspect. This is particularly true in spectra of very little structure. Even in some spectra possessing quite a lot of structure, there are very few distinguishing features which could facilitate a unique assigning of parameter values from a comparison of theory and experiment. A distinction between similar spectra may be made by considering the higher order moments of the bands. However, such an analysis is beyond the scope of this classical model.

(2) The band shape formula used to compute the spectra applies only at the absolute zero of temperature. However, the formulation of the classical Franck-Condon approximation in references [90] and [19], alludes to a rough estimate of the temperature dependence of the band shapes which is obtainable from the absolute zero formulation. A modification of the variance of the source deviates in the computational prescription, mimics the temperature dependence of the mean square radius of oscillations, and leads to a rough estimate of the

temperature dependence of the corresponding band shapes.

(3) Non-linear electron-lattice interactions have not been accounted for in the model. These non-linear interactions may manifest themselves in real systems as an extra cause of asymmetry in the band shapes at higher temperatures.

Chapter 7

Concluding remarks.

Since the theoretical prediction of the Jahn-Teller effect in 1937, many parallel advances in theory and experiment have taken place in the field. Among these have been the treatment of systems of higher symmetry, the inclusion of spin-orbit coupling and refinements such as the introduction of ground state reduction factors (Ham factors) and considerations of Berry's phase.

Systems of symmetry as high as that of the icosahedron, did not figure largely in discussions of the Jahn-Teller effect until the relatively recent discovery of the C_{60} molecule. As a source for Jahn-Teller studies, icosahedral systems prove to be a fascinating set of problems, exhibiting some properties that are not seen in systems of lower symmetry. The mathematical treatment of icosahedral systems has mainly been in the strong coupling régime. Jahn-Teller modes active in the various icosahedral electronic manifolds, possess relatively high dimensionalities and the symmetries of the corresponding oscillator Hamiltonians appertain to the higher unitary groups ($U(9)$ or even $U(14)$). A knowledge of the symmetry subduction paths from these higher unitary groups to I is necessary for the treatment of the weak coupling régime. However, detailed studies of these subduction paths have yet to be expounded and therefore the weak coupling problem remains relatively unmanageable.

The work presented in this thesis, primarily explores the ground state properties of strongly coupled $G \otimes (g \oplus h)$. The introduction of a biharmonic parametrization for this problem, leads to the possibility of incorporating results from the hyperspherical formulation of quantum field models, which greatly simplify the visualization of the resulting phase spaces. The consequences of this have proved to be quite important for these studies. To date, only a general topological understanding of the structure of these phase spaces has been expounded, and a study of what has become known as the "topography" of these phase spaces is necessary for more specific details such as ground state reduction factors (Ham factors) and Berry phases. In a biharmonic

parametrization, a study of the salient features in the topography of $G \otimes (g \oplus h)$ is very accessible.

In Chapter 4, an extension of the methods employed in Chapter 3 facilitate the calculation of reduction or Ham factors for operators acting within the low-lying states of $G \otimes (g \oplus h)_{eq}$, $G \otimes g$, $G \otimes h$ and $H \otimes g$. A complication, peculiar to icosahedral systems, arises from the energy-proximity of the low-lying sublevels which is most conveniently described by an extension of the standard definition of the Ham factor. A further complication which is not seen in systems of symmetry lower than that of the icoahedron, is the multiplicity of H operators which act within an H manifold. This leads to a multiplicity of Ham factors for H operators which in the case of $H \otimes g$ leads to the introduction of a matrix of Ham factors.

In Chapter 5, the equal coupling Hamiltonian is perturbed by a fourth-order icosahedral field term which has a very simple form in terms of the biharmonic parametrization. The interaction matrix is very complicated and not very sparse, but with the implementation of some organizational considerations, the problem becomes relatively simple to compute. Numerically computed ground state properties of the system interpolate very well between those appropriate to coupling to g and h-modes separately (these are properties which have already been calculated in Chapters 3 and 4). Some interesting remarks are also made regarding the experimental manifestations of these ground state properties.

The model presented in Chapter 5 is perturbative, and therefore its capabilities of modelling motion within the phase space of $G \otimes (g \oplus h)$, are limited to those of the zeroth order Hamiltonian. These limitations of the zeroth order Hamiltonian are discussed and compared with the predictions of group theoretical considerations.

Chapter 6 deals with the optical absorption line shapes arising in transitions from orbital singlet to G excited states in an icosahedral environment. The G excited state is subject to both spin-orbit and Jahn-Teller interactions and the resulting APESs are very complicated. The problem is made tractable by appealing to a classical Franck-Condon approximation and by means of numerical Monte Carlo integration, the absorption band shapes for a given set of adiabatic parameters are relatively easy to calculate. However, the limitations of this classical model would become apparent if one were to attempt a determination of unknown parameters by comparing theoretical and experimental spectra. The three main limitations of this model pertaining to resolution of band structure, temperature dependence and non-linear electron-lattice interactions are discussed.

It is hoped that this thesis has indicated the importance of a well chosen parametrization in analysing the invariably complicated phase spaces of icosahedral Jahn-Teller systems. Ground state properties, such as Ham factors and Berry phases, are most easily elucidated by assigning

a definite coordinate system to the phase space. It is therefore more informative, in the context of these experimentally accessible quantities, to consider the "topography" of the Jahn-Teller system rather than its more abstract "topology".

As is clear from a comparison of the introduction with the contents of this thesis. there is still any amount of work waiting to be done on this fascinating set of problems.

Appendix A

Matrix operators and quadratic forms appertaining to the G and H electronic manifolds.

A.1 Matrix representations of Jahn-Teller modes active in the G manifold.

$$\hat{\mathrm{g}}_{\alpha}^{G} = \begin{array}{c} \\ \langle G\alpha| \\ \langle G\beta| \\ \langle G\gamma| \\ \langle G\delta| \end{array} \begin{array}{c} \begin{array}{cccc} |G\alpha\rangle & |G\beta\rangle & |G\gamma\rangle & |G\delta\rangle \end{array} \\ \begin{pmatrix} 0 & 0 & 0 & -\frac{1}{\sqrt{6}} \\ 0 & 0 & -\frac{1}{\sqrt{6}} & 0 \\ 0 & -\frac{1}{\sqrt{6}} & 0 & -\frac{1}{\sqrt{6}} \\ -\frac{1}{\sqrt{6}} & 0 & -\frac{1}{\sqrt{6}} & 0 \end{pmatrix} \end{array} \quad \hat{\mathrm{g}}_{\beta}^{G} = \begin{pmatrix} 0 & 0 & -\frac{1}{\sqrt{6}} & 0 \\ 0 & 0 & 0 & \frac{1}{\sqrt{6}} \\ -\frac{1}{\sqrt{6}} & 0 & \frac{1}{\sqrt{6}} & 0 \\ 0 & \frac{1}{\sqrt{6}} & 0 & -\frac{1}{\sqrt{6}} \end{pmatrix},$$

$$\hat{\mathrm{g}}_{\gamma}^{G} = \begin{pmatrix} 0 & -\frac{1}{\sqrt{6}} & 0 & -\frac{1}{\sqrt{6}} \\ -\frac{1}{\sqrt{6}} & 0 & \frac{1}{\sqrt{6}} & 0 \\ 0 & \frac{1}{\sqrt{6}} & 0 & 0 \\ -\frac{1}{\sqrt{6}} & 0 & 0 & 0 \end{pmatrix}, \quad \hat{\mathrm{g}}_{\delta}^{G} = \begin{pmatrix} -\frac{1}{\sqrt{6}} & 0 & -\frac{1}{\sqrt{6}} & 0 \\ 0 & \frac{1}{\sqrt{6}} & 0 & -\frac{1}{\sqrt{6}} \\ -\frac{1}{\sqrt{6}} & 0 & 0 & 0 \\ 0 & -\frac{1}{\sqrt{6}} & 0 & 0 \end{pmatrix},$$

$$\hat{\mathrm{h}}_{\theta}^{G} = \begin{pmatrix} \frac{1}{2} & 0 & 0 & 0 \\ 0 & \frac{1}{2} & 0 & 0 \\ 0 & 0 & -\frac{1}{2} & 0 \\ 0 & 0 & 0 & -\frac{1}{2} \end{pmatrix}, \quad \hat{\mathrm{h}}_{\epsilon}^{G} = \frac{1}{\sqrt{3}} \begin{pmatrix} 0 & 0 & \frac{1}{2} & 0 \\ 0 & 0 & 0 & -\frac{1}{2} \\ \frac{1}{2} & 0 & 1 & 0 \\ 0 & -\frac{1}{2} & 0 & -1 \end{pmatrix},$$

$$\hat{\mathrm{h}}_x^G = \frac{1}{\sqrt{3}} \begin{pmatrix} -1 & 0 & \frac{1}{2} & 0 \\ 0 & 1 & 0 & \frac{1}{2} \\ \frac{1}{2} & 0 & 0 & 0 \\ 0 & \frac{1}{2} & 0 & 0 \end{pmatrix}, \quad \hat{\mathrm{h}}_y^G = \frac{1}{\sqrt{3}} \begin{pmatrix} 0 & 1 & 0 & -\frac{1}{2} \\ 1 & 0 & \frac{1}{2} & 0 \\ 0 & \frac{1}{2} & 0 & 0 \\ -\frac{1}{2} & 0 & 0 & 0 \end{pmatrix}, \quad \hat{\mathrm{h}}_z^G = \frac{1}{\sqrt{3}} \begin{pmatrix} 0 & 0 & 0 & \frac{1}{2} \\ 0 & 0 & \frac{1}{2} & 0 \\ 0 & \frac{1}{2} & 0 & -1 \\ \frac{1}{2} & 0 & -1 & 0 \end{pmatrix}.$$

Here the matrix $\hat{\mathrm{g}}_\alpha^G$ displays the column and row designations for all these matrices.

A.2 G and H tensors constructed from the components of a $|G\rangle$ vector.

$$\begin{aligned}
\mathcal{Q}_{\mathrm{g}\alpha}^G &= -\sqrt{\frac{2}{3}}\,(a_\alpha a_\delta + a_\beta a_\gamma + a_\delta a_\gamma), \\
\mathcal{Q}_{\mathrm{g}\beta}^G &= \frac{1}{\sqrt{6}}\,(2a_\beta a_\delta - a_\delta^2 - 2a_\alpha a_\gamma + a_\gamma^2), \\
\mathcal{Q}_{\mathrm{g}\gamma}^G &= \sqrt{\frac{2}{3}}\,(-a_\alpha a_\beta - a_\alpha a_\delta + a_\beta a_\gamma), \\
\mathcal{Q}_{\mathrm{g}\delta}^G &= \frac{1}{\sqrt{6}}\,(-a_\alpha^2 + a_\beta^2 - 2a_\beta a_\delta - 2a_\alpha a_\gamma), \\
\mathcal{Q}_{\mathrm{h}\theta}^G &= \frac{1}{2}\,(a_\alpha^2 + a_\beta^2 - a_\gamma^2 - a_\delta^2), \\
\mathcal{Q}_{\mathrm{h}\epsilon}^G &= \frac{1}{\sqrt{3}}\,(-a_\beta a_\delta - a_\delta^2 + a_\alpha a_\gamma + a_\gamma^2), \\
\mathcal{Q}_{\mathrm{h}x}^G &= \frac{1}{\sqrt{3}}\,(-a_\alpha^2 + a_\beta^2 + 2a_\beta a_\delta + a_\alpha a_\gamma), \\
\mathcal{Q}_{\mathrm{h}y}^G &= \frac{1}{\sqrt{3}}\,(2a_\alpha a_\beta - a_\alpha a_\delta + a_\beta a_\gamma), \\
\mathcal{Q}_{\mathrm{h}z}^G &= \frac{1}{\sqrt{3}}\,(a_\alpha a_\delta + a_\beta a_\gamma - 2a_\delta a_\gamma).
\end{aligned}$$

A.3 Matrix representations of Jahn-Teller modes active in the H manifold.

$$\hat{\mathrm{g}}_\alpha^H = \begin{array}{c|ccccc} & |H\theta\rangle & |H\epsilon\rangle & |Hx\rangle & |Hy\rangle & |Hz\rangle \\ \hline \langle H\theta| & 0 & 0 & 0 & 0 & \frac{-1}{\sqrt{5}} \\ \langle H\epsilon| & 0 & 0 & 0 & \frac{-1}{2\sqrt{15}} & 0 \\ \langle Hx| & 0 & 0 & 0 & \frac{-2}{\sqrt{15}} & \frac{1}{2\sqrt{15}} \\ \langle Hy| & 0 & \frac{-1}{2\sqrt{15}} & \frac{-2}{\sqrt{15}} & 0 & 0 \\ \langle Hz| & \frac{-1}{\sqrt{5}} & 0 & \frac{1}{2\sqrt{15}} & 0 & 0 \end{array} \qquad \hat{\mathrm{g}}_\beta^H = \frac{1}{\sqrt{15}} \begin{pmatrix} 0 & -\sqrt{3} & 0 & 0 & 0 \\ -\sqrt{3} & 0 & \frac{-1}{2} & 0 & 0 \\ 0 & \frac{-1}{2} & 2 & 0 & 0 \\ 0 & 0 & 0 & -2 & \frac{-1}{2} \\ 0 & 0 & 0 & \frac{-1}{2} & 0 \end{pmatrix}.$$

$$\hat{g}_{\gamma}^{H} = \frac{1}{\sqrt{15}} \begin{pmatrix} 0 & 0 & 0 & -\sqrt{3} & 0 \\ 0 & 0 & 0 & \frac{1}{2} & 2 \\ 0 & 0 & 0 & 0 & \frac{1}{2} \\ -\sqrt{3} & \frac{1}{2} & 0 & 0 & 0 \\ 0 & 2 & \frac{1}{2} & 0 & 0 \end{pmatrix}, \quad \hat{g}_{\delta}^{H} = \frac{1}{\sqrt{15}} \begin{pmatrix} 0 & 0 & \sqrt{3} & 0 & 0 \\ 0 & -2 & \frac{1}{2} & 0 & 0 \\ \sqrt{3} & \frac{1}{2} & 0 & 0 & 0 \\ 0 & 0 & 0 & 0 & \frac{-1}{2} \\ 0 & 0 & 0 & \frac{-1}{2} & 2 \end{pmatrix},$$

$$\hat{h}_{2\theta}^{H} = \frac{1}{\sqrt{14}} \begin{pmatrix} 2 & 0 & 0 & 0 & 0 \\ 0 & -2 & 0 & 0 & 0 \\ 0 & 0 & 1 & 0 & 0 \\ 0 & 0 & 0 & 1 & 0 \\ 0 & 0 & 0 & 0 & -2 \end{pmatrix}, \quad \hat{h}_{2\epsilon}^{H} = \frac{1}{\sqrt{14}} \begin{pmatrix} 0 & -2 & 0 & 0 & 0 \\ -2 & 0 & 0 & 0 & 0 \\ 0 & 0 & -\sqrt{3} & 0 & 0 \\ 0 & 0 & 0 & \sqrt{3} & 0 \\ 0 & 0 & 0 & 0 & 0 \end{pmatrix},$$

$$\hat{h}_{2x}^{H} = \frac{1}{\sqrt{14}} \begin{pmatrix} 0 & 0 & 1 & 0 & 0 \\ 0 & 0 & -\sqrt{3} & 0 & 0 \\ 1 & -\sqrt{3} & 0 & 0 & 0 \\ 0 & 0 & 0 & 0 & \sqrt{3} \\ 0 & 0 & 0 & \sqrt{3} & 0 \end{pmatrix}, \quad \hat{h}_{2y}^{H} = \frac{1}{\sqrt{14}} \begin{pmatrix} 0 & 0 & 0 & 1 & 0 \\ 0 & 0 & 0 & \sqrt{3} & 0 \\ 0 & 0 & 0 & 0 & \sqrt{3} \\ 1 & \sqrt{3} & 0 & 0 & 0 \\ 0 & 0 & \sqrt{3} & 0 & 0 \end{pmatrix},$$

$$\hat{h}_{2z}^{H} = \frac{1}{\sqrt{14}} \begin{pmatrix} 0 & 0 & 0 & 0 & -2 \\ 0 & 0 & 0 & 0 & 0 \\ 0 & 0 & 0 & \sqrt{3} & 0 \\ 0 & 0 & \sqrt{3} & 0 & 0 \\ -2 & 0 & 0 & 0 & 0 \end{pmatrix}, \quad \hat{h}_{4\theta}^{H} = \frac{1}{\sqrt{70}} \begin{pmatrix} -6 & 0 & 0 & 0 & 0 \\ 0 & -1 & 0 & 0 & 0 \\ 0 & 0 & 4 & 0 & 0 \\ 0 & 0 & 0 & 4 & 0 \\ 0 & 0 & 0 & 0 & -1 \end{pmatrix},$$

$$\hat{h}_{4\epsilon}^{H} = \frac{1}{\sqrt{70}} \begin{pmatrix} 0 & -1 & 0 & 0 & 0 \\ -1 & 0 & \frac{7}{\sqrt{3}} & 0 & 0 \\ 0 & \frac{7}{\sqrt{3}} & \frac{2}{\sqrt{3}} & 0 & 0 \\ 0 & 0 & 0 & \frac{-2}{\sqrt{3}} & \frac{7}{\sqrt{3}} \\ 0 & 0 & 0 & \frac{7}{\sqrt{3}} & 0 \end{pmatrix}, \quad \hat{h}_{4x}^{H} = \frac{1}{\sqrt{70}} \begin{pmatrix} 0 & 0 & 4 & 0 & 0 \\ 0 & \frac{7}{\sqrt{3}} & \frac{2}{\sqrt{3}} & 0 & 0 \\ 4 & \frac{2}{\sqrt{3}} & 0 & 0 & 0 \\ 0 & 0 & 0 & 0 & \frac{-2}{\sqrt{3}} \\ 0 & 0 & 0 & \frac{-2}{\sqrt{3}} & \frac{-7}{\sqrt{3}} \end{pmatrix},$$

$$\hat{h}_{4y}^{H} = \frac{1}{\sqrt{70}} \begin{pmatrix} 0 & 0 & 0 & 4 & 0 \\ 0 & 0 & 0 & \frac{-2}{\sqrt{3}} & \frac{7}{\sqrt{3}} \\ 0 & 0 & 0 & 0 & \frac{-2}{\sqrt{3}} \\ 4 & \frac{-2}{\sqrt{3}} & 0 & 0 & 0 \\ 0 & \frac{7}{\sqrt{3}} & \frac{-2}{\sqrt{3}} & 0 & 0 \end{pmatrix}, \quad \hat{h}_{4z}^{H} = \frac{1}{\sqrt{70}} \begin{pmatrix} 0 & 0 & 0 & 0 & -1 \\ 0 & 0 & 0 & \frac{7}{\sqrt{3}} & 0 \\ 0 & 0 & 0 & \frac{-2}{\sqrt{3}} & \frac{-7}{\sqrt{3}} \\ 0 & \frac{7}{\sqrt{3}} & \frac{-2}{\sqrt{3}} & 0 & 0 \\ -1 & 0 & \frac{-7}{\sqrt{3}} & 0 & 0 \end{pmatrix}.$$

Here the matrix $\hat{g}_{\alpha}^{H}$ displays the column and row designations for all these matrices.

A.4 G, $2H$ and $4H$ tensors constructed from the components of a $|H\rangle$ vector.

$$
\begin{aligned}
\mathcal{Q}^H_{\mathrm{g}\alpha} &= \frac{1}{3\sqrt{5}}(-\sqrt{3}a_\epsilon a_y - 4\sqrt{3}a_x a_y - 6a_\theta a_z + \sqrt{3}a_x a_z),\\
\mathcal{Q}^H_{\mathrm{g}\beta} &= \frac{1}{3\sqrt{5}}(-6a_\epsilon a_\theta - \sqrt{3}a_\epsilon a_x + 2\sqrt{3}a_x^2 - 2\sqrt{3}a_y^2 - \sqrt{3}a_y a_z),\\
\mathcal{Q}^H_{\mathrm{g}\gamma} &= \frac{1}{3\sqrt{5}}(\sqrt{3}a_\epsilon a_y - 6a_\theta a_y + 4\sqrt{3}a_\epsilon a_z + \sqrt{3}a_x a_z),\\
\mathcal{Q}^H_{\mathrm{g}\delta} &= \frac{1}{3\sqrt{5}}(-2\sqrt{3}a_\epsilon^2 + \sqrt{3}a_\epsilon a_x + 6a_\theta a_x - \sqrt{3}a_y a_z + 2\sqrt{3}a_z^2),\\
\mathcal{Q}^H_{\mathrm{h}2\theta} &= \frac{1}{\sqrt{14}}(-2a_\epsilon^2 + 2a_\theta^2 + a_x^2 + a_y^2 - 2a_z^2),\\
\mathcal{Q}^H_{\mathrm{h}2\epsilon} &= \frac{1}{\sqrt{14}}(-4a_\epsilon a_\theta - \sqrt{3}a_x^2 + \sqrt{3}a_y^2),\\
\mathcal{Q}^H_{\mathrm{h}2x} &= \sqrt{\frac{2}{7}}(-\sqrt{3}a_\epsilon a_x + a_\theta a_x + \sqrt{3}a_y a_z),\\
\mathcal{Q}^H_{\mathrm{h}2y} &= \sqrt{\frac{2}{7}}(\sqrt{3}a_\epsilon a_y + a_\theta a_y + \sqrt{3}a_x a_z),\\
\mathcal{Q}^H_{\mathrm{h}2z} &= \sqrt{\frac{2}{7}}(\sqrt{3}a_x a_y - 2a_\theta a_z),\\
\mathcal{Q}^H_{\mathrm{h}4\theta} &= \frac{1}{\sqrt{70}}(-a_\epsilon^2 - 6a_\theta^2 + 4a_x^2 + 4a_y^2 - a_z^2),\\
\mathcal{Q}^H_{\mathrm{h}4\epsilon} &= \frac{1}{3}\sqrt{\frac{2}{35}}(-3a_\epsilon a_\theta + 7\sqrt{3}a_\epsilon a_x + \sqrt{3}a_x^2 - \sqrt{3}a_y^2 + 7\sqrt{3}a_y a_z),\\
\mathcal{Q}^H_{\mathrm{h}4x} &= \frac{1}{3\sqrt{70}}(7\sqrt{3}a_\epsilon^2 + 4\sqrt{3}a_\epsilon a_x + 24a_\theta a_x - 4\sqrt{3}a_y a_z - 7\sqrt{3}a_z^2),\\
\mathcal{Q}^H_{\mathrm{h}4y} &= \frac{1}{3}\sqrt{\frac{2}{35}}(-2\sqrt{3}a_\epsilon a_y + 12a_\theta a_y + 7\sqrt{3}a_\epsilon a_z - 2\sqrt{3}a_x a_z),\\
\mathcal{Q}^H_{\mathrm{h}4z} &= \frac{1}{3}\sqrt{\frac{2}{35}}(7\sqrt{3}a_\epsilon a_y - 2\sqrt{3}a_x a_y - 3a_\theta a_z - 7\sqrt{3}a_x a_z).
\end{aligned}
$$

Appendix B

Fourth-order quartet and quintet invariants.

B.1 Quartet invariants.

$$
\begin{aligned}
((G\cdot G)_A\cdot(G\cdot G)_A)_A &= (q_\alpha^2+q_\beta^2+q_\gamma^2+q_\delta^2)^2. \qquad \text{(B.1)}\\
((G\times G)_G\cdot(G\times G)_G)_A &= (((G\times G)_G\times G)_G\cdot G)_A = \frac{1}{6}(q_\alpha^4+2q_\alpha^2q_\beta^2+q_\beta^2+\\
&\quad 12q_\alpha^2q_\beta q_\delta-4q_\beta^3q_\delta+8q_\alpha^2q_\delta^2+8q_\alpha^2q_\delta^2-\\
&\quad 4q_\beta q_\delta^3+q_\delta^4+4q_\alpha^3q_\gamma-12q_\alpha q_\beta^2q_\gamma+8q_\alpha^2q_\gamma^2+\\
&\quad 8q_\beta^2q_\gamma^2+12q_\beta q_\delta q_\gamma^2+2q_\delta^2q_\gamma^2-4q_\alpha q_\gamma^3+q_\gamma^4).\\
((G\times G)_H\cdot(G\times G)_H)_A &= (((G\times G)_H\times G)_G\cdot G)_A = \frac{1}{4}(7q_\alpha^4+14q_\alpha^2q_\beta^2+7q_\beta^4-\\
&\quad 24q_\alpha^2q_\beta q_\delta+8q_\beta^3q_\delta+2q_\alpha^2q_\delta^2+2q_\beta^2q_\delta^2+\\
&\quad 8q_\beta q_\delta^3+7q_\delta^4-8q_\alpha^3q_\gamma+24q_\alpha q_\beta^2q_\gamma-24q_\alpha q_\delta^2q_\gamma+\\
&\quad 2q_\alpha^2q_\gamma^2+2q_\beta^2q_\gamma^2-24q_\beta q_\delta q_\gamma^2+14q_\delta^2q_\gamma^2+8q_\alpha q_\gamma^3+7q_\gamma^4).
\end{aligned}
$$

B.2 Quintet invariants.

$$
\begin{aligned}
((2H\cdot 2H)_A\cdot(2H\cdot 2H)_A)_A &= (q_\theta^2+q_\epsilon^2+q_x^2+q_y^2+q_z^2)^2. \qquad \text{(B.2)}\\
((2H\times 2H)_G\cdot(2H\times 2H)_G)_A &= (((2H\times 2H)_G\times 2H)_{2H}\cdot 2H)_A = \frac{1}{15}(2q_\epsilon^4+6q_\epsilon^2q_\theta^2-\\
&\quad 2q_\epsilon^3q_x-2\sqrt{3}q_\epsilon^2q_\theta q_x+q_\epsilon^2q_x^2-2\sqrt{3}q_\epsilon q_\theta q_x^2+6q_x^2q_\theta^2-\\
&\quad 2q_\epsilon q_x^3+2q_x^4+q_\epsilon^2q_y^2+2\sqrt{3}q_\epsilon q_\theta q_y^2+6q_\theta^2q_y^2+6q_\epsilon q_x q_y^2+\\
&\quad 4q_x^2q_y^2+2q_y^4+6q_\epsilon^2q_yq_z-4\sqrt{3}q_\epsilon q_\theta q_yq_z+
\end{aligned}
$$

$$
\begin{aligned}
& & & 4\sqrt{3}q_\theta q_x q_y q_z - 6q_x^2 q_y q_z + 2q_y^3 q_z + 4q_\epsilon^2 q_z^2 + \\
& & & 6q_\theta^2 q_z^2 + 6q_\epsilon q_x q_z^2 + 2\sqrt{3}q_\theta q_x q_z^2 + q_x^2 q_z^2 - \\
& & & 2q_y q_z^3 + 2q_z^4).
\end{aligned}
$$

$$
\begin{aligned}
((2H \times 2H)_{2H} \cdot (2H \times 2H)_{2H})_A &= (((2H \times 2H)_{2H} \times 2H)_{2H} \cdot 2H)_A \\
&= \frac{2}{7}(q_\epsilon^2 + q_\theta^2 + q_x^2 + q_y^2 + q_z^2)^2.
\end{aligned}
$$

$$
\begin{aligned}
((2H \times 2H)_{2H} \cdot (2H \times 2H)_{4H})_A &= (((2H \times 2H)_{2H} \times 2H)_{4H} \cdot 2H)_A \\
&= \frac{1}{14\sqrt{5}}(2q_\epsilon^2 + 18q_\epsilon^2 q_\theta^2 - 12q_\theta^4 - 14q_\epsilon^3 q_x - \\
& \quad 14\sqrt{3}q_\epsilon^2 q_\theta q_x - 17q_\epsilon^2 q_x^2 - 14\sqrt{3}q_\epsilon q_\theta q_x^2 + \\
& \quad 18q_\theta^2 q_x^2 - 14q_\epsilon q_x^3 + 2q_x^4 - 17q_\epsilon^2 q_y^2 + \\
& \quad 14\sqrt{3}q_\epsilon q_\theta q_y^2 + 18q_\theta^2 q_y^2 + 42q_\epsilon q_x q_y^2 \\
& \quad 4q_x^2 q_y^2 + 2q_y^4 + 42q_\epsilon^2 q_y q_z - 28\sqrt{3}q_\epsilon q_\theta q_y q_z + \\
& \quad 28\sqrt{3}q_\theta q_x q_y q_z - 42q_x^2 q_y q_z + 14q_y^3 q_z + 4q_\epsilon^2 q_z^2 + \\
& \quad 18q_\theta^2 q_z^2 + 42q_\epsilon q_x q_z^2 + 14\sqrt{3}q_\theta q_x q_z^2 - \\
& \quad 17q_x^2 q_z^2 - 17q_y^2 q_z^2 - 14q_y q_z^3 + 2q_z^4).
\end{aligned}
$$

$$
\begin{aligned}
((2H \times 2H)_{4H} \cdot (2H \times 2H)_{4H})_A &= (((2H \times 2H)_{4H} \times 2H)_{4H} \cdot 2H)_A \\
&= \frac{2}{105}(13q_\epsilon^4 + 12q_\epsilon^2 q_\theta^2 + 27q_\theta^4 + \\
& \quad 14q_\epsilon^3 q_x + 14\sqrt{3}q_\epsilon^2 q_\theta q_x + 47q_\epsilon^2 q_x^2 + \\
& \quad 14\sqrt{3}q_\epsilon q_\theta q_x^2 + 12q_\theta^2 q_x^2 + 14q_\epsilon q_x^3 + \\
& \quad 13q_x^4 + 47q_\epsilon^2 q_y^2 - 14\sqrt{3}q_\epsilon q_\theta q_y^2 + 12q_\theta^2 q_y^2 - \\
& \quad 42q_\epsilon q_x q_y^2 + 26q_x^2 q_y^2 + 13q_y^4 - 42q_\epsilon q_y q_z + \\
& \quad 28\sqrt{3}q_\epsilon q_\theta q_y q_z - 28\sqrt{3}q_\theta q_x q_y q_z + 42q_x^2 q_y q_z - 14q_y^3 q_z + \\
& \quad 26q_\epsilon^2 q_z^2 + 12q_\theta^2 q_z^2 - 42q_\epsilon q_x q_z^2 - 14\sqrt{3}q_\theta q_x q_z^2 + 47q_x^2 q_z^2 + \\
& \quad 47q_y^2 q_z^2 + 14q_y q_z^3 + 13q_z^4).
\end{aligned}
$$

Appendix C

C.1 The interaction matrix for $(\frac{1}{2},\frac{1}{2}) \otimes (1,1)$.

$$V_o \begin{pmatrix} -\frac{(q_1+\sqrt{2}q_8)}{2} & \frac{q_9}{\sqrt{2}} & -\frac{(q_2+q_4)}{2} & \frac{(q_3+q_5)}{2} \\ \frac{q_9}{\sqrt{2}} & -\frac{(q_1-\sqrt{2}q_8)}{2} & \frac{(q_3-q_5)}{2} & \frac{(q_2-q_4)}{2} \\ -\frac{(q_2+q_4)}{2} & \frac{(q_3-q_5)}{2} & \frac{(q_1-\sqrt{2}q_6)}{2} & \frac{q_7}{\sqrt{2}} \\ \frac{(q_3+q_5)}{2} & \frac{(q_2-q_4)}{2} & \frac{q_7}{\sqrt{2}} & \frac{(q_1+\sqrt{2}q_6)}{2} \end{pmatrix} \tag{C.1}$$

C.2 The matrices $\hat{\mathbf{Q}}^{Gg}$, $\hat{\mathbf{Q}}^{Gh}$ and $\hat{\mathbf{Q}}^{Hg}$.

C.2.1 $\hat{\mathbf{Q}}^{Gg}$ in units of (V_G^G/ω_G^2).

$p_1 = \sqrt{3/8}\cos(3\pi/10)$, $p_2 = \sqrt{3/8}\cos(\pi/10)$, $p_3 = \sqrt{3/8}\sin(3\pi/10)$, $p_4 = \sqrt{3/8}\sin(\pi/10)$.
The column normalization for this matrix is $\sqrt{15}/4$.

	q_α	q_β	q_γ	q_δ
min 1	0	$\sqrt{\frac{3}{8}}$	0	$-\sqrt{\frac{3}{8}}$
min 2	p_1	$-p_3$	$-p_2$	$-p_4$
min 3	$-p_2$	p_4	$-p_1$	p_3
min 4	p_2	p_4	p_1	p_3
min 5	$-p_1$	$-p_3$	p_2	$-p_4$

C.2.2 $\hat{\mathbf{Q}}^{Gh}$ in units of (V_H^G/ω_H^2).

$\mu_1 = \sqrt{5}/6$, $\mu_2 = \sqrt{5/12}x^{-4}/3$, $\mu_3 = 5x/(3\sqrt{12})$, $\mu_4 = \sqrt{5}x^4/(3\sqrt{12})$, $\mu_5 = 5x^{-1}/(3\sqrt{12})$,
$\mu_6 = \sqrt{5/12}/3$, $\mu_2 = 5x^3/(3\sqrt{12})$, $\mu_3 = 5x^{-3}/(3\sqrt{12})$, $\mu_4 = \sqrt{5}x^{-2}/18$, $\mu_5 = \sqrt{5}x^2/18$,
with $x = \sqrt{(\sqrt{5}-1)/2}$.
The column normalization for this matrix is $5/(3\sqrt{2})$.

	q_θ	q_ϵ	q_x	q_y	q_z
min 1	μ_1	μ_9	$-\mu_{10}$	0	0
min 2	μ_1	$-\mu_2$	$-\mu_4$	μ_3	μ_5
min 3	μ_1	μ_6	μ_6	μ_7	$-\mu_8$
min 4	μ_1	μ_6	μ_6	$-\mu_7$	μ_8
min 5	μ_1	$-\mu_2$	$-\mu_4$	$-\mu_3$	$-\mu_5$
min 6	$-\mu_1$	$-\mu_6$	$-\mu_6$	μ_8	μ_7
min 7	$-\mu_1$	μ_4	μ_2	μ_5	$-\mu_3$
min 8	$-\mu_1$	μ_4	μ_2	$-\mu_5$	μ_3
min 9	$-\mu_1$	$-\mu_6$	$-\mu_6$	$-\mu_8$	$-\mu_7$
min 10	$-\mu_1$	μ_{10}	$-\mu_9$	0	0

C.2.3 $\hat{\mathbf{Q}}^{Hg}$ in units of (V_G^H/ω_G^2).

	q_α	q_β	q_γ	q_δ
min 1	$b\cos(\pi/2)$	$b\sin(\pi/2)$	$a\cos(\pi/2)$	$a\sin(\pi/2)$
min 2	$b\cos(3\pi/10)$	$-b\sin(3\pi/10)$	$-a\cos(9\pi/10)$	$a\sin(9\pi/10)$
min 3	$-b\cos(\pi/10)$	$b\sin(\pi/10)$	$-a\cos(7\pi/10)$	$-a\sin(7\pi/10)$
min 4	$-b\cos(9\pi/10)$	$-b\sin(9\pi/10)$	$a\cos(7\pi/10)$	$a\sin(7\pi/10)$
min 5	$b\cos(7\pi/10)$	$-b\sin(7\pi/10)$	$-a\cos(\pi/10)$	$a\sin(\pi/10)$
min 6	$-a\cos(3\pi/10)$	$a\sin(3\pi/10)$	$b\cos(9\pi/10)$	$-b\sin(9\pi/10)$
min 7	$-a\cos(9\pi/10)$	$-a\sin(9\pi/10)$	$b\cos(7\pi/10)$	$b\sin(7\pi/10)$
min 8	$-a\cos(\pi/10)$	$-a\sin(\pi/10)$	$b\cos(3\pi/10)$	$b\sin(3\pi/10)$
min 9	$a\cos(3\pi/10)$	$a\sin(3\pi/10)$	$b\cos(\pi/10)$	$-b\sin(\pi/10)$
min 10	$a\cos(\pi/2)$	$-a\sin(\pi/2)$	$b\cos(\pi/2)$	$-b\sin(\pi/2)$

$a = \sqrt{\frac{2}{15}}\frac{2}{\sqrt{5}-1}$, $b = \sqrt{\frac{2}{15}}\frac{\sqrt{5}-1}{2}$.

The column normalization of this matrix for these values of a and b is just 1.

Appendix D

Matrices of vibronic mixing between G and H vibronic states.

D.1 In $G \otimes h$.

G_α	θ	ϵ	x	y	z
α	$\frac{5}{18\sqrt{10}}$	0	$\frac{-5}{9\sqrt{30}}$	0	0
β	0	0	0	$\frac{5}{9\sqrt{30}}$	0
γ	0	$\frac{5}{18\sqrt{30}}$	$\frac{5}{18\sqrt{30}}$	0	0
δ	0	0	0	$\frac{-5}{18\sqrt{30}}$	$\frac{5}{18\sqrt{30}}$

G_β	θ	ϵ	x	y	z
α	0	0	0	$\frac{5}{9\sqrt{30}}$	0
β	$\frac{5}{18\sqrt{10}}$	0	$\frac{5}{9\sqrt{30}}$	0	0
γ	0	0	0	$\frac{5}{18\sqrt{30}}$	$\frac{5}{18\sqrt{30}}$
δ	0	$\frac{-5}{18\sqrt{30}}$	$\frac{5}{18\sqrt{30}}$	0	0

G_γ	θ	ϵ	x	y	z
α	0	$\frac{5}{18\sqrt{30}}$	$\frac{5}{18\sqrt{30}}$	0	0
β	0	0	0	$\frac{5}{18\sqrt{30}}$	$\frac{5}{18\sqrt{30}}$
γ	$\frac{-5}{18\sqrt{10}}$	$\frac{5}{9\sqrt{30}}$	0	0	0
δ	0	0	0	0	$\frac{-5}{9\sqrt{30}}$

G_δ	θ	ϵ	x	y	z
α	0	0	0	$\frac{-5}{18\sqrt{30}}$	$\frac{5}{18\sqrt{30}}$
β	0	$\frac{-5}{18\sqrt{30}}$	$\frac{5}{18\sqrt{30}}$	0	0
γ	0	0	0	0	$\frac{-5}{9\sqrt{30}}$
δ	$\frac{-5}{18\sqrt{10}}$	$\frac{-5}{9\sqrt{30}}$	0	0	0

H_θ	θ	ϵ	x	y	z
α	0	0	0	0	$\frac{-\sqrt{5}}{9}$
β	0	$\frac{-\sqrt{5}}{9}$	0	0	0
γ	0	0	0	$\frac{-\sqrt{5}}{9}$	0
δ	0	0	$\frac{\sqrt{5}}{9}$	0	0

H_ϵ	θ	ϵ	x	y	z
α	0	0	0	$\frac{-\sqrt{5}}{18\sqrt{3}}$	0
β	$\frac{-\sqrt{5}}{9}$	0	$\frac{-\sqrt{5}}{18\sqrt{3}}$	0	0
γ	0	0	0	$\frac{\sqrt{5}}{18\sqrt{3}}$	$\frac{2\sqrt{5}}{9\sqrt{3}}$
δ	0	$\frac{-2\sqrt{5}}{9\sqrt{3}}$	$\frac{\sqrt{5}}{18\sqrt{3}}$	0	0

H_x	θ	ϵ	x	y	z
α	0	0	0	$\frac{-2\sqrt{5}}{9\sqrt{3}}$	$\frac{\sqrt{5}}{18\sqrt{3}}$
β	0	$\frac{-\sqrt{5}}{18\sqrt{3}}$	$\frac{2\sqrt{5}}{9\sqrt{3}}$	0	0
γ	0	0	0	0	$\frac{\sqrt{5}}{18\sqrt{3}}$
δ	$\frac{\sqrt{5}}{9}$	$\frac{\sqrt{5}}{18\sqrt{3}}$	0	0	0

H_y	θ	ϵ	x	y	z
α	0	$\frac{-\sqrt{5}}{18\sqrt{3}}$	$\frac{-2\sqrt{5}}{9\sqrt{3}}$	0	0
β	0	0	0	$\frac{-2\sqrt{5}}{9\sqrt{3}}$	$\frac{-\sqrt{5}}{18\sqrt{3}}$
γ	$\frac{-\sqrt{5}}{9}$	$\frac{\sqrt{5}}{18\sqrt{3}}$	0	0	0
δ	0	0	0	0	$\frac{-\sqrt{5}}{18\sqrt{3}}$

H_z	θ	ϵ	x	y	z
α	$\frac{-\sqrt{5}}{9}$	0	$\frac{\sqrt{5}}{18\sqrt{3}}$	0	0
β	0	0	0	$\frac{-\sqrt{5}}{18\sqrt{3}}$	0
γ	0	$\frac{2\sqrt{5}}{9\sqrt{3}}$	$\frac{\sqrt{5}}{18\sqrt{3}}$	0	0
δ	0	0	0	$\frac{-\sqrt{5}}{18\sqrt{3}}$	$\frac{2\sqrt{5}}{9\sqrt{3}}$

D.2 In $H \otimes g$.

G_α	θ	ϵ	x	y	z
α	$\frac{2}{9}$	0	$\frac{-4}{9\sqrt{3}}$	0	0
β	0	0	0	$\frac{4}{9\sqrt{3}}$	0
γ	0	$\frac{2}{9\sqrt{3}}$	$\frac{2}{9\sqrt{3}}$	0	0
δ	0	0	0	$\frac{-2}{9\sqrt{3}}$	$\frac{2}{9\sqrt{3}}$

G_β	θ	ϵ	x	y	z
α	0	0	0	$\frac{4}{9\sqrt{3}}$	0
β	$\frac{2}{9}$	0	$\frac{4}{9\sqrt{3}}$	0	0
γ	0	0	0	$\frac{2}{9\sqrt{3}}$	$\frac{2}{9\sqrt{3}}$
δ	0	$\frac{-2}{9\sqrt{3}}$	$\frac{2}{9\sqrt{3}}$	0	0

G_γ	θ	ϵ	x	y	z
α	0	$\frac{2}{9\sqrt{3}}$	$\frac{2}{9\sqrt{3}}$	0	0
β	0	0	0	$\frac{2}{9\sqrt{3}}$	$\frac{2}{9\sqrt{3}}$
γ	$\frac{-2}{9}$	$\frac{4}{9\sqrt{3}}$	0	0	0
δ	0	0	0	0	$\frac{-4}{9\sqrt{3}}$

G_δ	θ	ϵ	x	y	z
α	0	0	0	$\frac{-2}{9\sqrt{3}}$	$\frac{2}{9\sqrt{3}}$
β	0	$\frac{-2}{9\sqrt{3}}$	$\frac{2}{9\sqrt{3}}$	0	0
γ	0	0	0	0	$\frac{-4}{9\sqrt{3}}$
δ	$\frac{-2}{9}$	$\frac{-4}{9\sqrt{3}}$	0	0	0

$H_{2\theta}$	θ	ϵ	x	y	z
α	0	0	0	0	$\frac{-4}{3\sqrt{70}}$
β	0	$\frac{-4}{3\sqrt{70}}$	0	0	0
γ	0	0	0	$\frac{-4}{3\sqrt{70}}$	0
δ	0	0	$\frac{4}{3\sqrt{70}}$	0	0

$H_{2\epsilon}$	θ	ϵ	x	y	z
α	0	0	0	$\frac{-2}{3\sqrt{210}}$	0
β	$\frac{-4}{3\sqrt{70}}$	0	$\frac{-2}{3\sqrt{210}}$	0	0
γ	0	0	0	$\frac{2}{3\sqrt{210}}$	$\frac{8}{3\sqrt{210}}$
δ	0	$\frac{-8}{3\sqrt{210}}$	$\frac{2}{3\sqrt{210}}$	0	0

H_{2x}	θ	ϵ	x	y	z
α	0	0	0	$\frac{-8}{3\sqrt{210}}$	$\frac{2}{3\sqrt{210}}$
β	0	$\frac{-2}{3\sqrt{210}}$	$\frac{8}{3\sqrt{210}}$	0	0
γ	0	0	0	0	$\frac{2}{3\sqrt{210}}$
δ	$\frac{4}{3\sqrt{70}}$	$\frac{2}{3\sqrt{210}}$	0	0	0

H_{2y}	θ	ϵ	x	y	z
α	0	$\frac{-2}{3\sqrt{210}}$	$\frac{-8}{3\sqrt{210}}$	0	0
β	0	0	0	$\frac{-8}{3\sqrt{210}}$	$\frac{-2}{3\sqrt{210}}$
γ	$\frac{-4}{3\sqrt{70}}$	$\frac{2}{3\sqrt{210}}$	0	0	0
δ	0	0	0	0	$\frac{-2}{3\sqrt{210}}$

H_{2z}	θ	ϵ	x	y	z
α	$\frac{-4}{3\sqrt{70}}$	0	$\frac{2}{3\sqrt{210}}$	0	0
β	0	0	0	$\frac{-2}{3\sqrt{210}}$	0
γ	0	$\frac{8}{3\sqrt{210}}$	$\frac{2}{3\sqrt{210}}$	0	0
δ	0	0	0	$\frac{-2}{3\sqrt{210}}$	$\frac{8}{3\sqrt{210}}$

$H_{4\theta}$	θ	ϵ	x	y	z
α	0	0	0	0	$\frac{-4}{9\sqrt{14}}$
β	0	$\frac{-4}{9\sqrt{14}}$	0	0	0
γ	0	0	0	$\frac{-4}{9\sqrt{14}}$	0
δ	0	0	$\frac{4}{9\sqrt{14}}$	0	0

$H_{4\epsilon}$	θ	ϵ	x	y	z
α	0	0	0	$\frac{-2}{9\sqrt{42}}$	0
β	$\frac{-4}{9\sqrt{42}}$	0	$\frac{-2}{9\sqrt{42}}$	0	0
γ	0	0	0	$\frac{2}{9\sqrt{42}}$	$\frac{8}{9\sqrt{42}}$
δ	0	$\frac{-8}{9\sqrt{42}}$	$\frac{2}{9\sqrt{42}}$	0	0

H_{4x}	θ	ϵ	x	y	z
α	0	0	0	$\frac{-8}{9\sqrt{42}}$	$\frac{2}{9\sqrt{42}}$
β	0	$\frac{-2}{9\sqrt{42}}$	$\frac{8}{9\sqrt{42}}$	0	0
γ	0	0	0	0	$\frac{2}{9\sqrt{42}}$
δ	$\frac{4}{9\sqrt{14}}$	$\frac{2}{9\sqrt{42}}$	0	0	0

H_{4y}	θ	ϵ	x	y	z
α	0	$\frac{-2}{9\sqrt{42}}$	$\frac{-8}{9\sqrt{42}}$	0	0
β	0	0	0	$\frac{-8}{9\sqrt{42}}$	$\frac{-2}{9\sqrt{42}}$
γ	$\frac{-4}{9\sqrt{14}}$	$\frac{2}{9\sqrt{42}}$	0	0	0
δ	0	0	0	0	$\frac{2}{9\sqrt{42}}$

H_{4z}	θ	ϵ	x	y	z
α	$\frac{-4}{9\sqrt{14}}$	0	$\frac{2}{9\sqrt{42}}$	0	0
β	0	0	0	$\frac{-2}{9\sqrt{42}}$	0
γ	0	$\frac{8}{9\sqrt{42}}$	$\frac{2}{9\sqrt{42}}$	0	0
δ	0	0	0	$\frac{-2}{9\sqrt{42}}$	$\frac{8}{9\sqrt{42}}$

Bibliography

[1] Aitchison, I.J.R. *Physica Scripta*, **T23**:12, 1988.

[2] Aljie, H., Alvarez, M.M., Anz, S.J., Beck, R.D., Diederich, F., Fostiropulos, K., Huffman, D.R., Kratschmer, W., Rubin, Y., Schriver, K.E., Sensharma, D., and Whetten, R.L. *J. Phys. Chem.*, **94**:8630, 1990.

[3] Aspel, S.E., Chancey, C.C. and O'Brien, M.C.M. *Phys. Rev. B.* **45**:5251, 1992.

[4] Auerbach, A. and Kivelson, S. *Nucl. Phys. B*, **257**:799, 1984.

[5] Auerbach, A. and Manini, N. *Phys. Rev.*, **B49**:12998, 1994.

[6] Auerbach, A. and Manini, N. *Phys. Rev.*, **B49**:13008, 1994.

[7] Biedenharn, L.C. *J. Math. Phys.*, **2**:433, 1961.

[8] Bethe, H. *Ann. Phys. Lpz.*, **3**:133, 1929.

[9] Berry, M.V. *Proc. Roy. Soc. Lond.*, **A392**:45, 1984.

[10] Barut, A.O. and Rączka, R.A. *Theory of group representations and applications.* World Scientific, 1986.

[11] Butler, P.H. *Point group symmetry applications*, Plenum Press 1981.

[12] Ceulemans, A. *J. Chem. Phys.*, **87**:5374, 1987.

[13] Ceulemans, A. and Fowler, P.W. *Phys. Rev.*, **A39**:481, 1989.

[14] Ceulemans, A. and Fowler, P.W. *J. Chem. Phys.*, **93**:1221, 1990.

[15] Ceulemans, A., Beyens, D., and Vanquickenbourne, L.G. *Chem. Soc.*, **106**:5824, 1984.

[16] Ceulemans, A. and Vanquikenborne, L.G. *Structure and Bonding*, **71**:126, 1989.

[17] Chancey, C.C. and O'Brien, M.C.M. *J.Phys.: Condens. Matter*, **1**:47, 1989.

[18] Chelikwsky, J.R. and Phillips, J.C. *Phys. Rev. Lett.*, **63**:1653, 1989.

[19] Cho, K. *J. Phys. Soc. Japan*, **25**,5:1372, 1968.

[20] Cullerne, J.P. and O'Brien, M.C.M. *J. Phys.: Condens. Matter*, **6**:9017, 1994.

[21] Cullerne, J.P., O'Brien, M.C.M. and Angelova, M.N. *J. Phys.: Condens. Matter*, **7**:3247, 1995.

[22] Cullerne, J.P. *The $G \otimes (g \oplus h)$ eigenvalue problem near the limit of equal coupling.* (Wigner Symposium: Mexico 1995).

[23] Cullerne, J.P. *Optical absorption line shapes for transitions from orbital singlet to G quartet states.* (Wigner Symposium: Mexico 1995).

[24] Cutkosky, R.E. *J. Math. Phys.*, **25**(4):939 1984.

[25] de Coulon, V., Martins, J.L. and Reuse, F. *Phys. Rev.*, **B45**:13671, 1992.

[26] Ebbesen, T.W., Tanigaki, K. and Kuroshima, S. *Chem. Phys. Lett.*, **181**:501, 1991.

[27] Elliott, J.P. and Dawber, P.G. *Symmetry in Physics Vol 1: Principles and simple applications.* Macmillan, 1985.

[28] Englman, R. *"The Jahn-Teller Effect in Molecules and Crystals"*, Wiley, 1972.

[29] Feng, J., Li, J., Wang, Z. and Zerner, M.C. *Intern. J. Quantum. Chem.*, **37**:599, 1990.

[30] Feng, J., Li, J., Li, Z. and Zerner, M.C. *Intern. J. Quantum. Chem.*, **39**:331, 1991.

[31] Fletcher, J.R., O'Brien, M.C.M., and Evangelou, S.N. *J. Phys. A*, **13**:2035, 1980.

[32] Fowler, P.W. *Chem. Phys. Lett.*, **131**:444, 1986.

[33] Gaunt, J.A. *Trans. Roy. Soc.(London)*, **A228**:195, 1928.

[34] Golding, R.M. *Mol. Phys.*, **26**:661, 1973.

[35] Gu B.L., Li Z.Q. and Zhu J.L. *J. Phys.:Condens. Matter*, **5**:5255, 1993.

[36] Haddon, R.C., Brus, L.E. and Raghavachari, K. *Chem. Phys. Lett.*, **125**:459, 1986.

[37] Ham, F.S. *Phys. Rev.*, **138**:A727, 1965.

[38] Ham, F.S. *Phys. Rev.*, **166**:307, 1968.

[39] Ham, F.S. *"Electron Paramagnetic Resonance"*. ed. S.Gershwin. New York Plenum pp1, 1972.

[40] Ham, F.S. *Phys. Rev. Lett.*, **58**:725, 1987.

[41] Ham, F.S. *Proc. Roy. Soc.*, **A392**:45, 1987.

[42] Hare, J.P., Kroto, H.W. and Taylor, R. *Chem. Phys. Lett.*, **177**:394, 1991.

[43] Henry, C.H., Shnatterly, S.E. and Slichter, C.P. *Phys. Rev.* , **137**:A2, 1965.

[44] Herzberg, G. and Longuet-Higgins, H.C. *Discuss. Faraday soc.* **35**:77, 1963.

[45] Hoare, M.R. and Pal, P. *Adv. Phys.*, **20**:161, 1971.

[46] Huang, Z.H., Feuchtwang, T.E., Cutler, P.H. and Kases, E. *Phys. Rev. A* **41**:32, 1990.

[47] Jahn, H.A. and Teller, E. *Proc. Roy. Soc.*, **A161**:220, 1937.

[48] Jahn, H.A. *Proc. Roy. Soc.*, **A164**:117, 1938.

[49] Judd, B.R. *Proc. Roy. Soc.*, **A241**:122, 1957.

[50] Judd, B.R. *Can. J. Phys.*, **52**:999, 1974.

[51] Joshi, A.W. *Elements of Group Theory for Physicists. 3rd. ed.* Wiley, 1982.

[52] Kapur, P.L. and Peierls, R. *Proc. Roy. Soc. A* **163**:606, 1937.

[53] Khlopin, V.P., Polinger, V.Z. and Bersuker, I.B. *Theoret. Chim. Acta (Berl.)*, **48**:87, 1978.

[54] Kroto, H.W., Heath, J.R., O'Brien, S.C., Curl, R.F., and Smalley, R.E. "C_{60}: Buckminsterfullerene," *Nature*,**318**:162, 1985.

[55] Lannoo, M., Baraff, B.A, Schlüter, M. and Tomanek, D. *Phys. Rev. B*, **44**:12106, 1991.

[56] Larsson, S., Volosov, A. and Rosén, A. *Chem. Phys. Lett.*, **137**:501, 1987.

[57] Laszlo, I. and Udvardi, L. *Chem. Phys. Lett.*, **136**:418, 1987.

[58] Laszlo, I. and Udvardi, L. *J.Mol. Struct.*, **183**:271, 1989.

[59] Leach, S., Vervloet, M., Desprès, A., Bréheret, E., Hare, J.P., Dennis, T.J., Kroto, H.W., Taylor, R. and Walton, R.M. *Chem. Phys.*, **160**:451, 1992.

[60] Lister, G.M.S. and O'Brien, M.C.M. *J.Phys. C:Solid St. Phys.*, **17**:3975, 1984.

[61] Longuet-Higgins, C.M. *Mol. Phys.* , **6**:455, 1963.

[62] Longet-Higgins, H.C., Öpik, U., Pryce, M.H.L. and Sack, R.A. *Proc. Roy. Soc.*, **A244**:1, 1958.

[63] Longuet-Higgins, H.C. *Advan. Spectr.* **2**:249, 1961.

[64] Mead, C.A. *Chem. Phys.* **49**:23, 1980.

[65] Mead, C.A. *Chem. Phys.* **49**:33, 1980.

[66] McLachlin, A.D. *Mol. Phys.* **4**:417, 1961.

[67] Murray-Rust, P., Bürgi, H.B., and Dunitz, J.D. *Acta Crystallo.*, **A35**:703, 1979.

[68] Negri, F., Orlandi, G. and Zerbetto, F. *Chem. Phys. Lett.*, **144**:31, 1988.

[69] Numerical Recipes in FORTRAN. Press, W.H., Teukolsky, S.A., Vetterling, W.T. and Flannery, B.P. (Cambridge University Press.) 2nd. ed. 1992.

[70] O'Brien, M.C.M. *Phys. Rev.*, **187**:407, 1969.

[71] O'Brien, M.C.M. *J.Phys. C:Solid St. Phys.*, **4**:2045, 1971.

[72] O'Brien, M.C.M. *J.Phys. C:Solid St. Phys.*, **4**:2524, 1971.

[73] O'Brien, M.C.M. *J.Phys. C:Solid St. Phys.*, **9**:3153, 1976.

[74] O'Brien, M.C.M. *J.Phys. A:Math.Gen.*, **22**:1779, 1989.

[75] O'Brien, M.C.M. and Chancey, C.C. *Am. J. Phys.*, **61** (8):688, 1993.

[76] O'Brien, M.C.M. and Shelton, D.G. *J.Phys. Condens. Matter*, **6**:7725, 1994.

[77] Öpik, U. and Pryce, M.H.L. *Proc. Roy. Soc.*, **A238**:425, 1957.

[78] Ozaki, M. and Takahashi, A. *Chem. Phys. Lett.*, **127**:242, 1986.

[79] Pooler, D.R. *J. Phys. A:Math. Gen.*, **11**,6:1045, 1978.

[80] Pooler, D.R. *J. Phys. C:Solid St. Phys.*, **13**:1029, 1980.

[81] Pooler, D.R. *J. Phys. A:Math. Gen.*, **13**:1197, 1980.

[82] Polinger, V.Z., Kirk, P.J., Dunn, J.L. and Bates, C.A. *J. Phys. :Condens. Matter.* **5**:2213, 1993.

[83] Ranfagni, A. *Physics Letters*, **62A**:395, 1977.

[84] Rantala, T.T., Stockman, M.I., Jelski, D.A. and George, T.F. *Cluster and Cluster-Assembled Materials.* (Pittsburgh, PA: MRS) p85, 1991.

[85] Rotenberg, M., Bivens, R., Metropolis, N. and Wooten, J.K. *The 3j and 6j symbols.* Technology Press. M.I.T. 1959.

[86] Röthlisberger, U., Andreoni, W. and Giannozzi, P. *J. Chem. Phys.*, **96**:1248, 1992.

[87] Sakamoto, N. *Phys. Rev. B Vol 26*, **12**:6438, 1982.

[88] Sturge, M.D. *"Solid State Physics"*. Academic Press N.Y., 1967.

[89] The Dynamical Jahn-Teller effect in localized systems. *Modern problems in condensed matter physics.* Vol 7. Ed. Perlin, YU.E. and Wagner, M. Elsevier Science Pub. 1984.

[90] Toyozawa, Y. and Inoue, M. *J. Phys. Soc. Japan*, **21**,9:1663, 1966.

[91] Wang, Y. *J. Phys. Chem.*, **96**:764, 1992.

[92] Wilczek, F. and Zee, A. *Phys. Rev. Lett.* **52**:2111, 1984.

[93] Wigner, E.P. *Nuchrichten der Akademie der Wissenschaften zu Göttingen. Math.-Kl.Physik.,Berlin*, 133, 1930.

[94] Wigner, E.P. *Am. J. Math.* **63**:57, 1941.